Ord, Emily N.J. (2012) *Combination therapy in ischaemic stroke.* PhD thesis.

https://theses.gla.ac.uk/3384/

Combination Therapy in Ischaemic Stroke

Emily N. J. Ord BSc (Hons)

Submitted in the fulfilment of the requirements of the

degree of Doctor of Philosophy in the Faculty of

Medicine, University of Glasgow

Institute of Cardiovascular and Medical Sciences
Faculty of Medicine
University of Glasgow

March 2012

© E. N. J. Ord 2012

Author's Declaration

I declare that this thesis has been written entirely by myself and is a record of work performed by myself, excluding Figure 3.1 which was performed by Dr. L. M. Work and Dr. C. McCabe and Figure 4.3 and Figure 4.4 which were performed by Dr. R. Shirley. Green fluorescent protein-expressing canine adenovirus was provided by Dr. Eric Kremer and green fluorescent protein-expressing lentiviral plasmid was provided from laboratory stocks at the BHF GCRC. This thesis has not been previously submitted for a higher degree. The research was carried out in the Institute of Cardiovascular and Medical Sciences, University of Glasgow, under the supervision of Dr. L. M. Work.

Emily Ord

March 2012

Acknowledgements

First and foremost I would like to thank my supervisor Dr. Lorraine M. Work for her invaluable wisdom, patience, guidance and kindness over the last three and a half years; far above and beyond the role of supervisor. I would also especially like to thank Prof. Andrew H. Baker, Prof. I. Mhairi Macrae and Dr. Chris McCabe for their support and supervision over the duration of my PhD. I would also like to thank Dr. Eric J. Kremer and all the members of his lab for their help during my time in Montpellier, and the Student Networking Award Association for funding the trip. I would also like to acknowledge the IMB for funding my PhD.

I have been lucky enough to make a number of very good friends during my time at the GCRC, and would especially like to thank my office mates Margaret Duffy, Lynsey Howard, Aiste Monkeviciute and Wendy Crawford for keeping me smiling even during the more stressful times, and Alette Brinth for all the running / therapy sessions. Special thanks to the Baker group for their patience with me in the lab (especially at the start), and the famous nights out! I would also like to thank Dr. Rachel Shirley for teaching me to keep the faith and showing me the humour in it all, and Dr. Lynda Coughlan and Dr. Katie White for helping with my "conference networking skills".

An extra special thank you to all my wonderful friends outside the world of science, you know who you are and you have all been the greatest distraction I could have asked for. You're motivational texts and chats have meant more than you can ever know, and I look forward to seeing a lot more of all of you now this is over!

To my wonderful family, thank you all so much for your unfaltering support. Mum and Dad, I don't know how long you've spent on the phone to me over the years celebrating my highs and helping me through the lows, but I appreciate and value every minute.

Last but most definitely not least I would like to thank my future husband (!!), Chris. You have always had 100% faith in me and supported me. Whether it be by listening to my numerous presentations on repeat without complaint, by picking me at stupid-O'clock from

work, or the hours you have spent listening to my science related problems, you've been a rock. Without exaggeration, I could not have done this without you and you cannot tell you how grateful I am for everything, it has meant the world.

Table of Contents

List of Figures

List of Tables

Abstracts

ASGCT 15th Annual Meeting – May 2012
Oral Presentation
E. N. J. Ord, R. Shirley, C. McCabe, J.D. McClure, E. J. Kremer, I. M. Macrae & L. M. Work
"Combined gene- and drug-based intervention is protective following cerebral ischaemia / reperfusion."

Integrative Mammalian Biology (IMB) Symposium – March 2012
Oral Presentation – Shortlisted for Young Investigator Award
E. N. J. Ord, R. Shirley, C. McCabe, E. J. Kremer, I. M. Macrae & L. M. Work.
"Combined anti-oxidant and anti-apoptotic intervention is protective following *in vitro* hypoxia / reoxygenation and transient middle cerebral artery occlusion *in vivo*."

British Society for Gene Therapy Annual Conference – October 2011
Oral Presentation - Shortlisted for Fairbairn Award
E. N. J. Ord, R. Shirley, C. McCabe, E. J. Kremer, I. M. Macrae & L. M. Work
"A novel gene- and drug-based intervention for stroke is neuroprotective in vitro and in vivo?"

XXVth International Symposium on Cerebral Blood Flow, Metabolism and Function – May 2011
Poster Presentation
E. N. J. Ord, R. Shirley, C. McCabe, E. Kremer, I. M. Macrae, A. H. Baker & L. M. Work
"Combined efficacy of anti-oxidant and anti-apoptotic interventions following hypoxia/reoxygenation in B50 neuronal cells."

British Society for Gene Therapy Annual Conference – April 2010
Poster Presentation
E. N. J. Ord, C. McCabe, I. M. Macrae, A. H. Baker & L. M. Work
"Upregulation of Neuroglobin as a Putative Neuroprotectant Following Ischaemia-Reperfusion Injury."

IMB & Physiological Society's 7th James Black Conference – September 2009
Poster Presentation
E. N. J. Ord, C. McCabe, I. M. Macrae, A. H. Baker & L. M. Work
"Upregulation of Neuroglobin as a Putative Neuroprotectant Following Ischaemia-Reperfusion Injury."

Abbreviations

ΔΨm	Mitochondrial Membrane Potential
4-HNE	4-Hydroxynonenal
AA	Arachidonic Acid
AAV	Adeno-associated Virus
Ab	Antibody
ABTS	2,2'-azino-bis - 3-ethylbenzothiazoline-6-sulphonic acid
ACA	Anterior Cerebral Artery
Ad	Adenovirus
ADA	Adenosine Deaminase
AIF	Apoptosis-Inducing factor
AMP	Ampicillin
AMPA	2-Amino-3-(5-methyl-3-oxo-1,2- oxazol-4-yl) Propanoic Acid
AngII	Angiotensin II
ANOVA	Analysis of Variance
ANT	Adenosine Nucleotide Translocator
AP-1	Activator Protein 1
APAF-1	Apoptosis-Activating Factor
APE / Ref-1	Human Apurinic Endonuclease / Redox-Factor 1
APS	Ammonium Persulphate
ASK	Apoptosis Signal-Regulating Kinase
ATF	Activating Transcription Factor
ATP	Adenosine Triphosphate
AUC	Area under Curve
BA	Basilar Artery
BBB	Blood-Brain Barrier
BCA	Bicinchoninic Acid
BDNF	Brain Derived Neurotrophic Factor
bFGF	Basic Fibroblast Growth Factor
BHT	Butylated Hydroxytoluene
BID	Bcl2 Interacting Proteins

BP	Blood Pressure
bp	Base Pairs
BSA	Bovine Serum Albumin
CAD	Caspase-Activated DNase
CAR	Coxsackie Virus and Adenovirus Receptor
CAV	Canine Adenovirus
CAV2	Canine Adenovirus Serotype 2
CCA	Common Carotid Artery
cDNA	Complementary DNA
CED	Convection Enhanced Delivery
CMV	Cytomegalovirus
CNS	Central Nervous System
CO_2	Carbon Dioxide
$CoCl_2$	Cobalt Chloride
COX	Cyclooxygenase
CPH	1-hydroxy-3-carboxy-2,2,5,5-tetramethylpyrrolidine
$cPLA_2$	Cytosolic Phospholipase A2
CPP	Cell Penetrating Peptide
CsCl	Caesium Chloride
CSF	Cerebral Spinal Fluid
ct	Cycle Threshold
CVD	Cardiovascular Disease
CyD	Cyclophilin D
Cygb	Cytoglobin
CytC	Cytochrome C
dATP	Deoxyadenosine Triphosphate
Daxx	Death-Associated Protein 6
DD	Death Domain
DED	Death Effector Domain
Dfx	Deferoxamine
dH_2O	Distilled Water
DISC	Death Inducing Signalling Complex
DMEM	Dulbecco's Minimal Essential Medium

DMSO	Dimethyl Sulphoxide
DNA	Deoxyribonucleic Acid
dNTP	Deoxyribonucleotide Triphosphate
DR	Death Receptor
DWI	Diffusion Weighted Imaging
ECA	External Carotid Artery
ECL	Electrochemiluminescence
EDTA	Ethylene Diamine Tetraacetic Acid
EGTA	Ethylene Glycol Tetraacetic Acid
ELISA	Enzyme-Linked Immunosorbent Assay
eNOS	Endothelial NOS
EPO	Erythropoietin
EPR	Electron Paramagnetic Resonance
ER	Endoplasmic Reticulum
ERK	Extracellular Signal-Regulated Kinase
EtOH	Ethanol
FADD	Fas Associated Protein with Death Domain
FasL	Fas Ligand
FasR	Fas Receptor
FCS	Foetal Calf Serum
Fe(II)	Ferrous
Fe(III)	Ferric
FITC	Fluorescein Isothiocyanate
G418	Geneticin
GABA	Gamma-Aminobutyric Acid
GADD34	Growth Arrest and DNA Damage-inducible 34
GAPDH	Glyceraldehyde 3-phosphate dehydrogenase
GDNF	Glial-Derived Neurotrophic Factor
GFP	Green Fluorescent Protein
GLT-1	Glutamate Transporter 1
GluR6	Glutamate Receptor 6
GPCR	G-Protein Coupled Receptor

GPx	Glutathione Peroxidase
GSH	Glutathione
GSSG	Glutathione Disulphide
H & E	Haematoxylin & Eosin
H^+	Hydrogen Ion
H_2O	Water
H_2O_2	Hydrogen Peroxide
hAd	Human Adenovirus
Hb	Haemoglobin
HB-EGF	Heparin-Binding EGF-like Growth Factor
Hd-CAV	Helper-Dependant Canine Adenovirus
HdAd	Helper-Dependant Adenovirus
HEPES	4-(2-Hydroxyethyl)-1-Piperazineethanesulfonic Acid
HIF-1	Hypoxia-Inducible Factor-1
HIV	Human Immunodeficiency Virus
HO-1	Heme Oxygenase
HRE	Hypoxia Response Element
HRP	Horseradish Peroxidase
HSP27	Heat Shock Protein 27
HSPG	Heparin Sulphate Proteoglycans
HSV	Herpes Simplex Virus
IAP	Inhibitors of Apoptosis
IC_{50}	Half Maximal Inhibitory Concentration
ICA	Internal Carotid Artery
ICAD	Inhibitor of Caspase-Activated DNase
ICAM-1	Intercellular Adhesion Molecule 1
ICC	Immunocytochemistry
ICH	Intracerebral Haemorrhage
IDLV	Integration-Deficient Lentiviral Vector
IGF-1	Insulin-like Growth Factor
IgG	Immunoglobulin G
IHC	Immunohistochemistry
iNOS	Inducible NOS

iu	Infectious Units
JBD	JNK Binding Domain
JIP	JNK Interacting Protein
JNK	c-Jun N-terminal Kinase
K_2HPO_4	Dipotassium Phosphate
kb	Kilobase
KCl	Potassium Chloride
kDa	Kilodaltons
KO	Knock Out
LB	Luria Base
LSD	Lysosomal Storage Disorder
LV	Lentivirus
MAPK	Mitogen-Activated Protein Kinase
MAPKK	Mitogen-Activated Protein Kinase Kinase
MAPKKK	Mitogen-Activated Protein Kinase Kinase Kinase
Mb	Myoglobin
MCA	Middle Cerebral Artery
MCAO	Middle Cerebral Artery Occlusion
MCS	Multiple Cloning Site
MDA	Malondialdehyde
MEK	Mitogen Activated Protein Kinase Kinase
MEM	Minimal Essential Medium
$MgCl_2$	Magnesium Chloride
mGluR	Metabotropic Glutamate Receptor
$MgSO_4$	Magnesium Sulphate
Mito-K_{ATP}	Mitochondrial AT-sensitive Potassium Channel
MK	Midkine
MMP	Mitochondrial Membrane Potential
MNNG	Methylnitronitrosoguanidine
MOI	Multiplicity of Infection
MPS IIIA	Mucopolysaccharide IIIA
MRI	Magnetic Resonance Imaging

mRNA	Messenger RNA
mRS	Modified Rankin Scale
mTOR	Mammalian Target of Rapamycin
MTP	Mitochondrial Permeability Transition Pore
MTT	3-(4,5-Dimethylthiazol-2-yl)-2,5-Diphenyltetrazolium Bromide
MW	Molecular Weight
NaCl	Sodium Chloride
NADH	Nicotinamide Adenine Dinucleotide
NADPH	Nicotinamide Adenine Dinucleotide Phosphate
$NaHCO_3$	Sodium Bicarbonate
NaOAc	Sodium Acetate
$NF\text{-}_{\kappa}B$	Nuclear Factor – Kappa B
Ngb	Neuroglobin
Ngb-Tg	Neuroglobin Transgenic Mouse
NMDAR	N-Methyl-D-aspartic Acid Receptor
nNOS	Neuronal NOS
NO	Nitric Oxide
$\cdot NO_2$	Nitric Dioxide Radical
NOS	Nitric Oxide Synthase
O_2	Oxygen
$O_2\cdot^-$	Superoxide
OD	Optical Density
OGD	Oxygen-Glucose Deficiency
OMM	Outer Mitochondrial Membrane
$ONOO^-$	Peroxynitrite
$PaCO_2$	Arterial Carbon Dioxide Tension
PARP-1	Poly [ADP-ribose] polymerase 1
PBN	α-Phenyl-*tert*-butyl-nitrone
PBS	Phosphate Buffer Saline
PCA	Posterior Cerebral Artery
PCD	Programmed Cell Death
PCR	Polymerase Chain Reaction

PDB	Protein DataBase
PFA	Paraformaldehyde
pfu	Plaque Forming Units
PI3K	Phosphoinositide 3-kinase
PILs	PEGylated Immunoliposomes
PKC	Protein Kinase C
PLA$_2$	Phospholipase A2
pMCAO	Permanent Middle Cerebral Artery Occlusion
PMSF	Phenylmethanesulfonylfluoride
PNS	Peripheral Nervous System
PPA	Pterygopalatine
PTP	Permeability Transition Pore
PWI	Perfusion Weighted Imaging
qRT-PCR	Quantitative Real-Time PCR
RBC	Red Blood Cell
RFP	Red Fluorescent Protein
RIPA	Radioimmunoprecipitation Assay Buffer
RNA	Ribonucleic Acid
ROS	Reaction Oxygen Species
rpm	Revolutions Per Minute
RQ	Relative Quantification
RT	Reverse Transcription
rt-PA	Recombinant Tissue Plasminogen Activator
RyR	Ryanodine Receptor
SAH	Subarachnoid Haemorrhage
SAP	Shrimp Alkaline Phosphatase
SCID	Severe Combined Immunodeficiency
SDS-PAGE	Sodium Dodecyl Sulfate Polyacrylamide Gel Electrophoresis
SEM	Standard Error Mean
SERCA	Sarco/Endoplasmic Reticulum Ca^{2+}-ATPase
SGSH	N-sulphoglucosamine Sulphohydrolase
SHR	Spontaneously Hypertensive Rat

shRNA	Short Hairpin RNA
SHRSP	Stroke-Prone Spontaneously Hypertensive Rat
SNAP	S-nitroso-N-acetyl-dl-Penicillamine
SO	Superoxide
SOC	Super Optimal Broth
SOD	Superoxide Dismutase
STAIR	Stroke Therapy Academic and Industry Roundtable
TAK	Transforming Growth Factor B-activated Kinase
TBE	Tris/Borate/EDTA
tBID	Truncated BID
TBS	Tris-Buffered Saline
TBS-T	Tris-Buffered Saline with Tween
TEMED	Tetramethylethylenediamine
TIA	Transient Ischaemic Attack
TIMP	Tissue Inhibitor of Metalloproteinases
TK	Thymidine Kinase
TLR	Toll-like Receptor
Tm	Melting Temperature
tMCAO	Transient Middle Cerebral Artery Occlusion
TNF	Tumour Necrosis Factor
TRADD	Tumour Necrosis Factor Receptor Associated Death Domain
TRAF2	Tumour Necrosis Associated Factor
TRITC	Rhodamine Dye
Trx	Thioredoxin
TTC	2, 3, 5-Triphenyltetrazolium Chloride
TU	Tranfecting Units
TUNEL	Terminal Deoxynucleotidyl Transferase dUTP Nick-end Labelling
UTP	Uridine-5'-triphosphate
UV	Ultra Violet
VDAC	Voltage Dependant Anion Channel
VEGF	Vascular Endothelial Growth Factor
VHL	Von Hippel–Lindau

vp	Virus Particles
VSVG	Vesicular Stomatitis Virus
WHO	World Health Organisation
WKY	Wistar Kyoto Rat
WT	Wild-Type

Summary

Stroke is the 3rd leading cause of death worldwide, second to heart disease and cancer, and is the leading cause of acquired adult long-term disability. Despite substantial advancement in the understanding of the pathogenesis of ischaemic stroke, development of treatments for stroke patients has been largely unsuccessful. As a result, administration of the thrombolytic, recombinant tissue plasminogen activator (rt-PA), in the acute stages following onset of ischaemia, remains the only clinically approved therapy. However, the 4.5 h "door-to-needle" time window observed with ischaemic stroke in addition to rt-PA's potential haemorrhage risk, results in only 2 – 5 % of all stroke patients receiving this therapy. Stroke is therefore a disease with largely unmet clinical needs.

Following its discovery in 2000, neuroglobin (Ngb) has been reported to mediate neuroprotection via a number of different pathways in both *in vitro* models of hypoxia ± reoxygenation and pre-clinical *in vivo* models of stroke, when upregulated from endogenous levels. c-Jun N-terminal Kinase (JNK) is a well-documented downstream mediator of apoptosis. Inhibition of JNK, by a number of different strategies, has been reported to be neuroprotective following hypoxia ± reoxygenation *in vitro* and ischaemia ± reperfusion *in vivo*. Although a regularly utilised strategy in the treatment of other cardiovascular diseases (CVD) and cancers, combination therapy is not currently employed in the treatment of stroke. Therefore it was the aim of this PhD to assess the effect of gene delivery-mediated upregulation of Ngb in combination with pharmacological pan-inhibition of JNK, using SP600125. The benefit of these therapies would first be assessed in an *in vitro* model of hypoxia / reoxygenation to provide the proof-of-concept required to perform a comprehensive *in vivo* study. *In vivo* analysis would include randomised and blinded assessment of neurological deficit longitudinally across a recovery period of 14 days and final lesion size in a rat strain exhibiting a number of the co-morbidities of CVD, the stroke-prone spontaneously hypertensive rat (SHRSP).

It was first necessary to determine the optimal viral vector for use in both the *in vitro* and *in vivo* intervention studies. Canine adenovirus serotype 2 (CAV2) had been reported to travel with great efficiency from the injection site following stereotactic injection into the striatum, with substantial reporter-gene expression observed in afferent structures such as the cortex. As the cortex is widely accepted as the location of the penumbra following

ischaemia / reperfusion in the present middle cerebral artery occlusion (MCAO) model, the level of cortical expression was of significant importance and as such compared following both striatal and cortical injection of CAV2-GFP 7 days post-injection in male SHRSPs. Significantly greater cortical transduction was observed following direct injection into the cortex with 3×10^9 vp CAV2-GFP in comparison to striatal injection. To ensure CAV2 was the best possible viral vector for use in this study, an additional comparative analysis with a GFP-expressing lentivirus was assessed. 4×10^7 vp lenti-GFP was administered stereotactically into the cortex over two injection sites, spanning the perceived region of penumbral tissue - owing to its previously reported inefficient transduction from injection site. Analysis at 7 days post-injection demonstrated a significantly reduced level of transduction in comparison to CAV2-GFP. Therefore a Ngb-expression CAV2 was generated. *In vitro* analysis of CAV2 demonstrated an inability to transduce the B50 rat neuronal cell line being utilised for the *in vitro* model. Therefore, a Ngb-expressing lentivirus was generated to mediate Ngb overexpression in the *in vitro* model with CAV2-Ngb utilised *in vivo*.

The effect of pre-treatment with MOI 5 vp / cell lenti-Ngb in combination with 20 μM SP600125 was examined in an *in vitro* model of 9 h hypoxia and serum deprivation with 24 h reoxygenation in complete medium using B50 rat neuronal cells. The results showed that pre-treatment with lenti-Ngb in combination with SP600125 lowered levels of oxidative stress and apoptosis to that equivalent of normoxic control cells, assessed all across four assays of cell viability. The four assays included two oxidative stress assays [Electron paramagnetic resonance (EPR) to assess superoxide (SO) production and a bioluminescent malondialdehyde (MDA) assay as a marker of lipid peroxidation], and two apoptosis assays (a cell death ELISA and caspase-3 immunocytochemistry). Interestingly, although it had initially been perceived to act as an anti-oxidant, Ngb upregulation was shown to significantly mediate neuroprotection through both anti-oxidant and anti-apoptotic parameters. Additionally, SP600125 pre-treatment alone was shown to have no effect on SO levels but potentiated Ngb's action when administered in combination, assessed by EPR. Furthermore, the anti-apoptotic agent, SP600125, completely abolished levels of lipid peroxidation, used as a marker of oxidative stress, when administered alone.

A pilot *in vivo* study of 45 min transient middle cerebral artery occlusion (tMCAO), using the intraluminal thread model, with 14 days recovery was performed in 12 SHRSP in order to assess the reproducibility of infarct in addition to assessing the sensitivity of the desired

neurological tests. Results demonstrated a substantial variation in infarct size between animals, with 4 out of 12 animals being excluded from the study as they did not exhibit an infarct. Average results from neurological tests in remaining animals were not significantly different from baseline at day 14. Additionally, one neurological test (the cylinder test) was discontinued mid-study as animals at baseline and post-tMCAO failed to rear onto hind legs at any point making analysis impossible. This pilot *in vivo* study allowed for procedural surgical issues to be 'flagged' and for refinement of technique prior to initiation of the intervention study. In addition, the pilot study allowed for experience to be gained in outcome assessments including neurological scoring and *ex vivo* infarct analysis, to ensure minimal user variation following initiation of the intervention study.

Further methodological refinement for the tMCAO model was implemented as a result of high mortality rates observed within control animals following initiation of the *in vivo* intervention study. It was observed that following stereotactic administration of control virus (CAV2-GFP), although there was no significant difference in neurological score between CAV2-GFP and control animals, mortality was significantly reduced in CAV2-GFP treated animals. Subsequent analysis determined no significant difference in lesion size between control animals and CAV2-GFP treated animal. This led to the hypothesis that the administration of a small (1 mm diameter) craniectomy (although immediately sealed with dental cement following injection) and subsequent piercing of the dura attributed to the stereotactic procedure perhaps allowed for a reduction in intracranial pressure in the acute stages following tMCAO improving survival. Additionally, it has been reported that pre-conditioning animals to isoflurane may mediate neuroprotection, as is observed in the present study to carry out a pre-tMCAO surgical procedure. However, although it is likely this would have been reflected in final lesion size, the present study may be weighted to only observe animals exhibiting a lesion within a certain threshold.

Finally, an *in vivo* intervention study was performed to determine the effect of pre-treatment with 3×10^9 vp CAV2-Ngb in combination with 1 mg / kg SP600125 in a model of tMCAO in male SHRSP with 14 days recovery. CAV2-Ngb or CAV2-GFP was administered into the cortex in a total of 2 μl 5 days prior to tMCAO, and SP600125 was administered *i.v.* 15 min pre- and 3 h post-tMCAO onset. Results of the intervention study showed that combined treatment of CAV2-Ngb and SP600125 reduced final infarct greater than either therapy alone, by 58 % in comparison to untreated controls. Treatment with SP600125 alone reduced infarct by 36 % and CAV2-Ngb treatment resulted in a reduction

of 38 %. This was reflected in neurological outcome where combined treatment mediated an improvement in neurological recovery assessed by 32-point neurological (where a healthy animal scores 32) from 18 in control animals to 26 in those receiving the combined intervention at day 14. Treatment with either SP600125 or CAV2-Ngb alone improved 32-point neurological score to 20 at day 14. Additionally, percentage footfalls were significantly improved from 45 % of all steps taken in control animals to ~ 28 % in animals administered with either single or combined treatment at day 14, no further improvement was noted with combined treatment assessed by this outcome.

This study represents the first anti-oxidant and anti-apoptotic combination study of cerebral ischaemia and additionally the first time a CAV2 vector has been utilised in a model of experimental stroke. In conclusion, research presented in this thesis demonstrates the combined neuroprotective action of Ngb upregulation in combination with JNK inhibition in an *in vitro* model of hypoxia / reoxygenation improves neuronal cell viability greater than either therapy alone. Subsequently, a robust pre-clinical *in vivo* model of tMCAO utilising the SHRSP, demonstrated a substantial reduction in lesion size and improvement neurological score, mediated by combined therapy greater than singular treatment.

Chapter 1:

Introduction

1.1 STROKE EPIDEMIOLOGY

Stroke is the 3rd leading cause of death worldwide, accountable for 8.6 % of all deaths in males and 11.0 % of deaths in females (WHO Global Infobase, 2004). A map of age standardised comparisons of stroke incidence in the UK is shown below for males and females (Figure 1.1 A & B), with the south-west of Scotland having some of the highest mortality rates from stroke in the UK.
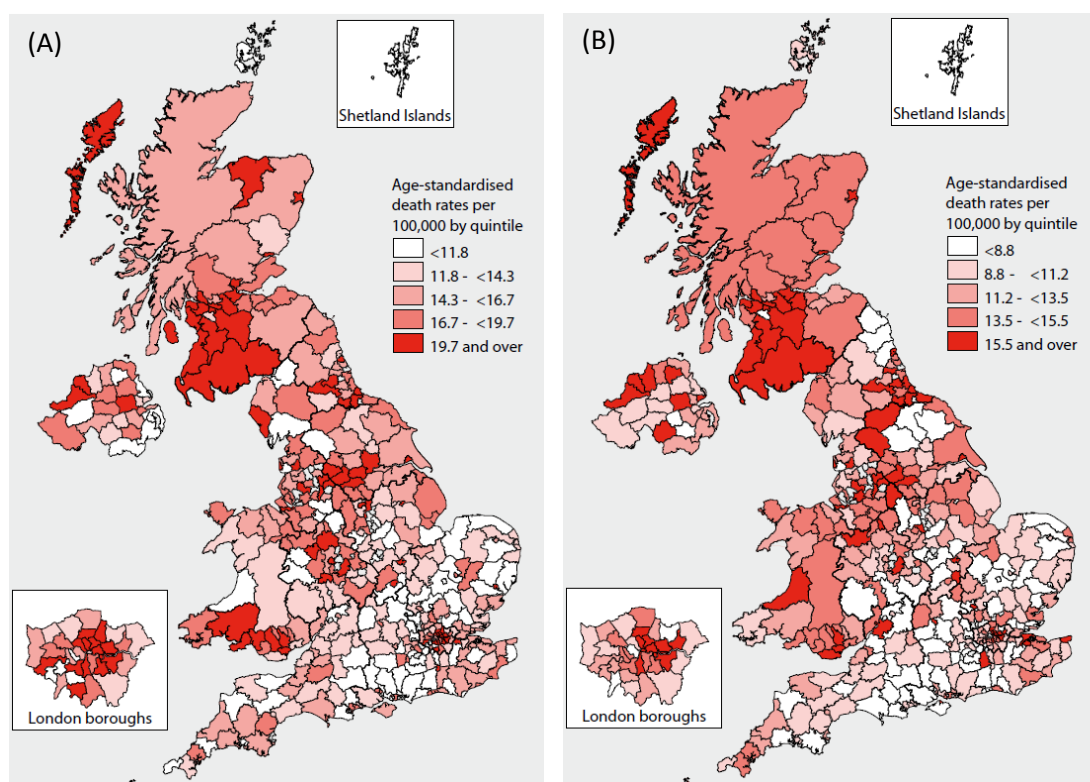
Figure 1.1:   Age Standardised Death Rates in the UK

Age standardised death rates from 100,000 population from stroke for men (A) and women (B) under 75 by local authority in the UK 2005/2007 (taken from, (Scarborough *et al.*, 2009))

In the UK, the occurrence of age specific stroke incidence fell by 29 % between 1999 and 2008, attributable to an improvement in primary care management of cardiovascular risk and the 56-day mortality after first stroke in the UK fell by 43 % between 1999 and 2008 (www.theheart.org). However, stroke patients currently occupy around 20 % of all acute hospital beds and 25 % of long-term beds and stroke is still the leading cause of adult acquired disability and as such presents a substantial financial burden when considering secondary care. In the UK alone, stroke care totalled an annual cost of > £ 2.6 billion to

the NHS in 2008. Although an age specific decline in stroke occurrence has been observed due to improvements in cardiovascular disease (CVD) management, overall stroke occurrence is set to dramatically increase over the next 50 years as a result of an ageing population. Additionally, with stroke incidence increasing by over 100 % in developing countries (Itrat *et al.*, 2011) it is clear that more needs to be offered clinically for patients.

1.2 CLASSIFICATIONS OF STROKE

1.2.1 Haemorrhagic Stroke

Stroke can be divided into haemorrhagic and ischaemic stroke, of which haemorrhagic stroke accounts for 20 % of all cases (Broderick *et al.*, 2007). Although haemorrhagic stroke only represents 20 % of all stroke cases, incidence is on the rise due to increased prescription of anti-platelet and anti-coagulant therapies in response to CVD. Haemorrhagic stroke results from a rupture of a blood vessel causing a bleed within the skull which can be further divided into intracerebral and subarachnoid haemorrhage, depending on the location of the bleed. Intracerebral haemorrhage (ICH) occurs within the brain tissue, of either the parenchyma or ventricles of the brain: almost half of affected patients die without recovering and more than half of survivors remain permanently disabled (Shiber *et al.*, 2010). Subarachnoid haemorrhage (SAH) occurs on the surface of the brain within the subarachnoid space between the arachnoid membrane and the pia mater surrounding the brain. Although mortality rates are comparable to ICH, outcome is somewhat better in that only 1 / 3rd of survivors remain dependant.

1.2.2 Ischaemic Stroke

Ischaemic stroke results from a blockage to a cerebral artery and accounts for ~ 80 % of all stroke cases. The blockage can be atherothrombotic or embolic, and generally defined by 1 of 5 classifications; a large artery stenosis, tandem arterial pathology, cardiac embolism, lacunar infarction or undetermined cause. Classifications of ischaemic stroke provided are defined by the TOAST multicentre clinical trial (Adams *et al.*, 1993). Large artery stenosis refers to complete occlusion or significant stenosis of a major brain artery or branch cortical artery, resultant from atherosclerosis. Tandem arterial pathology (also known as artery-to-artery embolism) is identical to large artery stenosis; however the occlusion originated from an embolism from an atherosclerotic lesion situated proximally

to an otherwise healthy branch. The pathophysiology of cardioembolic stroke is identical to the previously described subtypes; however the embolus arises from the heart. Also known as small artery occlusion, the pathophysiology of a lacunar infarction is significantly different to those described previously. It arises from occlusion of one of the deeply penetrating arteries, branching from the circle of Willis, the cerebellar arteries or basilar arteries by either microatheroma or, tandem- or cardio-embolism.

1.3   THERAPEUTIC CHALLENGES OF STROKE

Stroke treatment is a very complex process for a number of reasons. The brain is a highly metabolic organ that relies on constant oxygen and glucose supply from the circulation. Although amounting to only 2-3 % of the total body weight the brain utilises 20 % of the total oxygen and 25 % of the total glucose of the body from 15 % of cardiac output (Herculano-Houzel, 2011). Storage of energy and metabolites within the brain is extremely low and as such the brain is very sensitive to interruptions in blood flow. Although the brain is protected from systemic toxins under normal physiological conditions by the blood-brain barrier (BBB), this is broken down during cerebral ischaemia allowing infiltration of inflammatory mediators and other potentially toxic molecules. There are numerous pathways involved in brain damage initiated by cerebral ischaemia, with extensive interactions between them and in main, existing as positive feedback loops. In addition, the majority of damage occurs within minutes and the acute hours following cerebral ischaemia and as such, stroke treatment at present remains mainly preventative.

1.3.1   Anatomy of Cerebral Ischaemia

The tissue of the brain affected by ischaemic stroke can be divided into two regions: the core and the penumbra. Within the core of the ischaemic territory cells are entirely dependent on the blocked artery for blood flow and as such, receive very little or no blood from the onset of occlusion. Therefore, the cells of the core quickly use up available ATP levels with almost immediate depletion, causing subsequent ionic disruption and metabolic failure, resulting in rapid cell death by excitotoxicity and necrosis (Baron *et al.*, 1999). Between the irreversibly damaged core and the normal non-ischaemic brain lies the penumbra (Astrup *et al.*, 1981) (Figure 1.2). The reduction in cerebral blood flow within penumbra is less severe than in the core and the tissue receives supplementary flow from collateral blood vessels. Cells therefore deteriorate more slowly within this region, as

collateral blood flow is sufficient to maintain cellular structure and some function in the short term. However, the penumbra is destined to become irreversibly damaged (infarct) over time, generally 6 - 24 h following permanent ischaemia (del Zoppo *et al.*, 2011). This is in contrast to the ischaemic core where cells may only be salvaged by rapid reperfusion, as is observed in transient ischaemic attacks (TIAs). However in somewhat of a paradox, reperfusion in the later stages following the onset of ischaemia causes cell death within the penumbra to be exacerbated, in a phenomenon known as reperfusion injury, discussed later (section 1.7.1.4 & 1.8.1).
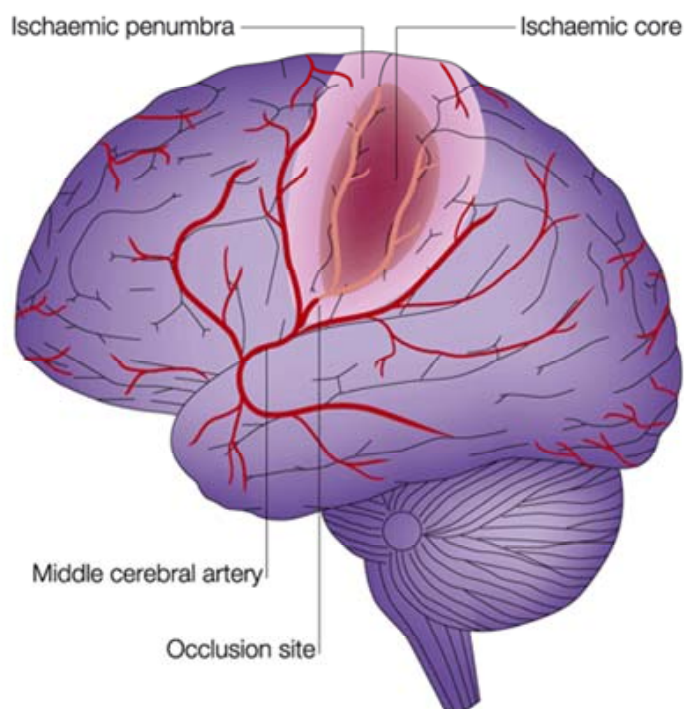
Figure 1.2:   Anatomy of Cerebral Ischaemia

Middle cerebral artery occlusion (MCAO) results in an ischaemic core of tissue surrounded by a penumbra, where cells may be salvaged within a given time (taken from Allan and Rothwell, 2001).

1.3.2   Prevention

As aforementioned, current therapies for stroke are predominantly preventative with the greatest risk factor for stroke being hypertension (O'Donnell *et al.*, 2010b). A recent study into modifiable risk factors for stroke across 22 countries and with a sample size of 3000

patients, demonstrated that the significant and modifiable risk factors for stroke (arranged in order of severity) are; history of hypertension; current smoking; waist-to-hip ratio; diet risk score; regular physical activity; diabetes, alcohol intake; and psychosocial stress (O'Donnell *et al.*, 2010a). However, a number of risk factors are non-modifiable such as, age, family history of CVD, male gender, African American race, increased fibrinogen and history of migraine (reviewed in (Sacco, 2001)). Improved outcome has been observed following control of life style risk factors common to all CVD such as: cessation of cigarette smoking (Wolf *et al.*, 1988); increased physical activity in men (Gillum *et al.*, 1996) and women (Hu *et al.*, 2000); and improvement in dietary intake of whole grains (Liu *et al.*, 2000), omega-3 (Iso *et al.*, 2001), and fruits and vegetables (Joshipura *et al.*, 1999). As hypertension demonstrates the most significant risk factor for stroke occurrence, it is not surprising that the most successful preventative treatment for stroke is blood pressure (BP) reduction. A number of classess of anti-hypertensive drugs exist with extent of stroke reduction observed varying between each class. BP reduction is generally mediated through prescription of angiotensin-converting enzyme inhibitors or angiotensin receptor blockers (A); beta receptor blockers (B); Ca^{2+} receptor blockers (C); or diuretics (D); in what is known as the ABCD algorithm (Brown *et al.*, 2003; Williams, 2003). The algorithm is based on two simple principles, firstly younger patients (< 55 years) generally respond better to intervention with A or B classed drugs, and older patients respond better to intervention with C or D classed drugs. Secondly, if BP is unresponsive following single administration combined intervention can be prescribed, with multiple low doses often resulting in more significant reduction in BP than a high dose with a single intervention. Pharmacological preventative interventions also include warfarin anti-coagulation treatment and anti-platelet agents such as aspirin, with preventative treatment mediated by anti-platelets showing a more successful reduction in stroke occurrence than anti-coagulants (Segal *et al.*, 2000). However, unwanted side effects have been associated with long-term aspirin administration, such as gastrointestinal (Trialists'Collaboration, 2002) and asthmatic (McGeehan *et al.*, 2002) complications. In addition to anti-coagulation and anti-platelet treatment, the cholesterol inhibitors, statins, (3-hydroxyl-methylglutaryl-coenzyme A reductase inhibitors) have been reported as safe (Ose *et al.*, 2000) and successful agents in stroke prevention (Cheung *et al.*, 2004; Sever *et al.*, 2003). Hyperlipidemia has not been suggested as a risk factor for stroke, yet a significant decrease in stroke has been observed in stroke patients receiving treatment for this vascular disease. Interestingly, the noted benefit of statins is independent of baseline cholesterol and patients with normal cholesterol levels exhibit the same reduction in stroke occurrence as patients

with elevated systemic cholesterol (HPSCG, 2002). In addition to inhibiting the generation of cholesterol statins may exhibit anti-inflammatory effects by upregulating endothelial nitric oxide synthase (eNOS), inhibiting inducible nitric oxide synthase (iNOS), and reducing levels of the inflammatory mediator, C-reactive protein (Albert *et al.*, 2001).

1.3.3   Thrombolytics

The majority of ischaemic strokes are caused by thromboembolic occlusions of cerebral arteries. Lysis of blood clots, allowing reperfusion of blood to the previously ischaemic area, forms the basis of thrombolytic therapy. Indeed the thrombolytic, recombinant tissue plasminogen activator, (rt-PA or Alteplase™), is the only approved treatment available to stroke patients following the onset of ischaemia. However as the risk of haemorrhage associated to all thrombolytics increases with time from stroke onset (Wang *et al.*, 2004), treatment is currently limited to the short therapeutic window of 4.5 h. This therapeutic window was recently increased from 3 h following a placebo-controlled study in clinical trial of 228 patients which showed a beneficial effect of rt-PA following administration between 3 and 4.5 h after initial ischaemic onset (Hacke *et al.*, 2008). rt-PA treatment is nearly twice as effective when administered within the first 90 min following the onset of cerebral ischaemia as it is when administered within 90 to 180 min following onset, and less so beyond this time (Hacke *et al.*, 2004). The therapeutic window remains a significant barrier to the potential administration of rt-PA, as stroke patients tend to present out with this time (Alberts *et al.*, 1993). Even within this time-scale there is occasional unease to administer rt-PA due an increased risk of haemorrhage in patients with advanced CVD and as a result, only 2 - 5 % of all stroke patients currently receive this clinical intervention (Deng *et al.*, 2006). Within the treated 2-5 %, effect size of thrombolysis is low. For 1 patient to have a favorable outcome following stroke (0 - 1 assessed by the modified Rankin scale), the number needed to treat with rt-PA is 14 within 4.5 h (Hacke *et al.*, 2008).

1.3.4   Stroke Unit Care and Outcome

Organised and high standard stroke unit (SU) care has been shown provide the greatest improvement in recovery following stroke. Indeed, SU care has been demonstrated as the only treatment option for acute stroke with proven reduction in death (SUTC's, 2002). SU care defined by the Stroke Unit Trialists' Collaboration includes the availability of a

consultant physician with responsibility for stroke, continuing education programs for staff, and links with external patient and carer organisations.

When performed in combination with early supported discharge (ESD) – in which less disabled patients can be discharged early to undergo further rehabilitation at home – SU care has also been demonstrated demonstrate a significantly cost effective management for stroke patients.

1.4   PREVIOUSLY ASSESSED NEUROPROTECTIVE STRATEGIES

The last three decades have seen dissection of the complex pathways of stroke and as a result, significant advancement in the field of neuroprotection. Neuroprotection can be defined as the administration of agents alone or in combination that interrupts the biomolecular cascades that eventuate in cell death following cerebral ischaemia. Although multiple pre-clinical studies have demonstrated the undoubtable proof-of-principle benefit of neuroprotection, clinical trials have not reflected this neuroprotection within the designated 4 - 6 h window deemed to be essential for feasible neuroprotection. Some of the main strategies and subsequent clinical trials are described below.

1.4.1 Ca^{2+} Channel Blockers

Ca^{2+} influx following cerebral ischaemia was shown to not only result in early cell death through oedema and necrosis but also programmed cell death in the penumbra through a variety of mechanisms. Therefore, as a result of the dissection of the role of Ca^{2+} influx in stroke and also the success of routine use of Ca^{2+} channel blockers in pathologies such as angina, hypertension and some arrhythmias, Ca^{2+} channel blockers were seen as a potential route for neuroprotection. Nimodipine is a 1,4-dihydropyridine-Ca^{2+} channel blocker that was believed to exert neuronal specific effects and also be preferential vasodilator of the cerebral vasculature, with a lesser effect observed on the peripheral vasculature (reviewed in (Tomassoni *et al.*, 2008)). Pre-clinical animal studies of the effect of nimodipine in stroke were widely accepted as successful and as such a total of 13 clinical trials were initiated for nimodipine, however 8 of these were early-phase non-definitive studies of < 200 patients. The first of the five larger trials (TRUST, 1990) assessed 1215 patients administered oral nimodipine or placebo within 48 h of stroke onset. The primary endpoint using the Barthel Index at 6 months was negative; however a significant

improvement at 3 weeks was reported (TRUST, 1990). In 1992, the American Nimodipine Study Group (ANSG) completed a study of 1064 patients (ANSG, 1992). Nimodipine or placebo was again administered orally within 48 h for a total of 21 days. Using the Toronto Scale and motor strength as primary outputs, no significant difference was observed between groups but a post-hoc sub-group analysis showed significant improvement when administered within 18 h of cerebral ischaemia. In 1994, a smaller trial using *i.v.* administration of nimodipine in 295 patients at 24 h following stroke onset for 5 days showed a detrimental effect of nimodipine at both the higher and lower dose (Wahlgren *et al.*, 1994). In 1995, a meta-analysis of all clinical trials with nimodipine was performed and showed no overall significance of nimodipine treatment unless administered within 12 h (Warner, 1995). However, a subsequent meta-analysis failed to confirm these positive results (Horn *et al.*, 2000). Post analysis of pre-clinical data showed that of the 250 documented animal studies, only 20 administered nimodipine following the onset on stroke and of those only 10 reported positive results. Of these 10 positive studies, several were administering nimodipine within $\leq$ 15 min of the onset of cerebral ischaemia. Studies administering nimodipine $\geq$ 1 h following onset of ischaemia demonstrated non-significant results overall. One of the reasons for these failed studies could be the lack of neuronal specificity of action. The action of Ca^{2+}-channel blockers within the vasculature results in significant vasodilatation and subsequent hypotension, which is highly detrimental in the acute stages following cerebral ischaemia.

1.4.2 Glutamate Antagonists

It is well established that excess glutamate release mediates a number of detrimental pathways following cerebral ischaemia, through activation of a number of glutamate receptors, primarily the NMDAR and AMPAR. However, the NMDAR has been demonstrated to have a more complex role in apoptosis than initially believed. Extensive pre-clinical studies using a variety of NMDAR antagonists such as the non-competitive antagonist, MK-801 (reviewed in (Ginsberg, 1995)); the competitive antagonist, CGS 19775 or selfotel (Simon *et al.*, 1990); and the active(glycine)-site antagonist, gavestinal (Bordi *et al.*, 1997); have demonstrated improvement in stroke outcome. However, clinical trials with these agents have not mirrored the pre-clinical success. In the case of MK-801, clinical trials were halted in the pilot phase as a result of adverse and severe side effects following administration (Albers *et al.*, 1995). Selfotel trials were halted immediately following a small phase I safety and tolerability study, as all patients treated with 2 mg / kg

showed adverse effects (Grotta *et al.*, 1995). Gavestinel demonstrated a superior clinical tolerance profile (Dyker *et al.*, 1999), and two large randomised, double-blind phase III clinical trials were initiated, of 1646 subjects (Sacco *et al.*, 2001) and 1804 subjects (Lees *et al.*, 2000). Although no adverse side effects were observed, primary outcome at 3 months was neutral in both trials. In a variety of pre-clinical animal models of stroke, AMPAR antagonists demonstrated neuroprotective actions in both global and focal ischaemia (Gill, 1994; Li *et al.*, 1993; Xue *et al.*, 1994). However, in a phase II double-blind multicentre clinical trial of the AMPAR antagonist, ZK200755, transient worsening of the NIHSS score attributable to depressed consciousness (coma) was reported (Elting *et al.*, 2002).

1.4.3   Magnesium (Mg)

Mg could be described as an endogenous antagonist of Ca^{2+} that initiates protection through multiple mechanisms such as NMDAR blockade, inhibition of neurotransmitter release, blockade of Ca^{2+} channels, and vascular smooth muscle relaxation (Muir, 2001). Considering the well-established benefit of magnesium sulphate ($MgSO_4$) treatment in pre-eclampsia (Witlin *et al.*, 1998), Mg was considered as a potential neuroprotective agent for the treatment of stroke. Pre-clinical stroke studies using Mg have been limited, but have shown an overall improvement in infarct reduction with treatment of $MgSO_4$ (Izumi *et al.*, 1991; Marinov *et al.*, 1996; Westermaier *et al.*, 2005; Yang *et al.*, 2000). A large multicentre trial of 2589 patients with acute stroke was initiated, in which patients were either administered *i.v.* $MgSO_4$ or placebo within a 12 h of stroke onset. Both primary and secondary outcomes at day 90 were negative, with mortality in the Mg treated group being slightly higher. A recent review of pre-clinical data suggested the neuroprotective action observed at the pre-clinical level was possibly as a result of a confounding influence of Mg-induced hypothermia (Meloni *et al.*, 2006). However, a phase III clinical trial (FAST-MAG) is still ongoing in California where ischaemic stroke patients are administered 4 g $MgSO_4$ *i.v.* within the ambulance and a further 16 g over the course of the subsequent 24 h in hospital, results are yet to be reported.

1.4.4   Antioxidants

1.4.4.1   Spin Traps

Spin-trapping is a technique that allows scavenging of free radicals. It involves the addition of a free radical, to a nitrone spin trap resulting in the formation of a spin adduct, without the formation of further free radicals and as such can terminate radical chain reactions. A number of pre-clinical studies confirmed the neuroprotective action of the spin trap, NXY-059, in infarct reduction and neurological recovery across a variety of stroke models in both rodents (Kuroda *et al.*, 1999; Sydserff *et al.*, 2002; Zhao *et al.*, 2001) and non-human primates (Marshall *et al.*, 2003; Marshall *et al.*, 2001). Following these extensive and successful pre-clinical studies, NXY-059 was studied in two large randomised and double-blinded trials. The initial trial (SAINT I) involved 1722 patients (Lees *et al.*, 2006), and the following year SAINT II enrolled 3306 subjects (Shuaib *et al.*, 2007). In both trials, patients were assigned to receive either a 72 h infusion of NXY-059 or placebo, starting within 6 h of the onset of cerebral ischaemia. SAINT I showed a significant improvement in NXY-059 treated patients assessed by the modified Rankin score, but not by the NIHSS scale or Barthel index. However, the subsequent SAINT II trial published entirely negative results in primary and secondary endpoints. The difference in the outcomes of these trials have been attributed to statistical weakness of the SAINT I trial (Koziol *et al.*, 2006; Saver, 2007) and the poor BBB permeability of NXY-059 (Fisher *et al.*, 2006).

1.4.4.2   Other Antioxidants

Two examples of additional antioxidants which have undergone clinical trials with over 200 patients are tirilazad and ebselen. Tirilazad mesylate (U-74006F) is an inhibitor of lipid peroxidation that was studied extensively in pre-clinical models in the mid-1990s (Park *et al.*, 1994; Xue *et al.*, 1992). A meta-analysis of the previously published data was released in 2007 (Sena *et al.*, 2007), where an overall improvement in both lesion size and neurological recovery was reported. Across 19 publications, tirilazad was demonstrated to reduce lesion size by an average of 29 % and improve neurological score by 48 % (Sena *et al.*, 2007). Maximum efficiency of tirilazad treatment was observed when administered prior to focal ischaemia, with a decreasing efficiency in action with administration time from ischaemic onset thereafter. The largest clinical trial of tirilazad comprised 660 patients, in which tirilazad was administered within 6 h of the onset of cerebral ischaemia (RANTTAS, 1996). Primary outcome of disability measured by the Glasgow Outcome

Scale and Barthel index at 3 months showed no change between groups at an independent interim analysis of 556 patients, and the trial was subsequently terminated. It was later determined that women metabolise tirilazad up to 60 % more efficiently than men, and therefore had perhaps not been administered a high enough dose to mediate neuroprotection, reducing the efficacy across the whole trial (Fleishaker *et al.*, 1995). Ebselen is an inhibitor of glutathione peroxidase-like activity, and also reacts with and subsequently scavenges ONOO⁻. In pre-clinical rodent models of focal ischaemia pre-treatment (Namura *et al.*, 2001) with ebselen or administration at point of reperfusion (Imai *et al.*, 2001) in transient occlusion models improved ischaemic damage and neurological deficit, respectively. Post-treatment at 30 min following onset of ischaemia in a rodent model of permanent occlusion resulted in modest protection (Takasago *et al.*, 1997). However, a randomised and blinded trial of 302 ischaemic stroke patients who were administered ebselen at 48 h post ischaemia for 2 weeks failed to replicate the protective effects seen in the pre-clinical models at 3 months, although improvements in the ebselen treated groups were observed prior to this at 1 month (Yamaguchi *et al.*, 1998).

1.4.5 Leukocyte Inhibition

Inhibition of intercellular adhesion molecule-1 (ICAM-1) expression on endothelial cells following cerebral ischaemia through administration of enlimomab, an ICAM-1 antibody, was thought to have potential in reducing inflammation following stroke. In transient MCAO but not in permanent MCAO a reduction in lesion size was observed following administration at 1 h following stroke onset (Huang *et al.*, 2000). However, clinical trials of 625 patients randomised to enlimomab or placebo, administered within the 6 h following stroke onset, resulted in a highly significant worsening of outcome assessed by the modified Rankin scale at 90 d (Sherman *et al.*, 2001). To address and elucidate these results, a pre-clinical focal ischaemia model in rats was carried out using anti-rat ICAM-1 (Vemuganti *et al.*, 2004). Results showed not only a failure to reduce lesion size but also an upregulation of host antibody production and circulating neutrophil and complement levels, suggesting a potential reason for the negative effects observed in the clinical trial.

1.4.6 Therapeutic Hypothermia

Therapeutic hypothermia refers to controlled reduction of core temperature to below 36 °C; with 34 - 35.9 °C delineating mild, 32 – 33.9 °C moderate, and 30 – 31.9 °C moderate /

deep and < 30 °C deep hypothermia. Hypothermia reduces the oxygen consumption of the brain by a rate of ~ 6 % per 1 °C temperature change, allowing preservation of potentially viable brain tissue for longer periods of time (Welsh *et al.*, 1990). A meta-analysis of pre-clinical models of therapeutic hyperthermia showed hypothermia improves neurological outcome by ~ 33 % under clinically-feasible conditions. Cooling is also effective in animal strains exhibiting co-morbidities of CVD and up to 3 h following the onset of stroke, warranting the initiation of clinical trials (van der Worp *et al.*, 2007). Although a number of small trials were carried out, enrolment numbers were never greater than 50 and results were varying (Els *et al.*, 2006; Georgiadis *et al.*, 2001; Kammersgaard *et al.*, 2000; Schwab *et al.*, 1998). However, a single centre phase II clinical trial is currently underway is Edinburgh assessing the benefit of hypothermia in the acute stages following ischaemic stroke, although no results have been published as of yet.

1.5 CEREBRAL ISCHAEMIA / REPERFUSION: PATHOPHYSIOLOGY OF NECROSIS AND APOPTOSIS

1.5.1 Necrosis

Necrosis represents one of the two types of ischaemia-induced cell death and is the main mechanism of cell death that occurs within the ischaemic core. Necrosis is a passive degeneration of cells, it is irreversible and is characterised by membrane dysfunction, cell swelling and normally results in a subsequent inflammatory response. Although necrosis has long been described to be uncontrolled, research suggests it could in fact be a tightly regulated process (reviewed in (Golstein *et al.*, 2007)), which has been specifically assessed in neurons (Yamashima *et al.*, 2003).

1.5.2 Energy & Excitotoxicity

1.5.2.1 Normal Respiration

Neurons work at an extremely high metabolic rate under normal circumstances. The brain counts for 2 % of the total body but requires 20 % O_2 and 25 % of the entire body's glucose consumption, although it performs no mechanical work or external secretory activity (Herculano-Houzel, 2011). Energy is required for maintenance of membrane potentials, ionic transport, maintenance of cell structure, and biosynthesis and transport of neurotransmitters and cellular elements. ATP, used to power this work, is generated by

degrading high-energy exogenous compounds such as glucose into low-energy compounds such as CO_2 and H_2O. Due to this high metabolic rate during normal respiration neurons are avid generators of free radicals, dealt with by the numerous endogenous antioxidants within the brain. Neurons require a constant supply of O_2 and glucose as they lack storage of energy substrates (Pauwels *et al.*, 1985), therefore disruption of blood flow and subsequent energy generation results in rapid brain disruption. For example, during cardiac arrest and subsequent global ischaemia consciousness is lost within ten seconds (Rincon *et al.*, 2006).

Oxidation of pyruvate (from glycolysis of glucose) in the mitochondria leads to the formation of a proton gradient across the inner mitochondrial membrane that is utilised by ATP synthase to generate ATP. This proton gradient is also necessary for Ca^{2+} uptake by the mitochondria, to maintain low intracellular Ca^{2+} levels. The generated ATP is then used to maintain the ionic Na^+ / K^+ ATPase, the Ca^{2+} ATPase and the proton ATPase in the synaptic vessel membrane. The ion gradients formed by these channels are used by membrane transporters to translocate transmitters, ions and cellular components to regulate cellular function and are essential for normal respiration and function to occur.

1.5.2.2 *Energy Failure & Excitoxicity*

Severe energy failure, through cerebral ischaemia, initially leads to a phenomenon known as excitotoxicity, causing oedema and subsequent necrosis. This is extremely rapid process and occurs within minutes of the initial onset of ischaemia. During complete ischaemia, glycolysis is up-regulated by seven- to eight-fold; so within 30 seconds, glucose and glucagon stores are almost totally consumed, and within 1 min ATP, phosphocreatine, glucose and glucagon are entirely depleted (Gatfield *et al.*, 1966). Rapid consumption of available ATP is followed by rapid membrane depolarisation, releasing K^+ into the extracellular space and allowing sodium and Ca^{2+} to enter the cell. A 10,000-fold gradient across the plasma membrane is present under normal circumstances as $[Ca^{2+}]_i$ must be highly regulated. This is achieved by use of cellular Ca^{2+} uptake by the mitochondria and endoplasmic reticulum (ER), and plasma membrane Ca^{2+} exchangers and pumps. During ischaemia, Ca^{2+} accumulates in the cytosol due to failure of Ca^{2+} ATPases on the ER, reversal of the Na^+ / Ca^{2+} exchanger on the mitochondrial and plasma membrane as a result of increased $[Na^+]_i$ and loss of Na^+ gradient from failure of the Na^+ / K^+ ATPase. Ca^{2+} is further released from the high-capacity mitochondrial stores by loss of the ATP-mediated proton gradient through the Ca^{2+} uniporter. Ischaemia-induced increase in $[Ca^{2+}]_i$ has a

number of deleterious effects, one of which is the initiation of glutamate-mediated excitotoxicity (Budd *et al.*, 1996).

Synaptic glutamate concentration is approximately 10 mM, while its concentration within the synaptic vesicles is estimated at 100 mM. Glutamate release from neurons is propagated in the depolarised cell initially by direct action of Ca^{2+} on vesicles causing release of glutamate into the cytosol and subsequent release of the cytosolic glutamate into the extracellular space as a result of the loss of the plasma membrane's Na^+ gradient. This leads to increased synaptic levels of glutamate during ischaemia (Benveniste *et al.*, 1984; Rossi *et al.*, 2000). Following release into the synapse, the excess glutamate activates its family of receptors on the postsynaptic membrane; NMDAR, AMPAR, kainate receptors and the G-protein coupled metabotropic receptors (mGluRs). Glutamate activation of NMDAR's causes direct influx of Ca^{2+} and Na^+ causing further depolarisation. As a consequence of the influx of Ca^{2+} and Na^+, voltage operated K^+ channels open and K^+ floods down its concentration gradient, increasing extracellular $[K^+]$.

When sufficient $[K^+]_{ext}$ builds up a phenomenon known as spreading depression occurs. Spreading depression is a wave of sustained depolarisation, with subsequent Ca^{2+} and Na^+ cellular influx and K^+ efflux throughout the ischaemic region and beyond, as a result of ATP depletion (Takano *et al.*, 1996). Further depolarisation of previously compromised cells concludes in necrosis; H_2O enters the cell passively, driven by Ca^{2+} and Na^+ influx, and oedema follows, rupturing the cell.

1.5.3   Programmed Cell Death (PCD)

Traditionally cell death following cerebral ischaemia was believed to be entirely necrotic, however work throughout the last two decades has shown a number of cells in the ischaemic penumbra undergo PCD (or apoptosis) in the hours or days following stroke onset (reviewed in (Sims *et al.*, 2010)). In contrast to necrosis, apoptosis is reversible and as such the cells of the penumbra provide the focus of all acute stroke therapies. Apoptosis involves an active commitment of the cell to degrade its own DNA according to an internal program of destruction. It is an essential function during development and requires energy. Cells undergoing apoptosis are dismantled in an organised fashion that minimises damage and disruption to neighbouring cells, with minimal immune response. There are two general pathways for the activation of apoptosis, the intrinsic and extrinsic pathways. The

intrinsic pathway refers to initiation of a pro-apoptotic cascade in response to intracellular stimuli, and the extrinsic pathway refers to initiation of apoptosis in response to an extracellular stimulus.

1.5.3.1   Intrinsic Apoptosis

In addition to Ca^{2+} influx resulting in oedema subsequent necrosis within the region of the infarct, partial depolarisation, observed in the peri-infarct zone does not cause immediate necrosis but triggers a number of the intrinsic stimuli of apoptosis. Activation of NMDARs by glutamate increases NO and subsequent peroxynitrite ($ONOO^-$) production in the ATP depleted the post-synaptic cell. Neuronal nitric oxide synthase (nNOS) is physically anchored to NMDARs and following activation and influx of Ca^{2+}, Ca^{2+} binds calmodulin and rapidly activates nNOS generating nitric oxide (NO). NO reacts with superoxide anions ($\bullet O_2^-$), produced by anaerobic metabolism of the energy-depleted mitochondria, forming peroxynitrite ($ONOO^-$). Peroxynitrite mediates apoptosis through classic oxidative stress pathways described below (section 1.7).

Intrinsic ischaemia induced Ca^{2+} release from the ER by disruption of the ATP dependent sarco(endo)plasmic reticulum Ca^{2+}-ATPase (SERCA) pump and activation of Ca^{2+}-induced-Ca^{2+}-release by the ryanodine receptor (RyR), may lead to further intracellular Ca^{2+} release from the adjacent mitochondrial stores. Increased $[Ca^{2+}]_i$ from the ER is within close proximity to the mitochondria and causes Ca^{2+} "hotspots" at the mouth of the release channels of the mitochondria (Figure 1.3). This localised increase in $[Ca^{2+}]_i$ causes rapid uptake by the mitochondria, resulting in mitochondrial permeabilisation through a stress response known as the inner-membrane permeability transition. The voltage-operated pore becomes activated by high concentration of Ca^{2+} within the mitochondrial matrix, initially resulting in rapid and stochastic opening. This develops rapidly into persistent pore opening, allowing entry of solutes and water into the mitochondria, causing osmotic swelling of the mitochondria and potential rupture, and releasing pro-apoptotic mediators into the cytosol of the cell (Figure 1.4). Opening of the mitochondrial permeability transition pore (MTP) results in release of a number of pro-apoptotic agents from the mitochondria such as cytochrome *c* (Liu *et al.*, 1996b; Yang *et al.*, 1997b), Smac / DIABLO (Adrain *et al.*, 2001; Du *et al.*, 2000) and HtrA2 / Omi (Hegde *et al.*, 2002; Suzuki *et al.*, 2001; Verhagen *et al.*, 2002).
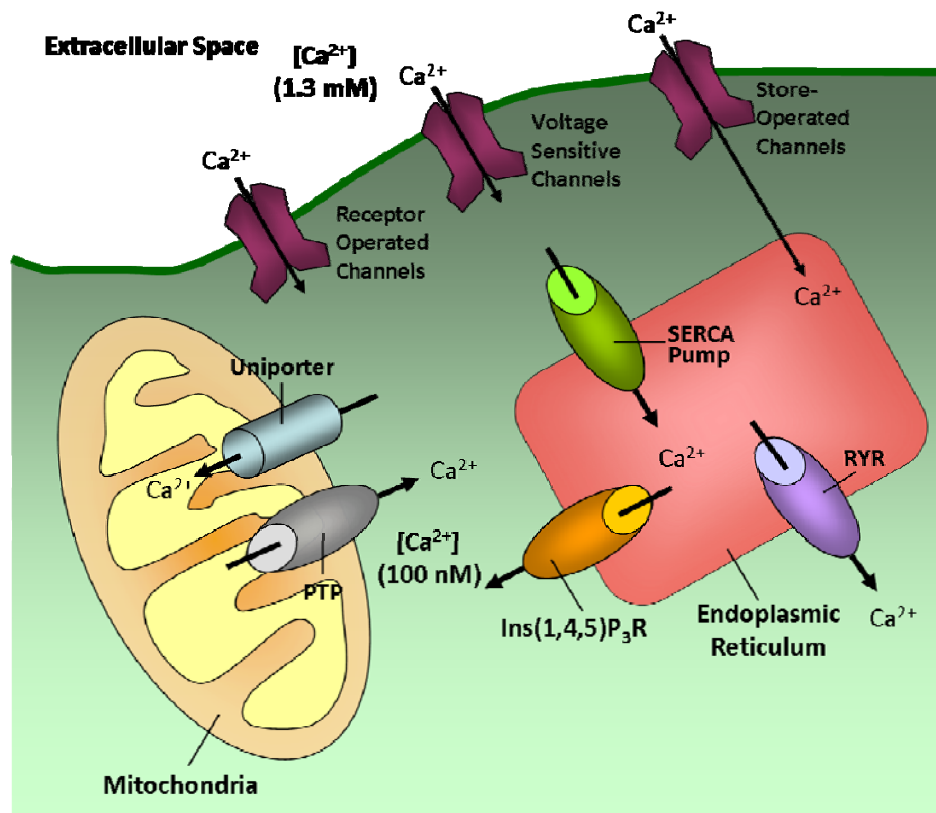
Figure 1.3:   Intracellular Ca^{2+} Compartmentalisation

Ca^{2+} import occurs through receptor operated, voltage-sensitive and store operated channels on the plasma membrane. On entry cytosolic Ca^{2+} is either inactivated by binding proteins or taken up by the mitochondria or ER (the largest store of intracellular Ca^{2+}, reaching mM levels), in order to keep cytosolic [Ca^{2+}] ~ 100 mM. In pathology, increased cytosolic [Ca^{2+}], results from reversal of ATP-dependent Ca^{2+} pumps on the plasma membrane and ER, reversal of Na$^+$ sensitive channels on the plasma membrane, loss of mitochondrial function and subsequent uniporter reversal and PTP opening, and direct action of products of anaerobic metabolism on the Ins(1,4,5)P3R Ca^{2+} receptor of the ER. (Modified from (Orrenius et al., 2003)).

The Bcl-2 family of proteins are vitally involved in neuronal survival and programmed cell death. This gene family contains both pro-apoptotic and anti-apoptotic proteins, and are classified by their expression of one or more Bcl-2 homology domains. The main anti-apoptotic proteins of this family consist of Bcl-2 and Bcl-x$_L$ which are contained within the outer membrane of the mitochondria as well as within the ER and peri-nuclear membrane. The anti-apoptotic members of the Bcl-2 family act by inhibiting the pro-apoptotic members, for example Bax and Bid (Figure 1.4). High [Ca^{2+}]$_i$ also activates release of pro-apoptotic mediators from the mitochondria through activation of calpains (Croall *et al.*, 1991). Calpains cleave the Bcl-2 interacting domain (BID) to its truncated and active form (tBID) (Chen *et al.*, 2001; Mandic *et al.*, 2002). BID is a member of the Bcl-2 pro-

apoptotic family of proteins that translocate to the mitochondria to initiate cell death. Once translocated to the mitochondrial membrane, tBID heterodimerises with the pro-apoptotic proteins Bak and Bax causing MTP opening (Figure 1.4).
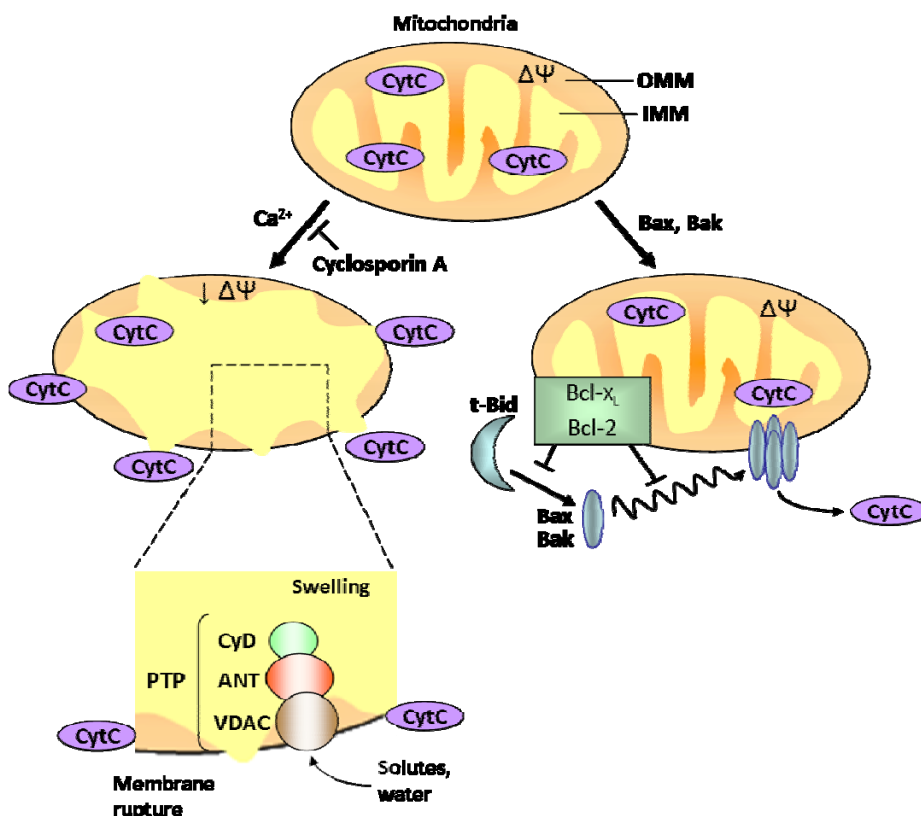
Figure 1.4: **Mechanisms of release of mitochondrial proteins by Ca^{2+}.**

Two of the three recognised mechanisms of outer mitochondrial membrane (OMM) permeabilisation initiated by increased [Ca^{2+}]$_i$ are shown. The left-hand side mechanisms depicts opening of the permeability transition pore (PTP), which consists of a voltage-dependant anion channel (VDAC), adenosine nucleotide translocator (ANT) and cyclophilin D (CyD). Pore opening results in subsequent oedema and swelling of the mitochondrial matrix, followed by rupture of the OMM and release of cytochrome *c* (CytC). The right-hand side mechanism depicts OMM permeabilisation through MTP opening and activation by the Bcl-2 family of proteins, Bax, Bak and tBid (modified from (Orrenius *et al.*, 2003)).

Ca^{2+} can also mediate mitochondrial permeabilisation though activation of cytosolic phospholipid A2 (cPLA$_2$). Activated cPLA$_2$ causes an increase in intracellular arachidonic acid release, which acts on the mitochondria to cause membrane permeabilisation. Levels of cPLA$_2$ are tightly regulated by [Ca^{2+}]$_i$ under normal conditions, however when [Ca^{2+}]$_i$ is in excess it readily binds to form a His-48 / Asp-99 / Ca^{2+} complex which activates cPLA$_2$. Activated cPLA$_2$ triggers arachidonic acid release by freeing it from an inhibiting

phospholipid molecule through an enzymatic process. Activated arachidonic acid has been shown to directly act on the MTP on mitochondria, possibly by modifying its putative voltage sensor (Scorrano *et al.*, 2001).

Release of pro-apoptotic CytC and Smac / DIABLO from the mitochondria result in initiation of the mitochondrial caspase-dependant intrinsic pathway of cell death. Following release, CytC forms a complex with cytosolic adapter protein (APAF-1) and caspase-9, known as the apoptosome, to mediate the activation of pro-caspase-9 in the presence of deoxy-ATP (dATP) (Figure 1.5). APAF-1 is a homologue of *C. elegans* cell-death gene product *CED-4* gene (Zou *et al.*, 1997), which is indispensible in apoptosis - APAF-1-null mice die *in utero* with a marked enlargement of the periventricular proliferative zone (Cecconi *et al.*, 1998). Activated caspase-9 cleaves and activates caspase-3, which initiates apoptosis through DNA fragmentation. Caspase-3 mediates DNA fragmentation by releasing the endonuclease caspase-activated DNase (CAD) from inhibition by cleaving its inhibitor ICAD (Figure 1.6) (Enari *et al.*, 1998), and is essential in the process of apoptosis (Jänicke *et al.*, 1998). CAD is a deoxyribose- and double-strand-specific enzyme (Hanus *et al.*, 2008) which preferentially cleaves the internucleosomal linker regions in chromatin (Widlak *et al.*, 2000). Smac / DIABLO and HtrA2 / Omi potentiate the intrinsic mitochondrial pathway of cell death by inhibiting one or more members of family of apoptosis inhibitory proteins (IAPs) (Figure 1.6) (Adrain *et al.*, 2001) which have been shown to directly inhibit caspase-3 and 7 (Deveraux *et al.*, 1997)
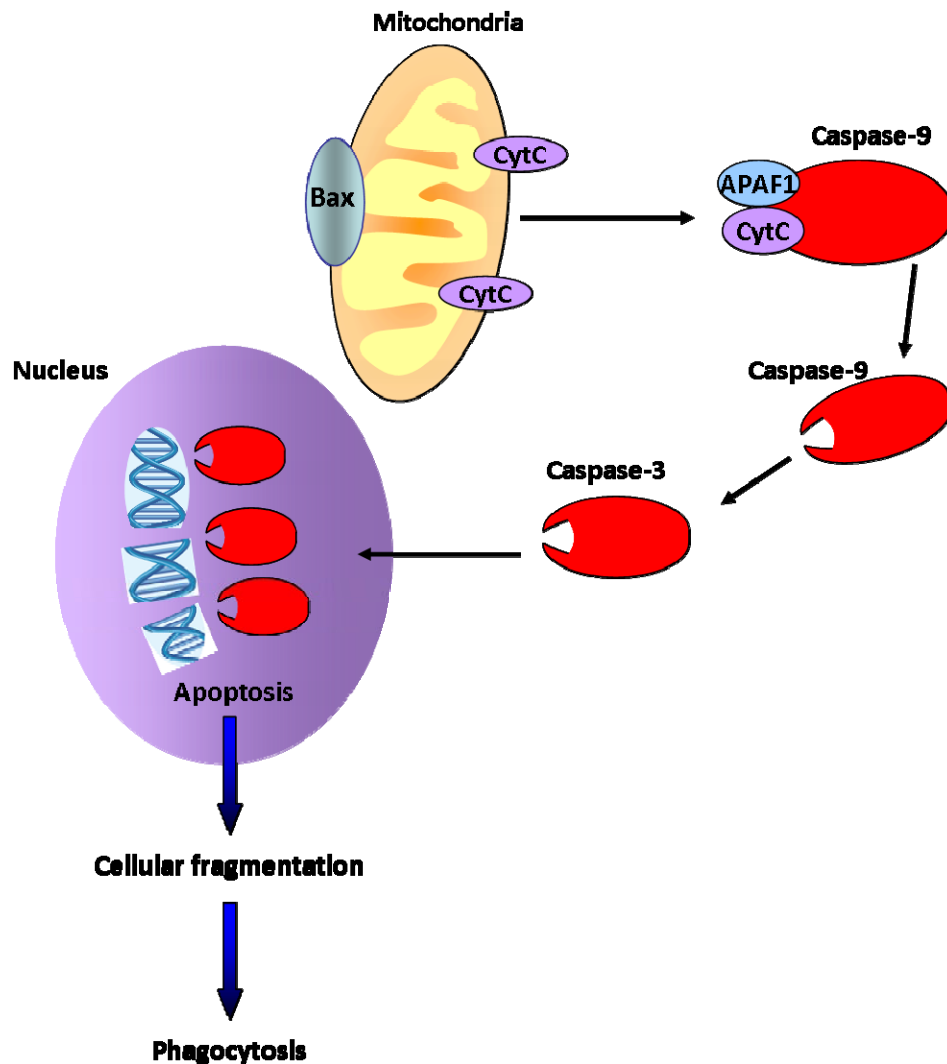
Figure 1.5:   Pathway of Caspase-Mediated Mitochondrial Programmed Cell Death

The intrinsic pathway involves the translocation to mitochondria of pro-apoptotic Bcl-2 family members such as Bax, which results in the release of cytochrome c into the cytosol, oligomerisation of Apaf-1 in a complex with caspase-9 (the apoptosome), and the subsequent activation of caspase-3. Activated caspase-3, releases caspase-dependant DNase from inhibition, initiating DNA fragmentation and subsequent PCD.

The intrinsic mitochondrial pathway of cell death can also occur via caspase-independent pathways. In addition to release of the caspase mediators CytC, Smac / DIABLO and HtrA2 / Omi, the mitochondria has been shown to also release apoptosis-inducible factor (AIF) (Cande *et al.*, 2002), endonuclease G (EndoG) (van Loo *et al.*, 2001) and more recently BNIP3 (Zhang *et al.*, 2007) following MMP. Following release AIF and EndoG translocate to the nucleus and initiate chromatin condensation and DNA fragmentation. Specifically, AIF causes large-scale DNA fragmentation and peripheral condensation of

nuclear chromatin, which is distinct from the global chromatin condensation and oligonucleosomal DNA fragmentation of caspase-dependent death (Cho *et al.*, 2008). Translocation of AIF to the nucleus may be mediated by poly(ADP-ribose) polymerase-1 (PARP-1) (Figure 1.6), observed *in vitro* by confocal analysis and cellular fragmentation analysis, which determined AIF was present within the nucleus of WT mouse fibroblasts following treatment with *N*-methyl-*N'*-nitro-*N*-nitrosoguanidine (MNNG) to induce apoptosis, but not in PARP-1 KO fibroblasts (Yu *et al.*, 2002). The mechanism by which PARP-1 mediates translocation of mitochondrial AIF is unknown. BNIP3 has been demonstrated as a mediator of intrinsic caspase-independent cell death through activation of EndoG (Zhang *et al.*, 2007). Primary cortical neurons were subjected to hypoxia and under normal hypoxic conditions, BNIP3 was shown to be upregulated within the mitochondria and EndoG was translocated to the nucleus following 24 h. A lentivirus expressing an inhibitory RNA (RNA$_i$) for BNIP3 was generated and following pre-treatment with lentivirus, inhibiting BNIP3, EndoG was delayed in translocation to the nucleus by 24 h. This suggested a novel role for BNIP3 mediated EndoG translocation in caspase independent cell death *in vitro*. More is known about AIF than EndoG, however, studies by Lee *et al.* showed that both EndoG and AIF could be detected within the nucleus at 4 - 24 h post-MCAO (Lee *et al.*, 2005). This suggests a complementary role for EndoG and AIF; however how they are purposely linked is unknown.
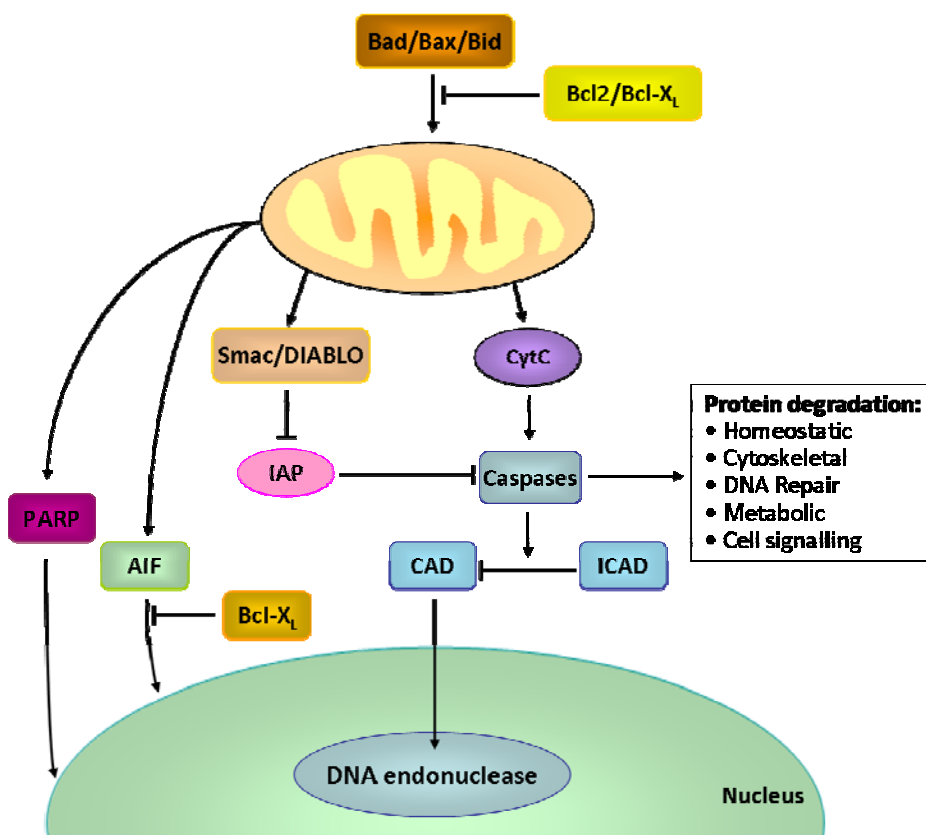
Figure 1.6: **Mitochondrial Pathways of Apoptosis**

The pro- and anti-apoptotic mediators of the Bcl-2 mediate release of CytC from the mitochondria, which activates downstream caspases through apoptosome formation (not shown). Caspase activation can be attenuated by secondary stimulation through Smac/Diablo suppression of the caspase inhibitors (IAPs). Caspases target a number of substances that cause cell dismantling by cleaving cytoskeletal and repair proteins. In addition, caspases activate caspase-activated deoxyribonuclease (CAD) resulting in DNA fragmentation. Caspase-independent apoptosis through AIF and EndoG (not shown) releases also mediates apoptosis (modified from (Lo *et al.*, 2003)).

1.5.3.2 *Extrinsic Apoptosis*

Extrinsic cell death is characterised by apoptosis initiated by activation of 'death receptors' expressed on the plasma membrane of the cells of the nervous system. The term 'death receptor' refers to a group of eight members of the tumour necrosis factor receptor (TNFR) superfamily of single pass transmembrane proteins (Ashkenazi, 2002). The main members of this family relevant to the nervous system that contain the 80-amino acid sequence that contains the so-called 'death domain' (DD) are the Fas receptor (FasR), TNF-R1, death receptors -4 and -5 (DR4 and DR5), and p75[NTR]. Activation of these receptors, leads to formation of a death inducing signalling complex (DISC) at the death domain sequence,

triggering apoptosis. However, of most importance in the pathogenesis following cerebral ischaemia are Fas and TNF-R1 (Martin-Villalba *et al.*, 1999; Rosenbaum *et al.*, 2000).

The FasR is switched on by Fas ligand (FasL) through either *cis* or *trans* activation (Figure 1.7). The best understood pathway of FasR mediated apoptosis is via the adapter protein FADD (Fas-associated death domain). FADD contains an NH_2-terminal death effector domain (DED) and a COOH-terminal DD, which binds FasR via a homeotypic DD-DD interaction. The NH_2-terminal DED of FADD binds cytosolic DED-containing pro-caspase 8 to the FasR complex via a DED-DED interaction and pro-caspase-8 is subsequently cleaved into active caspase-8. Caspase-8 can potentiate apoptosis through two pathways; cleavage of BID to tBID, activating MMP and release of pro-apoptotic agents or through direct cleavage of pro-caspase-3. Another well-established pathway of FasR mediated apoptosis is via the DD-independent mechanism using adapter protein Daxx (death-associated protein 6). Daxx was shown to be the link between FasR activation and the JNK-mediated apoptosis pathway (section 1.6) by Yang *et al.* in 1997 (Yang *et al.*, 1997c). A year later, Chang *et al.* demonstrated that FasR/Daxx activation of JNK occurred through activation of apoptosis signal-regulating kinase 1 (ASK1), by showing mutation of the conservative ATP binding loop of ASK1 completely abrogated Daxx-mediated cell death (Chang *et al.*, 1998) (Figure 1.7).

Following activation, TNF-R1 mediates cell death through a number of pathways initiated by the adapter protein TRADD (TNF receptor-associated death domain), which recruits additional adaptor proteins; TRAF2 (TNF-R-associated factor 2) and FADD (Figure 1.7). TRAF2 activates the JNK pathway of apoptosis (section 1.6) also through activation of ASK1 (Nishitoh *et al.*, 1998). Interestingly, TRAF2 also mediates an anti-apoptotic signalling cascade by activation of cellular inhibitor of apoptosis-1 (IAP-1) and cIAP-2 which suppress caspase-8 activation (Wang *et al.*, 1998).
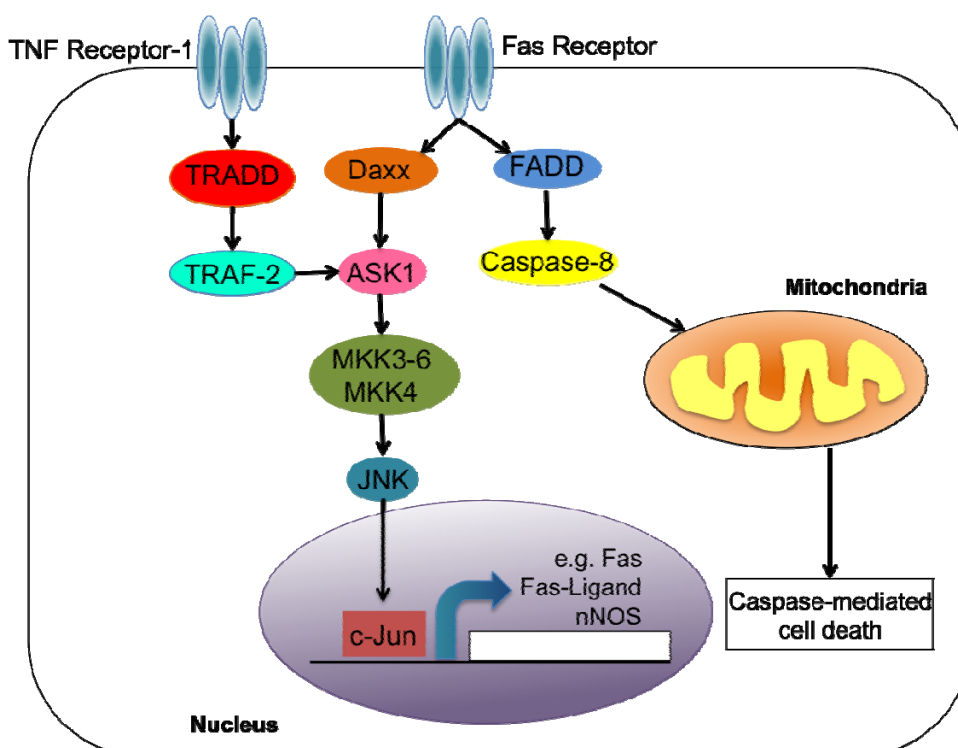
Figure 1.7:   Death Receptor Mediated Cell Death

Events regulated in the death receptor mediated or `extrinsic' pathway to apoptosis. *Cis* or *trans* ligation of cell surface death receptors, such as Fas or TNFR-1, by the appropriate ligand engages multiple intracellular signals leading to caspase or JNK activation and subsequent cell death.

1.6   THE IMPORTANCE OF JNK

As is the case with all mitogen activated protein kinases (MAPKs), c-Jun N-terminal kinase (JNK) activation occurs from a sequential activation cascade that includes MAPK kinase (MAPKK) and MAPK kinase kinase (MAPKKK) (Figure 1.8). JNK is activated by dual phosphorylation by MKK4 and MKK7, determined by gene targeting studies (Tournier *et al.*, 2001). The MAPKKK level of JNK activation is more diversely regulated, with activators including MAPK/ERK kinase kinases (MEKKs), mixed-lineage kinases (MLKs), dual leucine-zipper kinases (DLKs), activator of S-phase kinase (ASK), and transforming growth factor b-activated kinase (TAK). JNK mediates apoptosis through multiple pathways, including activation of the mitochondrial pathway cell death and through direct translocation to the nucleus and activation of pro-apoptotic transcription factors (Figure 1.8). JNK activates mitochondrial-mediated apoptosis by direct action on Bim / Bad, and subsequent Bax / Bak activation. Following translocation to the nucleus,

JNK activates the transcription factor c-Jun and ATF-2, leading to the formation of Jun-ATF-2 complex activator protein-1 (AP-1). The AP-1 pathway is involved in regulation of pro-apoptotic genes such as TNF-α, Fas-L and Bak (Fan *et al.*, 2001). In addition, JNK mediates the inhibition of a number of pro-apoptotic and pro-survival transcription factors, such as: JunD, ATF2, ATF3, Elk-1, Elk-3, p53, RXRα, RARα, AR, NFAT4, HSF-1, and c-Myc (Johnson *et al.*, 2007).
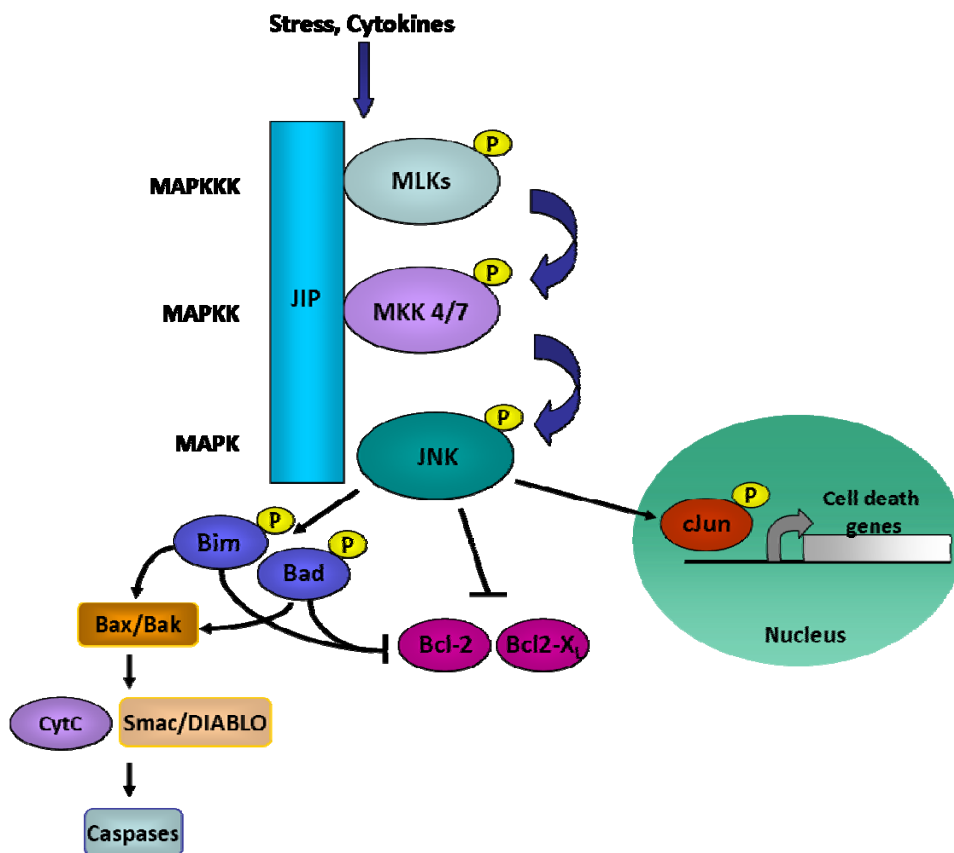
Figure 1.8:   JNK Pathway

Summary of the cascade of JNK signalling pathway and the downstream apoptotic mechanisms.

In addition, the release of pro-apoptotic factors from the mitochondria is increased by JNK through its direct inhibition of the anti-apoptotic mediator Bcl-2 (Deng *et al.*, 2001). JNK also mediates Bcl-2 inhibition indirectly through phosphorylation of Bad and Bim, which inhibit Bcl-2 when activated (Yu *et al.*, 2004). ROS specifically increase JNK activation through their direct interaction with the upstream mediator of JNK, ASK1 (Soberanes *et al.*, 2009). Under normal conditions, ASK1 remains inactive through binding with

thioredoxin (Trx), a ubiquitously expressed protein with a reduction / oxidation active site sequence.

1.6.1   JNK in Stroke

As JNK's role in cell death was elucidated, it was implicated to be a potentially important mechanism in neurological disorders such as stroke. In mammals, JNKs can be subdivided into 3 isoforms, JNK1, JNK2 and JNK3, coded for by genes *Jnk1*, *Jnk2* and *Jnk3*, respectively. As JNK3 expression is largely restricted to the brain, it has been a target of neuroprotective strategies using genetic strategies. Selective deletion of the *Jnk3* gene (*Jnk3* -/- mice) saved the neurons of the hippocampus from kainic acid-induced excitotoxicity, but this was not observed in *Jnk1* -/- or *Jnk2* -/- mice (Yang *et al.*, 1997a). Following cerebral ischaemia / reperfusion by occlusion of the MCA, an elevated level of c-Jun phosphorylation was observed in the peripheral area of ischaemic damage that co-localised with TUNEL-labelling, to detect apoptosis, in the brains of Sprague-Dawley rats (Herdegen *et al.*, 1998). Mice lacking the JNK scaffold protein (Figure 1.8), JIP1, (*Jip1* -/- mice) exhibited increased resistance to glutamate-induced excitotoxicity (Whitmarsh *et al.*, 2001) and demonstrated a reduced lesion size following focal transient cerebral ischaemia (Im *et al.*, 2003). Further studies have also demonstrated that *Jnk3* -/- mice had increased resistance to global ischaemia and reduced Bim and Fas expression (Kuan *et al.*, 2003). *In vitro* studies demonstrated *Jnk3*-null hippocampal neurons release less CytC release following oxygen-glucose deprivation (Kuan *et al.*, 2003).

1.6.2   Inhibition of c-Jun N-terminal Kinases in Models of Cerebral Ischaemia

As previously described, JNKs are critical in both the intrinsic and extrinsic pathways of PCD. JNKs can mediate cell death by activating pro-apoptotic genes through specific activation of transcription factors. In addition, JNK can mediate PCD through modulation of the mitochondrial Bcl-2 family of pro- and anti-apoptotic proteins. In this way, JNK can initiate and modulate co-ordinated regulation of the nuclear and mitochondrial pathways of PCD, and as such ensures efficient execution of apoptosis. Therefore, JNK offers an attractive therapeutic target for inhibition in a neuroprotective strategy.

1.6.2.1 Gene Knockout Studies

As a result of the initial absence of selective chemical inhibitors of JNK, gene knockout studies of JNK or the components of the JNK pathway were seen as an effective method in dissecting its role in both development and pathology. However, disruption of components of the upstream JNK signalling pathway were ineffective in assessing JNKs role due to reduced specificity when targeting upstream (e.g. MKK4 and MKK7) and by losing actions of alternative substrates when targeting downstream (e.g. c-Jun), such as the mitochondrial Bcl-2 proteins. Following permanent occlusion of the MCA, *Jnk3* -/- mice showed a 42 % reduction in lesion size (Pirianov *et al.*, 2007).

1.6.2.2 Peptide Inhibitors of JNK

Peptide inhibitors of JNK are derived from the direct interacting partners of JNK and its substrates. There are a number of peptide inhibitors of JNK, including the cell permeable JNK peptide inhibitor derived from the δ-domain of the substrate, c-Jun. However, this TAT-c-Jun peptide is only effective in blocking the nuclear pathways of JNK mediated apoptosis (Holzberg *et al.*, 2003). More effective blockade of JNK action has been observed using peptides derived from the JNK scaffold protein, JNK-interacting protein (JIP1). These peptides include the L-amino acid containing peptides TI-JIP, TAT-TIJIP and L-JNK-I, in addition to the D amino acid-containing peptide, D-JNK-I, which all act in a protein–substrate competitive manner (Barr *et al.*, 2004). Of these peptides L-JNK-I and D-JNK-I have most commonly been used in models of cerebral ischaemia with successful neuroprotection. It was demonstrated that stereotactic administration of 15.7 ng D-JNK-I resulted in a significant reduction in lesion size when administered at 1 h prior, 3 h post and 6 h post-tMCAO in male ICR-CD1 mice, by ~ 88 % (Borsello *et al.*, 2003a). No significant reduction in lesion size was observed following administration of D-JNK-I at 12 h post-tMCAO. Following permanent focal ischaemia in P14 rats, D-JNK-I mediated a significant reduction (~ 68 %) in lesion size when administered at 0.5 h prior, and 6 h post-MCAO but not 12 h post-MCAO (Borsello *et al.*, 2003a). Additionally, it was reported that *i.c.v.* administration of 40 nmol D-JNK-I following permanent MCAO in male ICR-CD1 mice significantly reduced lesion size (by ~ 25 %) when administered at 3 h post but not 6 h post MCAO (Hirt *et al.*, 2004).

1.6.2.3   CEP-1347

The first small molecule inhibitor of JNK was the 3,9-disubstituted [(alkylthio)methyl]-
and (alkoxymethyl)-K252a derivative, CEP-1347. The initial study using CEP-1347
demonstrated its effectiveness in saving neuronal cells from apoptosis through inhibition of
JNK, with an IC_{50} of 20 nM (Maroney *et al.*, 1998). To date there have been > 80 studies
assessing the anti-apoptotic ability of CEP-1347 across a wide range of pathologies
including; Huntington's disorder (Conforti *et al.*, 2008); Parkinson's (Investigators, 2007);
neuroAIDS (Eggert *et al.*, 2010); and stroke (Carlsson *et al.*, 2009). CEP-1347 acts
upstream to JNK, at the membrane proximal location of the MAPK pathway, as an ATP-
competitive inhibitor of the mixed-lineage kinases (MLK1, MLK2, and MLK3). The
neuroprotective effect of CEP-1347 remains to be determined; however, a Phase II/III
clinical trial into its effect in Parkinson's disease reported negative results in a sample size
of 806 patients across all 3 doses (PRECEPT, 2007).

1.6.2.4   SP600125

SP600125 (anthra[1,9]pyrazol-6(2H)-one) is a small molecule inhibitor of JNK, identified
in 2001, following screening of a proprietary library for small inhibitors of the JNK2 - c-
Jun interaction (Bennett *et al.*, 2001). SP600125 is a reversible ATP-competitive inhibitor
of JNK, with a similar IC_{50} for all three isoforms; JNK1, 40nM; JNK2, 40nM; and JNK3
90 nM. It has been shown to be highly selective with > 300-fold selectivity when
incubated with 16 other similar protein kinases (Bennett *et al.*, 2001). Co-crystallisation
studies have further explored the SP600125-JNK interactions, (Figure 1.9). The specific
residues of JNK not conserved in p38 are highlighted in Figure 1.9; namely I70, V79,
V196, L206 and Q155. These residues produce an ATP-binding pocket which
accommodates the planar structure of the SP600125, contributing to the specificity of this
small molecule inhibitor (Scapin *et al.*, 2003).

Studies comparing the efficacy of TAT-c-Jun peptide and SP600125 (Holzberg *et al.*,
2003), demonstrated that combined intervention resulted in 20 of the interleukin-induced
genes being downregulated. Of these 20 only 4 were downregulated by both, whilst 10
were downregulated by SP600125 alone and 6 by TAT-c-Jun peptide alone. This study
confirmed a different mode of action between the two inhibitors, perhaps explained by the
different modes of action on the nucleic or mitochondrial routes of apoptosis.

SP600125 has also been successfully used as an inhibitor of apoptosis and protective agent in a number of pathologies including ischaemia / reperfusion of the lung (Bogoyevitch *et al.*, 1996), liver (Bendinelli *et al.*, 1996), brain (Guan *et al.*, 2005), kidney and heart (Yin *et al.*, 1997).
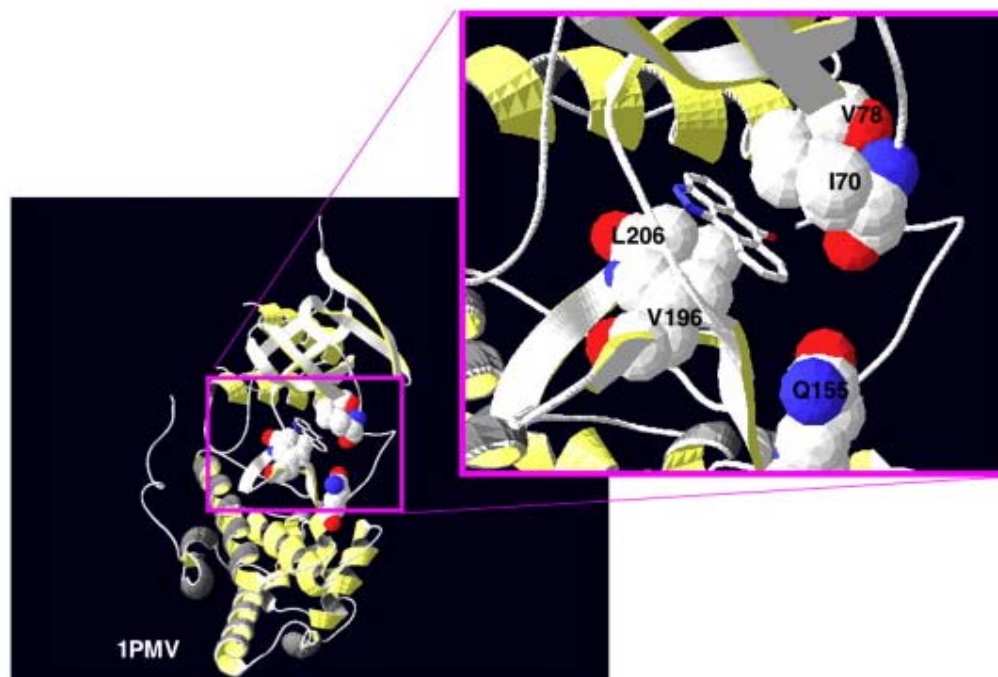
Figure 1.9:   **Crystal Structure of JNK3 and SP600125 Complex**

SP600125 has been co-crystallised with JNK3, and the resulting structure has been recorded in the Protein DataBase (PDB) as 1PMV (taken from (Bogoyevitch *et al.*, 2008))

1.7 CEREBRAL ISCHAEMIA / REPERFUSION: PATHOPHYSIOLOGY OF OXIDATIVE STRESS

Oxidative stress as a result of excess production of reactive oxygen species (ROS) is a fundamental mechanism of cell damage following cerebral ischaemia, where ROS refers to molecular oxygen (O_2) or its derivatives. Under normal cellular conditions, ROS have functions in neuronal signalling in both the PNS and the CNS (Droge, 2002). Although oxidative stress has been implicated in numerous pathologies across a variety of organs, including cancer, atherosclerosis and neurodegenerative diseases, the brain is particularly sensitive to oxidative damage (reviewed in (Uttara *et al.*, 2009)). There are several reasons

for this; the high consumption of oxygen under basal conditions, high concentrations of peroxidisable lipids, and high levels of iron that acts as a pro-oxidant during stress. Lactate acid and H^+ production from glycolysis and reversal of the H^+ uniporter on the mitochondrial membrane in the oxygen- and ATP-depleted cell contributes to excess cytosolic H^+ build-up and subsequent acidosis. Acidosis contributes to oxidative stress by providing H^+ for the conversion of $\bullet O_2^-$ into hydrogen peroxide (H_2O_2) or the more reactive hydroxyl radical ($\bullet OH$). In addition to H_2O_2 and $\bullet OH$ production, peoxynitrite ($ONOO^-$) is formed by the reaction of $NO\bullet$ and $\bullet O_2^-$. ROS have a number of detrimental effects which result in cell damage and tissue destruction, such as: lipid peroxidation, protein denaturing, disruption of DNA and multiple cell signalling effects resulting in initiation of apoptosis (Figure 1.10).
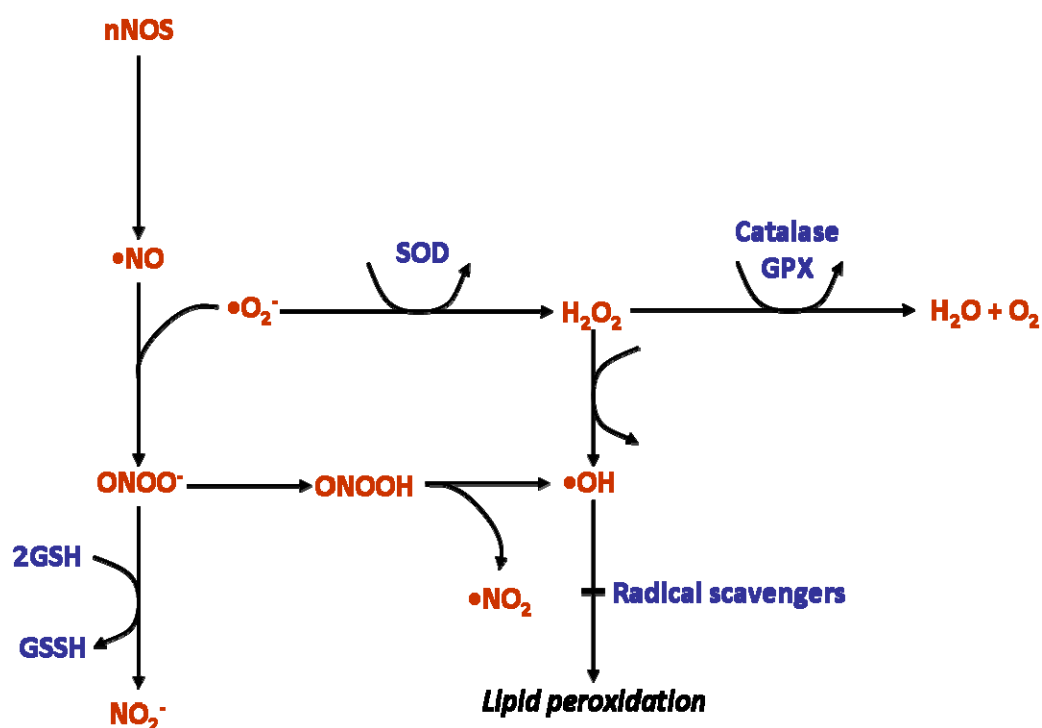
Figure 1.10:   Production and decomposition of ROS

Production pathways of ROS following cerebral ischaemia and their subsequent decomposition by their endogenous and specific antioxidants.

1.7.1.1   ROS and Lipid Peroxidation

Lipid peroxidation is the main mechanism by which ROS cause damage within the brain. Initiation of lipid peroxidation results in a positive-feedback loop of damage (Figure 1.11).

The •OH initiates removal of one H^+ from a polyunsaturated fatty acid resulting in formation of a lipid radical that reacts readily with O_2 to form a lipid peroxyl radical and another lipid radical. The lipid radical by-product will further react with oxygen causing a positive feedback reaction. As an example of the positive-feedback loop of lipid peroxidation: excess ROS can activate PLA_2 which in turn releases and activates AA and a by-product of the activation of AA is ROS. ROS act directly on lipids to ultimately produce aldehydes, dienals or alkanes, such as 4-HNE. 4-HNE induces apoptosis following cerebral ischaemia in neurons (McCracken *et al.*, 2000) and has been shown to be upregulated in a time-dependent manner in the ipsilateral striatum following focal ischaemia in rats (Matsuda *et al.*, 2009).
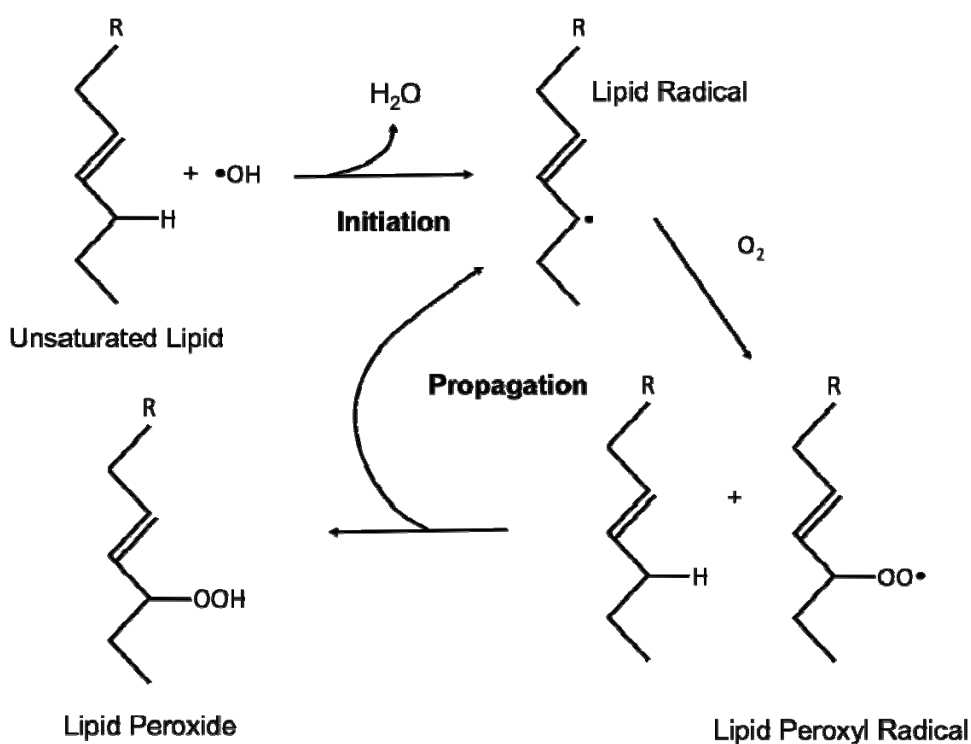
Figure 1.11: Lipid Peroxidation Positive Feedback

Process of lipid peroxidation by •OH.

1.7.1.2   ROS and DNA Modifications

Oxidative damage of DNA differs to endonuclease-mediated DNA fragmentation in that it occurs at earlier time-points following cerebral ischaemia and is potentially reversible. Oxidative damage to DNA occurs from direct attack of ROS on DNA, resulting in primarily DNA base damage and single-strand breaks (SSBs), observed in rodent models

of cerebral ischaemia (Chen *et al.*, 1997; Liu *et al.*, 1996a; Nagayama *et al.*, 2000). Although oxidative damage is potentially reversible, in cerebral ischaemia the multiple mechanisms that induce ROS and the subsequent positive feedback loop of ROS observed in many pathways ultimately generates fatal DNA damage to neuronal cells (Chen *et al.*, 1997; Kawase *et al.*, 1999).

1.7.1.3   *ROS and Cell Signalling*

The primary site for generation of ROS following cerebral ischaemia is the mitochondria, where they exert their most detrimental role in initiation of cell death via CytC release (Kirkland *et al.*, 2002; Sugawara *et al.*, 2002). However, in addition to mediating CytC release in the mitochondria, ROS have been shown to have a direct interaction with nuclear factor $_KB$ (NF-$_KB$) and on activation of the MAPK / JNK pathway of cell death.

NF-$_KB$ is known to be activated by the redox state of the cell in a number of disease pathologies and activation can be inhibited through use of antioxidants (Dalton *et al.*, 1999). The downstream gene targets of NF-$_KB$ include, NOS, cyclooxygenase-2 (COX-2), matrix metalloproteinase-9 (MMP-9), intracellular adhesion molecules (ICAMs) and cytokines which are involved in a number of detrimental pathways of cerebral ischaemia such as, apoptosis, BBB breakdown, and inflammation. ROS has been shown to activate the MAPK, JNK, resulting in initiation of JNK-mediated cell death, as previously described (section 1.6). In the presence of excess ROS, Trx is actively oxidised and ASK1 dissociates from the inhibitory complex and is subsequently phosphorylated and activated by an unknown kinase. Activated ASK1 recruits the homodimer TRAF2 and the resultant complex activates MKK's (Tobiume *et al.*, 2002).

1.7.1.4   *ROS, Reperfusion and Hyperperfusion*

In the reperfusion period, hyperperfusion is well established as a frequent occurrence as part of reperfusion (Marchal *et al.*, 1996). Hyperperfusion can cause oedema and haemorrhage within the brain. Following 60- or 120- minute tMCAO in cats, hyperperfusion was observed at an extent of 300 % of pre-occlusion values. The most severe hyperperfusion observed was linked to mortality within the study, where infarct was significantly larger (Heiss *et al.*, 1997). Hyperperfusion also results in substantial upregulation of ROS in the early period of reperfusion, as the resupply of O_2 to the damaged ischaemic respiratory chain cannot be fully utilised (Frantseva *et al.*, 2001). This

increase in ROS leads to further permeabilisation of the BBB and to enhance leukocyte infiltration .

1.8 CEREBRAL ISCHAEMIA / REPERFUSION: PATHOPHYSIOLOGY OF THE INFLAMMATORY RESPONSE

In the CNS, microglia are the source of production and release of inflammatory mediators during cerebral ischaemia (Figure 1.12). In the minutes following cerebral ischaemia, there is increased accumulation of ATP or UTP in the extracellular space (Melani *et al.*, 2005) of the brain parenchyma as a result of cellular membrane breakdown. Increased ATP activates the P2X7 receptors of the microglia, leading to release of pro-inflammatory mediators (Korcok *et al.*, 2004), such as cytokines, ROS and NO. In the later stages following cerebral ischaemia, a large number of molecular signals are released from the intracellular compartment of dead / dying cells, known as danger-associated molecular pattern molecules (DAMPs). DAMPs act on the Toll-like receptors of the microglia to further activate release of pro-inflammatory mediators. Under normal conditions, cell-to-cell interaction between neurons and microglia maintains the quiescence of the microglia. Disruption of these interactions results in activation of the microglia, and potentiates the release of pro-inflammatory mediators. For example, the membrane protein CD200 expressed on neurons interacts with the CD200R on microglia and enforces the resting phenotype (Lyons *et al.*, 2007). During ischaemia, expression of this protein is reduced leading to activation of the microglia. In a similar fashion, the cell-surface bound neuronal chemokine, CX3CL1, acts on the microglial CX3CL1 receptor promoting quiescence during normal respiration (Denes *et al.*, 2008). Thus, during cerebral ischaemia loss of the CX3CL1 / CX3CL1R interaction, releases microglia from suppression and promotes the inflammatory response.
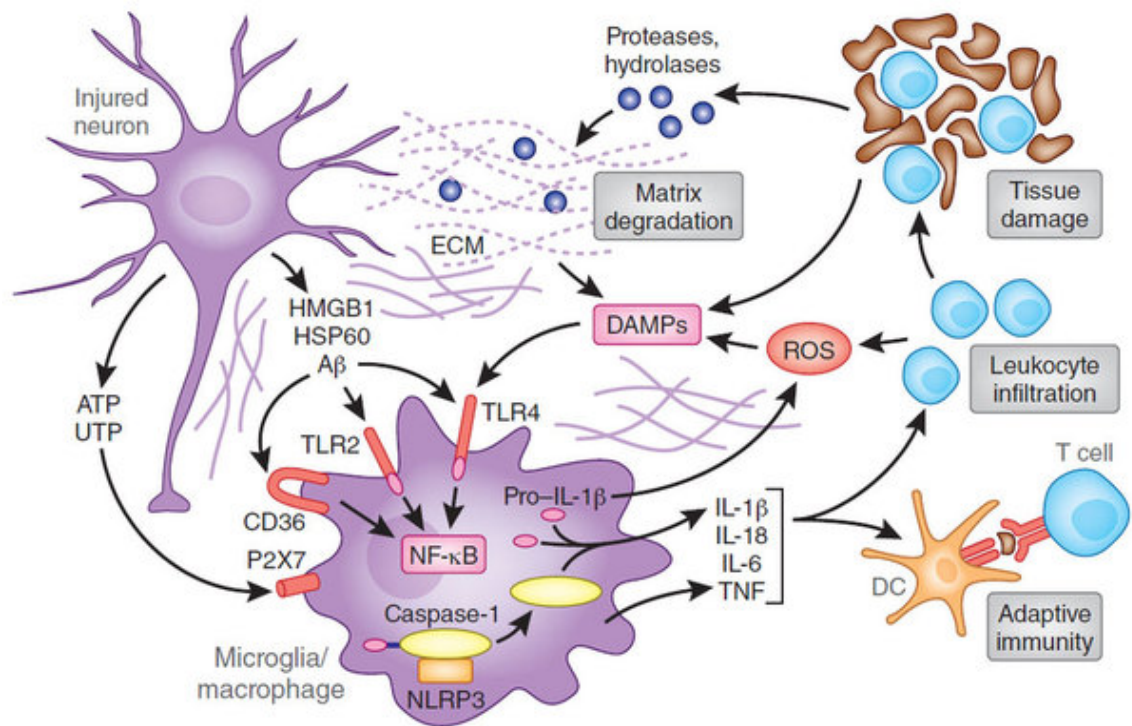
Figure 1.12:   Innate Immune Response

Release of ATP from damaged cells activates purinergic receptors on microglia and macrophages. Activation of microglia and macrophages leads to production of pro-inflammatory cytokines such as, IL-1β, IL-18, IL-6 and TNF. DAMPs, released by apoptotic cells, act on Toll-like receptors (TLRs) of the microglia, resulting in activation of the pro-inflammatory transcription factor NF-$_κ$B. Activation of these pathways enhance leukocyte infiltration and aggravate tissue damage, causing further release of these mediators (taken from (Iadecola *et al.*, 2011)).

1.8.1   Inflammatory Response in Reperfusion

Although significant inflammation is observed during ischaemia as a result of microglial activation, the vast majority of the inflammatory response is observed following reperfusion to the previously ischaemic area (Figure 1.13). Beginning in the intravascular compartment, platelets and endothelial cells are activated in response to hypoxia, ROS and shear stress (reviewed in (Carden *et al.*, 2000)). Animal studies have provided evidence of leukocyte-mediated injury as a result of reperfusion. When comparing 2-hour tMCAO with permanent MCAO, it was found that neutrophil accumulation occurred to a greater extent and at earlier timepoints in reperfused animals. In addition, it was found that reperfused animals had a larger final infarct than those subjected to permanent occlusion (Zhang *et al.*, 1994). In further support of neutrophils' role in reperfusion injury, Bednar *et al.* (1991) demonstrated an improvement in cerebral blood flow in rabbits treated with anti-neutrophil antiserum from < 10 ml / 100 g / minute to 20-30 ml / 100 g / minute following

tMCAO, and a corresponding decrease in final infarct in neutropenic animals (Bednar *et al.*, 1991).
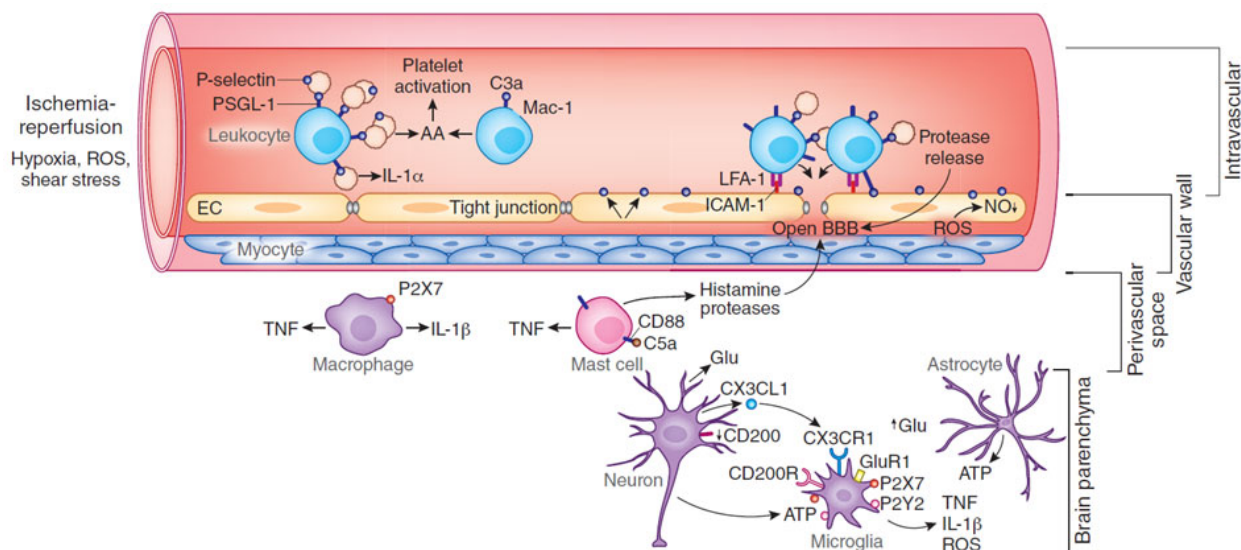
Figure 1.13:   The Vascular Inflammatory Response in Stroke

Following reperfusion to a previously ischaemic region, the inflammatory response is initiated. Expression of P-selectin on leukocytes and of P- and E-selectin on endothelial cells provides a platform for low-affinity leukocyte adhesion. Firm adhesion is obtained following endothelial ICAM-1 expression and interaction with the β2 integrins of leukocytes. Vasoconstriction occurs from loss of vascular NO bioavailability, enhancing leukocyte and platelet aggregation. Cerebral ischaemia results in BBB breakdown, which allows leukocyte infiltration into the perivascular space and brain parenchyma, mediating further inflammation (taken from (Iadecola *et al.*, 2011).

The adhesion molecule P-selectin is translocated to the membrane and expressed onto platelets and endothelial cells within minutes of cerebral ischaemia (Atkinson *et al.*, 2006). The bioavailability of potent vasodilator, NO, is rapidly degraded within the endothelial cells of the cerebral vasculature as a result of oxidative stress, causing vasoconstriction (Sehba *et al.*, 2000). Extreme vasoconstriction in combination with expression of adhesion molecules results in leukocyte adhesion to the vascular wall. Oxidative stress and protease release from leukocytes permeabilises the BBB, and upregulates the pinocytotic transport vehicles of the endothelial cells, allowing for leukocyte infiltration into the brain parenchyma (Cipolla *et al.*, 2004). Endothelial production of proteins responsible for the tight junctions between endothelial cells is also downregulated by leukocytes, leading to further BBB permeabilisation (Xu *et al.*, 2005). In addition to intravascular mediated BBB disruption, in the perivascular space the complement system is activated and C5a acts on

the CD88 receptor of mast cells causing degranulation and release of histones, TNF and proteases, which acts on the BBB to cause further breakdown and enhances expression of adhesion molecules on endothelial cells (Konsman *et al.*, 2007).

Following infiltration, inflammatory leukocytes kill via a number of pathways. Inflammatory mediators result in excess release of ROS. Virtually all inflammatory cells express the enzyme NADPH oxidase and as a result produce excess $\cdot O_2^-$ (Cathcart, 2004) and subsequent $ONOO^-$ due to the *de novo* expression of iNOS (Iadecola *et al.*, 1995), and H_2O_2 and $\cdot OH$ via the Haiber-Weiss reaction facilitated by acidosis and increased bioavailability of free iron. ROS mediate cell damage and apoptosis. Additionally, apoptosis is induced through activation of the 'death-receptors', FasR and TNF-R1. FasL is present within the inflammatory migroglial cytotoxic T cells, $\gamma\delta T$ cells and natural killer (NK) cells (Kagi *et al.*, 1994). Furthermore, TRAIL is expressed following cerebral ischaemia within astrocytes and microglia and TNF-α is released by a number of immune cells. Activation of the innate complement system cascade initiates necrosis through activation of the final subunit C9, which forms a pore in the membrane of cells resulting in cell lysis (Ziporen *et al.*, 2009). Complement activation also signals for phagocytosis of activated cells.

1.9 NEUROGLOBIN

Neuroglobin is a member of the globin superfamily. It is believed that in very early evolution, when aerobic metabolism became predominant, O_2 binding and delivery was a function acquired to the globins. Haemoglobin (Hb) and myoglobin (Mb) are well characterised members of the globin superfamily and are responsible for O_2 delivery within the blood stream and muscles, respectively. Indeed, Hb and Mb are among the most characterised proteins in history; however they are evolutionarily young in respect to the globin superfamily. The turn of the new millennia saw the advent of new abilities to access genetic bioinformatics and as such new proteins were discovered, and the globin superfamily was expanded. Neuroglobin (Ngb) (Burmester *et al.*, 2000) and Cytoglobin (Cygb) (Burmester *et al.*, 2002) were found to be evolutionarily older and more discreet globins, expressed at lower levels than Hb and Mb. Ngb is expressed in the CNS, PNS, CSF, retina and endocrine tissues (Trent *et al.*, 2002). Ngb's localisation to neurons has generated most scientific interest, although its expression is ~ 100-fold higher in the retina

(Schmidt *et al.*, 2003). Ngb's distribution within the rat brain has shown to be extensive, with expression across the cerebral cortex, hippocampus and sub-cortical structures such as thalamus, hypothalamus, olfactory bulb and cerebellum. Although Ngb has been the subject of a vast amount of interest, its function and mechanism has yet to be fully elucidated.

The three-dimensional structure of Ngb has been solved in its different oxidation states. Although Ngb shares only 21 – 25 % sequence homology to Hb and Mb, the same fold sequence is observed (Figure 1.14). In addition, there is conservation of the key amino acids of Hb and Mb function. Ngb was shown to contain a heme-binding group and initial studies demonstrated and ability to reversibly bind oxygen (Trent *et al.*, 2001), leading to the hypothesis of its role as an O_2 transporter within the brain. Assessing the O_2 affinity of Ngb proved to be challenging as Ngb auto-oxidises with a half life of $\sim$ 3 – 20 min depending on the environmental pH, however an initial study determined Ngb's O_2 half saturation pressure (P_{50}) $\sim$ 2 torr, similar to that of Mb (Dewilde *et al.*, 2001; Fago *et al.*, 2004). However, subsequent studies in physiological conditions demonstrated a P_{50} of $\sim$ 7.5 torr, almost five times greater (Fago *et al.*, 2004). Taken together with its relatively low overall concentration in the brain (1 µM) (Dewilde *et al.*, 2001) and the elucidation of its physiologically low O_2 binding affinity, the potential role of Ngb in O_2 storage or diffusion was abolished.

Although its exact mechanism and function are unknown, there has been a lot of interest in Ngb's role in pathophysiology of the brain. There is strong evidence of Ngb localisation around the mitochondria (Hundahl *et al.*, 2010), suggesting a role for Ngb in normal cell respiration, as such it may be expected that exposure to hypoxia may exert a strong effect on Ngb expression. However, *in vivo* hypoxia studies are far from conclusive. A combined analysis of brains from mice subjected to varying lengths of exposure (5 h – 2 weeks) and levels of hypoxia (6 - 12 % O_2), showed highly variable Ngb concentrations (Burmester *et al.*, 2007). A number of *in vivo* hypoxia studies reported no difference in Ngb expression between hypoxic and normoxic animals (Hundahl *et al.*, 2005; Milton *et al.*, 2006), whilst others have demonstrated a large induction of Ngb in response to hypoxia (Fordel *et al.*, 2007b; Khan *et al.*, 2006). However, under hypoxic conditions, the PO_2 inside brain neurons remains unclear. The intracellular PO_2 controls hypoxia-related gene expression and perhaps this explains the variability observed. Interestingly however, the *in vivo* response of Ngb following cerebral ischaemia is also variable. Studies of both focal (Hundahl *et al.*, 2006a; Sun *et al.*, 2001) and

global (Schmidt *et al.*, 2004) ischaemia showed no variation of Ngb mRNA levels assessed by *in situ* hybridisation and qRT-PCR.
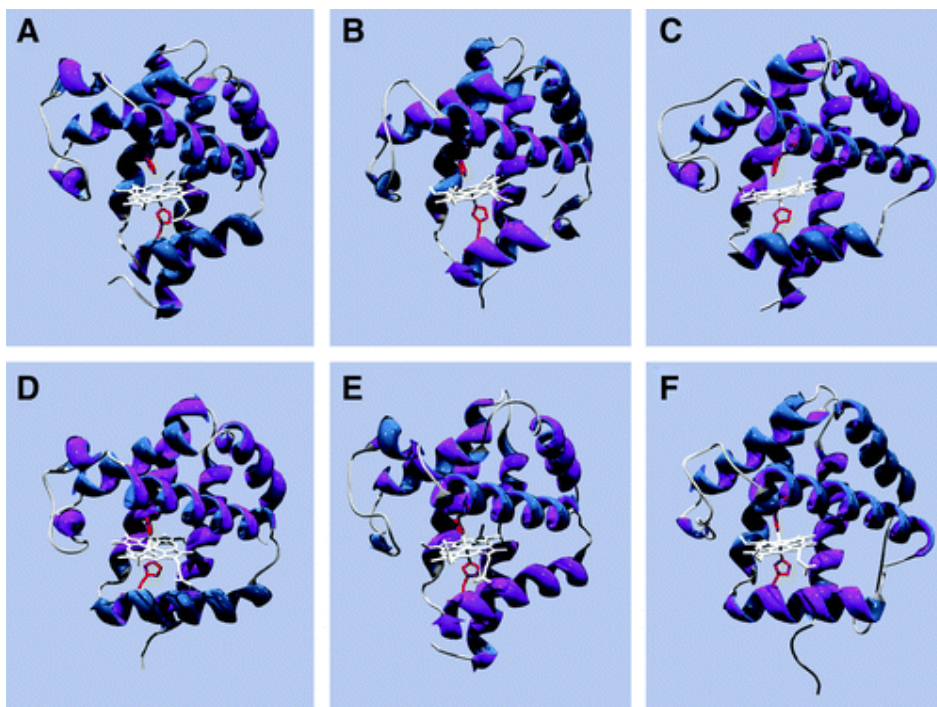
Figure 1.14:   Comparison of the Structure of Globins

Top row = pentacoordinate globins. (A) Sperm whale myoglobin, (B) human haemoglobin alpha subunit and (C) yellow lupine leg haemoglobin. Bottom row = hexacoordinate globins. (D) Human neuroglobin, (E) human cytoglobin, and (F) Asian rice non-symbiotic haemoglobin. Heme moiety and proximal and distal histidines are shown in ball and stick, (taken from(Reeder, 2010))

It is unlikely that under normal conditions mammals are likely to experience low O_2 as adults, and as such brains are not highly adapted for it. Therefore studies were carried out to assess Ngb expression within the brains of hypoxia-tolerant fish and turtles. Specifically, analysis of the brains of zebrafish (*Danio rerio*) (Roesner *et al.*, 2006) and the anoxia-tolerant turtle (*Trachemys scripta*) (Milton *et al.*, 2006) showed significant Ngb upregulation in response to exposure to a low oxygen environment. From these data, Burmester *et al.* (2009) studied Ngb levels in the subterranean blind mole rat (*Spalax ehrenbergi*), a mammal known to be able to survive exposure to hypoxia for significant lengths of time without neuronal damage (Burmester *et al.*, 2009). Ngb levels were reported to be significantly higher in the *Spalax* mole rat, than its evolutionary cousin the

common rat (Avivi *et al.*, 2010). This suggests the presence of Ngb within the human brain is an early-evolutionary remnant from a period before entirely aerobic respiration. This strengthens the argument for its safe upregulation from current endogenous levels by a gene delivery approach.

Although Ngb's endogenous expression following hypoxia or cerebral ischaemia / reperfusion could not be elucidated in *in vivo* rodent models*, in vitro* studies reported more success. Sun *et al.*, (2001) were the first to demonstrate that not only was Ngb time-dependently upregulated in response to oxygen-glucose deprivation (OGD) in neuronal cell culture, but also that further upregulation of Ngb from endogenous levels using adeno-associated virus (AAV) serotype 1 mediated gene delivery protected neurons from OGD *in vitro* (Sun *et al.*, 2001). In the following years the same group reported AAV-mediated Ngb overexpression protected rat neurons from damage in an *in vivo* model experimental stroke (Sun *et al.*, 2003), demonstrating the powerful neuroprotective ability of this endogenous agent. The mechanism of this protection is unknown but has been shown to have multiple neuroprotective actions, such as:

i) Hypoxia signalling (Khan *et al.*, 2008)
ii) Free radical scavenging (Li *et al.*, 2011)
iii) NADH oxidase action to sustain anaerobic glycolysis (Brunori *et al.*, 2005)
iv) Inhibition of CytC-mediated PCD (Fago *et al.*, 2006b)

Upregulation of Ngb has been shown to be protective across a number of *in vitro* and *in vivo* models of cerebral ischaemia and / or reperfusion, which will be discussed at greater lengths within chapter 3 and 5.

1.10 LIMITATIONS OF PRE-CLINICAL STUDIES

1.10.1 Stroke Therapy Academic Industry Roundtable (STAIR) Guidelines

From the previous section it has been demonstrated that there have been a substantial number of failed clinical trials of neuroprotective agents, that had previously been shown to be effective in pre-clinical animal models. The reason behind this is unclear but a number of factors may play a part in this anomaly, for example factors such as, the choice

of animal model, the physiological monitoring utilised and the outcome measures assessed. For this reason, and in order to address these issues, a conference of academics and industry representatives was convened to suggest a set of guidelines for the evaluation of pre-clinical therapies known as the Stroke Therapy Academic Industry Roundtable (STAIR) initially in 1999, and reviewed in 2009 (Fisher *et al.*, 2009). The main guidelines are detailed in Table 1.1

Table 1.1: STAIR recommendations for preclinical stroke drug development

1.	Evaluate the candidate drug in permanent and temporary occlusion models and in both rodent and higher animal species
2.	Evaluate an adequate dose–response effect over a reasonable time window.
3.	Appropriate physiological monitoring and blinding should be performed.
4.	Histological and functional outcome measures should be assessed with prolonged survival to ensure that early treatment effects are not lost.
5.	If feasible, treatment effects should be confirmed in both sexes and aged animals.
6.	Treatment effects should be replicated in several laboratories, including both industry and academic location.
7.	Data, both positive and negative, should be published.

A systematic review by O'Collins *et al.* in 2006 of ~ 3500 articles published addressing various neuroprotective strategies between 1957 and 2003 showed that only 5 out of 550 of the drugs reported to be effective met the standards set by the STAIR guidelines (O'Collins *et al.*, 2006). One of the main findings within the review was a lack of randomisation and blinding, resulting in an overestimated efficacy of therapies. In fact, although there has been an overall trend towards improvement in stroke study design, only 36 % of studies report randomisation, 11 % report concealment, 29 % report blinded assessment of outcome, and 3 % reported use of power calculations in generation of sample size (Sena *et al.*, 2007).

1.10.2   Cerebral Ischaemia Models

There are a large number of pre-clinical brain ischaemia animal models in use for the study of stroke (reviewed in (Macrae, 2011)). They can largely be divided into global ischaemia, multifocal ischaemia or focal ischaemia. Global ischaemia is a model of circulatory failure, induced by cardiac arrest or cervical compression by neck cuff but cannot be truly regarded as a model of stroke. Multifocal ischaemia can be induced by injection of embolus material into a brain-supplying artery (Orset *et al.*, 2007). Focal ischaemia occurs as a result of reduction of blood flow in a specific region of the brain by occlusion of a major cerebral artery, such as the MCA – which is the most commonly affected blood vessel in human ischaemic stroke (Mohr *et al.*, 1986). The MCA can be occluded intravascularly using the intraluminal thread model (Longa *et al.*, 1989), or extravascularly by surgical occlusion by ligation, clipping, electrocauterisation (Tamura *et al.*, 1981) or by administration of the potent vasocontrictor endothelin-1 topically (Macrae *et al.*, 1993) or intraparenchymally (Sharkey *et al.*, 1993). All of these models can be adjusted to cause transient or permanent occlusion, with the exception of electrocoagulation models which are not reversible. Embolic stroke models have a number of advantages; embolic vessel occlusion is the most frequent cause of ischaemic stroke in humans and as such has good pathophysiological relevance. However, there is large variability in lesion size, distribution and location within this model (Brown *et al.*, 2010). This variability can be improved by placing the thrombi directly into the proximal MCA, although this is a very technically demanding procedure. Extravascular or surgical MCAO requires craniotomy and incision of the dura, which has been shown to alter brain temperature, intracranial pressure and BBB permeability (Hudgins *et al.*, 1970). Additional disadvantages include damage to autonomic nerves, potentially affecting cerebral blood-flow, and technical intricacy of procedure.

The intraluminal thread model used in the present study was developed by Koizumi *et al.* (1986) in rats, and uses an occluding suture or monofilament that is advanced into the internal carotid artery until it blocks the origin of the MCA, subjecting its vascular territory to ischaemia (Figure 1.15) (Koizumi *et al.*, 1986). The suture may be removed to allow for reperfusion or left in place for permanent occlusion. This model can produce a large and reproducible infarction, whilst being minimally invasive and not requiring a craniotomy. As with the alternative models there are a number of complications such as ipsilateral visual injury (Steele *et al.*, 2008), ECA ischaemia (Dittmar *et al.*, 2003), intraluminal thrombus formation (Muller *et al.*, 1994), and inadequate MCAO (Schmid-Elsaesser *et al.*,

1998). However, use of standardised monofilaments has been shown to reduce the incidence of these complications and as such none of these complications were noted in the present study. Although mainly reproducible, large variation in lesion size is present across animal species, strains and ages.
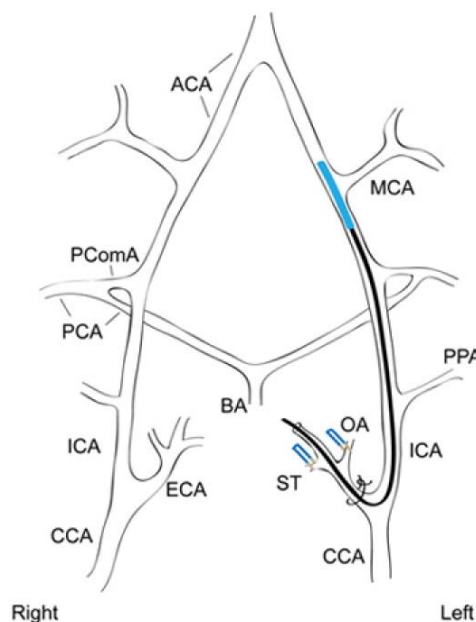
Figure 1.15:   Intraluminal thread model of focal ischaemia.

Filament is shown in the advanced position at the origin of MCAO, mediating occlusion.

ACA = Anterior Cerebral Artery;   MCA = Middle Cerebral Artery

PCA = Posterior Cerebral Artery;   ICA = Internal Cerebral Artery

ECA = External Carotid Artery;   CCA = Common Carotid Artery

BA = Basilar Artery;   PPA = Pterygopalatine Artery

1.10.3   Monitoring Physiological Variables

Other factors perhaps contributing to the poor bench-to-bedside translation include factors such as anaesthesia, monitoring of physiological variables, and experimental endpoint. Inhaled anaesthesia is superior to intraperitoneal or *i.v.* anaesthetics, as there is greater control of the depth and duration of anaesthesia (Zausinger *et al.*, 2002). In addition, mechanical ventilation shows decreased infarct variability in comparison to animals breathing spontaneously (Zausinger *et al.*, 2002). Physiological variables including brain temperature, blood pressure (BP), and blood gases can contribute to outcome and as such should be monitored where possible throughout the study. A reduction in BP could further

compromise cerebral blood flow (CBF) in ischaemic brain as a result of the subsequent loss of autoregulation; a raised BP will potentiate oedema and subsequent intracranial pressure. Additionally, levels of arterial CO_2 ($PaCO_2$) are a important in cerebral ischaemia as elevated $PaCO_2$ causes and increase in CBF and low $PaCO_2$ results in a reduction of CBF. Brain temperature is of significant importance as hypothermia has been shown to reduce infarct size and alter distribution (Busto *et al.*, 1989). An example of this was noted in a study of the NMDA receptor antagonist, MK-801, which had been shown to be protective in rodent models of MCAO, as previously described (section 1.4.2). However, further analysis showed administration of MK-801 induced hypothermia, and returning the animal to normothermia abolished any protective effect seen. Problems with these variables can be addressed in a pilot study, and although information regarding suture size, occlusion time and surgical procedures are available in the literature, these parameters may not be optimal for the desired model.

1.11 COMBINATION THERAPY

Taking into account the complex and "cross-talking" pathways that lead to cell damage following cerebral ischaemia, effective treatment could be achieved through administration of combined or serial treatments of a variety of agents. This approach has proven successful in other pathologies of CVD. Indeed, the majority of pre-clinical studies indicate that treatment with thrombolytics is suboptimal if not in combination with neuroprotective agents. At least additive but also synergistic effects have been demonstrated by combination of thrombolytics with neuroprotectants in pre-clinical models including, free radical scavengers (Asahi *et al.*, 2000), glutamate receptor antagonists (Meden *et al.*, 1993; Zivin *et al.*, 1991), anti-leukocyte adhesion molecules (Bowes *et al.*, 1995) and hypothermia (Kollmar *et al.*, 2004). A small randomised clinical trial using rt-PA in combination with the NMDA antagonist, lubeluzole, (Grotta, 2001) showed promising results, but was terminated early due to funding withdrawal as a result of the failure of the Diener Trial, 2000. A common problem in patients receiving rt-PA is the subsequent re-occlusion of cerebral vessels as a result of platelet activation in the ischaemic brain, early clinical trials combining rt-PA with anti-platelets such as tirofiban (Seitz *et al.*, 2004), abciximab (Gahn *et al.*, 2010), eptifibate (Pancioli *et al.*, 2008) and argatroban (Barreto *et al.*, 2008) have demonstrated lower rates of re-occlusion and yield higher rates of artery recanalisation.

Although the vast majority of combination studies have been addressing improvement in the action of rt-PA and reperfusion therapy, combined neuroprotective strategies have been used with some success in pre-clinical animal models. For example, NMDA receptor antagonists have been co-administered with a large number of neuroprotective agents. Combination of NMDA receptor antagonist (MK-801) with a GABA receptor agonist (muscimol) is synergistically effective with administration up to 3 h following onset of ischaemia in a rodent model of permanent focal ischaemia (Lyden *et al.*, 2000). MK-801 and the free radical scavenger α-Phenyl-*tert*-butyl-nitrone (PBN) in an *in vitro* model of OGD demonstrated substantial synergistic effects in combination (Barth *et al.*, 1996). Combination of MK-801 with the neuroprotective agent citicoline, demonstrated synergistic neuroprotection following 90 minute tMCAO in Sprague-Dawley rats, assessed mortality and infarct volume (Onal *et al.*, 1997). The NMDA receptor antagonist, dextrorphan, and the protein synthesis inhibitor, cycloheximide, demonstrated additive neuroprotective effects in a rodent model of 90 minute tMCAO. The combination reduced infarct by ~ 65 % when administered 15 min prior to ischaemia (Du *et al.*, 1996). Peptide inhibitors of the caspase family (z-VAD.FMK and z-DEVD.FMK) showed synergistic efficacy when used in combination with MK-801 following 2 h tMCAO in mice. This study demonstrated a synergistic effect with pre-treatment, and treatment at 1 h following ischaemia onset but not following 1 h reperfusion (Ma *et al.*, 1998). In *in vitro* brain slices basic fibroblast growth factor (bFGF) enhances and augments the protective effects of MK-801 against OGD.

In addition to neuroprotective combinations with NMDA receptor antagonists, synergistic effects have been observed with two different antioxidants, U-74389G and U-101033E. Sprague-Dawley rats were subjected to 90-minute tMCAO, and treatment was administered 15 min prior to ischaemia, during ischaemia 15 min prior to reperfusion and 45 min following reperfusion. Synergistic improvement was observed in functional recovery but no improvement with combined therapy was noted regarding lesion size at 7 d (Schmid-Elsaesser *et al.*, 1999). Treatment with erythropoietin, the enhancer of RBC production, has been shown to be neuroprotective in pre-clinical models of stroke (reviewed in (Minnerup *et al.*, 2009)). Erythropoietin (EPO) treatment in combination with the AngII receptor inhibitor and vasodilator, olmesartan, increased survival and neurological recovery at day 30 to a greater extent than either treatment alone (Faure *et al.*, 2006) in gerbils subjected to carotid artery ligation.

In addition to improving the safety of reperfusion therapy, and increasing the therapeutic window, the use of combined therapies may enable a decrease in the doses required of either agent, resulting in a subsequent improvement in adverse side effects / dangers. Combinations of neuroprotective agents represent a relatively new field of stroke therapy, with incredibly large potential.

In the present study combined anti-oxidant and anti-apoptotic intervention is assessed, through gene delivery and pharmacological interventions, respectively. Utilising a gene delivery-mediated antioxidant strategy allows for long-term overexpression of the endogenous protective agent, Ngb. Whereas, transient inhibition of the apoptotic agent JNK through pharmacological intervetion, allows for the biphasic regenerative response of JNK in the late stages following cerebral ischaemia.

1.12 GENE THERAPY

Gene therapy can be broadly described as the insertion of a gene into an organism in an attempt to correct defective genes or for delivery of therapeutic genes. In 1972 Friedmann and Roblin published a paper in Science proposing a role for genetic modifications of cells using exogenous DNA (Friedmann *et al.*, 1972). This was shown to be possible in 1977, when the thymidine kinase (TK) gene was successfully transferred into TK$^-$ L mammalian cells (Wigler *et al.*, 1977) using herpes simplex virus. Eight years later, successful gene therapy occurred *in vivo* using the retroviral vector N2 to express the NeoR marker gene (Eglitis *et al.*, 1985). Gene transfer was originally considered for the treatment of monogenic diseases such as Duchenne's muscular dystrophy and cystic fibrosis where replacement of a non-functioning gene should restore a normal phenotype. However, gene therapy can now be utilised across a wide range of acquired diseases including cancer, cardiovascular disease and neurological disorders. Up to March 2011, there have been a total of 1714 gene therapy clinical trials worldwide (Figure 1.16). At present, the vast majority of clinical trials are for cancer gene therapy (64.6 %), with the second most common being CVD at 8.5 %, and 2 % of all worldwide clinical trials for gene therapy being for neurological disorders. In 1990, the first human clinical trial was embarked on to treat the genetic disorder, adenosine deaminase (ADA) deficiency, in two children. ADA deficiency is a rare form of severe combined immunodeficiency (SCID), in which the highly metabolically active T and B cells of the immune system are unable to divide as a result of deoxyadenosine build-up. In addition, there is a build-up of S-

adenosylhomocysteine which is toxic to immature lymphocytes. Subsequently, the immune system in patients with this disorder is severely compromised or completely absent. T-lymphocytes of the 2 patients were removed and transduced *ex vivo* with retroviral-mediated transfer of ADA gene. Transduced cells were selected and expanded *ex vivo* before being returned to the patient. This trial ultimately led to the normalisation of both cellular and humoral immune responses, and ten years post transfection the ADA wild-type gene could still be detected within one of the patients (Muul *et al.*, 2003). This groundbreaking study demonstrated for the first time the enormous clinical potential of gene therapy.
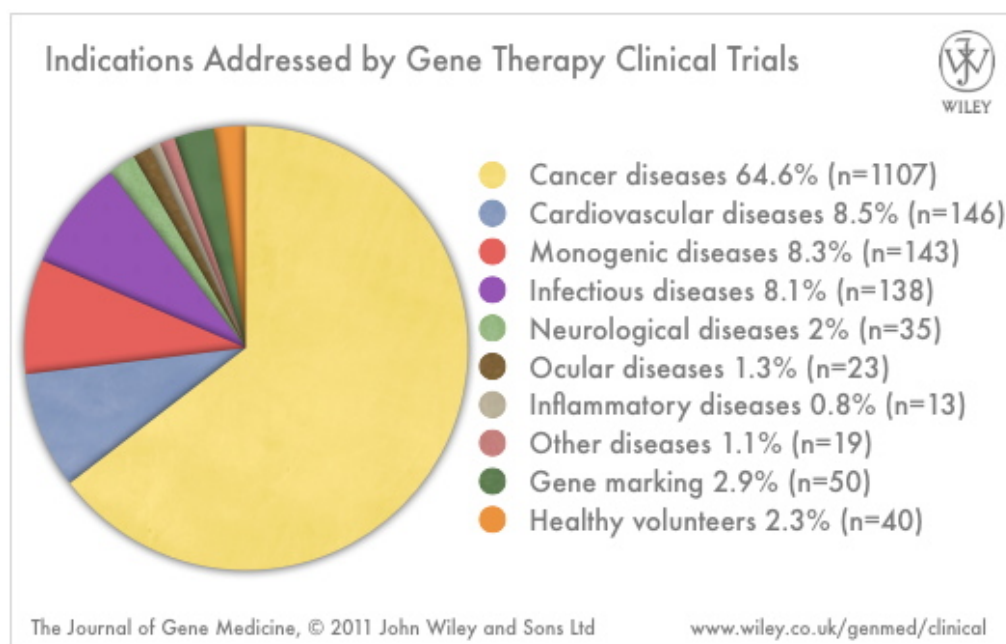
Figure 1.16:   Gene Therapy Clinical Trials

Disease targets for gene therapy presented as a proportion of ongoing clinical trials. Data taken from (http://www.abedia.com/wiley/indications.php).

1.13   GENE THERAPY IN THE BRAIN

1.13.1   Routes of Administration

The majority of chronic neurological diseases, both genetic and acquired, do not respond well to small molecule or pharmacological interventions, and have no approved long-term therapy. Gene therapy offers therapeutic potential in both genetic and acquired

neurological disorders, but clinical advances have been slow in this field. Route of administration remains the main obstacle of gene delivery for the nervous system, as entrance to the CNS is limited by both skeleton structure and by tight regulation of the chemical microenvironment by the BBB (Shi *et al.*, 2000). Predictably, the BBB prevents the vast majority of gene transfer vehicles from entering the CNS following systemic administration. Therefore, the most utilised route of administration has been direct injection into specific structures of the brain parenchyma; however spread from injection site is low following direct stereotactic injection. Convection-enhanced delivery (CED) has been shown to vastly improve the distribution of viral vectors, by slowly injecting a larger volume under pressurised conditions (Bobo *et al.*, 1994). However, even with use of CED, distribution of viral vectors remains limited to the selected brain structure. Gene transfer vehicles can also be administered into the CSF via the intrathecal space or lateral ventricles. In the neonatal mouse brain, direct injection into the CSF allows for widespread delivery throughout the nervous system and provides an ideal therapy for the treatment of monogenic neurological disorders (Passini *et al.*, 2001). However, in adult rodent models the distribution pattern is greatly restricted following injection into the CSF, reducing the benefit of this delivery route in the treatment of neurological diseases. By far the most convenient and clinically relevant delivery of gene transfer vehicles to the brain would be by systemic administration. PEGylated immunoliposomes (PILs) can be defined as molecular 'Trojan horse' technology that carries plasmid DNA or RNA with brain-specific promoters in the interior of a nanocontainer to mask the agent from the host's immune system (Zhang *et al.*, 2002c). The PILs are targeted to the brain by formulation with monoclonal antibodies for specific receptors such as transferrin and insulin – abundant on the brain capillary endothelium. Numerous studies have shown abundant biodistribution of reporter genes in the CNS, with minimal transduction in other organs, following systemic administration of brain-targeted PILs, however gene expression duration has been shown to be transient in comparison with viral vector-mediated gene transfer.

1.13.2   Viral Vectors

Human adenoviral vectors (hAds) (24.2 %) and retroviral vectors (20.7 %) make up the vast majority of the viral vectors used in all clinical trials, with adeno-associated viruses (AAVs) and lentiviral vectors (LVs) only making up 4.7 % and 2.3 % of all trials, respectively (Figure 1.17). However, the challenging conditions of directing treatment to

the brain means the selection of the appropriate viral vector for the specific disease model is vital in optimising its efficiency as a tool for treating neurological disease. Indeed, retroviral vectors are not utilised in the treatment of neurological disorders as the terminally differentiated state of most neurons precludes the use of this vector that is reliant on cell replication for stable maintenance in cells. To date, AAVs are the most commonly utilised viral vectors for gene delivery to the brain.
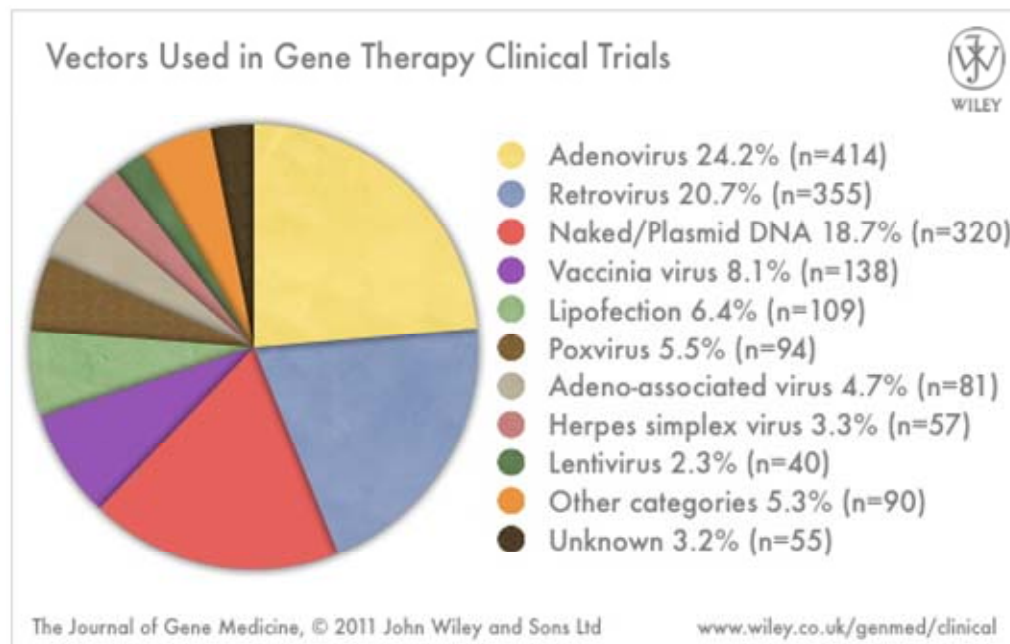
Figure 1.17:   Viral Vectors Used in Clinical Trials

Viral vectors used in gene therapy clinical trials presented as a proportion of ongoing clinical trials. Data taken from (http://www.abedia.com/wiley/indications.php).

1.13.2.1   Adeno-Associated Virus (AAV)

AAVs are non-enveloped viruses of the parvovirus family with a linear single-stranded 4.7 kb DNA genome. There are approximately 35 known serotypes of AAV and over 100 variants which have been isolated and at least 10 serotypes have been engineered into rAAV vectors. The long-term expression observed from AAVs is enabled as a result of the low levels of innate immune response present following administration. Indeed, only transient infiltration of neutrophils and chemokines has been detected following AAV administration (Zaiss *et al.*, 2002). The AAV2 serotype was the first to be cloned into bacterial plasmids in 1982 (Samulski *et al.*, 1982). Since then rAAV2 vectors have made

up the majority of the research conducted using AAV-based vectors due to their broad tissue tropisms and safety. However, recently more attention has been paid to alternate serotypes, including mixed capsid vectors. When considering neurological disorders, it has been demonstrated that rAAV8 and rAAV9 (among others) have significantly higher distribution and transduction of neurons than rAAV2 in the CNS. The transduction efficiency of rAAV serotypes in the CNS is discussed fully in Results Chapter 3.

Since 2003, 6 therapeutic genes in 8 experiments of pre-clinical stroke have been delivered using rAAV vectors, outlined in Table 1.2. All studies utilised either intraparenchymal or intracerbroventricular delivery of transgenes mediated by rAAV1 or rAAV2. Although greater transduction of the CNS has been demonstrated with AAV8 and AAV9, these vectors are yet to be utilised in a model of cerebral ischaemia.

Table 1.2:   **rAAV-mediated gene delivery experiments for ischaemic stroke**

Transgene	Stroke model	Animal strain	rAAV	Delivery	Total virus	Delivery time	Reference
Netrin-1	tMCAO	CD-1 mice	rAAV1	Basal ganglia	2×10^9	1 w prior	(Lu *et al.*, 2012)
GLT-1	tMCAO	Fisher 344 rats	rAAV1	Striatum	6×10^{10}	3 w prior	(Harvey *et al.*, 2011)
Netrin-1	tMCAO	Unspecified rats	rAAV1	Striatum	2×10^{10}	1 h post	(Sun *et al.*, 2011)
IGF-1	pMCAO	CD-1 mice	rAAV2	Caudate	2×10^{10}	24 h post	(Zhu *et al.*, 2009)
IGF-1	pMCAO	CD-1 mice	rAAV2	Caudate	2×10^{10}	3 w prior	(Zhu *et al.*, 2008)
VEGF	tMCAO	CD-1 mice	rAAV1	Lateral ventricle, caudate	4×10^9	5 d prior	(Shen *et al.*, 2008)
VEGF	tMCAO	CD-1 mice	rAAV2	Lateral ventricle, caudate	1×10^{10}	5 d prior	(Shen *et al.*, 2006)
AIP	tGCI	Sprague-Dawley rats	rAAV2	Hippocampus	2×10^{10}	5 d prior	(Cao *et al.*, 2004)
Ngb	tMCAO	Sprague-Dawley rats	rAAV2	Cortex, striatum	2.4×10^{11}	3 w prior	(Sun *et al.*, 2003)

Growth factors represent the most commonly utilised transgenes for treatment of cerebral ischaemia. Zhu *et al.*, (2008) initially reported rAAV2-mediated insulin-like growth factor-1 (IGF-1) upregulation 3 weeks prior to pMCAO resulted in a significantly improved neurological deficit and a significantly reduced lesion size compared to reporter gene-expressing control. They demonstrated this improvement was as a result of

neovascularisation and neurogenesis within the ischaemic hemisphere (Zhu *et al.*, 2008). This study was replicated in 2009 by the same group, but rAAV2-IGF-1 was administered 24 h following the initial onset of ischaemia. They reported neovascularisation and neurogenesis in the post-ischaemic brain however neurological deficit and lesion size were not assessed (Zhu *et al.*, 2009). The benefit of VEGF upregulation on potential neovascularisation and subsequent protection from brain ischaemia utilising rAAV1 and rAAV2 vectors was assessed (Shen *et al.*, 2006). Following administration of rAAV2-VEGF 5 d prior, CD-1 mice were submitted to 45 min tMCAO with 7 d recovery. rAAV-2 mediated overexpression of VEGF significantly reduced lesion volume in comparison to reporter-gene expressing and saline controls – neurological deficit or extent of neovascularisation was not assessed in this study (Shen *et al.*, 2006). In 2008, the same group assessed the effect of utilising a VEGF transgene which could be 'switched-on' under hypoxic conditions by HIF-1, to address the problems with observed long-term, uncontrolled overexpression of VEGF in the brain, such as hemangioma (Shen *et al.*, 2008). It was reported that increased VEGF mediated subsequent neovascularisation in the brains of rAAV1-VEGF treated mice that had undergone tMCAO procedure in comparison to normoxic controls. However, the effect of increased CBF through neovascularisation on lesion size or neurological deficit was not reported (Shen *et al.*, 2008). It has been demonstrated that upregulation of the angiogenic factor netrin-1 by rAAV1 had no effect on lesion size but improved motor function recovery following tMCAO in rats (Sun *et al.*, 2011) (Lu *et al.*, 2012). Sun *et al.* (2011) occluded the MCA for 60 min and animals were recovered for 56 days, with behavioural testing at day 35. rAAV1-netrin-1 was administered following 1 h reperfusion, post-ischaemia. Netrin-1 treated animals exhibited increased microvessel density in the peri-infarct area, which related to significantly improved motor function at day 35, but no improvement in lesion size (Sun *et al.*, 2011). 7 days following injection with rAAV1-netrin-1, Lu *et al.* (2012) occluded the MCA of CD-1 mice for 60 min with 7 d recovery. They also reported no change in lesion size but an improvement in behavioural recovery following tMCAO at d 7 (Lu *et al.*, 2012).

Neuroprotective agents represent the other category of transgenes upregulated by rAAV vectors in pre-clinical models of cerebral ischaemia. Neuroprotection afforded by rAAV2-mediated Ngb upregulation in a model of tMCAO was assessed 3 weeks following administration of rAAV-Ngb in male Sprague-Dawley rats exposed to 90 min ischaemia with recovery for 24 h (Sun *et al.*, 2003). rAAV2-Ngb treated animals exhibited a significantly reduced lesion size and a reduced neurological deficit compared to reporter-

gene expressing rAAV and saline control (Sun *et al.*, 2003). Upregulation of the glutamate transporter-1 (GLT-1) by rAAV1 was shown to reduce lesion size, assessed by TTC staining, and improve neurological deficit when administered 3 w prior to 60 min tMCAO in Sprague-Dawley rats (Harvey *et al.*, 2011).

Although rAAV mediated transgene expression represents a safe and effective system for ischaemic stroke gene delivery, there are a number of drawbacks associated with this vector. Neuroprotective strategies require administration prior to insult as a result of the relatively long transcriptional period observed with AAVs. Additionally, serotypes with improved neurotropism are yet to be assessed in models of cerebral ischaemia.

1.13.2.2   *Adenoviral Vectors*

Adenoviruses are non-enveloped dsDNA viruses with an icosahedral capsid consisting of 3 main structural proteins, hexon, fiber and penton base and several minor capsid proteins. Adenoviruses were first isolated from tonsils and adenoid tissue [Rowe et al. 1953] and are infectious human viruses, which often cause mild infection of the gastrointestinal and upper respiratory tract. As adenoviruses are non-integrating viral vectors the risk of insertional mutagenesis is removed, and in the non-dividing cells of the nervous system transgene expression can be maintained for several months. However, the major shortcoming of adenoviral vectors is their immunogenicity. Many individuals already possess immunity to adenoviral vectors, and will produce neutralising antibodies and T-cells directed at Ad proteins. This response can be ameliorated through use of third generation or helper-dependant / "gutless" adenoviruses. Helper-dependant viruses have essential regions of the virus genome deleted and rely on essential virus functions from a helper virus. By deleting the majority of the viral genome transgene expression is sustained with mimimal activation of the immune response. Ad serotype 5 is the most commonly utilised serotype for adenoviral gene delivery studies, and is infact the only serotype that has been used in the pre-clinical studies of cerebral ischaemia (Table 1.3).

In accordance with studies assessing AAV-mediated VEGF upregulation, replication-deficient Ad5 (rdAd5)-mediated upregulation of VEGF was reported to reduce levels of apoptosis and improve neurological recovery following permanent ligation of the CCA with 2 h subsequent hypoxia (H/I) in neo-natal Sprague-Dawley rats (Zheng *et al.*, 2010). Interestingly, 5 x 10^9 pfu rdAd5-VEGF was administered stereotactically into the cortex 3

days post H/I. However, although a significant improvement was observed from saline control, improvement could be partly attributed to the 2 week post-natal period of rapid neurological growth and development, and as such this study serves only as a model of neo-natal hypoxia-ischaemic brain damage (Zheng *et al.*, 2010).

Table 1.3:   Adenovirus-mediated gene delivery experiments for ischaemic stroke

Transgene	Stroke model	Animal strain	rAAV	Delivery	Total virus (pfu)	Delivery time	Reference
VEGF	H/I	Sprague-Dawley rats	rdAd5	Lateral ventricle	1×10^8	3 d post	(Zheng *et al.*, 2010)
BDNF	tMCAO	KM mice	rdAd5	Caudate	?	7 d prior	(Shi *et al.*, 2009)
GluR6	tGCI	Sprague-Dawley rats	rdAd5	Hippocampus	1×10^{10}	5 d prior	(Li *et al.*, 2009)
APE/Ref-1	tMCAO	C57BL/6J mice	rdAd5	Cortex, striatum	1.2×10^7	3 d prior	(Kim *et al.*, 2009)
MK	pMCAO	SHR	rdAd5	Lateral ventricle	9×10^8	90 min post	(Ishikawa *et al.*, 2009)
TIMP-1 TIMP-2	tGCI	C57BL/6J mice	rdAd5	Striatal	5×10^3	72 h prior	(Magnoni *et al.*, 2007)
COX-1	tMCAO	Long-Evans rats	rdAd5	Lateral ventricle	1×10^8	72 h prior	(Lin *et al.*, 2006)
HB-EGF	tMCAO	Wistar rats	rdAd5	Lateral Ventricle	1.1×10^8	3 d post	(Sugiura *et al.*, 2005)

Brain-derived neurotrophic factor (BDNF) has been shown to be protective in a number of models of cerebral ischeamia, through promotion of survival and differentiation of neuronal tissue. However, long-term overexpression of BDNF causes negative side effects including seizure risks. It has therefore been demonstrated that controlled upregulation of BDNF under hypoxic / ischaemic conditions, utilising an hypoxia response element (HRE) activated promotor, attenuated infarct volume and neurological deficit following 60 min tMCAO in KM mice (Shi *et al.*, 2009). Animals were pre-treated with an undisclosed amount of virus 7 days prior to tMCAO, and control studies were performed to ensure BDNF was upregulated only in response to hypoxia *in vitro* or tMCAO procedure *in vivo* (Shi *et al.*, 2009). Apurinic/apyrimidinic endonuclease/redox effector factor-1 (APE/Ref-1) is a multifunctional enzyme responsible for repairing apurinic/apyrimidinic (AP) sites in DNA, generated by reactive oxygen species following cerebral ischaemia / reperfusion. Following double injection (1.4×10^7 total pfu) of rdAd5-APE/Ref-1 3 d prior to onset of

tMCAO (60 min), infarct volume is reduced from ~ 140 mm^3 to < 10 mm^3 in C57BL/6J mice, assessed by TTC staining (Kim *et al.*, 2009). However *n* numbers were particularly low for this *in vivo* study (*n* = 3 / group). Midkine (MK) is a neuroprotective agent which acts through various biological activities including chemotaxis of inflammatory cells, promotion of angiogenesis and migration of neuronal cells. Post-ischaemic upregulation of MK by rdAd5 (9 x 10^8 pfu, 90 min post onset) administered stereotactically into the striatum resulted in a significant reduction in lesion size and increase in migration of neuronal precursor cells in spontaneously hypertensive rats (SHRs) (Ishikawa *et al.*, 2009).

1.13.2.3   Lentiviral Vectors

Lentiviruses are a subclass of retroviruses that are being studied and developed for use in neurodegenerative disorders owing to their ability to transduce the post-mitotic cells of the nervous system (Naldini *et al.*, 1996b). Lentiviruses have a relatively large packaging capacity of up to 8 kb and an ability to infect a wide range of cells. They are minimally immunogenic having been shown to sustain gene expression for several months (Zhang *et al.*, 2002b) without detectable pathology (Abordo-Adesida *et al.*, 2005; Azzouz *et al.*, 2004). Gene transfer through lentivirus is relatively stable as the transgene integrates into the host genome. However this integration raises one of the main concerns of lentivirus' safety profile, insertional mutagenesis resulting in transcription of pro-oncolytic genes. In response to this safety concern, a new generation of lentiviral vectors have been engineered, non-integrating lentiviral vectors. They are considered much safer than their integrating counterparts as a result of mutations in the conserved acidic residues in the viral integrase gene, catalytic site or chromosome binding site. These mutations render the vectors integration defective without interrupting viral DNA synthesis or accumulation in the nucleus (Apolonia *et al.*, 2007; Leavitt *et al.*, 1996). Efficient sustained transgene expression *in vivo* has been demonstrated in the rat ocular and brain tissue at high levels (Yanez-Munoz *et al.*, 2006). Although the safety profile is highly improved in non-integrating lentiviral vectors, they have yet to be utilised in a study of cerebral ischaemia (Table 1.4).

Table 1.4: **Lentivirus-mediated gene delivery experiments for ischaemic stroke**

Transgene	Stroke model	Animal strain	Integrating	Delivery	Total virus (TU)	Delivery time	Reference
Nampt	tMCAO	Sprague-Dawley rats	Yes	Lateral ventricle	2×10^6	3 w prior	(Wang *et al.*, 2011)
MMP-9 shRNA	tMCAO	Sprague-Dawley rats	Yes	Striatal	?	2 w prior	(Hu *et al.*, 2011)
nNOS-N$_{1-133}$	tMCAO	C57BL/6 mice	Yes	Cortex	4×10^6	5 d prior	(Zhou *et al.*, 2010)
GDNF	tMCAO	Wistar rats	Yes	Striatum	1×10^6	4 w prior	(Arvidsson *et al.*, 2003)

It has been demonstrated that lentiviral mediated overexpression of the neuroprotectant, nicotinamide phosphoribosyltransferase (Nampt), significantly reduced lesion size and improved neurological deficit in Sprague-Dawley rats following 2 h tMCAO with 24 h recovery, through the SIRT1-dependent AMPK pathways of survival (Wang *et al.*, 2011). Matrix metalloproteinases-9 (MMP-9) has been shown to be a key orchestrator of BBB breakdown following cerebral ischaemia / reperfusion (Hu *et al.*, 2009). Lentiviral-mediated inhibition of MMP-9 using a short hairpin RNA (shRNA) maintained the structural integrity of the brain following tMCAO; however no improvement in lesion size or neurological recovery was reported (Hu *et al.*, 2011). A comprehensive study by Zhou *et al.* (2010) into the activation of nNOS by PSD-95 demonstrated that lentivirus-mediated disruption of the nNOS/PSD-95 interaction by nNOS-N$_{1-133}$ reduced lesion size and improved neurological recovery following tMCAO. The same study assessed the specific activation of nNOS by PSD-95 as directly inhibiting nNOS has been demonstrated to cause severe side due to their key physiological functions in the CNS (Zhou *et al.*). Glial cell line-derived neurotrophic factor (GDNF) has been implicated as a potential therapeutic target for cerebral ischaemia in a number of pre-clinical models. However, lentiviral-mediated GDNF upregulation showed no improvement in lesion size or neurological deficit following tMCAO from reporter-gene expression lentivirus control (Arvidsson *et al.*, 2003).

1.13.2.4 *Herpes Simplex Virus (HSV)*

HSV type 1 (HSV-1) has a relatively large genome of 150 kb, which facilitates DNA inserts of up to 30 - 40 kb and is able to infect a broad range of cell types including non-

dividing cells. HSV-1 is neurotrophic and can establish lifelong presence in neurons. Due to this natural tropism, the majority of gene transfer applications of HSV-1 vector have been directed toward the nervous system. HSV-1 vector systems can be divided recombinant virus systems and amplicons, and recombinant viral vectors can be further divided into, replication-competent attenuated vector and replication-incompetent attenuated vector. Replication-competent HSV-1 vectors are useful in cancer therapy in the rapidly dividing cells of the tumour, but outwith this disease model exhibit cytopathic effects. Replication-incompetent HSV-1 vectors have a better safety profile as they exhibit diminished toxicity, but result in severely reduced transgene expression. Amplicons are similar to a helper-dependant adenovirus or 'gutless' DNA vector system where only a replication and packaging DNA sequence is present in the viral vector genome. Advantages of this system are a low immune response and reduced cellular toxicity compared to the recombinant HSV-1 vectors.

Table 1.5:   HSV-1-mediated gene delivery experiments for ischaemic stroke

Transgene	Stroke model	Animal strain	Recombinant / Amplicon	Delivery location	Total virus	Delivery time	Reference
TdGR	tMCAO	Sprague-Dawley rats	Amplicon	Striatum	3×10^4 particles	18 h prior & 2 h post	(Cheng *et al.*, 2009)
HSP27	tMCAO	Sprague-Dawley rats	Recombinant	Striatum	3×10^6 pfu	30 min post	(Badin *et al.*, 2009)
GADD34	tMCAO	C57BL/6 mice	Recombinant	Cortex	1×10^6 pfu	24 h prior	(McCabe *et al.*, 2008)
GDNF	tMCAO	Sprague-Dawley rats	Amplicon	Striatum	3×10^4 particles	4 d prior & 3 d post	(Harvey *et al.*, 2003)

Badin *et al.* (2009) demonstrated upregulation of HSP27 but not HSP70 by a replication-competent recombinant HSV-1 vector resulted in a significantly reduced lesion size following 30 min tMCAO with 24 h recovery. Importantly, this reduction in lesion size was reported with administration of vector 30 min post onset of cerebral ischaemia, however no subsequent improvement in neurological deficit was noted (Badin *et al.*, 2009). Replication-incompetent recombinant HSV-1 vectors represent an improved safety profile in comparison to replication-competent recombinant vectors, however transduction efficiency is compromised. In accordance with this, it was demonstrated that replication-incompetent recombinant HSV-1-mediated upregulation of GADD34 had no effect on lesion size following endothelin-1 induced tMCAO (McCabe *et al.*, 2008). HSV-1 amplicons are the most clinically relevant of the HSV-1 vector systems in that they have

the best safety profile following administration to the brain. HSV-1 amplicon-mediated upregulation of GDNF was initially demonstrated to have no significant improvement in lesion size in comparison to reporter-gene-expressing control virus but demonstrated a significant improvement in neurological recovery at day 7 post tMCAO (Harvey *et al.*, 2003). More recently selective overexpression of a dominant negative glucocorticoid receptor was shown to inhibit the detrimental actions of glucocorticoids following cerebral ischaemia, when administered 18 h prior to but not 2 h post onset of ischemia in a model of tMCAO (Cheng *et al.*, 2009).

1.13.3 Future Prospects of Gene Delivery in Stroke

At present no clinical trials have been initiated utilising gene delivery as a therapeutic strategy for stroke, there are a number of reasons for this. With the minimal success observed for pre-clinical models to identify an effective pharmacological strategy for clinical translation, the road towards clinical trials for the far newer science of gene-therapy remains arduous. Although a significant amount of progress has been made in vector safety and targeting, still far more needs to be done with optimisation of vectors and delivery routes. The time delay in protein expression following administration of viral vector also remains an obstacle for gene delivery, as the vast majority of neuronal damage occurs within hours to days following onset of ischaemia. In addition, 'door-to-needle' time in stroke patients is notoriously long and as such gene delivery has often been regarded as only having a clinical future as a preventative parameter or as a neuroregenerative strategy. Currently a Phase I single administration dose escalation study for neuroregeneration is being performed in Glasgow's Southern General Hospital, known as the Pilot Investigation of Stem Cells in Stroke (PISCES). 12 patients who have been left disabled by ischaemic stroke are being administered ascending doses of ReN001 neuronal stem cells, and will be assessed by the modified Rankin Score and Barthel Index at 1 year post-administration. However, as the vast majority of the currently available therapies for stroke are preventative, identification of a safe neuroprotective agent to be upregulated long-term by gene delivery offers a novel, safe strategy in stroke treatment. This would prevent the side-effects observed with chronic administration of anti-platelet or anti-coagulant preventative drugs, including increased risk of haemorrhagic stroke. Additionally, gene delivery mediated neuroprotective pre-treatment in combination with immediate pharmacological therapy at time of infarct represents a potentially effective

strategy in combating the multifactorial process involved with ischaemic stroke progression.

1.13.3.1   Canine Adenovirus

Despite successful transduction of CNS cells by a number of viral vectors, problems still impede the advancement of gene therapy strategies for neurological disorders. One of the most significant unmet needs is the limited diffusion of viral vectors from the injection site, resulting in the requirement for multiple stereotactic injections to guarantee sufficient spread across the affected area. Canine adenovirus serotype 2 (CAV2) is a xenogenic adenoviral vector, which induces a very low level of innate immune response in comparison to hAd5. It has been previously reported that CAV2 preferentially transduces neurones (Peltekian *et al.*, 2002) and spread from injection site is extensive following stereotactic injection (Soudais *et al.*, 2001). Recognition of CAV2 on the neuronal membrane is primarily CAR-dependant and trafficking from cell surface is endosomal and bidirectional, with a bias for retrograde transport (Salinas *et al.*, 2009). CAV2 has been researched thoroughly over the last decade and has been shown to mediate successful gene transfer resulting in improvement of neurological disorders across a number of pre-clinical studies. For example, CAV2-mediated gene transfer of sulfoglucosamine sulfohydrolase (SGSH) in a model of mucopolysaccharidosis IIIA (MPS IIIA), was reported to almost completely reverse presence of vacuoles in the brain (a symptom of MPS IIIA) following neonatal administration in MPS IIIA mice (Lau *et al.*, 2010). Ongoing studies are also assessing the reversal or inhibition of neurodegeneration in Parkinson's disease medated by CAV2. CAV2 mediates highly efficient and reliable gene transfer to the nervous system following single stereotactic injection with minimal immunogenicity, and as such offers a potential new viral vector for use in the treatment of ischaemic stroke among other neurological disorders.

1.14 AIMS

The principle aims of this thesis were to assess the neuroprotective efficacy of gene delivery-mediated Ngb upregulation alone and in combination with pharmacological (SP600125) inhibition of JNK. This was divided into four separate studies:

- Determining the optimal vector available for *in vitro* and *in vivo* delivery of Ngb. This was achieved by assessing transduction efficiency of reporter gene expressing viral vectors into a B50 rat neuronal cell line and transduction spread from injection site following stereotactic injection in SHRSPs.

- Assessing the efficacy of Ngb upregulation and JNK inhibition alone and in combination in an *in vitro* model of hypoxia / reoxygenation, using B50 rat neuronal cells, across a variety of cell viability assays.

- Conduct a pilot control *in vivo* study to optimise neurological assessments and *ex vivo* analysis following 45 min tMCAO, prior to *in vivo* intervention study.

- Conduct a randomised and blinded *in vivo* pre-clinical intervention study to determine the efficacy of Ngb upregulation and JNK inhibition following tMCAO in male SHRSP rats, with outcome measures of lesion size and neurological deficit.

Chapter 2:

Materials & Methods

2.1   CHEMICALS

All chemicals, unless otherwise stated, were obtained from Sigma-Aldrich (Poole, UK) and were of the highest grade obtainable. All cell culture reagents were obtained from Gibco (Paisley, UK) unless otherwise stated. Dulbecco's calcium and magnesium free phosphate buffered saline (PBS) were obtained from Lonza (Basal, Switzerland).

2.2   CELL CULTURE

All tissue culture work was performed using a biological safety class II vertical laminar flow cabinet in sterile conditions. Cell lines were maintained in the appropriate cell culture media (Table 2.1) and incubated at 37 °C in a 5 % CO2 atmosphere.

2.2.1 Maintenance of Established Cell Lines

Cells were grown as a monolayer and medium was replenished every 3 - 4 days. Cells were routinely passaged at approximately 80 % confluence to prevent overgrowth and loss of surface contact. To passage, cells were washed twice in PBS and incubated in 5 ml of trypsin-ethylenediamine tetra-acetic acid (trypsin-EDTA; Gibco, Paisley, UK) for approximately 5 min at 37 °C or until the majority of the cells had detached from the flask. The action of trypsin-EDTA was then prevented by the addition of 5 ml complete medium. Cells were pelleted by centrifugation at 1500 rpm for 5 min and resuspended in complete medium for passaging or plating.   Before plating, cells were counted using a haemocytometer to ensure the required seeding density.

2.2.2   Cryo-Preservation and Recovery of Cultured Cell Lines

Cells were harvested as described above and resuspended in 2 ml complete medium supplemented with 10% dimethyl sulphoxide (DMSO) per T-150 cm^3 cell culture flask of cells. 1 ml of cell suspension was aliquoted into cryo-preservation vials and cooled at a constant -1 °C / min to - 80 °C using isopropanol. Frozen vials were stored indefinitely in liquid nitrogen. Cryo-preserved cells were recovered by rapidly thawing to 37 °C followed by drop-wise addition of 10 ml pre-warmed complete medium, to allow for slow change in osmotic gradient. Cells were pelleted by centrifugation at 1500 rpm for 5 min then

resuspended in complete medium before addition to a T-25 cm^3 cell culture flask. Cells were incubated overnight at 37 °C and medium changed the following day.

2.2.3   Hypoxic Challenge

B50 rat neuronal cells were placed in a hypoxic chamber (Modular Incubator Chamber Mic-101, Bilrups-Rothenberg) in serum free medium for a time course of 3, 6, 9 or 18 h, with 24 h reoxygenation in the standard incubator before any experimental analysis. Cells were transduced with lentivirus overexpressing neuroglobin (lenti-Ngb) or lentivirus overexpressing green fluorescent protein (lenti-GFP) for four h in serum free medium as previously described, 48 h prior to hypoxia. JNK inhibitor (SP600125, 20 µM) or volume matched DMSO vehicle control was administered 10 min prior to hypoxia and re-administered for re-oxygenation period in fresh complete medium. The hypoxic chamber was perfused with gas (1 % O_2, 5 % CO_2 and balance N_2) at a rate of 25 L / min for 4 min to ensure all atmospheric air had been removed, before sealing and placing in a 37 °C incubator.

Table 2.1: **Cell lines and media used for culture cells used in this study**

Cell type	Description	Cell culture medium used
B50	Immortalised rat neurones from neuroblastoma	Dulbecco's Modified Eagle Medium (DMEM)/low glucose with no phenol red (Gibco, Paisley, UK) supplemented with 10 % (v/v) foetal calf serum (FCS), 1 % (v/v) penicillin, 100 µg/ml streptomycin and 2 mM L-glutamine
DK Zeo	Immortalised canine kidney cells	DMEM/Glutamax™ supplemented with 10% (v/v) FCS, 110 µg/ml sodium pyruvate, 100nM non-essential amino acids, 1% (v/v) penicillin, 100 µg/ml streptomycin, 500 µg/ml geneticin (G418)
293T	Transformed human embryonic kidney cell line	Minimum Essential Medium (MEM) (Gibco, Paisley, UK) supplemented with 10% (v/v) FCS, 1% (v/v) penicillin, 100 µg/ml streptomycin and 2 mM L-glutamine
293	Immortalised human embryonic kidney cell line	MEM (Gibco, Paisley, UK) supplemented with 10% (v/v) FCS, 2 mM L-glutamine, 1% (v/v) penicillin, and 100 µg/ml streptomycin
CHO	Immortalised Chinese hamster ovary cells	DMEM/F-12 medium (Gibco, Paisley, UK) supplemented with 10% (v/v) FCS, 2 mM L-glutamine, 1% (v/v) penicillin, and 100 µg/ml streptomycin
A549	Immortalised adenocarcinomic human alveolar basal epithelial cells	RPMI 1640 medium (Gibco, Paisley, UK) supplemented with 10% (v/v) FCS, 2 mM L-glutamine, 1% (v/v) penicillin, 100µg/ml streptomycin
Hep G2	Immortalised human liver carcinoma cell	MEM (Gibco, Paisley, UK) supplemented with 10% (v/v) FCS, 2 mM L-glutamine, 1% (v/v) penicillin, and 100 µg/ml streptomycin

2.3   GENERAL MOLECULAR BIOLOGY TECHNIQUES

2.3.1   RNA Extraction

Total RNA was extracted from cells using the RNeasy Mini Kit (QIAGEN, Crawley, UK) as per manufacture's instructions. Briefly, cells were harvested in Qiazol and pelleted by centrifugation at 1500 rpm for 5 min. 600 µl buffer RLT was added to the cell pellet and the mixture was vortexed to disrupt cells. Buffer RLT contains guanidine isothiocyanate which immediately inactivates RNases to ensure isolation of intact RNA. To ensure complete homogenisation of the sample, it was passed through a blunt 20-gauge needle five times. 70% ethanol was added to the lysates to ensure ideal binding conditions. The lysate was loaded onto the RNeasy Spin Column and centrifuged at room temperature to allow the RNA to bind to the silica-gel membrane of the spin column. The spin column was then washed with 700 µl buffer RWT, followed by two wash steps with 500 µl buffer RPE. Finally the RNA was eluted in 30 µl RNase-free water by centrifugation at 8000 x g for 1 min. The eluted RNA was passed through the spin column again to increase the RNA yield. The quantity of RNA in each sample was quantified by optical density (OD) utilising a NanoDrop™ (ND-1000 spectrophotometer [Labtech International, Ringmer, UK]).

2.3.2   DNase Treatment of RNA

DNase digestion is required for RNA applications that are sensitive to very small amounts of DNA (e.g. reverse transcription polymerase chain reactions (RT-PCR) analysis). This was carried out on RNA samples using TURBO DNA-free™ (Ambion, Texas, USA). To a 40 µl RNA sample, 4 µl 10x TURBO DNase Buffer and 1 µl TURBO DNase (2 U/µl) was added. After 20 min incubation at 37 °C, 4.5 µl DNase inactivation reagent was added and mixed before 2 min incubation at room temperature. The sample was then centrifuged at $10,000 \times g$ for 90 secs and supernatant collected as DNA free sample.

2.3.3   cDNA Synthesis

1 µg RNA was used to synthesis cDNA using Advantage RT-for-PCR Kit (Clontech, CA, USA) as per manufacture's instructions. Briefly, 1 µg RNA samples were diluted to a total volume of 12.5 µl and 1 µl random hexamer primer (50 µM) was added. Samples were then incubated at 70 °C for 2 min before placing on ice. To each RNA sample, 4.4 µl

MgCl$_2$ (25 mM), 4 µl 5 x reaction buffer, 1 µl dNTP mix (10 mM each), 0.5 µl recombinant RNase inhibitor (20 U/µl) and 1 µl MMLV reverse transcriptase (50 U/µl) was added and mixed by pipetting. The samples were incubated initially at 25 °C to allow for primer annealing followed by incubation at 42 °C for 1 h to allow for cDNA synthesis to occur and then heated to 94 °C for 5 min to stop the cDNA synthesis reaction and to destroy any DNase activity.

2.3.4   DNA Extraction

2.3.4.1   *Preparation of Plasmid DNA*

An ampicillin or kanomyocin (100 µg/ml) containing luria base (LB) agar plate (0.5 g/L, sodium chloride; 10 g/L, tryptone; 5 g/L yeast extract; and 15 g/L agar) was streaked with bacteria containing the plasmid DNA to be amplified from a glycerol stock and incubated overnight at 37 °C. A single colony was then picked from the plate and used to inoculate a starter culture of 10 ml luria broth (LB) containing ampicillin (100 µg/ml).   The starter culture was incubated in an orbital shaker for 8 h at 37 °C and 180 rpm. The cloudy starter culture was either taken for Mini-Prep extraction or then added to 500 ml LB broth with ampicllin (100 µg/ml) in a 2 l flask and incubated in an orbital shaker overnight at 37 °C and 180 rpm for a Maxi-Prep. The bacterial cells were harvested by centrifugation at 6000 x g for 15 min at 4 °C. Glycerol stocks of positive colonies were produced by mixing 150 µl sterile glycerol with 850 µl of culture, and vortexing before storing at - 80 °C.

2.3.4.2   *Large-scale Isolation of Plasmid DNA (Maxiprep)*

The plasmid DNA was extracted from the bacteria using the Plasmid Maxi Kit (QIAGEN, Crawley, UK) as per manufacture's instructions.   Briefly, the bacterial pellet was re-suspended in 10 ml of the lysis Buffer P1. Buffer P1 contains Tris and EDTA. EDTA chelates divalent metals (primarily magnesium and calcium). Removal of these cations destabilises the cell membrane, producing lysis of the bacterial cells, and also inhibits DNases. In addition, Buffer P1 also contained RNase A (a ribonuclease to degrade RNA). 10 ml of Buffer P2 was added, the solution mixed thoroughly by inverting 4 - 6 times and incubated at room temperature for 5 min. Buffer P2 contains sodium hydroxide and SDS. SDS is a detergent that disrupts the phospholipids of the cell membrane and sodium hydroxide disrupts the cell walls. This results in release of plasmid DNA and sheared cellular DNA from the cells.   Sodium hydroxide also denatures the DNA, producing linearisation of cellular DNA. 10 ml of Buffer P3 was added (chilled to 4 °C), the solution

mixed thoroughly by inverting 4 - 6 times and incubated on ice for 20 min. Buffer P3 is a neutralisation buffer containing potassium acetate and allows precipitation of genomic DNA, proteins, cell debris and KDS (combination of acetate and SDS). The circular plasmid DNA is also allowed to renature. The solution was then centrifuged at 20000 x g for 30 min at 4 °C and the supernatant containing the plasmid DNA was removed. A QIAGEN-tip 500 was equilibrated by addition of 10 ml Buffer QBT and the column allowed to empty by gravity flow.

The supernatant was applied to the anion-exchange QIAGEN-tip and allowed to enter the resin by gravity flow, where the plasmid DNA selectively binds under low-salt and pH conditions. The QIAGEN-tip was washed twice with 30 ml Buffer QC, a medium-salt wash to remove RNA, proteins, metabolites and other low-molecular-weight impurities. The plasmid DNA was then eluted from the QIAGEN-tip by addition of 15 ml Buffer QF, a high-salt buffer. As DNA is negatively charged, the addition of salt masks the charges and allows DNA to precipitate. The plasmid DNA was then concentrated and desalted by isopropanol precipitation. 10.5 ml of isopropanol was added to the plasmid DNA and centrifuged immediately at 15000 x g for 30 min at 4 °C. The supernatant was subsequently removed, and the pellet washed by addition of 5 ml 70 % (v/v) ethanol and centrifuged at 15000 x g for 10 min. The supernatant was again removed and the pellet air-dried for 5 - 10 min. The dried plasmid DNA was re-dissolved in 100 μl sH$_2$O before quantification of yield by OD utilising a NanoDrop™.

2.3.4.3   Small-scale Isolation of Plasmid DNA (Miniprep)

Bacterial cells from starter cultures were harvested by centrifugation at 6000 x g for 15 min at 4 °C, and the pellet resuspended in 300 μl lysis buffer P1 (as previously described). 250 μl buffer P2 was added, and solution mixed thoroughly by inversion. 250 μl buffer N3 was added, mixed immediately by inversion (4 - 6 times), and mixture was centrifuged at 13000 rpm for 10 min. Supernatant was applied to the QIAprep spin column, centrifuged for 60 secs at 13000 x g and the flow through discarded. The spin column was then washed by addition of 750 μl buffer PE followed by centrifugation at 13000 x g for 60 secs. The flow through was discarded and DNA was eluted in 50 μl sH$_2$O.

2.3.4.4   Isolation of DNA from Mammalian Cells

Total genomic DNA was isolated using the QIAamp DNA Mini Kit (QIAGEN, Crawley), according to manufacturer's instructions. Briefly, culture medium was removed, cells

were washed twice in PBS then 200 μl of PBS was added to each well and cells scraped with a rubber policeman. Detached cells were transferred into fresh 1.5 ml eppendorfs and 20 μl of proteinase K was added to each sample. Proteinase K is a broad-spectrum serine protease that works to break down the contaminating proteins present during DNA extraction, including nucleases. 200 μl of lysis buffer AL (SDS, EDTA and guanidine hydrochloride) was then added to the sample and incubated for 10 min at 56 °C for optimal lysis. As previously mentioned, SDS is a detergent that disrupts the phospholipids of the cell membrane and EDTA chelates divalent metals (primarily magnesium and calcium), which destabilises the cell membrane, producing lysis of the cells in addition to further inhibiting DNases. Guanidine hydrochloride is a chaotropic salt, which allows adsorption of DNA (but not RNA, polysaccarides, proteins, etc.) onto the silica-gel membrane in the following steps. 200 μl of 100 % EtOH was added to each sample, mixed by pulse-vortex for 15 sec, briefly centrifuged and loaded onto the QIAamp spin column. Samples were centrifuged at 6000 x g for 1 min to allow DNA to be adsorbed onto the silica-gel membrane and flow-through was discarded. Spin column was washed with 500 μl buffer AW1 (guanidine hydrocholide and EtOH) and centrifuged at 6000 x g for 1 min, followed by a second wash of buffer AW2 (EtOH) and centrifuged at 20000 x g for 3 min. Finally, each spin column was placed into a clean Eppendorf, and 50 μl sH$_2$O was added to each column and left for 5 min to elute DNA before centrifuging at 6000 x g for 1 min. This final elution step was repeated to maximise DNA yield, and DNA quantified by NanoDrop™.

2.3.5   DNA Purification

2.3.5.1   Phenol-Chloroform Extraction

An equal volume of phenol-chloroform was added to the sample and mixed by inversion thoroughly before spinning at 13000 x g for 3 min. Phenol-chloroform is a solvent mixture of low polarity that when mixed with a protein / DNA "soup" changes the environment of the mixture from one of reasonable polarity (H$_2$O) to one of extremely low polarity. In a low polar environment, the negatively charged hydrophilic DNA (from negative charges of the phosphate backbone) remains in the water phase and all other proteins etc remain in the phenol-chloroform phase. The upper aqueous layer was therefore kept and ethanol precipitated as follows: add 1/10 volume 3 M NaOAc and mix before adding 2 volumes ice-cold 100 % EtOH and incubating on ice for 30 min. Addition of sodium acetate quenches the negative charge of DNA by binding through the positively charged sodium

ions, making the DNA much less water soluble, ethanol is added to facilitate this reaction by reducing the dielectric constant of the solution. The mixture was then centrifuged at 13000 x g for 10 min at 4 °C and the supernatant removed. The pellet was washed in 70 % EtOH by centrifugation to remove any residual salt and the pellet redissolved following air-drying in sH_2O.

2.3.5.2 Gel Extraction for PCR Products or Linearised Plasmid Isolation

Gel extraction was performed using Wizard® SV Gel and PCR Clean-Up System (Promega, UK). Following electrophoresis to separate DNA fragments (100 ml 2 % (w/v) agarose, in 1 x Tris/Borate/EDTA (TBE) with 7 µl ethidium bromide), the band of interest was excised by visualisation using a long-wavelength UV lamp and the gel slice put into a pre-weighed 1.5 ml Eppendorf. The weight of the gel slice was calculated and the membrane binding solution is added at a ratio of 10 µl per 10 mg, and incubated at 55 °C with intermittent vortexing for 10 min, until the gel slice is completely dissolved. Membrane binding solution contains guanidinium isothiocyanate, which is a very powerful protein denaturant. The tube is centrifuged briefly to collect all the contents and the dissolved gel mixture is transferred to the SV Minicolumn and incubated for 1 min at room temperature. The column was centrifuged at 16000 x g for 1 min and the flow through discarded. 700 µl Membrane Wash Solution, previously diluted with 95 % EtOH, was added to the column and centrifuged at 16000 x g for 1 min and wash step repeated with 500 µl Membrane Wash Solution and centrifugation at the same speed for 5 min. Column was re-centrifuged dry to allow evaporation of residual ethanol before elution of DNA in 50 µl sH_2O.

2.3.6 Quantitative Real Time Polymerase Chain Reaction (qRT-PCR)

TaqMan™ qRT-PCR (Applied Biosystems, ABI Prism, 7900HT Sequence Detection System) was used to quantify the relative concentration of mRNA present in both cells and tissue. This quantitative measurement is based on the detection of a fluorescent signal produced proportionally during amplification of a PCR product. The amount of fluorescence released during the amplification cycle is proportional to the amount of product generated in each cycle and can be measured directly. Acquisition of data occurs when PCR amplification was in the exponential phase. The Taqman™ detection system (Applied Biosystems, Warrington, UK) was used at the following conditions: denaturation, 95 °C for 10 min; amplification, 95 °C for 15 sec; annealing, 60 °C for 1 min (40 cycles); dissociation, 95 °C for 15 sec; 60 °C for 15 sec and 95 °C for 15 sec.

2.3.7 Shrimp Alkaline Phosphatase (SAP) Dephosphorylation

Dephosphorylation of 2.5 µg of digested plasmid was performed using 5 U shrimp alkaline phosphatase (SAP) (Promega, Southampton, UK) by incubation at 37 °C for 15 min. SAP was inactivated by incubation at 65 °C for 15 min.

2.3.8   Ligations & Transformations

2.3.8.1   *StrataClone Ligation and Transformation Technique*

Ligation mixture was prepared by combining 3 µl StrataClone Cloning Buffer, 2 µl of diluted PCR product or 2 µl StrataClone Control Insert, 1 µl StrataClone Vector Mix. The ligation reaction was mixed gently by pipetting and incubated at room temperature for 5 min before being placed on ice. 1 µl ligation mixture was added to one tube of StrataClone SoloPack competent cells and the transformation reaction incubated on ice for 20 min. The reaction was placed in a 42 °C water bath for 45 secs and then placed back on ice for 2 min. 250 µl of pre-warmed super optimal broth with catabolite repression (SOC) medium (20 g/L bactotryptone, 5 g/L yeast extract, 10 mM NaCl, 2.5 mM KCl, 20 mM glucose) was added and ligation reaction placed in an orbital shaker for at least 1 h at 37 °C with shaking (180 rpm). During the outgrowth period, LB amplicillin (100 µg/ml) agar plates were prepared for blue-white colour screening by spreading 40 µl of 2 % 5-bromo-4-chloro-3-indolyl-β-D-galactopyranoside (X-gal) on each plate. 5 µl or 100 µl of the transformation mixture was spread on the colour screening plates and incubated overnight at 37 °C. Several white (positive) colonies were picked from each plate and amplified overnight in 5 ml LB broth containing ampicillin (100 µg/ml). Plasmid DNA was isolated using the Qiagen plasmid mini preparation kit (QIAGEN Ltd., Crawley, UK) as previously described (section 2.3.4.3). Diagnostic restriction digestion of individual clones was performed to determine which plasmids contained a single copy of the Ngb insert.

2.3.8.2   *General Ligation and Transformation Technique*

Dephosphorylated plasmid and Ngb insert was ligated using Quick T4 ligase (New England BioLabs, Hitchin, UK). 50 ng of vector was mixed with a 3-fold molar excess of insert and volume adjusted to 9 µl with dH_2O, 10 µl of 2x Quick Ligation Buffer and 1 µl of Quick T4 DNA Ligase was added and solution mixed. Solution was centrifuged briefly and incubated at room temperature (25 °C) for 5 min before chilling on ice prior to transformation. The ligated plasmid was then transformed into JM109 competent *E. coli*

(Promega, Southampton, UK) using a standard heat shock protocol. Briefly, 10 µl of the ligation reaction was incubated with 50 µl competent cells on ice for 30 min. The reaction was placed in a 42 °C water bath for 30 secs and then placed back on ice for 2 min. To the tube was added 450 µl of SOC medium, which was then placed in an orbital shaker for 3 - 4 h at 37 °C with 180 rpm shaking. 20 µl or 200 µl of culture was plated onto LB agar plates (10 g/L bactotryptone, 5 g/L bactoyeast extract, 5 g/L NaCl, 15 g/L agar, pH 7.5) supplemented with 100 µg/ml ampicillin and incubated overnight at 37 °C. Several colonies were picked from each plate and amplified overnight in 5 ml LB broth. Plasmid DNA was isolated using the Qiagen plasmid mini preparation kit (QIAGEN Ltd., Crawley, UK) as before (section 2.3.4.3). Diagnostic restriction digestion (section 2.3.9) of individual clones was performed to determine which plasmids contained a single copy of the Ngb insert.

2.3.9   Restriction Digestion

Restriction digests contain the DNA, one or two specific enzymes flanking the digestion site, the relevant buffer and water. The exact concentrations of constituents are described for each reaction within the text. All contents are added to an Eppendorf and mixed thoroughly by pipetting. The mixture is subsequently incubated at the optimal enzymatic temperature for a given period, depending on enzyme and quantity of DNA. Finally successful digestion was assessed by gel electrophoresis.

2.3.10   Sequencing

Sequencing reactions contained 100 ng plasmid DNA, 3.2 pmoles primer, 1 µl v3.1 Ready Reaction mix (Applied Biosystems, MA, USA), 4 µl v3.1 sequencing buffer (Applied Biosystems, MA, USA) in a 20 µl reaction. The cycle conditions were denaturing at 96 °C for 45 secs, annealing at 50 °C for 25 secs and extension at 60 °C for 4 min, for 25 cycles. Sequencing products were cleaned using CleanSEQ® (Agencourt Bioscience Corporation, MA, USA) as per manufacturer's instructions. Briefly, 10 µl CleanSEQ® and 62 µl 85 % EtOH was added to each sample and the sample plate was placed onto an Agencourt SPRIPlate 96R for 3 - 5 min or until solution was clear. The cleared supernatant was discarded, the samples cleaned with 100 µl 85 % EtOH and left on the magnet for 60 secs before the EtOH was removed and the cleaning step repeated twice more. After the final wash, samples were left to air-dry for 5 – 10 min on magnet before removal from the

magnet and addition of 40 μl elution buffer. Following 5 min incubation in elution buffer the plate was returned to the magnet for 3 – 5 min, to allow the sample to separate and the solution to clear. Finally, 35 μl of clear sample was transferred to a new plate for analysis on the ABI 3730 automated sequencer, using SeqScape v2.0.

2.4   FUNCTIONAL *IN VITRO* ASSAYS

2.4.1   Virus Transductions

Cells were seeded in a 12- or 6-well plate at a seeding density of 2 x 10^5 or 4 x 10^5 cells / well, respectively, and incubated overnight at 37 °C to produce 70 – 80 % confluence the following day. Viruses were diluted to the desired concentration in serum free medium. Cells were washed twice in PBS before being transferred to serum free medium. Wells were subsequently infected with the required multiplicity of infection (MOI) of virus and incubated for 4 h at 37 °C. Cells were washed twice in PBS to remove unbound virus then placed in fresh complete medium and incubated for 48 h before transgene expression was assessed or cells were placed into hypoxia / reoxygenation before functional outcome measured.

2.4.2   Determination of Protein Concentration in Cell and Tissue Lysates

The amount of protein in cell lysates was determined using the bicinchoninic acid (BCA) assay kit (Pierce, Rockford, USA) as per manufacturer's instructions. Briefly, a standard curve was generated using dilutions of BSA ranging from 25 μg / ml to 2000 μg / ml. 200 μl of BCA working reagent (Reagent A:B, 50:1 dilution) was added to 25 μl of cell lysate or standard, in duplicate in a 96 well plate. The plate was protected from light and incubated at 37° C for 30 min. The absorbance was measured at 570 nm on the Wallac Victor² plate reader (Wallac, Turku, Finland).

2.4.3   Western Blotting

To determine the relative expression of either Ngb or phospho-JNK protein levels, sodium dodecyl sulphate polyacrylamide gel electrophoresis (SDS-PAGE) and western blotting were performed. A 12 % polyacrylamide gel [containing 40 % (v/v) polyacrylamide (30 %), 11.25 mM Tris pH 8.8, 0.1 % (v/v) SDS, 300 μl 10 % (w/v) ammonium persulphate

(APS) and 30 µl N,N,N',N'-tetramethylethylenediamine (TEMED)] was prepared. Cells were harvested and lysed in radio immunoprecipitation assay buffer (RIPA buffer; 20 mM Tris pH 7.5, 150 mM NaCl, 2.5 mM Na.Pyrophosphate, 1 mM ß-glycerophosphate, 1 mM Na_3VO_4, 1 mM EDTA, 1 mM EGTA, 1 % (v/v) Triton X, 1µg / ml leupeptin and 1 mM PMSF). Samples were also passed through a blunt 20-gauge needle five times to produce complete lysis of the cells. Protein concentration was determined by BCA assay (Perbio Science, Cramlington, UK) as described above and equal protein loaded for each sample. Ngb levels were determined using standard western procedures and phospho-JNK was assessed using an initial immunoprecipitation step before running on the gel. Briefly, 1 µl of phospho-JNK primary antibody was added to 50 µg (in 200 µl with PBS) protein and samples rotated overnight at 4 °C. 20 µl protein-A Sepharose beads were added to sample and incubated with rotation at 4 °C for 4 h, before centrifugation for 10 min at 13000 x *g*. Supernatant was discarded and beads washed with lysis (RIPA) buffer three times, before adding 40 µl 2 x reducing loading buffer (125 mM Tris pH 6.8, 4 % (v/v) SDS, 10 % (v/v) glycerol, 0.006 % (w/v) bromophenol blue and 2 % (v/v) β-mercaptoethanol) and boiling at 95 °C for 5 min to denature and separate protein from beads. The mixture was finally centrifuged, 13000 x *g* for 5 min, and protein containing supernatant kept for electrophoresis.

Protein samples were diluted to the same concentration in a total volume of 40 µl and mixed with 2 x reducing loading buffer (125 mM Tris pH 6.8, 4 % (v/v) SDS, 10 % (v/v) glycerol, 0.006 % (w/v) bromophenol blue and 2 % (v/v) β-mercaptoethanol). The samples were heated to 95 °C for 5 min before loading onto the gel. 40 µl of a full range (MW 225 – 12 kDa) rainbow ladder (Amersham Bioscience UK Ltd, Buckingham, UK) was also added to the gel as a marker of protein size. Samples were electrophoresed at 80 V in running buffer (0.025 M Tris-HCl, 0.2 M glycine, 0.001 M SDS) overnight to achieve separation of the proteins on the gel.

Proteins were transferred onto Hybond-P membrane (Amersham Bioscience UK Ltd, Buckingham, UK) for approximately 6 h at 300 mAmps at 4 °C in transfer buffer (0.025 M Tris, 0.2 M glycine, 20 % (v/v) methanol, 0.001 M SDS). The membrane was then blocked in 10 % (w/v) fat-free milk powder in TBS / Tween20 (TBS-T; 150 mM NaCl, 50 mM Tris, 0.1 % (v/v) Tween-20) for 4 h at room temperature with agitation. The membrane was incubated overnight at 4 °C with a 1:1000 dilution in 1 % (w/v) BSA blocking solution of antibody. The membrane was washed by two 5 min washes in 10 %

(w/v) milk blocking solution then incubated in a 1:1000 dilution of horseradish peroxidase (HRP) secondary antibody (Dako, Denmark) in a 10 % (w/v) milk blocking solution for 1 h at room temperature with agitation. The membrane was finally washed with four 15 min washes in blocking solution with an additional two 15 min washes with TBS-T.

Proteins were visualised using enhanced luminol-based chemiluminescent (ECL) detection system (Amersham Bioscience UK Ltd, Buckingham, UK) as per the manufacture's instructions. Briefly, equal quantities of the two solutions from the ECL kit were mixed and poured onto the membrane. After 1 min, the excess ECL was drained off and films (Medical X-ray Film, Kodak) were exposed for up to an hour before processing through a developer (X-OMAT 1000, Kodak) to determine the presence of the specific protein bands.

2.4.4 Immunocytochemistry (ICC)

Cells were fixed on coverslips in 4 % paraformaldehyde at room temperature for 15 min or overnight at 4 °C. After three 5 min washes in PBS, cells were permeabilised in 0.1 % Triton for 15 min then washed a further 3 times in PBS. Cells were then incubated with the primary antibody (diluted in PBS and 20 % (v/v) serum of animal in which secondary antibody was raised) for 1 h. Cells were then washed three times in PBS before being incubated with the secondary FITC or TRITC labelled antibody (1 µg/ml diluted in PBS and 20 % (v/v) serum) for 1 h. Concentrations and specific conditions of individual antibodies are described in Table 2.2. After three 5 min PBS washes, the back of the coverslip was washed in water and the coverslip mounted onto a glass slide using Prolong Gold® (Invitrogen, Carlsbad, CA, USA).

2.4.5 Electron Paramagnetic Resonance (EPR)

Oxidative stress was assessed by analysing superoxide (SO) release from B50 rat neuronal cells 24 h after 9 h hypoxia. SO levels were detected by EPR (e-scan R; Bruker BioSpin GmbH, Rheinstetten Germany) with the spin probe 1-hydroxy-3-carboxy-2,2,5,5-tetramethylpyrrolidine (CPH; Noxygen, Elzach, Germany). Cells were incubated *in situ* with Krebs buffer (composition in mmol/L: NaCl 99.01, KCl 4.69, $CaCl_2$ 1.87, $MgSO_4$ 1.20, K_2HPO_4 1.03, $NaHCO_3$ 25.0, Na-HEPES 20.0, and glucose 11.1; pH 7.4) and CPH in a total volume of 1 ml for 60 min at 37 °C. In the presence of SO, CPH is oxidised to the

nitroxide CP radical and the triple-line spectrum is read giving the EPR amplitude in proportion to the amount of CP• reflecting the interaction of ROS with CPH after 60 min giving a rate of SO production calculated in counts per minute. Each sample was normalised to protein concentration through use of the BCA assay kit (Pierce, Rockford, USA) as before (section 2.4.1). Instrument settings were: centre field of 3392 G, modulation amplitude of 5.08 G, sweep time of 10.49 s, sweep width of 120 G and 30 scans.

2.4.6 Malondialdehyde (MDA) Assay

A spectrophotometric assay (Tebu-Bio, France) for malondialdehyde was used to determine lipid peroxidation levels following hypoxia / reoxygenation. Malondialdehyde is a product of lipid peroxidation and can therefore be used as a marker of oxidative stress. The principle of this assay is based on the reaction of one chromogenic reagent (NMPI) with MDA at 45 °C, yielding a stable carbocyanine dye, which can be read at 586 nm on a spectrophotometer. Cells were harvested in 500 μl PBS containing a final concentration of 5 mM of the antioxidant butelyated hydroxytoluene (BHT), using a rubber policeman. 5 μl of 500 mM BHT in acetonitrile was added into 500 μl PBS to deter further lipid peroxidation occurring during homogenisation.

Assay was carried out as per manufacturer's instructions. Briefly, cells were lysed by 2 to 3 freeze / thaw cycles and cell debris removed by centrifugation at 3000 x g for 10 min at 4 °C, supernatant was kept for assay. A standard curve was generated by stepwise dilution of supplied standard; 4 μM, 3 μM, 2 μM, 1 μM, 0.5 μM and sH$_2$O blank. 10 μl probucol (a powerful anti-oxidant, supplied), 200 μl sample and 640 μl diluted R1 reagent (supplied) was added to a clean microcentrifuge tube and sample mixed. 150 μl reagent R2 was added and sample mixed again, before being incubated at 45 °C for 60 min. The turbid samples were then centrifuged at 10000 x g for 10 min to obtain a clear supernatant and the sample supernatant and standards were transferred to clear cuvettes and absorbance read at 586 nm. Readings were normalised to input protein using the BCA assay (section 2.4.1).

Table 2.2: Antibodies Used in Experimental Procedures

Primary / Secondary	Antibody	Raised In	Source	Clone No.	Final Concentration Used At		
					ICC	IHC	Western
Primary	Neuroglobin	Mouse Monoclonal	Abcam, Cambridge, UK	13C8	10 µg / ml	10 µg / ml	1 µg / ml
	Caspase 3	Rabbit Monoclonal	Abcam, Cambridge, UK	E87	35 µg / ml	N/A	N/A
	GFP	Rabbit Polyclonal	Abcam, Cambridge, UK	N/A	25 µg / ml	25 µg / ml	N/A
	Mouse IgG	Mouse	Dako, Denmark	N/A	Equivalent to 1° Ab	Equivalent to 1° Ab	N/A
	Rabbit IgG	Rabbit	Dako, Denmark	N/A	Equivalent to 1° Ab	Equivalent to 1° Ab	N/A
Secondary	Goat Anti-Mouse	Goat	Invitrogen, California, US	N/A	4 µg / ml	4 µg / ml	N/A
	Goat Anti-Rabbit	Goat	Invitrogen, California, US	N/A	4 µg / ml	4 µg / ml	N/A

2.4.7   Cell Death ELISA

The cell death ELISA (Roche, West Sussex, UK) is a measure of apoptosis based on the quantitative sandwich-enzyme-immunoassay principle using antibodies directed against DNA and histones. In addition to multiple other processes, endogenous endonucleases cleave double stranded DNA generating mono- and oligonuclesomes during apoptosis. The DNA fragments are multiples of a 180 bp subunit that can be detected as a "DNA ladder" on agarose gels after extraction. The principles of this assay are based on coating the walls of a 96 well plate with an anti-histone antibody and blocking any non-specific binding with blocking solution. The cell samples are then added in duplicate and nucleosomes bind via their histone components. An anti-DNA-peroxidase is added to react with the DNA part of the nucleosome and unbound peoxidase conjugate is removed by washing. Finally, the cytoplasmic histone-associated DNA fragments are quantified by photometric analysis through the addition of ABTS. The assay was carried out as per manufacturer's instructions. Briefly, 5×10^4 of pelleted sample cells were resuspended in 500 µl incubation (lysis) buffer (supplied) and incubated at room temperature for 30 min. The lysate was centrifuged at 20000 x g for 10 min and 400 µl or supernatant containing the cytoplasmic fraction was removed and diluted 1:10 with incubation buffer. 100 µl coating solution (supplied) was added to each of the required wells in the supplied 96-well plate and incubated at room temperature for 1 h. Coating buffer was removed and 200 µl incubation buffer added to each well and plate incubated at room temperature for 30 min. Incubation buffer was removed and well washed three times with washing solution (supplied). 100 µl sample, positive or negative controls were added in duplicate and incubated at room temperature for 90 min. Samples were removed and wells washed three times in washing buffer, before 100 µl conjugate solution (supplied) was added to each well and incubated at room temperature for 90 min. The solution was removed and wells washed three times in washing solution before 100 µl substrate solution (supplied) was added to each well. The plate was finally incubated at room temperature with agitation at 250 rpm until the colour development was sufficient for photometric analysis (~ 20 min) at 405 nm. Values were blank corrected for background apoptosis.

2.5   HISTOLOGY

2.5.1   Paraffin Processing

Brains were cut into approximately 7 (~ 2 mm) coronal slices using a matrix (Harvard Apparatus, UK) placed in individual cassettes in a tissue processor (Shandon Excelsior, Thermo Scientific), and dehydrated through a serial alcohol gradient and xylene before embedding in paraffin wax ready for subsequent histological analysis

1. 70 % (v/v) EtOH   2 h

2. 80 % (v/v) EtOH   3 h

3. 95 % (v/v) EtOH   4 h

4. 100 % (v/v) EtOH (1)   4 h

5. 100 % (v/v) EtOH (2)   5 h

6. 100 % EtOH (3)   5 h

7. 100 % EtOH (4)   6 h

8. 50 % EtOH / 50 % Xylene (v/v) 4 h

9. Xylene (1)   5 h

10. Xylene (2)   5 h

11. Wax (1)   5 h

12. Wax (2)   5 h

13. Wax (3)   6 h

2.5.2   Sectioning of Tissue

Serial 6 μm sections of paraffin embedded brains were cut on a manual rotary microtome (RM2235, Leica) at 7 pre-determined coronal levels, throughout the middle cerebral artery territory, and collected onto poly-L-lysine coated slides (Starfrost® Adhesive Microscope Slides).   Three slides were obtained from each level with three or four sections on each slide. Sections were baked on to slides at 60 °C for 4 h followed by 40 °C overnight. One slide from each coronal level was stained with haemotoxylin and eosin (H&E), as described below to delineate areas of infarction. Frozen tissue was cut at 20 μm on a

cryotome (Cryotome E, Thermo Scientific) and coronal sections collected onto poly-L-lysine coasted slides (Starfrost® Adhesive Microscope Slides), before storing at - 20 °C.

2.5.3 Haematoxylin and Eosin Staining

Haemotoxylin and eosin staining is commonly used to demonstrate areas of ischaemic damage. Haemotoxylin stains nuclei dark blue and eosin stains the cell cytoplasm and surrounding neuropil pink (Figure 2.1). Following removal of wax in Histoclear (National Diagnostics) and rehydration through a series of graded alcohols (100 %, 90 % and 70 %) and water, sections were placed in haemotoxylin for 1 min and then washed in running water. The sections were placed in 70 % alcohol and placed in eosin for 1 min. The tissue was then dehydrated, cleared in Histoclear for 2 x 7 min and mounted using Histomount mounting medium (National Diagnostics).
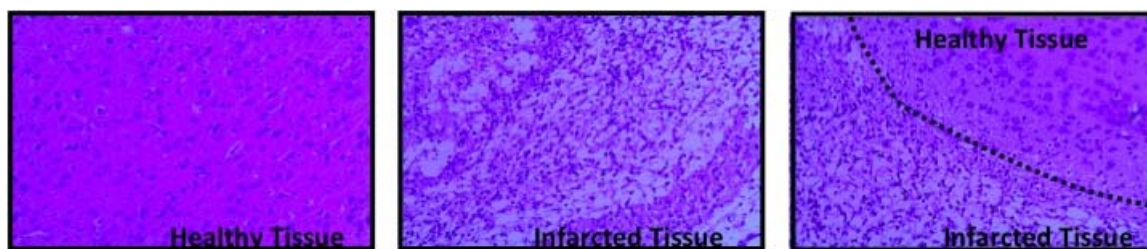
Figure 2.1:   Haematoxylin & Eosin Staining of Infarcted Brain
Normal brain tissue morphology (left) is shown by even distribution and round nuclei (blue) of cells. Infarcted tissue (centre) is represented by neurons displaying the morphological features of ischaemic damage. The region of infarct can be delineated onto scale diagrams (**Figure 2.3**) by identifying the boundary between infarct and normal tissue which is easily identifiable at 14 d after MCAO (right).

2.5.4 Immunohistochemistry (IHC)

2.5.4.1 Antigen Retrieval

Formalin fixation forms protein cross-links that can mask the antigenic sites in tissue specimens. Antigen retrieval methods are designed to break these protein cross-links, and therefore unmask antigens. Two methods were used; sodium citrate buffer and trypsin. Briefly, sodium citrate buffer (10 mM Sodium Citrate, 0.05 % Tween 20, pH 6.0) was heated in a microwave until temperature reached 95 – 100 °C. Slides were immersed in

the buffer and incubated for 15 min. Slides were subsequently washed twice in deionised water and the immunohistochemical protocol followed from the blocking step.

For trypsin retrieval methods, sections were covered with trypsin working solution (0.1 % trypsin, 0.1 % CaCl2, pH 7.8) and incubated for 10 min at 37 °C. Sections were then washed in PBS and then blocking carried out.

2.5.4.2   IHC Protocol

Paraffin wax was removed from the sections by 2 x 7 min washes in Histoclear (Fisher Scientific, Leicestershire, UK). Sections were rehydrated by passing through an alcohol gradient of 100 %, 95 %, 70 % EtOH for 7 min each. Slides were washed in sH$_2$O for 5 min. Endogenous peroxidase activity was quenched by incubating slides for 30 min in 3 % (v/v) hydrogen peroxide in methanol at room temperature before being washed twice in sH$_2$O for 5 min. Antigen unmasking was carried out if required using the previously described method (section 2.5.4.1). IHC was carried out using fluorescent secondary antibodies. Briefly, sections were placed in blocking solution (10 % goat or horse serum) and incubated for 1 h at room temperature in a humidified chamber to prevent sections drying out. The primary antibody and the isotype matched IgG control were diluted in blocking solution (dilutions in Table). Antibodies were incubated on sections overnight at 4 °C or at room temperature for 1 h in a humidified tray. Slides were then washed 3 times in PBS. The secondary antibody was diluted to 0.01 mg / ml in blocking solution and incubated on the slides for 1 h at room temperature. Slides were washed 3 times in PBS and the coverslips mounted using ProLong® Gold with Dapi nuclei counter-stain.

2.6   VIRUS GENERATION

2.6.1 Polymerase Chain Reaction (PCR)

The human Ngb coding region was amplified by PCR using specific primers containing enzymes flanking regions to facilitate cloning into the relevant plasmid (Table 2.3). Each PCR reaction contained 200 μM of each dNTP (Promega, Southampton, UK.), 1.25 U Taq DNA polymerase (Promega, Southampton, UK.) and 0.125 μM each primer in 2.5 mM MgCl2, 50 mM KCl, 10 mM Tris-HCl (pH 9.0) and 0.1% Triton X-100. The reactions were subjected to 40 cycles of denaturing at 94 °C for 1 min, annealing at 52 °C for 1 min

and extension at 72 °C for 1 min. PCR products were analysed by agarose gel electrophoresis and subsequent ligations were performed directly on a 1:10 dilution of the PCR reaction.

Table 2.3:   Sequence of Specific Ngb Primers

Virus	Plasmid	Forward / Reverse	Enzyme	Sequence
Lentivirus	pSFFV	Forward	*Bam*HI	5' CAGT–GGATCC-T-ATGGAGCGCCCGGAGTCA 3'
		Reverse	*Xho*I	5' CTCG-CTCGAG-A-TTACTCCCCATCCCAGCCT 3'
Canine Adenovirus	ptCAV	Forward	*Xho*I	5' CAGT-CTCGAG-T-ATGGAGCGCCCGGAGTCA 3'
		Reverse	*Avr*II	5' CTCG-CCTAGG-A-TTACTCCCCATCCCAGCCT 3'

2.6.2   Subcloning of *Ngb* into Intermediate Stratagene pUC18 Control Plasmid

Ngb was inititally subcloned from PET3a_Ngb, a kind gift from Prof D. Greenberg (Buck Institute for Research on Aging, Novato, California), into pUC18 control plasmid. This cloning step was achieved using the StrataClone PCR Cloning Kit, a blue/white screening cloning technique, by means of the ligation and transformation steps previously described (section 2.3.8.1).

2.6.3   Subcloning of Ngb into Lentiviral Construct Plasmid

Fifty µg of lentiviral vector construct plasmid with spleen focus forming virus (SFFV) promoter and multiple cloning site (pHR'SIN-cPPT-SFFV-MCS-WPRE, referred to as pSFFV herein) was digested overnight at 37 °C with 10 U/µl enzyme *Bam*HI (Promega, Southampton, UK) or 10 U/µl *Xho*I (Promega, Southampton, UK) in a 100 µl reaction using enzyme buffer D, as previously described (section 2.3.9). Digested plasmid was subsequently dephosphorylated to prevent re-circularisation and re-ligation of the linearised lentiviral vector (section 2.3.7). Ligations and transformation were carried out following the general ligation and transformation protocol (section 2.3.8.2) using Quick T4 ligase (New England Biolabs, Hitchin, UK) and transformation into JM109 competant *E. coli* (Promega, Southampton, UK). Several colonies were picked from each transformation

plate and amplified overnight in 5 ml LB broth. Plasmid DNA was isolated using the Qiagen plasmid mini preparation kit (QIAGEN Ltd., Crawley, UK) as before (section 2.3.4.3). Diagnostic restriction digestion of individual clones was performed to determine which plasmids contained a single copy of the Ngb insert. Positive clones were sequenced (section 2.3.10) to confirm they contained a single unmutated copy of the insertion in the correct orientation. Large-scale plasmid DNA preparations of correctly sequenced plasmids were then carried out using the Qiagen Plasmid Maxi Preparation Kit (Qiagen Ltd, Crawley, UK) following the manufacturer's instructions as previously described (section 2.3.4.2).

2.6.4 Production of Lentivirus

Lentivirus was produced in low passage 293T cells by standard triple transient transfection with pSFFV-Ngb vector construct encoding the viral genome (50 μg), envelope plasmid (pMDG) (17.5 μg), and second-generation packaging plasmid (Int 8.74) (32.5 μg). Low passage 293T cells were seeded in six T-150 flasks to reach 70 – 80 % confluence following overnight incubation at 37 °C at 5 % CO_2. In a single 50 ml falcon tube, 50 μg pSFFV-Ngb vector construct, 17.5 μg pMDG envelope plasmid and 32.5 μg Int 8.74 packaging plasmid were added to 5 ml OptiMEM before sterile filtration through a 0.22 μm filter. In a 2nd 50 ml falcon tube, 1 μl of 10mM PEI was added to 5 ml OptiMEM and sterile filtered, as before. The 2 falcon tubes were combined and incubated for 20 min at room temperature to allow plasmid DNA and PEI to form polyplexes for transfection. During the incubation period, the 293T cells were washed gently with OptiMEM to remove any remaining serum. 10 ml of sterile triple tranfection mixture was added to each flask for 4 h at 37 °C in 5 % CO_2 before being removed and replaced with 20 ml fresh 10 % MEM. The virus-containing medium was collected at 48 h, filtered through a 0.22 μM filter unit to remove cellular debris due to its cytotoxic effect, stored at 4 °C overnight and medium replaced with 10 ml fresh 10 % MEM. 72 h post-transfection virus-containing medium was removed and filtered as before, and collected together with 48 h medium.

2.6.5 Concentration of Lentivirus

Virus was concentrated by ultracentrifugation in a Beckman Optima L-80 XP Ultracentrifuge (Beckman Coulter Ltd, Buckinghamshire, UK). Six 15 ml Beckman ultra-clear centrifuge tubes (Beckman Coulter) were sterilised in 70 % EtOH, and the sterile

virus-containing medium (~ 15 ml each) added. The tubes were loaded into a SW-32.1 Ti rotor bucket (Beckman Coulter), placed in the SW32 Ti rotor (Beckman Coulter) and centrifuged at 90353 x g for 1 h at 4 °C. Supernatant was immediately and carefully removed, without disruption to the lentivirus pellet, and tubes re-filled with remaining medium until total volume had been ultracentrifuged. After the final spin, supernatant was decanted as before and tubes were left to sit upside down on fresh tissue paper for 2 min to remove any excess supernatant. 50 µl of Opti-MEM I reduced serum medium with GlutaMax I was added to each tube and left to incubate on ice for 20 min. Each pellet was subsequently subjected to pipetting up and down several times to resuspend fully. Finally, tubes were pooled before aliquoting in 5 µl aliquots and storing at - 80 °C.

2.6.6   Lenti-X™ Concentrator

Lenti-X™ Concentration (Clontech, California) is a method for concentrating lentivirus stocks giving a reduced volume, high titre stock. This is necessary for *in vivo* stereotactic injections where there are tight constraints on total volume injected with ~ 3 µl being maximal. At the final stage of lentivirus prep, following pellet resuspension and pooling of stock, 1/3 volume of Lenti-X™ Concentrator is added, mixed by inversion and incubated at 4 ºC for 30 min. Sample is centrifuged at 1500 x g for 45 min at 4 ºC, after which an off white pellet is visible. The supernatant is carefully removed and the pellet resuspended in 50 µl PBS, 1 µl is removed for titration and the remainder aliquoted and stored at - 80 ºC.

2.6.7   Titre of Lentivirus

A 12-well plate was seeded with 293T cells at 5 x 10^4 cells / well and 24 h later the medium removed and replaced with 1 mL fresh MEM medium supplemented with 10 % (v/v) FCS, 1 % (v/v) penicillin/streptomycin and 1 % (v/v) glutamate. A serial dilution of concentrated freeze-thawed lentivirus stock, ranging from 10^{-2} to 10^{-6} was prepared and 30 or 100 µl of sequential lentivirus dilutions were added to each well in duplicate. The titre plate was incubated for 72 h (37 ºC, 5 % CO_2) before the 293T cells were washed in PBS and removed in 200 µl PBS for DNA isolation (section 2.3.4.4). Lentivirus genomic copy number was quantified in DNA extracted from 293T cells, 3 days post-transduction by Taqman™ quantitative PCR (qPCR) according to a published protocol (Butler *et al.*, 2001) for late reverse transcriptase amplicon quantification. Standard curves for quantification

were prepared by serial dilution of lentiviral vector construct plasmid DNA of known concentrations, based upon the following equations.

1.   To determine molecular weight of plasmid DNA:

(bp) x (330 Daltons x 2 nt / bp) = Daltons
Daltons = g / mole

2.   Determine weight of one copy of plasmid DNA (molecule)

g / mole ÷ Avogadro's constant (molecules / mole) = g / molecule

3.   Determine copy number of plasmid DNA per ml in plasmid DNA stock

Concentration of plasmid (g / ml) ÷ g / molecule = copy number of plasmid (molecules of plasmid) / ml

4.   Preparation of top standard:

Copy number of plasmid DNA / ml ÷ top standard required = initial dilution for top standard

5.   Convert to microlitres:

1000 ÷ initial dilution factor for top standard = µl of plasmid DNA stock required for 1 ml

For each 12.5 µl reaction of the 384-well TaqMan™ plate the following was added: 6.25 µl of 2 x TaqMan universal mastermix (containing AmpliTaq Gold DNA polymerase, dNTP's, passive reference and optimised buffer components (Applied Biosystems)), 3.13 µl primer/probe mix, 250 ng DNA or 1 µl plasmid DNA standard, and 2.13 µl sH$_2$O. Each standard and sample was run in triplicate. A non-template control, replacing the sample DNA with 1 µl sH$_2$O was also run in triplicate to eliminate false positives. Primer/probe mix contains late RT forward primer, MH531 5'-TGTGTGCCCGTCTGTTGTGT-3' (T_m: 59.4 °C) and late RT reverse primer, MH532 5'-GAGTCCTGCGTCGAGAGAGC-3' (T_m: 59.4 °C) at final concentrations of 300 nM and the late RT fluorescent probe 5'-[fluorescein amidite (FAM)]-CAGTGGCGCCCGAACAGGGA-[teramethylrhodamine(TAMRA)]-3' (T_m: 59.4 °C) at a final concentration of 100 nM.

The plate was run on an Applied Biosystems 7900HT fast real-time PCR system, subjected to the following parameters: initial incubations at 50 °C for 2 min and initial denaturing at 95 °C for 10 min, followed by 40 cycles of amplification consisting of 15 secs for denaturing at 95 °C and annealing / extending for 1 min at 60 °C. The amount of late RT

amplicons during each cycle was detected by measuring the increase in FAM fluorescence (quenched by TAMRA) with excitation / emission at 540 nm / 570 nm, respectively. Acquisition of data occurred at the exponential phase.

The raw cycle number [cycle-threshold (Ct)] for standards and samples were exported from the SDS v2.3 software (Applied Biosystems™) and imported into Excel®. The standard curve of the standards were plotted using x = log (x) in order to form a linear regression, and the equation of the line calculated. Titre samples were averaged across the triplicates and corrected using the equation of the line. Infectious viral units per ml (iu / ml) of each sample diluent were based upon the following sequential equations.

1. **Total DNA extracted**

    = concentration of DNA (ng / µl) x volume of DNA eluted.

2. **% Total DNA added to the TaqMan when using 250 ng**

    = (250 ng / total DNA extracted) x 100

3. **Cell number used in TaqMan qPCR reaction**

    = (5×10^4) x (% Total cell DNA added to TaqMan when using 250 ng) / 100

4. **Amplicon copy number per cell**

    = Corrected samples from Excel® / cell number used

5. **Infectious viral units per ml (iu / ml)**

    = [(Dilution factor x 1000) / volume µl of virus added to plate] x copy number / cell

The average of all sample diluents from the initial titre plate were averaged and any outliers removed to give the final titre (iu / ml).

2.6.8   Confirmation of Lentiviral Transgene Expression

After generation of lentivirus, functionality was assessed by transducing cells as previously described (section 2.4.1) at increasing MOI's and confirming the presence of the specific mRNA and protein through Taqman™ qRT-PCR (section 2.3.6) and immunocytochemistry (section 2.4.4), as previously described.

2.6.9   Cloning of Canine Adenoviral Plasmid
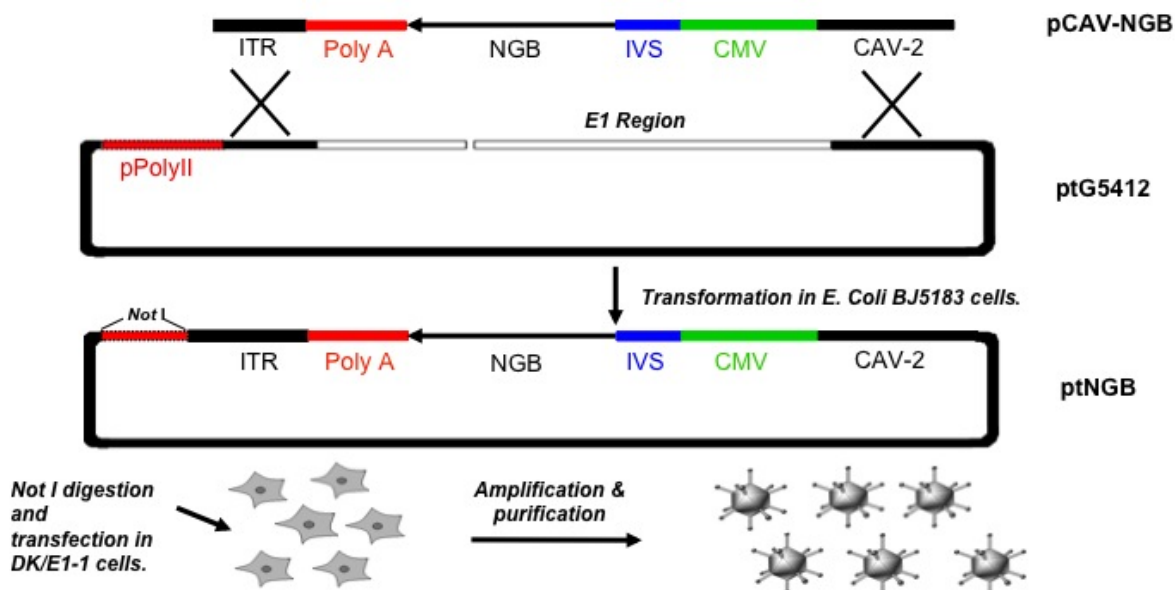
Figure 2.2:   **Schematic of Canine Adenovirus Cloning and Amplification Protocol**

The Ngb insert was amplified from the lentivirus pSSFV-Ngb plasmid by PCR using specific primers (Table 2.3). The forward primer incorporated a *Xho*I restriction site and the reverse incorporated the *Avr*II restriction site onto the Ngb insert to allow for cloning into the multiple cloning site (MCS) of the ptCAV plasmid, utilised for the initial step of cloning, as previously described (section 2.6.1).

20 µg of ptCAV plasmid was digested at *Xho*I and *Avr*II (New England Biolabs,) overnight at 37 °C. 2.5 µl (5 U/µl) enzyme *Xho*I and 2.5 µl (5 U/µl) enzyme *Avr*II in 5 µl (10 x) buffer 2 was added to 20 µg DNA in a total reaction of 50 µl made up with sH$_2$O and heat inactivated at 65 °C for 30 min. The digested plasmid was extracted by phenol-chloroform precipitation (section 2.3.5.1) and dephosphorylated to prevent re-ligation using SAP (section 2.3.7).

150 ng dephosphorylated ptCAV plasmid and 100 ng or 50 ng Ngb insert was ligated using Quick T4 ligase (New England BioLabs, Hitchin, UK) before transforming into JM109 competent *E. coli* (Promega, Southampton, UK) using a standard heat shock protocol (section 2.3.8.2). Several colonies were picked from each transformation plate and

amplified overnight in 10 ml LB broth with 100 µg/ml kanomyocin. Plasmid DNA was isolated using the Qiagen plasmid mini preparation kit (QIAGEN Ltd., Crawley, UK) (section 2.3.4.3). Diagnostic restriction digestion of individual clones was performed to determine which plasmids contained a single copy of the Ngb insert and positive clones were subsequently sequenced to confirm the correct sequence and orientation (section 2.3.10). Large-scale plasmid DNA preparations of correctly sequenced ptCAV-Ngb plasmids were performed using the Qiagen Plasmid Maxi Preparation Kit (Qiagen Ltd, Crawley, UK) (section 2.3.4.2). ptCAV-Ngb plasmid was subsequently digested at *Pac*I and *Ssp*I and insert (pCAV-Ngb) removed and cleaned by gel purification (section 2.3.5.2) for subcloning into the final pTG541 plasmid (Figure 2.2).

The 34 Kb pTG541 plasmid was linearised at *Swa*I (New England Biolabs) for 2 h at room temperature in the following reaction: 5 µg (2 µl) pTG541, 2 µl enzyme *Swa*I (5 U/µl), 2 µl buffer 3 + BSA in a 20 µl reaction made up with sH$_2$O. Linearisation was assessed by agarose gel electrophoresis, and the remainder of the digested pTG541 plasmid extracted from digestion mixture by ethanol precipitation. Briefly, digestion mixture was made up to 50 µl with sH$_2$O, 150 µl 100 % EtOH and 5 µl (3 M) NaOAc was added and mixed before being incubated at - 80 °C for 20 min. Reaction was thawed and spun at 4 °C for 10 min at 12000 rpm. Supernatant was removed and pellet was washed with 70 % EtOH at room temperature for 2 min at 12000 rpm. EtOH was removed and pellet was left to air dry before resuspension in 15 µl sH$_2$O.

100 ng of linearised pTG541 plasmid and 300 ng pCAV-Ngb insert was then transformed without ligation into electrocompetent BJ5183 *E. coli* cells. Briefly, 100 ng linearised pTG5412 plasmid, 300 ng pCAV-Ngb insert or 100 ng pTG5412 plasmid with 300 ng pCAV-Ngb insert was added to 60 µl BJ5183 *E. coli* cells and left to incubate on ice for 15 min. The mixture was transferred into a 0.2 cm electroporation cuvette and pulser set to the conditions: 4.5 ms time constant, 200 W resistance and 25 mFD capacitance with 2.5 kV and the cells pulsed once. 500 µl pre-warmed SOC was immediately added to the cuvette to recover cells and after gentle mixing, the cells / SOC mixture it was removed and left at 37 °C for 1 h. 100 µl or 400 µl of separate conditions were plated at on AMP resistant LB agar plates overnight at 37 °C.

As a result of the large size of pTG541 plasmid (34 Kb), successful cloning was suggested by both clear control plates and few very small colonies on experimental plates. A large

selection of colonies were picked from experimental plates and grown up overnight in 5 ml LB broth at 37 °C with agitation (180 rpm). Starter cultures were DNA extracted, as previously described (section 2.3.4.3), and run on 1 % agarose gel. Samples showing a very small quantity of DNA, expressed ideally in one very large band were selected for transformations into DH5α cells, by heat shock (section 2.3.8.2). Several colonies were picked from each successful transformation plate and amplified all day in 5 ml LB broth. Starter cultures were DNA extracted (section 2.3.4.3) and samples *Eco*RI diagnostic digested (10 µl DNA, 1 µl *Eco*RI (5 U/µl, NEB) and 2 µl (10 x) buffer 3 with BSA, in a 20 µl reaction at 37 °C for 1 h) to check for presence of single copy of Ngb insert.

Large-scale plasmid DNA preparations of correctly digested plasmids were then carried out using the Qiagen Plasmid Maxi Preparation Kit (Qiagen Ltd, Crawley, UK) as before (section 2.3.4.2).

2.6.10 Transfections of pT-CAV-Ngb

A 6-well plate was seeded with DK Zeo cells (Table 2.1) at 1×10^6 cells / well 24 h pre-transfection to allow for ~ 80 % confluency and time of transfection. pTCAV-Ngb was *Not*I enzyme digested to remove pPolyII region (Figure 2.2). For 4 wells (including one control), 4 µg of plasmid was digested at *Not*I for 2 h at 37 °C as follows; 4 µg pTCAV-Ngb, 2 µl *Not*I (10 U / µl) enzyme, 2 µl buffer 3 with BSA in a 20 µl reaction made up with sH$_2$O. Control digest was run on agarose gel to check successful digestion.

For transfections, digestion was mixed with 250 µl OptiMEM and in a second Eppendorf 250 µl OptiMEM was mixed with 16 µl lipofectamine and both left for 5 min at room temperature. Top row of wells, from 6-well plate, were washed twice in PBS and medium replaced with 1.5 ml Opti-MEM / well. The lipofectamine / OptiMEM was added to the DNA / OptiMEM and gently mixed before incubating at room temperature for 20 min. The mixture was added slowly to each well of the top row and left for 6 h at 37 °C at 5 % CO$_2$, after which the transfection mixture was removed from top row and added to medium on bottom row with the top row being replaced with 3 ml DMEM / Glutamax™ (Table 2.1) medium and incubated for 5 days.

2.6.11 Amplification of Canine Adenovirus

Following transfection, all the wells of the 6-well plate were scraped using a rubber policeman and pooled with medium into one falcon before 3 freeze / thaw cycles. After final thaw, cells were centrifuged at 4000 rpm for 10 min to remove cell debris and supernatant kept to incubate with a fresh monolayer of DK Zeo cells (two 10 cm dishes seeded at 7 x 10^6 cells / dish) and incubated for 48 h. Following the 48 h incubation period, dishes were subsequently scraped, cell / medium mixture freeze / thawed, and centrifuged before incubation on another fresh monolayer of cells. This amplification process was repeated 4 – 5 times, increasing the number of 10 cm dishes by two with each repeat. After the final repeat, the supernatant was used to infect 10 x T150 cm^3 flasks of 293T cells at ~ 80 % confluency for 48 h. The amplification process was repeated 4 – 5 times at this stage with gathered supernatant re-infecting 10 x T150 cm^3 flasks to increase concentration of virus until a complete cytopathic effect of the virus was noted at 48 h post-infection. At this stage, supernatant was finally incubated with 50 x T150 cm flasks for 48 h after which cells and supernatant were removed and centrifuged at 1500 x g for 10 min and cells re-suspended in 30 ml PBS and supernatant kept. Cell / PBS mixture was freeze / thawed 3 times and stored at - 80 °C until purification. The supernatant from 50 x T150 cm^3 flasks was sterile filtered and subjected to ammonium sulphate protein precipitation to remove any virus. Briefly, 9.7 g ammonium sulphate was added to 40 mls sterile supernatant and incubated at room temperature with agitation (180 rpm) for 4 h before centrifugation at 1160 x g for 15 min. Following centrifugation, supernatant was removed and all pellets resuspended in a total volume of 40 ml PBS and stored at - 80 °C until purification.

2.6.12 Purification of Canine Adenovirus using CsCl Density Gradient

To purify and concentrate crude CAV2 stocks, centrifugation on CsCl density gradients was used. 14 ml ultra-clear centrifuge tubes (Beckham Coulter Ltd, Buckinghamshire, UK) were sterilised with 70 % (v/v) EtOH and rinsed in sterile PBS. A CsCl gradient was produced by pipetting 2.5 ml 1.25 g/ml CsCl into a sterile centrifuge tube, followed by 2 ml of 1.4 g/ml CsCl being administered slowly below the initial layer, making two phases. ~ 7.5 ml of crude virus stock was overlayed carefully on top of the gradient, and the tube filled with PBS. The centrifuge tubes were loaded into a Sorvall Discovery 90 rotor container, placed in the rotor and centrifuged at 35000 rpm for 90 min at 18 °C, with

maximum acceleration and deceleration 9. Following centrifugation a white opalescent at the interface of 1.25 g/ml and 1.4 g/ml containing complete virus was seen. The virus band was removed by piercing the tube just below it with a 22-gauge needle and withdrawn in a minimal volume.

The removed virus was then subjected to a second isopycnic gradient to further purify the stock. Virus stock was added on top of 5 ml 1.34 g/ml CsCl as before and tubes filled with PBS. The tubes were centrifuged at 35000 rpm for 18 h at 18 °C, in a Sorvall Discovery 90 rotor container. The virus band was removed by piercing the tube just below it with a 22-gauge needle and withdrawn in a minimal volume, taking extra care at this stage not to extract virus in excess volume.

Purified virus was transferred to a Slide-A-Lyzer Dialysis Cassette (MW ≤ 10,000) (Perbio Science UK Ltd, Northumberland, UK) for desalting by dialysis. The virus was dialysed with 2 L of 0.01 M Tris pH 8 with 0.001 M EDTA for approximately 2 h and the buffer was replaced and dialysis repeated for an additional 2 h. Finally the buffer was changed, supplemented with 10 % (v/v) glycerol and the virus dialysed overnight. The virus was carefully removed from the cassette, aliquoted and stored at - 80 °C.

2.6.13 Titre of Canine Adenovirus

Physical titre of CAV2 was assessed optical density at 260 nm (OD_{260}). A 1:10 and 1:20 dilution of the freeze / thawed purified virus stock was made in PBS with 0.1 % (w/v) SDS. The samples was heated to 56 °C for 10 min to free DNA from the capsid and briefly centrifuged before determination of OD_{260} (NanoDrop 1000 spectrophotometer, Labtech International, Ringmer, UK). The conversion of 1 OD unit = 1.1×10^{12} vp/ml was used for final titre, taking into account initial dilution factors.

2.6.14 Functional Confirmation of Transgene Overexpression from Canine Adenovirus

Functional overexpression of titred virus was assessed by transducing cells as previously described (section 2.4.1) at increasing concentrations and confirming the presence of the specific Ngb mRNA and protein through Taqman™ (section 2.3.6) and immunocytochemistry (section 2.4.4), as previously described. HepG2 cells were utilised

for CAV2 transduction as B50 cells lacked expression of the coxsackie adenovirus receptor (CAR) utilised by CAV2.

2.7   *IN VIVO* METHODS

2.7.1   Animal Models

All animals were housed under controlled environmental conditions. Temperature was maintained at ambient (15 - 25 °C) temperature with 12 h light / dark cycles. Rats were fed standard rat chow (rat and mouse No.1 maintenance diet, Special Diet Services) and water provided *ad libitum.* Work with experimental animals was in accordance with the Animals Scientific Procedures Act 1986 under the project license held by Professor A.F. Dominiczak, PPL 60 / 3618. Inbred colonies of stroke-prone spontaneously hypertensive (SHRSP) were maintained "in-house" by brother, sister mating and routine in lab microsatellite screening was used to confirm homozygosity of all loci within a random group from each strain

2.7.2   Preparation of Animals for Surgery

All experiments were carried out under licence from the British Home Office and in accordance to the Animals (Scientific Procedures) Act, 1986.

Anaesthetic: Rats were anaesthetised in a Perspex chamber with 5 % isoflurane in 100 % oxygen. After 3 to 4 min, an intubation tube (16-gauge cannula) was carefully inserted into the trachea with use of a metal guidewire and the animals were artificially ventilated throughout the surgical procedure (2.5 ml stroke volume and 74 beats/min). Isoflurane levels were altered to maintain appropriate depth of anaesthesia (generally 2.5 - 3 %).

Temperature Monitoring: Throughout surgical procedures, body temperature was monitored using a rectal probe (VetTech Solutions Ltd, UK) and kept within physiological limits (37.5 °C ± 1 °C) using a heat lamp.

Blood Pressure Monitoring for Non-Recovery Procedures: The femoral artery was cannulated before induction of focal cerebral ischaemia to allow measurement of blood pressure. The femoral artery of the left hindlimb was exposed and a polythene cannula

(0.58 nm internal diameter, 0.96 nm external diameter, Portex) was prepared. The end of the cannula to be inserted into the artery was cut at an angle and rounded off to remove sharp edges. Heparinised saline (1 % heparin, Leo Laboratories Limited, Ireland) in 0.9 % saline was drawn into the cannula. The distal end of the exposed section of artery was ligated and the proximal end loosely tied with tension to prevent backflow. A small incision was made in-between, and the cannula inserted carefully and held in place using the proximal tie. The cannula was connected to a transducer and a calibrated physiological measuring system to measure mean arterial blood pressure (Biopac Systems Inc.).

Study Design: Studies were randomised and blinded where possible, to prevent bias in animal selection and data analysis. All data analysis was performed under blinded conditions, with random confirmation of scores on an additionl occasion by a 2nd blinded observer, in accordance to the most recent pre-clinical STAIR guidelines (S.T.A.I.R, 2009).

2.7.3 Middle Cerebral Artery Occlusion (MCAO)

Signifcant traning in the MCAO procedure was performed prior to initiation of both the pilot control study and the intervention study. A total of 4 cadavers were utilised to intitally learn procedure under supervision and 12 non-recovery MCAO procedures were performed under supervision to perfect technique. Rats were anaesthetised as previously described. The method of transient intraluminal filament occlusion used was a modified version of Longa and colleagues (Longa *et al.*, 1989). Under an operating microscope (M651; Leica Microsystems, UK) a midline neck incision was made and the left common carotid artery (CCA) exposed at the point of bifurcation into the internal and external carotid artery. The CCA was temporarily occluded by ligation using a 5/0 silk suture (Sofsilk; Covidien, UK) and the occipital artery and other small branches off the external carotid artery (ECA) were electrocoagulated. The ECA was then permanently ligated and a loop of suture fed around the internal carotid artery (ICA) and tension applied. The pterygopalatine artery (PPA) was temporarily ligated to prevent incorrect filament advancement. The ECA was electrocoagulated distal to the ligation and cut. A small incision was made approximately 3 mm above the point of CCA bifurcation. A silicone-coated nylon filament (diameter: 0.37 mm, Doccal Corporation, Redlands, CA, USA) was inserted into the ECA and gently advanced into the ICA, approximately 22 mm from the carotid bifurcation, until mild resistance was felt, indicating occlusion of the origin of the

middle cerebral artery (MCA). The filament was held in place with ligatures for 45 min during which time the ligation on the PPA was removed. The filament was then completely removed and the incision in the trunk of the ECA sealed by electrocoagulation. The ligature around the CCA was removed and the neck wound sutured with 4/0 vicryl absorbance suture. Anaesthesia was turned off but intubation tube remained intact and mechanical ventilation was maintained until independent breathing was observed. During this time animals were administered 2 ml saline *sc* to prevent dehydration during the acute phase of recovery. When fully conscious, animals were moved to the recovery room where they were monitored at least 3 times a day for the first 3 days and at least once a day thereafter.

2.7.4 Intracerebral Injection of Viral Vector

Rats were anaesthetised and intubated as previously described and their heads held in a stereotactic frame (model # 726336, Harvard Apparatus, UK). Using a dorsal approach, a small incision was made in the scalp and the underlying connective tissue was blunt dissected and retracted. A small craniectomy was made with a saline-cooled drill (Bone Microdrill system; Harvard Apparatus, UK) 0.7 mm posterior and 3 mm lateral (on the animal's left) to Bregma. When only a thin layer of bone remained, this and the dura underneath, were removed using a dural hook to expose the brain surface. The 0.4-gauge needle of a 1 µl Hamilton syringe (Microliter Syringe, Hamilton) was slowly lowered 2.5 mm below the brain surface into the cortex and left for 3 min before being retracted 0.5 mm and left for another 1 min. Virus was injected at a rate of 0.5 µl per min after which the needle was left in place for 4 min to allow for complete diffusion of injectate from the needle tip. The needle was then slowly withdrawn, the craniotomy filled with dental cement (Prontolute; Wright Cottrell, UK), the muscle and skin sutured with 4/0 vicryl and the animal administered with 2 ml *sc* saline to prevent dehydration. Once recovered from anaesthetic, the animal was moved to a recovery room where it was monitored at least daily.

2.7.4.1 Canine Adenovirus

For the intervention study, 3×10^9 virus particles (vp) of either CAV2-GFP control virus or CAV2-Ngb was administered 5 days prior to MCAO. Animals were injected a total volume of 2.2 µl at one location (co-ordinates = AP: - 0.7 mm, ML: + 3 mm, DV: - 2 mm).

2.7.4.2   Lentivirus

For the virus study, 2×10^7 vp of lenti-GFP was injected at two separate cortical locations (co-ordinates = AP: - 0.4 mm, ML: + 3.5 mm, DV - 2 mm: and, AP: - 2.4 mm, ML: + 4 mm, DV: - 2 mm). Animals were injected 7 days prior to sacrifice.

2.7.5   Mapping of the Brain

2.7.5.1   Detection of Areas of Ischaemic Damage and GFP Transduction

Areas of infarct were determined 14 d post-MCAO by identifying neurons and the surrounding neuropil which demonstrated the morphological features of ischaemic damage at 7 pre-determined coronal levels covering the territory of the MCA (Figure 2.3). The H&E stained sections were viewed under a light microscope at a range of magnifications (x 4, x 10 and x 20) to accurately determine the boundary of the infarct (specific characterizations of irreversible cell death were identified). Irreversibly damaged neurons were pyknotic (shrunken and triangular in shape) with cellular incrustations seen at a magnification of x 20. The neurons also showed an eosinphilic cytoplasm and the surrounding neuropil was disrupted, vacuolated and displayed pallor. Figure 2.1 shows examples of undamaged and infarcted tissue.

Levels of GFP expression were determined through similar means, but expression was assessed through use of both a fluorescence (Olympus 1X71) and confocal (Zeiss, LSM 510 Meta) microscope. Both epifluorescence and antibody detected GFP was quantified, using a GFP specific monoclonal antibody.

2.7.5.2   Measuring Affected Area in Brain

Areas of tissue infarction and GFP expression were identified on brain sections and their location transcribed onto scale line diagrams at the 7 pre-determined coronal levels (Figure 2.3) taken from the stereotaxic atlas of Paxinos and Watson. The area of infarct or GFP transduction of 3 sections at each coronal level were delineated onto the appropriate coronal line diagrams, and measured using image analysis (Image J, National Institues of Health, USA). The infarct volume (mm^3) for each brain was calculated by plotting the area (mm^2) of damage at each coronal level against the known anterior / posterior stereotaxic coordinates from Bregma and calculating the area under the curve.

2.7.6 Tail-Cuff Measurement of Blood Pressure

Systolic blood pressure monitoring was carried out by non-invasive computerised tail-cuff, which is based on the plethysmographic method (Davidson *et al.*, 1995). Rats were preheated to ~ 39 ºC for ~ 20 min and restrained by wrapping in surgical sheet, before a pneumatic pressure sensor was attached to the tail distal to a pneumatic pressure cuff, both under the control of a Programmed Electro-Sphygmomanometer. Systolic blood pressure values from each animal were determined by averaging a minimum of six separate indirect pressure measurements.
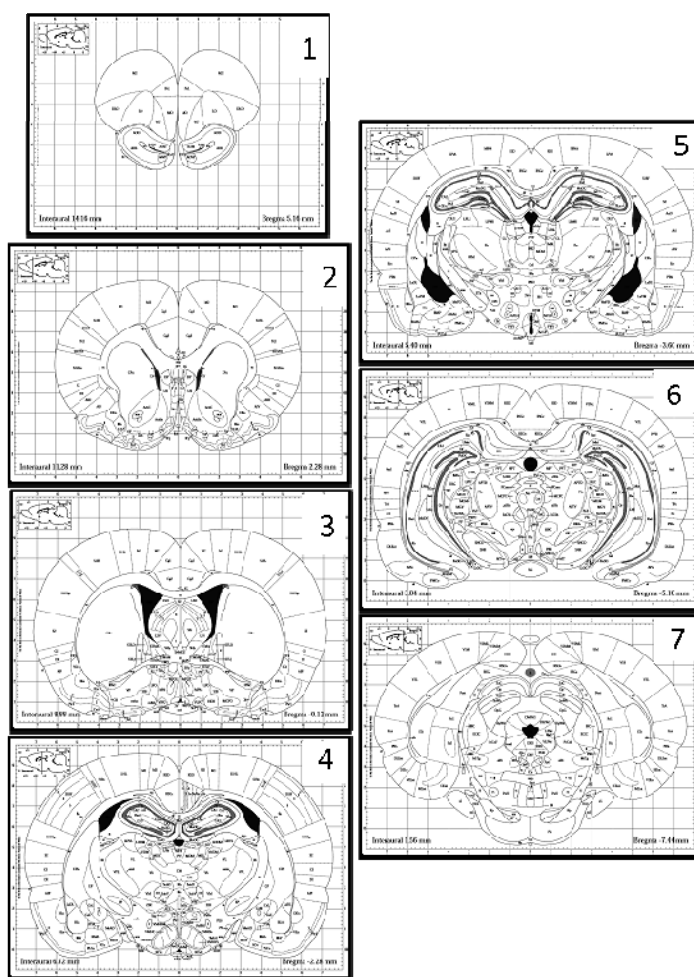
Figure 2.3: Seven Coronal Levels Used for Mapping Infarct and GFP Expression throughout MCA territory

Seven coronal levels at anterior/posterior co-ordinates; level 1= + 5.16; level 2 = + 2.28; level 3 = - 0.12; level 4 = - 2.28; level 5 =- 3.60; level 6 = - 5.16; level 7 = - 7.44, relative to bregma. Taken from Paxinos and Watson.

2.7.7 Behavioural Testing

Each animal was trained on the neurological assessments prior to MCAO to ensure reproducibility at performing tasks. Animals were then assessed on a single occasion 3 – 4 d prior to the experimental stroke procedure to ascertain a baseline score. The 32-point neurological score used was developed from a series of tests described by Hunter and colleagues (Hunter *et al.*, 2000) and consists of 10 separate tests which assessed limb function, mobility and general health, the lower the numerical score the greater the neurological deficit. In addition to the 32-point neurological score, animals were also assessed by the tapered beam test, quantifying the number of footfalls taken in one crossing of a tapered beam (2.7.7.2). The animals were tested across both tests at day 1, 2, 3, 7, 10, and 14 day's post-MCAO to monitor neurological deficit as a result of stroke. Neurological scoring was performed blinded and video recorded to allow for playback to both count footfalls from tapered beam assessment and to also allow for validation of scores of the 2 tests by a 2nd, blinded observer.

2.7.7.1 The 32-Point Neurological Score

The 32-point neurological score demonstrates a refined and more comprehensive measure of sensorimotor assessment in comparison to previous simplified assessments such as the commonly utilised Bederson scale (Bederson *et al.*, 1986). The score comprises of a battery of 10 tests, for which a healthy animal scores 32, that include assessment of paw placement, grip strength, ability to grip a horizontal bar, visual forepaw reaching, contralateral reflex, contralateral rotation, righting reflex, inclined plane, general condition, motility, and circling. The criteria used to score each test are outlined in Table 2.4.

Paw Placement: The animal was held lengthways at the edge of a table. Each paw on either side of the body was gently placed over the edge of the table. The animal scored a point for retracting the paw and placing it back on the table, giving a maximum score of 4.

Righting Reflex: The animal was held firmly in one hand and rotated until it was lying in a supine position in the palm of the hand with the back of the hand facing the floor. The animal scored 1 point for righting itself when the hand's grip was loosened (maximum score of 1).

Horizontal Bar: The animal was hung by its forepaws on a wooden bar. The animal scored points for hanging without falling and raising its hind legs to the bar without aid (maximum score of 3 if both hind legs raised to the bar).

Inclined Platform: The cage lid was held above the floor at an angle of approximately 45 ° to the floor. The animal was placed on the cage lid, facing downwards, towards the floor. The animal scored points for the speed at which it turned to face "uphill" towards the top of the cage lid (maximum score of 4).

Rotation: The animal was held by the base of its tail and rotated clockwise and then anti-clockwise. The animal scored a point if it twisted its body contralaterally to the direction of rotation (maximum score of 2).

Visual Forepaw Reaching: The animal was held at the base of the tail with its head just below the level of a tabletop. The animal was brought closer to the edge of the table until its vibrissae were almost touching it. The animal scored a point if it arched and placed a forepaw on the tabletop (maximum score of 2).

Circling: The animal was placed on the floor and allowed to move freely. The animal scored points for moving without preference to one side or circling (maximum score of 5).

Grip Strength: The animal was placed on the cage lid and lifted off by the base of the tail. The animal scored points (maximum of 3) based on the strength with which it gripped on to the cage lid when being lifted off.

Mobility: The animal was placed on the floor and allowed to move freely. The animal scored points for normal activity and mobility (maximum score of 4).

General Condition: The animal scored points for signs of well-being, such as coat condition, movement, weight gain and lack of secretions around eyes and nose (maximum score of 4).

Table 2.4:   Scoring Criteria for 32-point Neurological Score

Paw Placement	Score: 1 for each successful paw placement (max = 4)
Righting Reflex	Score: 1 for successful righting
Horizontal Bar	Score: 3 if both hindlimbs raised onto the bar 2 if one hindlimb raised onto the bar 1 if the animal hangs from the bar 0 if the animal falls
Inclined Platform	Score: 4 if the animal rotates immediately 3 if the animal rotates within 15 secs 2 if the animal rotates in 15-30 secs 1 if the animal rotates in over 30 secs 0 if the animal falls off the cage lid
Rotation	Score: 1 for each side (max = 2)
Visual Forepaw Reaching	Score: 1 for each successful paw placement (max = 2)
Circling	Score: 5 if the animal does not circle 4 if the animal tends to one side 3 for large circles (> 50 cm radius) 2 for medium circles (15-50 cm radius) 1 for small circles (> 15 cm radius) 0 for spinning
Grip Strength	Score: 3 for normal strength 2 for good but weakened strength 1 for weak strength 0 for no grip
Mobility	Score: 4 for normal mobility 3 for very active 2 for lively 1 for unsteady 0 if reluctant to move
General Condition	Score: 4 if normal 3 if very good, but less weight gain 2 if very good but secretions 1 if good 0 if fair
Maximum Score = 32	

2.7.7.2   Tapered Beam Test

In addition to the 32-point neurological score the animals were assessed on their ability to traverse a 130 cm tapered beam into their "home-cage" without footfalls onto the ledge below (Schallert *et al.*, 2000).   Each animal underwent training to ensure they were competent in running across the beam without footfalls prior to surgery and an average percentage of footfalls were taken from 3 trials across the beam at each timepoint.   The tapered beam test was filmed and assessed alongside the neurological score on days 1, 2, 3, 7, 10 and 14 post-MCAO.   The film was replayed to count footfalls, which were presented as a percentage of total steps taken.   The tapered beam walk test specifically assessed forelimb and hindlimb sensorimotor recovery following MCAO.

2.7.8 Termination of Experiment

2.7.8.1   Perfusion Fixation

After the assigned recovery period each animal was terminally anaesthetized before perfusion fixation under physiological pressure.   Chemical fixation is the common method used to preserve tissue and results in less distortion of the tissue than methods such as fresh freezing or heat based techniques.   Fixation with 10 % formalin maintains cellular definition of the tissue and, if carried out carefully, will produce few artefacts.

With the rat in a supine position, an incision was made below the sternum to expose the rib cage.   The diaphragm was cut away from the rib cage and the rib cage cut at either side to expose the heart.   A blunted 12-gauge needle attached to the perfusion apparatus was inserted into the apex of the heart and advanced into the aorta until visible.   The needle was clamped in place and the right atrium incised.   A constant pressure (~ 120 mmHg) was applied to allow perfusion of 300 ml heparinised (10 U/ml) saline.   When saline outflow from the atrium was bloodless, approximately 300 ml of fixative (10 % formalin) was perfused until the animal was rigid to the touch.

Following perfusion fixation, the head of the animal was immersed in 10 % formalin for 24 h.   The brain was then removed and left for a further 24 h in 10 % formalin before being stored in phosphate buffer until processing (as previously described).

2.7.8.2   2, 3, 5-Triphenyltetrazolium Chloride (TTC) Staining

TTC is a water-solutble salt, which is oxidised to a lipid soluble bright red formazan by mitochondrial enzyme systems. In undamaged tissue, dehydrogenase reduces TTC to formazan, which stains a deep red. In infarcted tissue, where the mitochondrial enzyme systems have been incapacitated, dehydrodgenase activity I is reduced or eliminated and areas remain unstained. TTC can delineate areas of ischaemic damage as early as 3 h post MCAO, but with a more accurate read-out at timepoints of 24 h post ischaemic onset (Bederson *et al.*, 1986). Although the size of infarction can be measured using this technique there can be no visualisation of the microscopic grey and white matters structure and individual cells. This stain was only used in early studies to validate surgical technique on non-recovery animals as it allows a quick and easy demonstration of successful tMCAO and ischaemic damage. The brain was cut into approximately 5 coronal slices and each one immediately immersed in 3 ml of a 2 % solution of TTC (Sigma) in saline. The brain slices were incubated in the TTC solution in a 37 ºC incubator until colour change was visible.

2.8   STATISTICAL ANALYSIS

2.8.1 In Vitro

All *in vitro* results are expressed as mean ± standard error of the mean (± SEM). *In vitro* experiments were performed in triplicate on at least three independent occasions and analysis was by unpaired Student's t test.   In the case of multiple comparisons, Bonferroni's post-hoc analysis was utilised.

2.8.2 In Vivo

In vivo experiments were performed with at least 8 rats per group in the intervention study. Comparison between the 6 groups was performed by repeated measures analysis of variance (ANOVA), as described previously (Davidson *et al.*, 1995) with Bonferroni's post test.

Chapter 3

Results:

Selection of Optimal Viral Vector for *In Vitro* and *In Vivo* Studies

3.1   INTRODUCTION

Viral vector-mediated gene delivery to the brain is notoriously challenging with problems ranging from immunogenicity and transduction efficiency to production of high titre virus and delivery time / route.   A number of diseases of the brain require widespread gene transfer, such as the neurogenetic disorder lysosomal storage diseases (LSDs), Alzheimer's, Parkinson's and brain ischaemia or stroke.   A number of methods have been assessed to enhance transduction efficiency following injection of low volumes of virus stereotactically into the brain parenchyma.   Convection-enhanced delivery is a physical system, enhancing transduction efficiency by relying on pressure a gradient to increase the distribution of agents through the solid tissue (Chen *et al.*, 2005).   The main viral vectors that have been studied for neurological gene transfer include adeno-associated viruses (AAV), human adenovirus (hAd), lentivirus (LV), herpes-simplex virus (HSV-1) and, more recently, non-human adenoviruses such as canine adenovirus (CAV2).

The majority of pre-clinical and clinical trials using gene therapy for neurological disorders have utilised AAVs.   These viral vectors are useful in that they result in prolonged gene expression for up to 8 years (Hadaczek *et al.*, 2010), express limited toxicity, have high titer production capacity (Monahan *et al.*, 2000) and have been shown to cross the BBB following systemic delivery in neo-natal and more recently in adult rodents (Foust *et al.*, 2009).   Although a number of clinical trials have shown direct injection of serotype 2 (AAV2) in humans to be well tolerated (Wu *et al.*, 2006}), transduction efficiency of this virus from injection site is low and a low level of pre-existing immunity exists in humans which increases in prevalence with age (73 % of 50 - 59 year olds worldwide exhibit seroprevalence to AAV2).   Therefore, efficient transduction of the brain would require multiple injections, or pre- or co-treatment with substances such as mannitol (Mastakov *et al.*, 2001) or heparin (Mastakov *et al.*, 2002) to allow transduction to larger areas of the brain.   Pre- or co-treatment with mannitol improves transduction efficiency following stereotactic administration of AAV2 by causing hyperosmolarity of CNS cells, allowing greater spread from injection site.   Pre- or co-treatment with heparin improves AAV2 interaction with its primary receptor, the heparin sulphate proteoglycan (HSPG), on the surface of the cells of the CNS – primarily neurones.   Due to these drawbacks a number of alternative AAV serotypes have been studied in pre-clinical rodent models, such as AAV1, 5, 7, 8, and 9.   A comparative study of AAV serotypes 2, 5, 6, 7, and 8 expressing reporter

gene, GFP, (Harding *et al.*, 2006) demonstrated that greater transduction following single stereotactic injection into the left striatum of the murine brain was afforded by AAV7 and -8, at an incidence of ~ 3.2-fold and ~ 2.4-fold, respectively. In addition, the rostra-caudal spread of GFP$^+$ cells was 3 mm greater in AAV7 and AAV8 injected brains for any other serotype. Another comparative study of AAV serotypes 7, 8, 9, and rh10 (Cearley *et al.*, 2006) demonstrated that following multiple injections into the cortex, striatum, hippocampus and thalamus the highest transduction levels were observed following injection with AAVrh.10, however, AAV9 demonstrated the furthest spread of transduction with reporter gene positive cells observed in the hippocampus of the contralateral hemisphere. Although *in situ* injection of these alternative serotypes has shown better transduction efficacy than AAV2, widespread and reliable transduction was still not achieved (Taymans *et al.*, 2007).

As an alternative to direct injection into the CNS, brain transduction following systemic administration of AAV vectors has also been assessed. In adult mice, gene delivery to the CNS following systemic administration is notoriously challenging. Nomoto *et al.*, (2009) demonstrated that systemic administration 1 x 10^{12} granule copies (g.c.) of an IL-10-expressing AAV1 virus into male SHRSP at 6 weeks prevented vascular remodelling and end-organ damage at 7 months after gene delivery compared to a reporter gene expressing AAV1 virus (Nomoto *et al.*, 2009). Xue *et al.*, (2010) reported a protective effect of a stereotactically administrated erthyropoietin (EPO) expressing AAV9 virus in a pre-clinical model of Parkinson's disease with protection being abolished following systemic administration of the same vector (Xue *et al.*, 2009). A study assessing the biodistribution of AAV2, AAV10 and AAV11 following systemic administration of 1 x 10^{10} – 2.5 x 102.1^{11} g.c in cynomolgus monkeys (*Macaca fascicularis*) (4 – 5 years, 3 – 5 kg) demonstrated inconsistent results (Mori *et al.*, 2006). Following systemic injection of 2.5 x 10^{10} g.c.of a β-gal expressing AAV2 virus, β-gal$^+$ cells were detected at 2 days and 3 months post-injection in the cerebellum of all animals, with half of the animals expressing β-gal$^+$ cells in the cerebrum. However, following systemic injection of 2.5 x 10^{11} g.c.of a GFP-expressing AAV2 virus, no GFP$^+$ cells were observed in the CNS 3 months post injection. Additionally, systemic injection of a GFP expressing AAV10 or AAV11 (1 x 10^{10} g.c.) resulted in no transduction to the CNS (Mori *et al.*, 2006).

It has been demonstrated that effective transgene expression within the CNS can be achieved following systemic delivery of AAV vectors into neonates. Both the BBB and

the immune system are developmentally immature during the perinatal period; AAV-mediated neonatal gene therapy is a promising strategy for treating genetic neurological diseases. Miyake *et al.*, (2011) performed a comparative analysis of neonatal systemic injection of 1.5×10^{11} g.c. of GFP-expressing AAV1, AAV8, AAV9 or AAV10 into C57BL/6J mice and demonstrated that although all serotypes demonstrated transduction to the CNS, GFP$^+$ cells were most abundant in the brains of AAV9-treated animals. Additionally, 18 months after systemic administration of AAV9 vector into neonatal mice, GFP expression in the CNS was undiminished and sustained (Miyake *et al.*, 2011). Neonatal delivery of 2×10^{11} g.c AAV2/9 has also shown extensive and widespread transduction to all structures of the CNS of MF1 mice (Rahim *et al.*, 2011). Neonatal gene therapy offers a very promising rationale in treating early onset neurological genetic diseases, in that it can prevent the onset of disease rather than attempting to reverse the effects.

In 1995 Byrnes *et al.* described a robust and long-term inflammatory response following stereotactic injection of human Ad5 (hAd5) in rats (Byrnes *et al.*, 1995). This inflammatory response has been attenuated through use of a helper-dependent hAd's (HdAd), which have been developed in an effort to evade the immune system. These are "gutless" adenoviruses, devoid of all viral genes, which in the presence of anti-adenoviral immunity transgene expression can remain stable in the brain for at least 1 year, compared to 4 weeks in first generation hAd (Barcia *et al.*, 2007). A recent study into the safety profile, biodistribution and efficacy of HdAd vectors in the presence of anti-Ad immunity as a prelude to a phase I clinical trial for glioblastoma multiforme (GBM) showed HdAd resulted in minimal immunogenicity following stereotactic injection of ($5 \times 10^8 - 5 \times 10^9$ vp) in Lewis rats, but also demonstrated minimal spread from injection site (Muhammad *et al.*, 2010).

LV vectors are useful and popular viral vectors of choice for gene delivery to the brain. LV can infect non-dividing cells, which although is not unique to LV, can allow stable gene transfer in post-mitotic cells such as mature neurons (Naldini *et al.*, 1996a). LV vectors have a large transgene capacity, of close to 10 kb, and exhibit long-term expression of up to 400 days following stereotactic injection (Deroose *et al.*, 2006). LV vectors do not transfer virus-derived coding sequences and thereby avoid recognition and destruction of transduced cells by the immune response. However, like AAV's, LV transport from the injection site is limited, and as such overall transduction is low. A comparative analysis of

AAV1, 2, 3, 4, 5, 6 and 8 with LV following a single stereotactic injection into the red nucleus of female adult Fisher F344 rats showed a far greater spread of transduction with AAV1 and AAV8 (~ 11-fold and ~ 10-fold, respectively) than LV, 1 month post injection (Blits *et al.*, 2010). Integration deficient lentiviral vectors (IDLVs) show promise for neurological gene therapy as they exist as long-term episomes in non-dividing cells and as such significantly reduce the risk of insertional mutagenisis, that have been observed in both pre-clinical (Seggewiss *et al.*, 2006) and clinical trials using integrating lentivirus (Hacein-Bey-Abina *et al.*, 2003). Stereotactic injection into the straitum and hippocampus of adult female C57Bl/6J mice with 5.2 x 10^5 transducing units (TU) GFP-expressing IDLV resulted in similar transduction efficiency to its integrating counterpart (Yanez-Munoz *et al.*, 2006). Rahim *et al.*, (2009) reported that pseudotyping IDLVs with vesicular stomatitis virus G protein (VSVG), rabies and gp64 envelopes did not alter IDLV transduction efficiency following stereotactic injection in adult Sprague-Dawley rats, however, retrograde transport was improved from injection site when pseudotyping IDLV with rabies virus (Rahim *et al.*, 2009). Therefore IDLVs offer a significantly safer clinical option in the treatment of neurological disorders, however transduction efficiency remained low following stereotactic administration.

HSV-1 provides an alternative viral vector to AAV and LV which is highly neurotropic and shows significant transduction from the point of injection. HSV travels by neuronal retrograde transport which is a trait of the life-cycle of the wild-type virus (Cook *et al.*, 1973). Although spread from injection site is vast, the efficiency of transduction at the point of injection is minimal (Lilley *et al.*, 2001), and as such it is difficult to predict where HSV-1 will traffic. If HSV-1 travels efficiently away from this injection site without transducing the neurons at the point of injection it remains to be seen whether it could be a useful tool in delivering genes to the nervous system. In addition, results are contradictory when assessing the immune response following *in situ* injection. Clinical trials using replication-competent (ICP 34.5 null) HSV-1 reported no adverse effects (Rampling *et al.*, 2000), however use of the same strain in the rodent brain has demonstrated severe inflammation (McMenamin *et al.*, 1998).

Research using a non-human adenovirus, canine adenovirus serotype 2 (CAV2), has shown preferential transduction of neurons following stereotactic delivery with efficient retrograde transport (Soudais *et al.*, 2001) and minimal immune response (Chillon *et al.*, 2001). Therefore, it was the initial aim of this chapter to assess the optimal viral vector to

overexpress Ngb for use in the *in vivo* tMCAO study. Transduction efficiency, location and spread were determined using viral vectors expressing eGFP reporter genes following cortical stereotactic injection.

3.2   RESULTS

3.2.1   *In Vivo* Comparison of Viral Vectors

3.2.1.1   Canine Adenovirus

Previous work from our group using MRI imaging had identified the location for the penumbra within the cortex in a model of tMCAO in WKY rats (Figure 3.1). In addition, previous work by collaborators had shown stereotactic injection of CAV2 into the striatum of the non-human primate, *microcebus murinus*, showed significant transduction through the brain and into a variety of afferent structures, such as the cortex, and in parts even crossing into the contralateral hemisphere (Bourgoin *et al.*, 2003).   Therefore, as the penumbra is the focus of all research into acute stroke therapies, an initial study was carried out to compare the spread and expression level of a reporter gene (GFP) expressing CAV2 following injection in both the cortex and the striatum using SHRSP. Animals were injected with one injection of 3 x 10^9 vp in a total volume of 2.1 µl. Animals receiving the striatal injection were injected at co-ordinates (AP: + 1.2 mm, ML: + 3 mm, DV: - 5 mm; relative to bregma), and animals receiving the cortical injection were injected at co-ordinates (AP: + 1.2 mm, ML: + 3 mm, DV: - 2 mm; relative to bregma). An antibody directed against GFP was used to determine total GFP expression although epifluorescence could also be detected from frozen coronal sections allowing comparison between these 2 measures (Figure 3.2).

Table 3.1:   Canine adenovirus injection protocols (*n* = 4).

Viral Vector	Number of injections	Co-ordinates (AP, ML, DV)	Weight	Virus Particles	Recovery	Processing
Canine Adenovirus	1	+1.2, +3, -2 mm	270 – 290 g	(1x) 3 x 10^9 vp	+ 7 Days	PFA fixed & OCT embedded

3.2.1.2   *Location of GFP Expression from CAV2-Injected Animals*

Location and brain volume of expression was determined by quantifying the area of GFP expression using scale line diagrams of cortical section, a modification of the technique used to measure infarct (Osborne *et al.*, 1987) (Figure 3.3). Cortical injection of 3 x 10^9 vp CAV2-GFP resulted in extensive rostra-caudal GFP expression, spanning a distance AP of ~ 7 mm, and transducing a total brain volume of 155.9 ± 11.1 mm^3 (Figure 3.3).
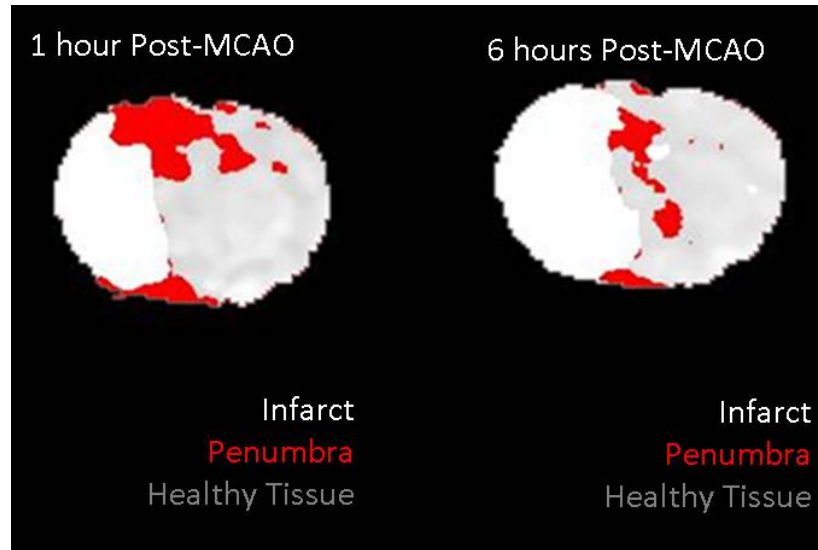
Figure 3.1:   MRI maps highlighting penumbral loss with time following MCAO
Maps of diffusion weighted / perfusion weighted imaging (DWI / PWI) mismatch, demonstrating location and size of penumbra in a representative WKY rat exposed to MCA occlusion. Region with perfusion deficit and displaying ischaemic injury on diffusion scan representing ischaemic core (white), region displaying perfusion deficit but not ischaemic injury representing penumbra (red) and normally perfused tissue representing healthy tissue (grey). Images courtesy of Dr L.M. Work and Dr C. McCabe.
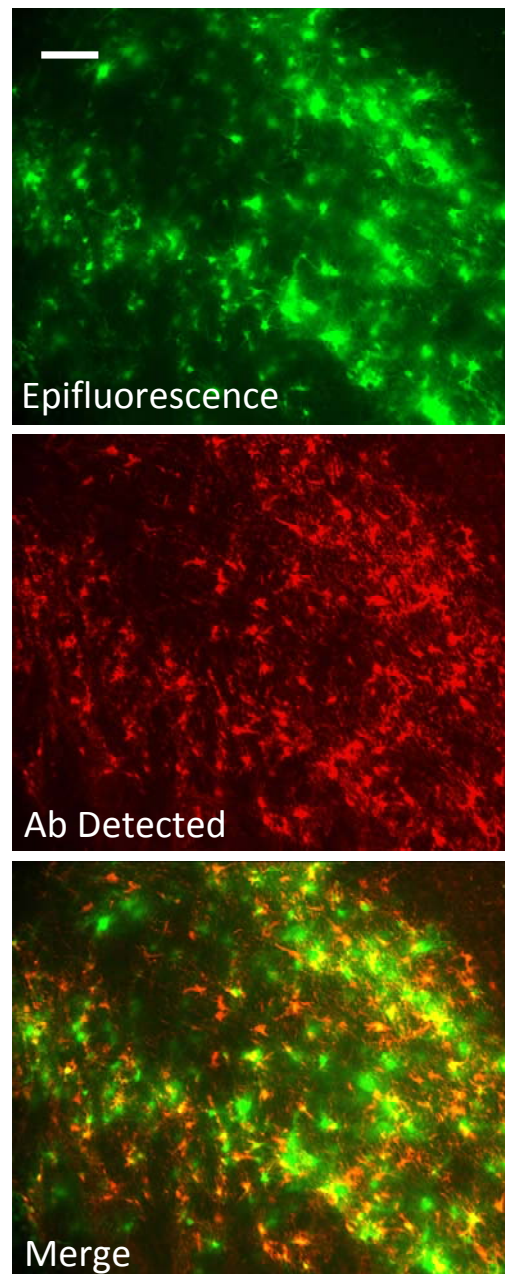
Figure 3.2:   Comparative Analysis of GFP Epifluorescence with Ab Detected GFP
GFP epifluorescence (far left) in comparison to antibody (Ab) detected GFP (centre) and merge (right). Scale bar = 50µm, x 25 magnification - applicable to all panels, images obtained using fluorescence microscopy.

(A)
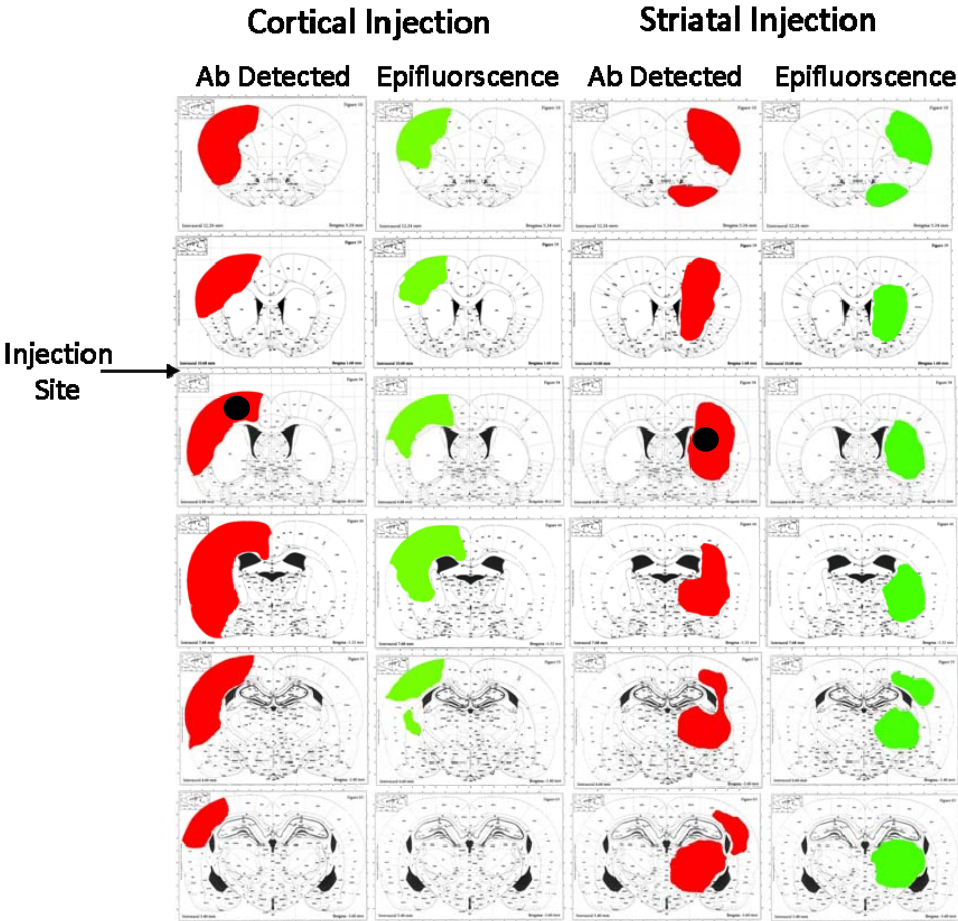
(B)
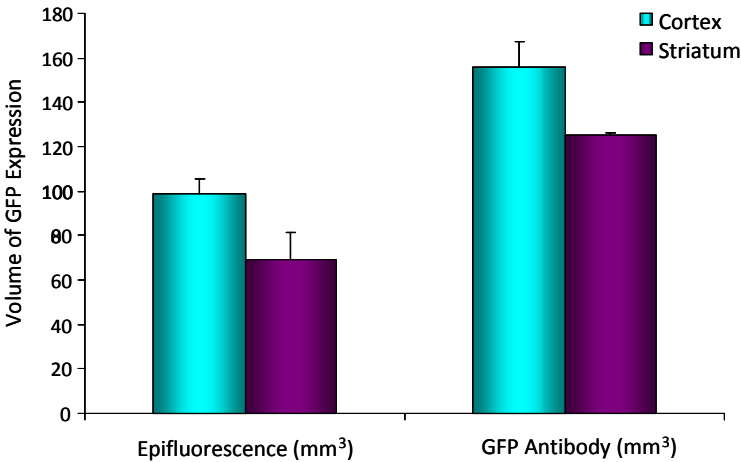
Figure 3.3:   Comparison of Distribution and Transgene Expression Following Striatal and Cortical Injection of CAV2-GFP

(A) Cortical injection of CAV2-GFP (left two columns) and striatal injection of CAV2-GFP (right two columns) (3 x 10^9 vp in 2.1 µl total volume) detected by epifluorescence (green) or specific α-GFP antibody (red) from a representative animal.   • = Injection site (B) Quantified volume of transduction from either injection site with both detection methods (section 2.7.5).

Although transduction of the cortex was also noted following striatal injection, transduction efficiency was lower and more variable as it was on the periphery of the total transduction zone (125.0 ± 2.6 mm^3; Figure 3.3).

3.2.1.3 Lentivirus

Research within our group in addition to previously reported studies, using a variety of models, have reported that although lentivirus is a highly neurotropic viral vector, spread from injection the site is minimal (Baekelandt *et al.*, 2002). However, in order to assess the efficiency of lentivirus in the present model, male SHRSP rats (*n* = 4) were stereotactically injected in the cortex with reporter gene (GFP) expressing lentivirus, protocol described in Table 3.2. As lentivirus is notoriously difficult to produce in high titres, animals receiving lentivirus were administered 2 x 10^7 vp at two separate locations within the cortex, rostral and caudal to the perceived infarct location. Brains were fixed in 4% PFA and embedded in OCT.

Table 3.2   Lentivirus injection protocols (*n* = 4).

Viral Vector	No. of Injections	Co-ordinates (AP, ML, DV)	Weight	Virus Particles	Recovery	Processing
Lentivirus	2	-0.4, +3, -2 mm -2.4, +4, -2 mm	270 – 290 g	(2x) 2 x 10^7 vp	+ 7 Days	PFA fixed & OCT embedded

3.2.1.4   Location of GFP Expression from Lentivirus Treated Animals

Sections were stained with a GFP-specific antibody and quantified using scale line diagrams of the relevant coronal sections (Osborne *et al.*, 1987), as previously described for CAV2. GFP expression of lentivirus treated animals was significantly lower than that of CAV2-treated animals (Figure 3.4). Antibody detection of GFP determined a total transduction volume of 19.8 ± 3.8 mm^3, in comparison to 13.3 ± 3.5 mm^3 determined by epifluorescence (Figure 3.4) with marked positive transgene expression within this discrete zone.

Eplifluorescence   Ab Detected

Injection sites
AP: -0.4 & -2.4
relative to Bregma
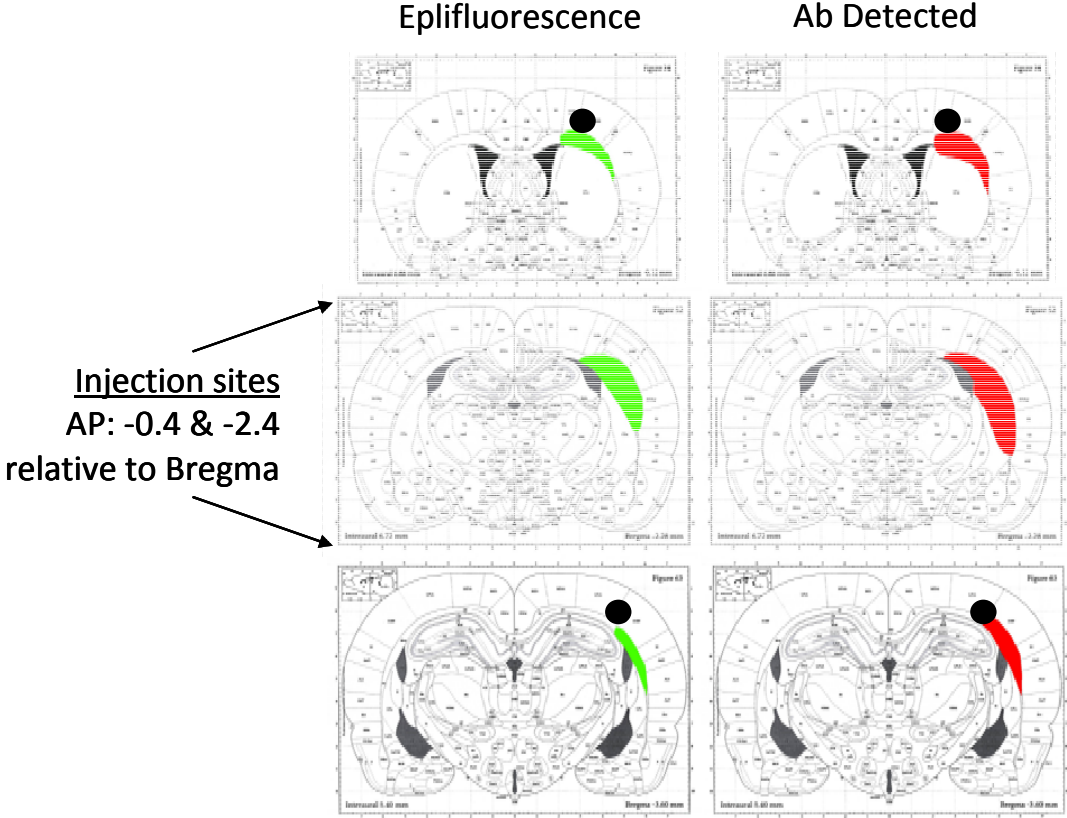
Figure 3.4:   Distribution and Transduction of Transgene Expression Following Injection of Lenti-GFP

Double cortical injection of 2 x 10^7 vp lenti-GFP at AP: - 0.4 mm, ML: + 3 mm, DV: - 2 mm and AP: - 2.4 mm, ML: + 4 mm, DV: - 2 mm, relative to bregma. Detection by epifluorescence (green) or specific α-GFP antibody (red) in a representative animal (n = 4). • = Injection site.

3.2.1.5   *Comparison of CAV2 and Lentivirus*

Within the cortical regions of transduction, both CAV2 and lenti-mediated GFP expression was extensive (Figure 3.5). However, cortical stereotactic injection of 3 x 10^9 vp CAV2-GFP mediated a ~ 8-fold increase of GFP expression in comparison to 4 x 10^7 vp lenti-GFP, across two cortical injection sites (Figure 3.6).

3.2.2   Optimisation of Injection Location

Results show injection into the cortex with CAV2-GFP resulted in significantly greater overall transgene expression than with LV-GFP. From these data it was concluded that CAV2 would be the vector of choice for use in the *in vivo* study. However, when assessing the location of GFP transduction, in comparison with the location of typical infarct following 45 min tMCAO, it was clear that moving the injection caudally from bregma would optimise the expression of virus to match the location of ischaemia (Figure 3.7). It was postulated that the co-ordinates, AP: - 0.7 mm, ML: + 3 mm, DV: - 2 mm, would allow for a greater potential transduction of neurons within the peri-infarct area (Figure 3.7).

3.2.3   Generation of a Ngb Overexpressing Canine Adenovirus

3.2.3.1   *Virus Generation*

A diagram of the cloning strategy for CAV2-Ngb is shown in the Materials and Methods Chapter (Figure 2.2). The initial step of cloning the Ngb insert into ptCAV was confirmed by sequencing using Ngb specific primers (

Figure 3.8). pCAV flanks the Ngb expression cassette on either side with complementary regions of the pTG5412 plasmid. The insert including the complementary regions and the expression cassette of pCAV2-Ngb was subcloned into pTG5412, containing the CAV2 genome, by homologous recombination in *Escherichia coli* electrocompetant BJ5183 cells, forming the final plasmid ptCAV-Ngb. Successful cloning was determined by *Eco*RI diagnostic digest, confirmed by virtual cut using Serial Cloner™ software (Figure 3.9).
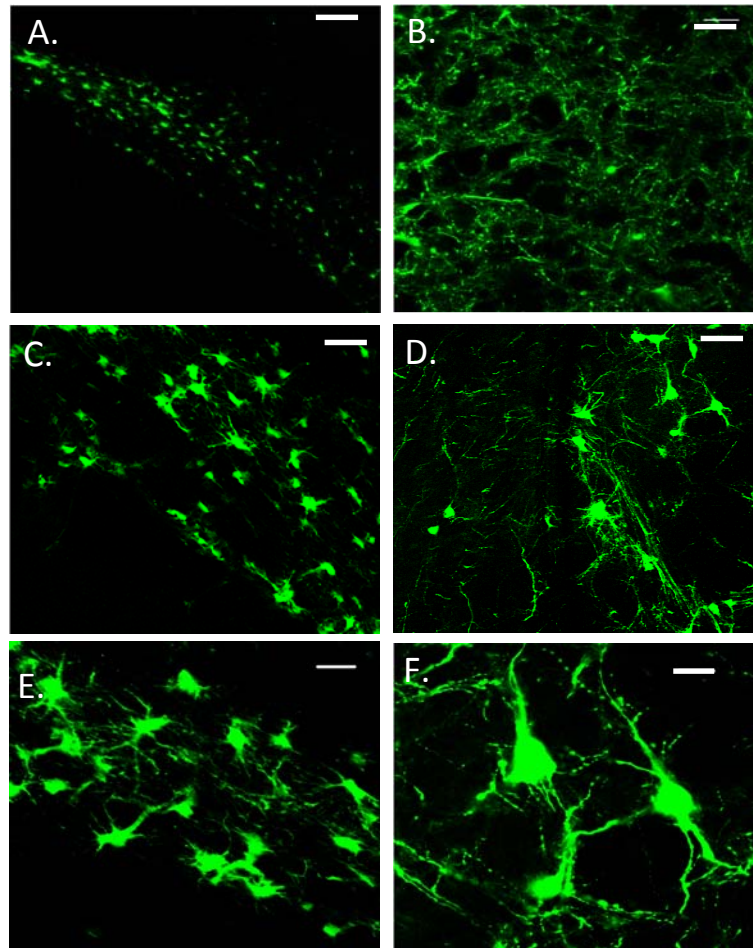
Figure 3.5:   Transduction Efficiency of Lentivirus and CAV2 in Region of Cortex

 (A, C & E) representative images of lenti-GFP cortical transduction at level 4 with increasing magnifications (x10, x25 and x63, respectively). (B, D & F) representative images of CAV2-GFP cortical transduction at level 4 with increasing magnifications (x10, x25 and x63, respectively). Scale bar A & B = 100µm; C & D = 50 µm; E & F = 20µm, images taken within cortex by confocal microscopy.
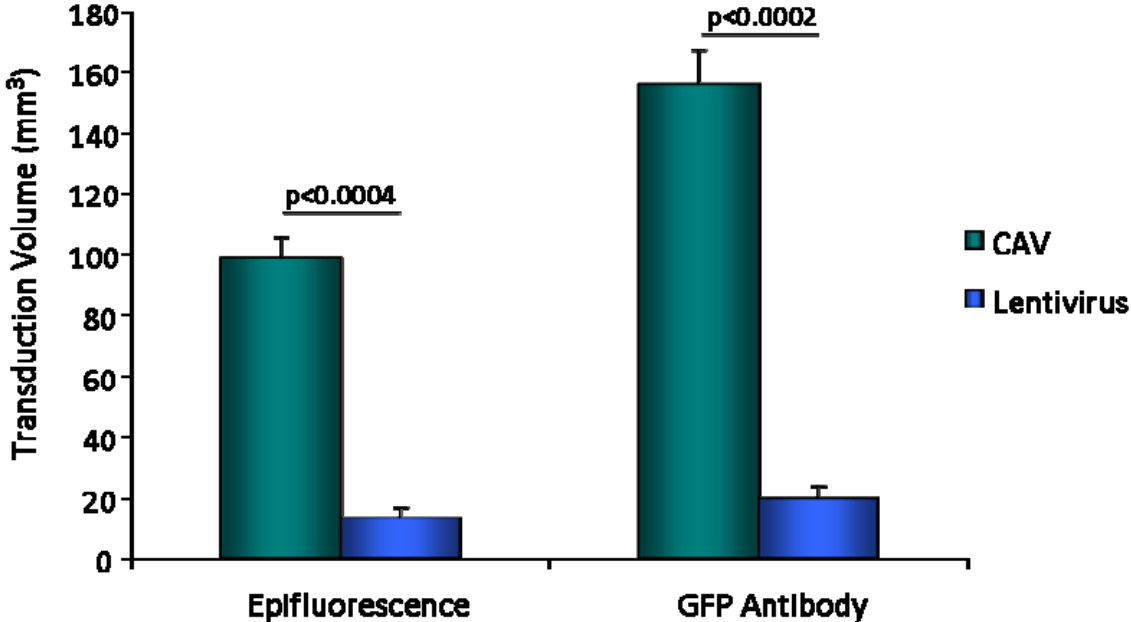
Figure 3.6: **Comparison of Transduction Volume Following Injection of Lentivirus or CAV2.**

Quantification of the total transduction volume from CAV2-GFP or lenti-GFP cortical injection, detected 7 days post-injection, by either epifluorescence or a specific anti-α-GFP antibody. p<0.0004 and p<0.0002, Student's unpaired t-test, n = 4 / group.

Previous Injection Site
AP: + 1.2 mm,
relative to Bregma

New Injection Site
AP: - 0.7 mm,
relative to Bregma
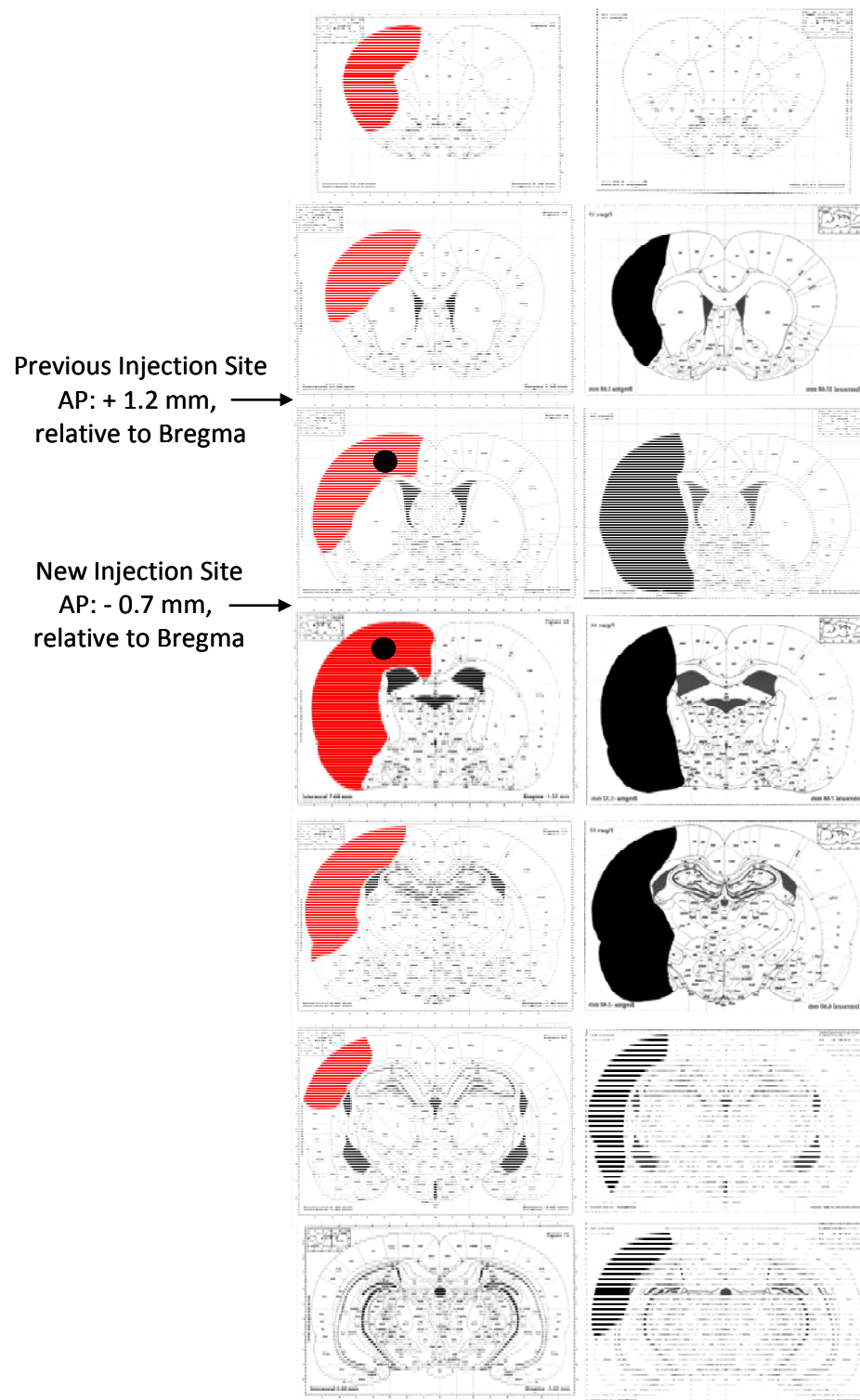
Figure 3.7:   Optimisation of Injection Location

Comparative analysis of transduction spread (red) following cortical injection of CAV2-GFP with location of infarct (black) from a representative animal from the *in vivo* control study. Proposed move of injection site is highlighted with arrows. • = Injection site.
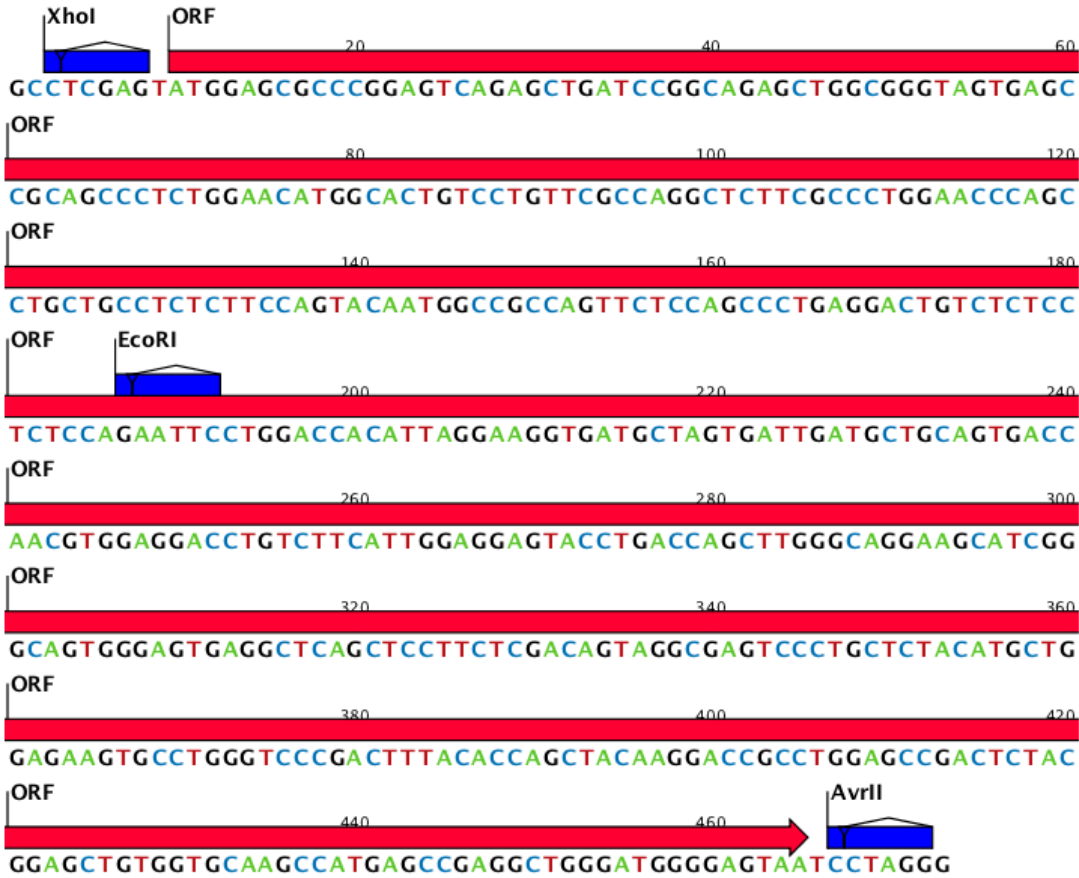
Figure 3.8: **Confirmation of CAV2-Ngb Cloning by Sequence Analysis**

Region of the open reading frame (ORF) of Ngb, shown in red, within pCAV2-Ngb. Restriction sites *Xho*I, *Eco*RI and *Avr*II are shown in blue. Image generated by CLC Sequence Viewer 6™ (Taipei, Taiwan).
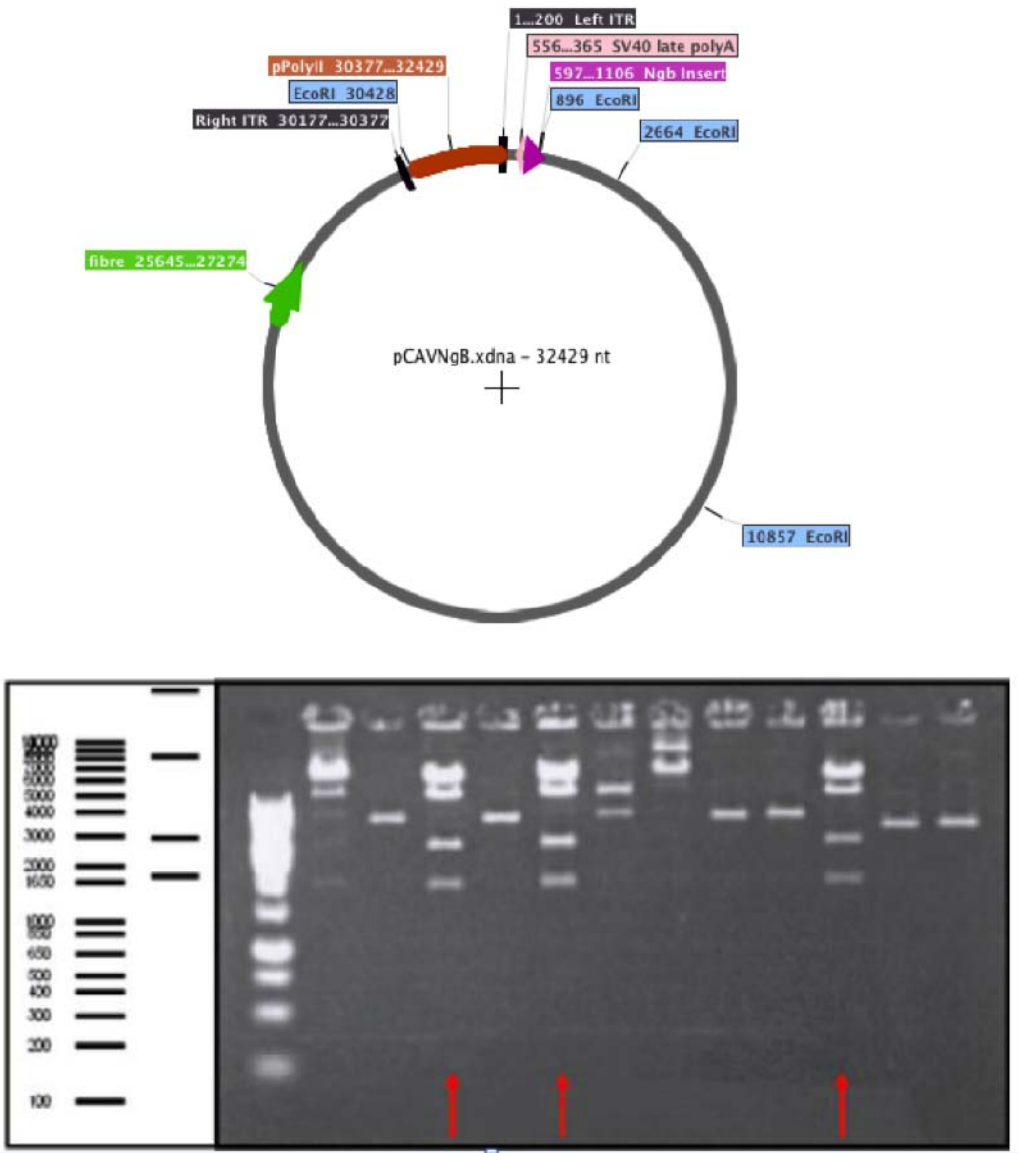
Figure 3.9:   Confirmation of CAV2-Ngb Cloning by Restriction Digest

*Eco*RI digest of pCAV-Ngb plasmid (top) was shown to result in 4 distinct bands demonstrated by Virtual Cut using Serial Cloner 2.5™ software (bottom left). Diagnostic digest with *Eco*RI of 12 selected clones demonstrated successful insertion of Ngb insert in clone 3, 5, and 10 – indicated with red arrows.

3.2.3.2   Confirmation of Functional Overexpression

To confirm the functional overexpression of Ngb from the newly generated CAV2, HepG2 cells were transduced with increasing MOI of CAV2-Ngb or control reporter gene expressing virus, CAV2-GFP (MOI of 1000, 5000, 10000 vp / cell). Inclusion of a control virus allowed any effect of canine adenovirus transduction alone on Ngb levels to be determined and also to show the transduction efficiency of this viral vector in this cell line. HepG2 cells were used as they express coxsackie adenovirus receptor (CAR), the receptor CAV2 binds; whereas the neuronal B50 cell line has low CAR expression (Figure 3.10 A & B). Transduction efficiency of HepG2 cells was assessed by transduction assay with increasing concentrations of CAV2-GFP and imaged at 36 h.

TaqMan™ qRT-PCR was performed on extracted RNA from HepG2 cells exposed to increasing concentrations of virus (Figure 3.11 A) 36 h after virus transduction. Levels of Ngb mRNA were dose-dependently increased in those cells transduced with CAV2-Ngb while those transduced with CAV2-GFP showed no significant alteration in Ngb mRNA levels. Ngb mRNA expression increased significantly in comparison to untreated control cells at MOI 1000, 5000, and 10000 (Control = 1.00 ± 0.1, *CAV2-Ngb MOI 1000 = 85.1 ± 93.6, *CAV2-Ngb MOI 5000 = 354.2 ± 45.8, *CAV2-Ngb MOI 10000 = 732.6 ± 55.0, CAV2-GFP MOI 1000 = 2.2 ± 0.4, CAV2-GFP MOI 5000 = 2.6 ± 0.3, CAV2-GFP MOI 10000 = 1.7 ± 0.1, $p < 0.001$, Student's unpaired t-test).

Over-expression of Ngb protein was determined by ICC in cells transduced with CAV2-Ngb or CAV2-GFP using a specific α-Ngb antibody. This demonstrated a marked increase in Ngb protein expression levels at MOI 1000, 5000 and 10000 vp / cell (Figure 3.11 B).

(A)
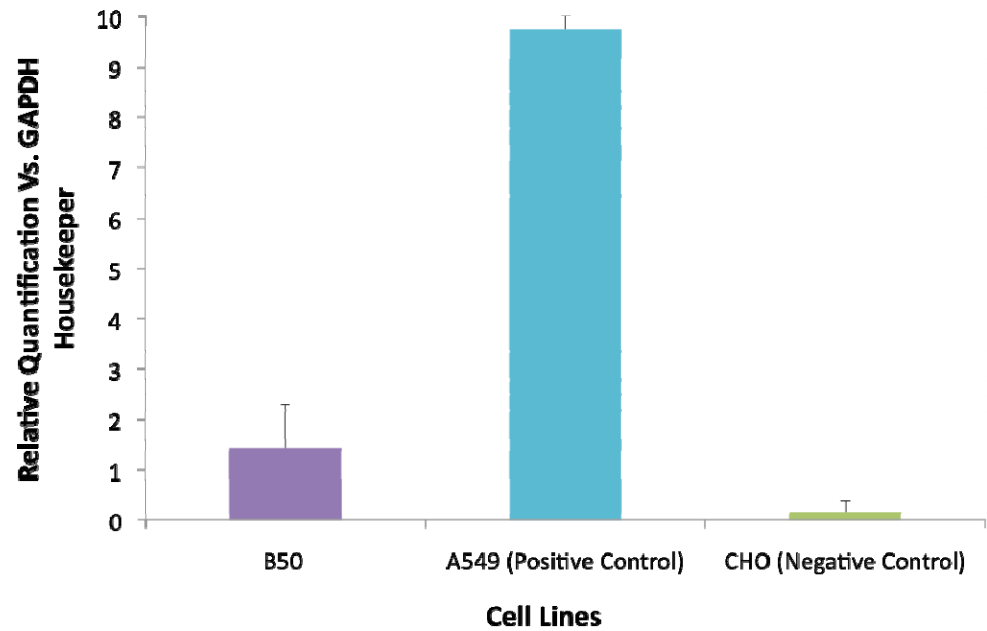
(B)
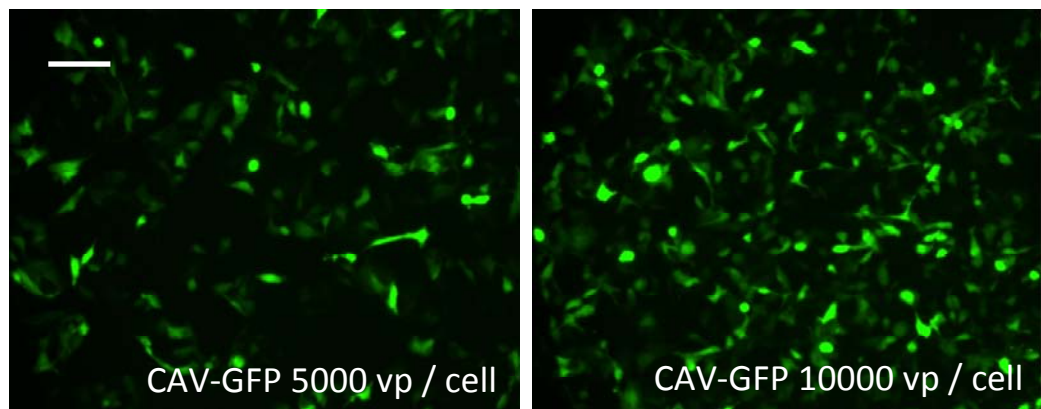
Figure 3.10:   Validation of HepG2 Cells for *In Vitro* CAV2 Study
(A) Assessment of CAR expression on B50 rat neuronal cells in comparison to CAR⁻ CHO cells and CAR⁺⁺ A549 cells, quantified by TaqMan™ qRT-PCR normalised to 18S housekeeper.   Relative quantification (RQ) was calculated from ΔΔCt (cycle threshold), *n* = 3 / group.   RQ ± RQmax is shown. (B) Transduction efficiency of CAR⁺ HepG2 (Lee *et al.*, 2004) cells with MOI of 5000 and 10000 vp CAV2-GFP. Scale bar = 100µm, x20 magnification – applicable to both panels, images obtained using confocal microscopy.

(A)

(B)
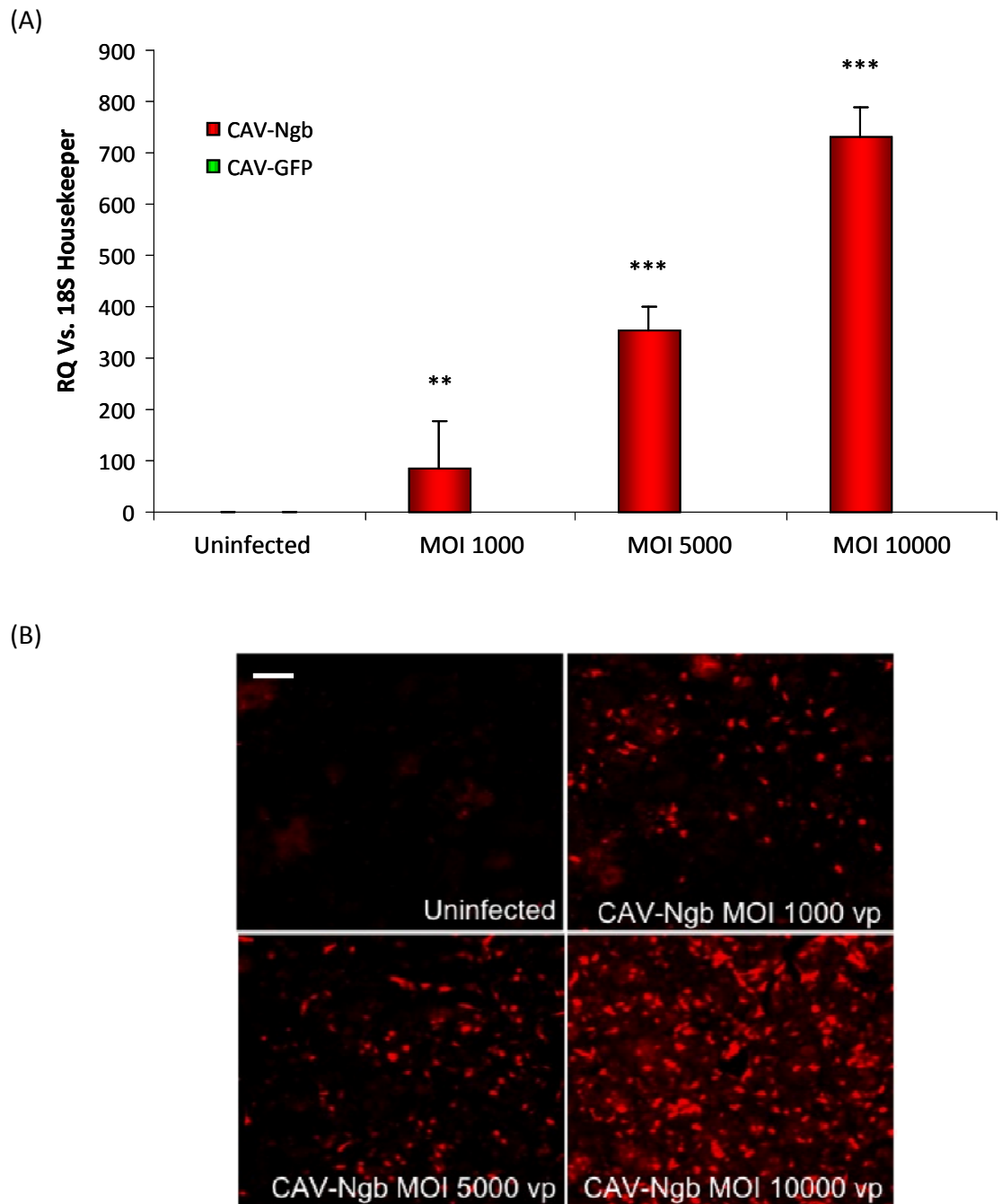
Figure 3.11:   Functional Overexpression of Ngb HepG2 cells.
(A) Increasing Ngb mRNA levels with MOI CAV2-Ngb quantified by TaqMan™ qRT-PCR and normalised to 18S in HepG2 cells. Relative quantification (RQ) was calculated from ΔΔCt (cycle threshold) and compared to levels observed in uninfected control cells. RQ ± RQmax is shown. (B) Functional overexpression of Ngb protein was demonstrated by ICC in HepG2 cells transduced with increasing MOI of CAV2-Ngb, 36 h post transduction. Ngb is stained in red (x10). Scale bar = 100μm, x20 magnification – applicable to all panels, images obtained using confocal microscopy.

3.2.4 Generation of a Ngb Overexpressing Lentivirus

From previous data (Figure 3.10 A) it was observed that B50 neuronal rat cells do not express CAR and as such CAV2-Ngb could not be utilised in the *in vitro* proof-of-concept study. Lentivirus was shown to transduce B50 neuronal rat cells at ~ 100 % efficiency (Figure 3.12 A), and therefore an Ngb-expressing lentivirus was generated to assess the benefit of Ngb overexpression in an *in vitro* model of hypoxia / reoxygenation.

3.2.4.1   *Lentivirus Generation*

Full description of lenti-Ngb generation is described in Chapter 2 (section 2.3.6). Briefly, pSFFV and PET3a_Ngb were digested overnight at *Bam*HI and *Xho*I. Ngb was gel extracted and ligations and transformations carried out with linearised pSFFV and Ngb using Quick T4 Ligase (New England Biolabs, Hitchin, UK) and transformation into JM109 competent *E. Coli* (Promega, Southampton, UK) (Figure 3.12 B).

Successful cloning was assessed by diagnostic digest at sites flanking Ngb, to show a single insert of Ngb (Figure 3.12 C). Clones exhibiting a Ngb insert assessed by diagnostic digest, were sequenced using Ngb specific primers, as shown previously (

Figure 3.8 A).

3.2.4.2   *Confirmation of Functional Overexpression*

To confirm the functional overexpression of Ngb from a newly generated lentiviral construct, B50 rat neuronal cells were transduced with increasing multiplicity of infections (MOI's) of lenti-Ngb or control reporter gene expressing virus, lenti-GFP (MOI 0.1, 1 or 5 vp / cell). Inclusion of a control virus allowed any effect of lentivirus transduction alone on Ngb levels to be determined and also to show transduction efficiency of lentivirus in B50 rat neuronal cells.

TaqMan™ qRT-PCR was performed on extracted RNA from B50 rat neuronal cells transduced with increasing concentrations of virus. Levels of Ngb mRNA were dose-dependently increased in those cells transduced with lenti-Ngb while those transduced with lenti-GFP showed no such increase (Figure 3.13). Ngb mRNA expression increased significantly in comparison to controls at an MOI of 1 vp / cell and 5 vp / cell but failed to

reach significance at the lowest MOI studied, 0.1 vp / cell (RQ for control = 1.00 ± 0.03, lenti-Ngb MOI 0.1 = 1.40 ± 0.08, **lenti-Ngb MOI 1 = 11.59 ± 0.47, **lenti-Ngb MOI 5 = 145.77 ± 6.75, lenti-GFP MOI 0.1 = 1.27 ± 0.07, lenti-GFP MOI 1 = 1.13 ± 0.03, lenti-GFP MOI 5 = 0.85 ± 0.04; **p<0.0001, unpaired t-test compared to uninfected control, using Bonferroni's correction).

Overexpression of Ngb protein was determined by ICC in cells transduced with increasing MOI using a specific α-Ngb antibody. A marked increase in Ngb expression levels was seen in the B50 rat neuronal cells transduced with the lenti-Ngb at an MOI of 5 vp / cell (Figure 3.14). IgG controls confirmed specificity of secondary antibody to specific Ngb antibody.

(A)

(B)

(C)
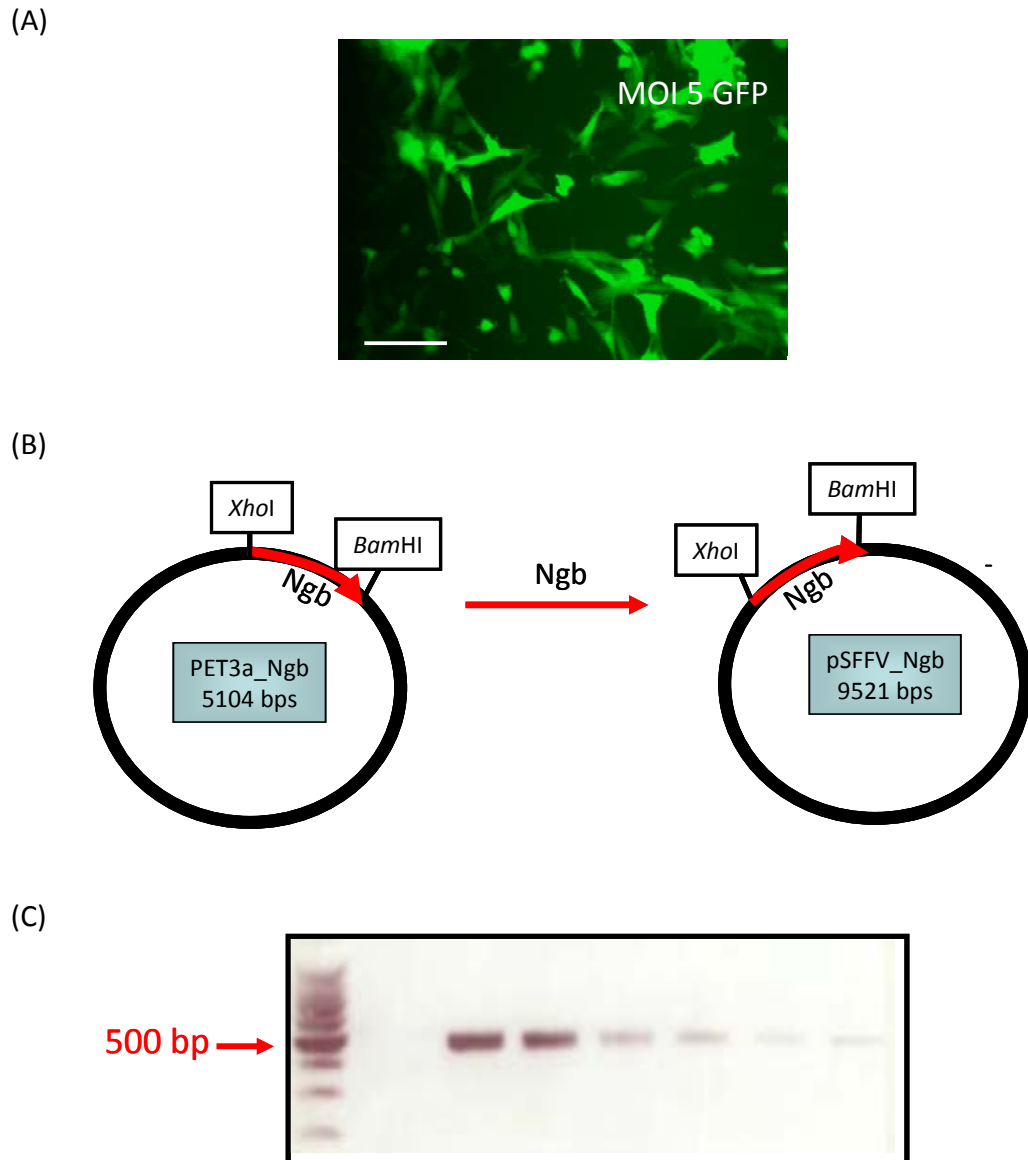
Figure 3.12: **Lentivirus Transduction Efficiency in B50 Rat Neuronal Cells and Confirmation of Subsequent Lenti-Ngb Cloning**

(A) Lenti-GFP transduced cells represent ~ 100 % transduction of B50 rat neuronal cells with lentivirus at an MOI of 5vp/cell. Scale bar = 100 µM, representative of *n*=3, images obtained using fluorescence microscopy. (B) Cloning strategy. (C) Diagnostic digest of Lenti/SFFV_Ngb assessing successful insertion of Ngb (500 bp).
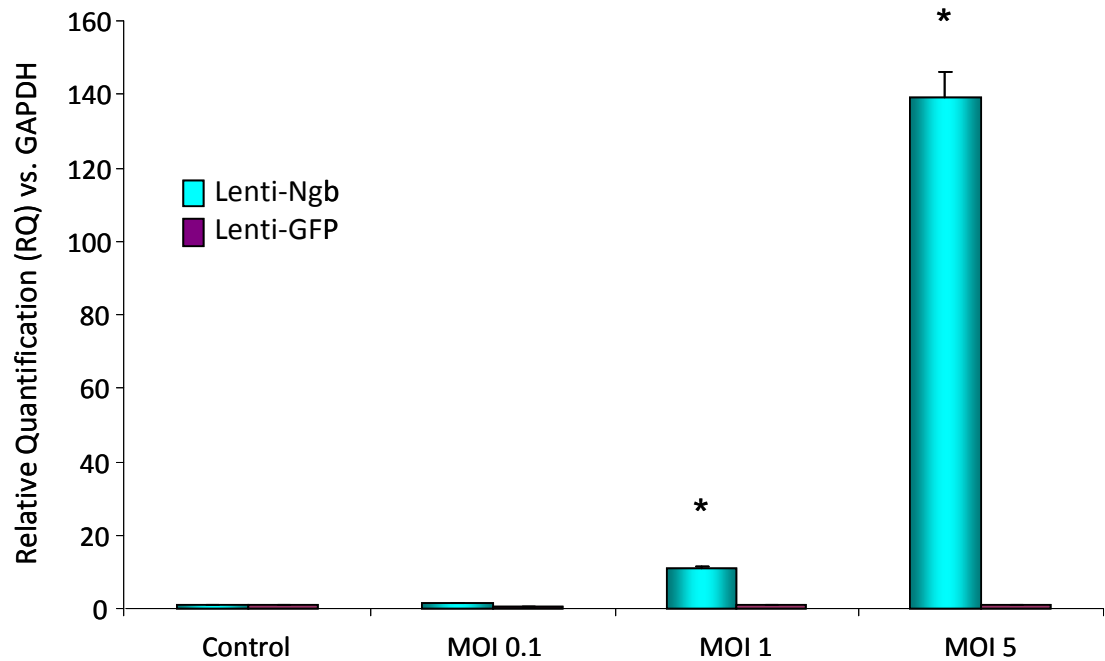
Figure 3.13:   Functional overexpression of Ngb mRNA from a lentiviral construct.

Levels of *Ngb* mRNA in B50 rat neuronal cells were quantified by TaqMan™ qRT-PCR and normalised to GAPDH following transduction with increasing concentration of virus (cells harvested for RNA extraction 3 days after virus transduction). Conditions were run in triplicate in a duplex reaction with a *Ngb* specific probe and GADPH housekeeper. Relative quantification (RQ) was calculated from ΔΔCt (cycle threshold) and compared to control virus levels. RQ ± RQmax is shown. *$p < 0.0001$, unpaired t-test compared to control virus, using Bonferroni's post-hoc correction.
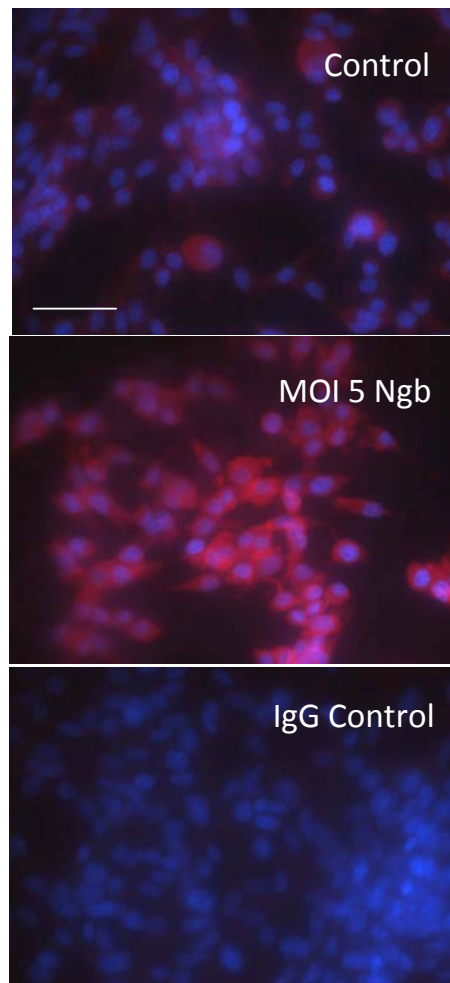
Figure 3.14:   Functional overexpression of Ngb protein from a lentiviral construct

Qualitative determination of Ngb overexpression by ICC in B50 rat neuronal cells following transduction with Ngb or GFP-overexpressing lentivirus (nuclei = blue, DAPI; Ngb = red, TRITC). Cells were fixed 3 days after virus transduction for ICC analysis. Negative staining in IgG controls demonstrates specificity of secondary antibody. Scale bar = 100 µM, applicable for all panels, images obtained using fluorescence microscopy. Representative of *n*=3.

3.3   DISCUSSION

Herein, the aim of this chapter was to determine the optimal vector for *in vivo* and *in vitro* studies.

Initially CAV2 transduction throughout the SHRSP brain was assessed following stereotactic injection into the cerebral cortex and striatum, and these data used to find the optimal injection location for transduction to the cortex. Results indicated increased cortical and overall transduction from direct injection into the cortex in comparison with striatal injection of CAV2. Subsequently, extent of transgene expression following cortical injection of lenti-GFP or CAV2-GFP was compared to allow for generation of the optimal Ngb-expressing virus for use in the *in vivo* intervention study. As the study is one of neuroprotection, transduction efficiency was of significant importance, as the greater number of neurons that could be transduced to overexpress Ngb the greater the potential protection mediated by Ngb. Results indicated significantly greater neuronal transduction and spread from a single injection of 3 x 10^9 vp CAV2-GFP in comparison to a double injection of 2 x 10^7 vp (4 x 10^7 vp total virus) lenti-GFP within the cortex of male SHRSP's, determined 7 days post-injection. In total less lentivirus was delivered in comparison to CAV2, however lentivirus is notoriously difficult to make in high titre stocks and volume of agents delivered in a single stereotactic injection cannot exceed 2 µl. To address this problem, lentivirus was super concentrated using the Lenti-X concentrator (section 2.6.6), and administered at two locations within the cortex perceived to span the region of potential penumbra. Additionally, it is necessary to note that CAV2 and lentivirus transgene expression was controlled using different promoters, CMV and SFFV, repectively. Although no specific comparative analysis of these two promotors in the nervous system *in vivo* has been assessed, *in vitro* analysis has demonstated no difference in transgene expression mediated by lentivirus under the control of either CMV or SFFV promotors (Bender *et al.*, 2007).

Previous work by collaborators had shown following striatal injection significant retrograde transport of CAV2 with subsequent gene expression into afferent structures such as the cortex, *substantia nigra*, and thalamus was observed (Soudais *et al.*, 2001). Co-injection of Sprague-Dawley rats with 1 x 10^9 vp CAV2-GFP and 1 x 10^9 vp Ad5 expressing reporter gene, red fluorescent protein (RFP), in a total volume of 2 µl at co-ordinates (AP: +1 mm, ML: +3.5 mm, DV: –5 mm, relative to Bregma) resulted in

significantly greater CAV2-mediated GFP expression in comparison to Ad-mediated RFP expression, with GFP^{+} cells found in the cortex of every coronal section from + 3 mm to – 9 mm (AP, relative to Bregma) (Soudais *et al.*, 2001). Within this region of expression, significant and equivalent neuronal specific expression spanned a rostra-caudal distance of ~ 3 mm (Soudais *et al.*, 2001), whereas the present model (using 3-fold the total vp, 3 x 10^9 vp CAV2-GFP) showed significant and equivalent expression in a region spanning ~ 7 mm rostra-caudally from injections into the cortex or striatum. The present study demonstrated retrograde transport into the cortex from a striatal injection, consistent with previous findings (Soudais *et al.*, 2001); however transduction into the cortex was relatively low and variable – perhaps due to the cortical expression making up the periphery of the total transduced area. As the region of the penumbra was perceived to exist within the cortex, the levels of CAV2-mediated cortical GFP expression following direct injection into the cortex (AP: + 1.2 mm, ML: + 3 mm, DV: - 2 mm) was assessed. This had not been assessed previously and results showed a significant and conserved expression of GFP within the cortex across the group, spanning an equivalent rostra-caudal distance of ~ 7 mm.

In order to compare this with lentivirus, animals were injected at two cortical sites with 2 x 10^7 vp lenti-GFP. Although lentivirus is highly neurotropic and currently being examined for use in a number of neurological disorders (reviewed in (Lundberg *et al.*, 2008)), *in vivo* distribution from injection site has been shown to be minimal (Baekelandt *et al.*, 2002; Blits *et al.*, 2010). This was confirmed within the present model where LV-mediated GFP expression was confined to the regions of injection. However, transduction efficiency was maximal within these regions in the present study (Figure 3.5).

The present study demonstrated reporter transgene expression at 7 days post injection. Studies have reported CAV2 mediated gene expression persists for at least 3 months (Keriel *et al.*, 2006) while lentivirus mediated expression, through integration into the host genome, is more stable and can last for at least 8 months (Mazarakis *et al.*, 2001), and has low transduction efficiency from injection site. However, LV can transduce both neurones and astrocytes very efficiently (Stitelman *et al.*, 2010) and expression is maintained for long periods. However, considering the ability of CAV2 to transduce the brain tissue, allowing it to potentially salvage a greater number of cells, a Ngb expressing CAV2 was generated for use in the *in vivo* intervention study. When comparing the location of transduction with the infarcted region following 45 tMCAO it was observed that the

injection site could be optimised my moving caudally, to maximise the neuroprotective potential of Ngb. As the injection site remained within the cortex it was not deemed necessary to assess transduction following injection at the modified location.

A Ngb expressing lentivirus was generated for use in the *in vitro* proof-of-concept study, as the B50 neuronal rat cell line was shown to have very low CAR expression, and as such could not be effectively transduced by CAV2. Efficient transduction by lentivirus was confirmed at ~ 100 % utilising an MOI of 5 vp / cell, and functional overexpression was demonstrated at both the mRNA and protein level.

This study has provided the evidence required to allow selection of the best available viral vector for use *in vitro* and *in vivo*, and shown the successful generation of these Ngb-overexpressing vectors.

Chapter 4

Results:

In Vitro Analysis of Neuroprotective Strategies

4.1 INTRODUCTION

In vitro models of hypoxia / reoxygenation to simulate the ischaemia / reperfusion observed in stroke can help to elucidate potential novel therapies prior to *in vivo* validation. Ultimately, the utility of an *in vitro* model is determined by how closely they can mimic the major cellular events observed during and after cerebral ischaemia *in vivo*. They provide a platform for allowing well-controlled, repeatable and environmentally isolated experiments without systemic confounders. These experimental models can be monitored in real time, and can isolate specific brain regions of interest. *In vitro* models have already been used successfully to ascertain details of specific mechanisms in the pathophysiology of stroke, not only furthering mechanistic understanding but also unlocking more areas for potential therapeutic development. However, some of the benefits of *in vitro* models are also what leaves them scientifically vulnerable to criticism. A lack of systemic input, bringing inflammatory mediators, and true co-culture systems leave a large portion of the mechanisms involved in lesion progression unconsidered, and may have an unknown effect on downstream signalling following injury. Also, the extracellular environment *in vitro* differs significantly to that seen *in vivo*. Some of these limitations can be addressed by manipulating studies in controlled ways to take them into account, but only if the action *in vivo* has been previously and completely reported, and even then there is no way of addressing all shortcomings. An *in vitro* model should always be validated against relevant *in vivo* models, in particular considering the specific pathways and proteins of interest. When considering the study of stroke there are a variety of tissue surrogates available including; primary cell cultures and immortalised cell lines; and brain slices or organotypic cell cultures. There are also a number of *in vitro* experimental models including; oxygen-glucose deprivation, and chemical-induced hypoxia.

Primary cell cultures are commonly used in *in vitro* experimental models of hypoxia / reoxygenation and provide the ability to examine the effect of injury on specific cell types or varying ratios of co-cultures. Co-cultures are beneficial when considering the mechanisms of stroke, as they allow examination of the interplay of neurones and glial cells in hypoxia. A confounding factor for the use of dissociated primary cultures is following mechanical and enzymatic dissociation from rat embryonic or young post-natal tissue, cells display significantly different characteristics in response to hypoxic injury from aged tissue (Lin *et al.*, 2002). In order to address this, cells need to undergo long-

term cell culture ($\sim$ 10 – 14 passages) to exhibit the classical excitotoxic response to glutamate. Immortalised cell lines provide a useful tool in *in vitro* models as they are easy to obtain, consistent, well characterised and can be grown for prolonged periods. However, the modifications that have been used to evade normal cellular senescence can cause disruption of normal intracellular signalling cascades and apoptotic machinery. Cell cultures, whether singular or co-culture primary systems, or immortalised cell lines face further limitations in that they are normally grown in a monolayer and cells of the nervous system have been shown to behave differently when grown in constructs (Fawcett *et al.*, 1989). Biodegradable macroporous hydrogels can be used as tissue scaffolding to allow co-cultures to be grown in 3D constructs, but does not allow for any anatomical organisation (Cullen *et al.*, 2007).

Hypoxia / reoxygenation (hypoxia / reoxygenation) can be initiated *in vitro* by two broad types of manipulation; oxygen ($\pm$ glucose / serum) reduction / deprivation, resulting in hypoxia or anoxia, respectively; or chemical initiation of hypoxic cascades. Chemical hypoxia induced by treatment with sodium cyanide (NaCN), potassium cyanide (KCN), hydrogen peroxide (H_2O_2,), or L-glutamate causes a greater release of reactive oxygen species than reduction or deprivation of oxygen (Arumugam *et al.*, 2006). When oxygen reduction or deprivation is teamed with glucose depletion, it is termed as either oxygen / glucose deprivation (OGD) or *in vitro* ischaemia. The model in the present study utilises a hypoxic environment (1% O_2) and a serum free, low glucose medium to induce ischaemia-like conditions in our immortalised B50 rat neuronal cell line.

A number of studies have confirmed *in vitro* injury-induced expression of neuroglobin (Ngb) as an endogenous mechanism of protection with increasing exposure to *in vitro* hypoxia / anoxia. Sun *et al.* (2001) first described Ngb expression to be increased with increasing exposure (4, 6, 16 and 24 h) to anoxia. Reoxygenation following anoxia varied per timepoint, with cells exposed to the remaining period of 24 h following hypoxia, (i.e. 20, 18, 8 and 0 h reoxygenation, respectively). The study utilised primary cultured neurones with glucose supplementation during anoxia, and Ngb expression was assessed at the protein level by western blot and immunocytochemistry. These data were largely supported in another study (Fordel *et al.*); using a 1 % O_2 infused hypoxic chamber and no reoxygenation, showing Ngb to be upregulated in a time-dependent manner from 4 h to 48 h in HN33 neuronal cells (an immortalised hippocampal neuronal cell line). Interestingly, this group went on to repeat this experiment at 3 % O_2 and found no significant difference

in Ngb upregulation occurring before 48 h (Fordel *et al.*). A later report (Rayner *et al.*, 2006) showed Ngb levels to be differentially expressed in ND15 cell (a hybrid dorsal root ganglia neuroblastoma cell line) with differing lengths of reoxygenation following 60 min of hypoxia induced by argon degasification (leaving < 1.2 % O_2) of medium before cells were incubated in an argon flushed chamber. They showed Ngb was significantly increased with 5 h reoxygenation but not with 2 or 24 h. Taken together these data suggested a role for Ngb in an endogenous injury-induced response to hypoxia / reoxygenation injury, however its regulation is clearly under dynamic control and varies according to experimental protocol.

Sun *et al.* (2001) further demonstrated that antisense-mediated knockdown of Ngb increased the neuronal cultures vulnerability to hypoxia / reoxygenation injury, whilst overexpression of Ngb using transfection with a recombinant plasmid containing Ngb cDNA in HN33 cells granted relative protection from anoxia-induced injury, signifying a neuroprotective role for Ngb (Sun *et al.*, 2001). Various groups have manipulated Ngb overexpression for neuroprotection *in vitro* with the majority finding this to be protective (Antao *et al.*, 2010; Jin *et al.*, 2008a; Li *et al.*, 2008b; Zhou *et al.*, 2008) in various *in vitro* models of experimental stroke. It was reported that a reduction in NO toxicity in HN33 cells pre-treated with a Ngb-expressing plasmid following initiation of chemical hypoxia using the NO-producing chemicals; S-nitroso-N-acetyl-dl-penicillamine (SNAP), diethylenetriamine NONOate (DETA/NONOate), and sydnonimine (SIN-1) (Jin *et al.*, 2008a). Using the same expression plasmid Li *et al.,* (2008a) demonstrated an improvement in cells survival in Ngb overexpressing cells following induction of chemical hypoxia using H_2O_2. In addition, they showed Ngb overexpression mediated cell survival through decreasing ROS/RNS production, inhibition of caspase 3/7 activity, decreasing lipid peroxidation and maintaining mitochondrial membrane potential. However, they also reported the improvement in cell survival observed was not attributed to an increase in SOD, GPX or catalase activity {Li *et al.*, 2008a}. SH-SY5Y neuroblastoma cells were challenged with H_2O_2 for 2 h following pre-treatment with a Ngb expressing plasmid (unspecified). Ngb transfected cells demonstrated an improvement in cell survival assessed by MTT assay; maintenance of mitochondrial membrane potential; a reduction in Ca^{2+} influx; and reduction in intracellular depletion of ATP; in comparison to control plasmid {Zhou *et al.*, 2008}. Conversely, Peroni *et al.* (2007) found a HIV-1 TAT protein to upregulate Ngb failed to protect neuronal cells against oxygen-glucose deprivation (Peroni *et al.*, 2007).

Following experimental hypoxia / reoxygenation or ischemia / reperfusion injury *in vivo*, the pattern and levels of endogenous Ngb expression remains unclear, with a number of contradictory reports. Studies in mice exposed to increasing lengths (4 – 48 h) of hypoxia (7 % O_2) with no re-oxygenation, Ngb was shown to be time-dependently increased at the mRNA level taken from whole hemisphere homogenates (Fordel *et al.*, 2007a). When reoxygenation was introduced in mice exposed to 48 h hypoxia, Ngb expression was increased with 8 h reoxygenation but not with 24 h, suggesting Ngb is upregulated in hypoxia but only transiently in reoxygenation. In relation to this, Hundahl *et al.* (Hundahl *et al.*, 2006b) found Ngb mRNA expression to be decreased in the ipsilateral hemisphere in spontaneously-hypertensive rats at 24 h following 90 min tMCAO in comparison to sham controls. However, IHC to localise Ngb expression one-week post-tMCAO showed no significant difference in levels or location in comparison to contralateral hemisphere or sham control. Schmidt-Kastner and colleagues (Schmidt-Kastner *et al.*, 2006) assessed Ngb expression following 12.5 min global brain ischaemia in different regions of the brain of male Wister rats. They found no significant change in Ngb expression using their experimental model of global cerebral ischaemia across the hippocampus, the dentate gyrus or the cortex at 0.5, 1, 3, 6 or 24 h post ischaemia.

Although Ngb is shown to be upregulated with hypoxia and transiently with hypoxia / reoxygenation *in vitro*, how this occurs is unknown but believed to be potentially activated by the transcription factor hypoxia-inducible factor 1-alpha (HIF-1α). In support of this mechanism of upregulation, Ngb was shown to be upregulated without hypoxic induction in the presence of cobalt and deferoxamine, two well-established activators of HIF-1α (Gong *et al.*, 2001). In addition, the 5'-untranslated region of Ngb contains consensus-binding sequences with HIF-1α, and HIF-1 (+ / -) knockout mice show a downregulation of Ngb expression following exposure to both 12 % and 7 % O_2 for 48 h in comparison to CD1 control mice (Fordel *et al.*, 2004b). In support of *in vitro* studies, endogenous upregulation of Ngb *in vivo* has been shown during hypoxia / ischaemia but reports addressing subsequent reoxygenation / reperfusion have been contradictory.

The c-Jun N-terminal Kinases (JNKs) are well-established mediators of apoptosis (reviewed in, (Borsello *et al.*, 2007)). They have been shown by the majority of *in vitro* cerebral ischaemia studies to be upregulated in response to hypoxic stress. Initial studies of *in vitro* ischaemia using primary neuronal cells and glutamate induction of excitotoxic stress illustrated a time-dependent increase in activated (phosphorylated) JNK (p-JNK) and

it's downstream target, c-Jun (p-c-Jun), with increasing exposure to glutamate (Kawasaki *et al.*, 1997a; Kawasaki *et al.*; Schwarzschild *et al.*, 1997a). Furthermore, utilising the excitotoxic glutamate receptor agonist (NMDA) as an initiator of excitotoxic stress (Borsello *et al.*, 2003b), demonstrated 10 - 30 min exposure to 100 μM NMDA resulted in a time-dependent increase in p-JNK, p-c-Jun and c-Jun in primary cortical neurones (Borsello *et al.*, 2003a). p-JNK was also shown to be increased after 3 h OGD in PC12 neuronal cells (Tabakman *et al.*, 2005). Interestingly, it has been reported that with increasing lengths of reoxygenation following 3 h OGD there is no significant change in p-JNK or p-c-Jun (Liu *et al.*, 2009) in primary cortical neurons. However, Chen and colleagues in 2011 (Chen *et al.*, 2011) reported an increase in p-JNK with increasing lengths of reoxygenation following 4 h OGD in primary cortical neurones. Collectively these *in vitro* studies demonstrate levels of JNK expression during hypoxia or excitotoxicity are consistently increased but changes in expression upon reoxygenation are contradictory.

In support of the role of JNK in cell death following cerebral ischaemia, a number of studies have assessed endogenous expression of JNK post ischaemia / hypoxia *in vivo*. Kuan *et al.* (Kuan *et al.*, 2003) showed increased c-Jun expression in the hippocampal subfield following cerebral ischaemia to be correlated with the presence of pyknotic nuclei of apoptosing cells. They went on to show that with increasing lengths of reperfusion, there was a time-dependent increase in p-c-Jun and p-JNK activity up to 24 h post insult, which was abolished in *Jnk3* knockout (-/-) mice. Interestingly, basal activity of c-Jun was reduced to 35 % of wildtype control in *Jnk1* -/- mice but no difference was noted in *Jnk2* or *Jnk3* -/- mice. Taken together these data suggest a role for JNK3 in stress-induced JNK signalling, and that JNK1 is primarily responsible for the high levels of basal JNK activity in the brain.

Given the inconsistencies in alterations in expression levels and activation of Ngb and JNK *in vitro* and *in vivo*, the first aim in this chapter was to determine changes in expression (mRNA and protein) in the *in vitro* model of hypoxia / reoxygenation using rat B50 neuronal cells. Second, to ascertain if these changes were reflected in the infarct core and / or tissue immediately surrounding it in the acute stages post tMCAO in *ex vivo* samples. Finally, to determine the *in vitro* effect of combined antioxidant and anti-apoptotic intervention through gene-based overexpression of Ngb alone and in combination with

JNK inhibition through the use of a pharmacological inhibitor, in a number of assays of oxidative stress and apoptosis.

4.2 RESULTS

4.2.1 Injury-Induced Synthesis of Ngb and JNK mRNA and Protein

4.2.1.1 *Hypoxic Induction of Ngb Synthesis In Vitro*

In order to determine the effect of *in vitro* hypoxia / re-oxygenation in the neuronal B50 rat cell line on endogenous injury-induced synthesis of Ngb, characterised at both the mRNA and protein level, cells were exposed to increasing lengths of hypoxia with serum starvation (3, 6, 9 and 18 h) with 24 h re-oxygenation in complete medium before lysis in QIAzol for RNA extraction and TaqMan™ qRT-PCR, lysis in RIPA buffer for western immunoblotting, or fixing on coverslips in 4 % (w/v) paraformaldehyde for ICC. Increasing exposure to hypoxia with reoxygenation resulted in a time-dependent increase in Ngb mRNA synthesis determined by TaqMan qRT-PCR, which reached statistical significance at 9 and 18 h (Figure 4.1). Samples exposed to 3 and 6 h of hypoxia showed no significant difference in Ngb synthesis in comparison to basal control levels (RQ for control = 1.00 ± 0.03, 3 h = 0.91 ± 0.04, 6 h = 1.04 ± 0.04, *9 h = 1.54 ± 0.13, **18 h = 2.59 ± 0.10, *n*=3, mean $\pm$ SEM).

The time-dependent hypoxia-induced increase in Ngb mRNA synthesis levels was reflected at the protein level determined by immunocytochemistry (ICC) (Figure 4.2). Of note, in addition to the increase in Ngb synthesis in B50 neuronal cells is the reduction in total cell number with increasing time in hypoxia prior to reoxygenation (Figure 4.2).
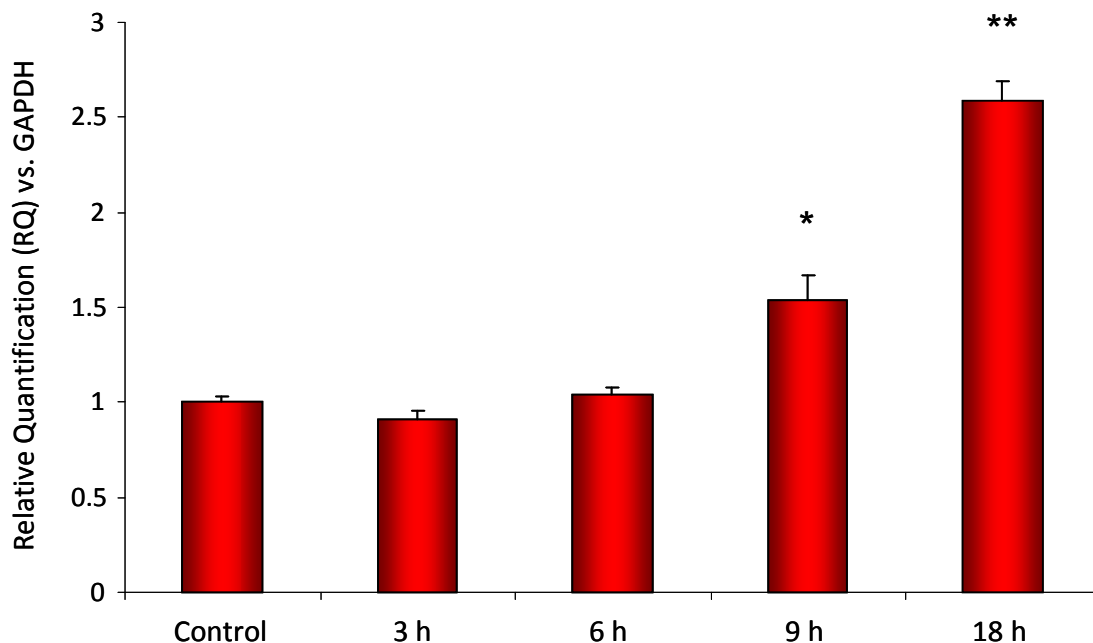
Figure 4.1:   Characterisation of endogenous injury-induced synthesis of Ngb mRNA.

Taqman™ analysis for Ngb vs. GAPDH loading control shows a time-dependent increase in Ngb at the mRNA level up to 18hr time point with 24 h reoxygenation. Conditions were run in triplicate in a duplex reaction with a Ngb specific probe and GADPH housekeeper probe with results normalised to GAPDH. Results shown are relative quantification (RQ) calculated from ΔΔCt (cycle threshold) compared to normoxic control RQ ± RQmax is shown, representative of *n*=3. *p<0.05 & **p<0.001, respectively, unpaired t-test compared to normoxic control, using Bonferroni's post-hoc correction.
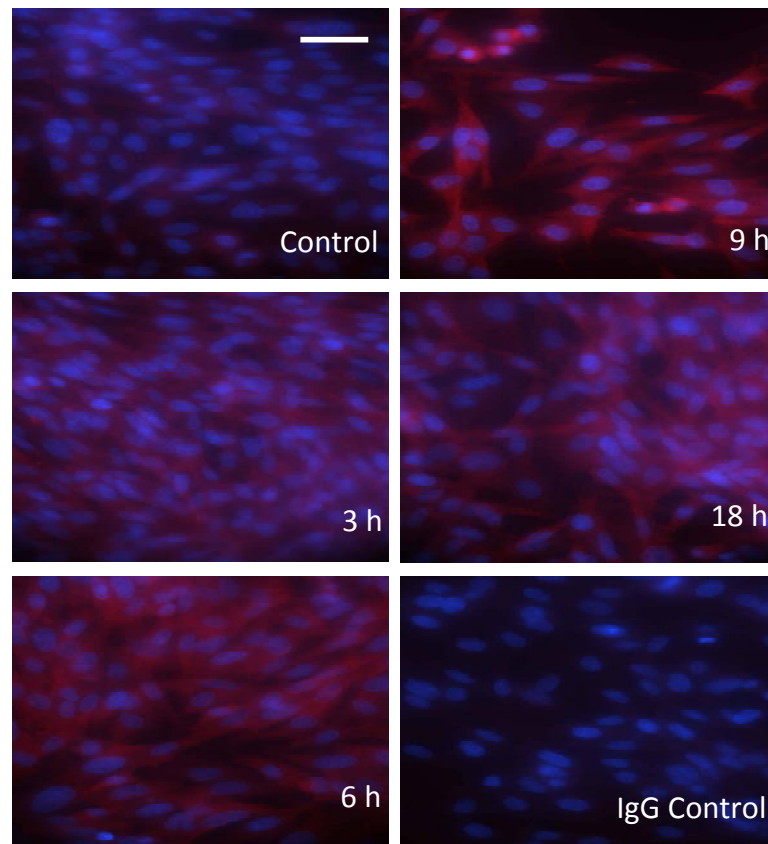
Figure 4.2:   Characterisation of endogenous injury-induced synthesis of Ngb protein, assessed by ICC.

Qualitative determination of Ngb synthesis in B50 rat neuronal cells by ICC following increasing exposure to hypoxia with 24 h reoxygenation shows an increase in protein synthesis with increasing exposure to hypoxia (nuclei = blue, DAPI; Ngb = red, TRITC). Representative of n = 3. Scale bar = 50 μm.

4.2.1.2 Hypoxic Induction of JNK Synthesis In Vitro

JNK is a well-characterised mediator of apoptosis. In order to characterise the efficacy of JNK inhibition it was necessary to firstly determine changes in mRNA and protein levels following the hypoxic challenge in B50 rat neuronal cells. Using specific probes for the 3 isoforms of the JNK gene (*Jnk1*, *Jnk2* and *Jnk3*), a significant upregulation of the *Jnk3* gene was seen following exposure to 6, 9 and 18 h of hypoxia with reoxygenation (Figure 4.3) (RQ for control = 1.00 ± 0.1, 1 h = 1.61 ± 0.1, 3 h = 2.11 ± 0.8, *6 h = 3.04 ± 2.1, *9 h = 3.10 ± 0.3, **18 h = 9.19 ± 0.1, mean $\pm$ SEM, $n=3$). No change in levels of *Jnk1* or *Jnk2* mRNA was observed following increasing exposure to hypoxia with reoxygenation (Figure 4.3). It has previously been reported that while *Jnk1* and *Jnk2* are expressed ubiquitously, *Jnk3* is almost entirely expressed in the brain and is the main mediator of neuronal JNK induced apoptosis (Kuan *et al.*, 2003). Immunoprecipitation was performed prior to SDS-PAGE and western blotting to determine synthesis of activated JNK3 protein (p-JNK3) following increasing exposure (1, 2, 4, 6, 9, and 18 h) to hypoxia with reoxygenation. A time-dependent increase in phospho-JNK3 was observed, reflecting data from qRT-PCR analysis (Figure 4.4).
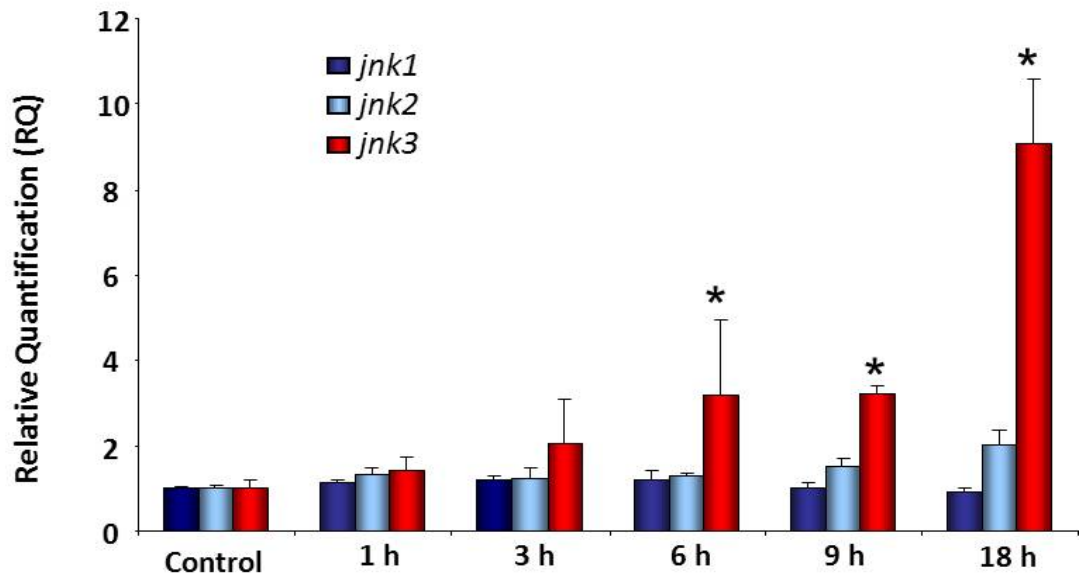
Figure 4.3: **Characterisation of *in vitro* endogenous injury-induced synthesis of *Jnk1*, *Jnk2* and *Jnk3*.**

Levels of *Jnk1, Jnk2* or *Jnk3* mRNA were quantified by TaqMan™ qRT-PCR from B50 rat neuronal cells exposed to increasing lengths of hypoxia before 24 h reoxygenation and normalised to GAPDH. Conditions were run in triplicate in a duplex reaction with *Jnk1*, *Jnk2*, and *Jnk3* specific probes and GADPH housekeeper. Relative quantification (RQ) was calculated from ΔΔCt (cycle threshold) and compared to control levels. RQ ± RQmax is shown. *p<0.016, unpaired t-test compared to normoxic control, using Bonferroni's post-hoc correction.
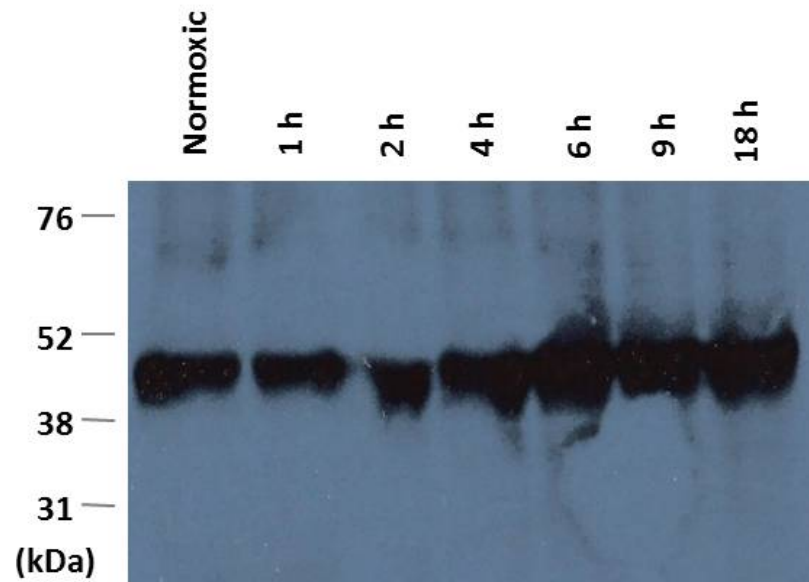
Figure 4.4:   Characterisation of endogenous injury-induced synthesis of p-JNK3 *in vitro*.

Western blot of phospho-JNK synthesis in B50 rat neuronal cell lysates (50 μg protein normalised by BCA) exposed to increasing times of hypoxia prior to 24 h reoxygenation. Cell lysates were immunoprecipitated using a α-total phosphorylated JNK antibody and subjected to SDS-PAGE. Membranes were then probed with a α-JNK3 specific antibody. Representative of *n*=3.

4.2.1.3 Neuroglobin Expression Following Cerebral Ischaemia / Reperfusion In Vivo

To ascertain if the altered levels of Ngb mRNA determined *in vitro* were reflected *in vivo*, TaqMan™ qRT-PCR was performed on brain tissue from rats exposed to 45 min tMCAO. *Ex vivo* analysis was performed by flash-freezing brain tissue at increasing time-points (3, 6, and 24 h) following tMCAO. Synthesis levels of Ngb mRNA were assessed by TaqMan™ from RNA extracted from brain homogenate, taken from the perceived anatomical regions of the peri-infarct or infarct. To serve as controls, the corresponding anatomical regions of the sham-operated brains were collected and RNA extracted for baseline Ngb mRNA synthesis levels.

In the region of the infarct, Ngb synthesis was significantly increased compared to samples from sham procedure brains at 3 h post-tMCAO whilst at 6 h post-tMCAO Ngb synthesis was significantly lowered compared to sham control (Figure 4.5). At 24 h Ngb synthesis levels exhibited no difference from sham controls (RQ for sham = 1 ± 0.05, *3 h = 1.46 ± 0.09, *6 h = 0.74 ± 0.03, 24 h = 0.86 ± 0.09, unpaired t-test using Bonferroni's correction ($p \leq 0.016$), compared to sham control). Due to a lack of available tissue, Ngb expression levels could not be assessed in the peri-infarct region.

4.2.1.4 Jnk1, Jnk2, and Jnk3 Expression Following Cerebral Ischaemia / Reperfusion In Vivo

To ascertain if the altered levels of *Jnk1*, *Jnk2*, and *Jnk3* determined *in vitro* were reflected *in vivo*, TaqMan™ qRT-PCR for the 3 *Jnk* isoforms was also performed on brain tissue exposed to 45 min tMCAO, using specific *Jnk1*, *Jnk2*, and *Jnk3* probes.

In the region of the infarct (Figure 4.6), levels of *Jnk1* mRNA were not significantly changed with increasing time post-tMCAO compared to sham control (RQ for sham = 1 ± 0.18; 3 h = 0.86 ± 0.13; 6 h = 1.02 ± 0.10; 24 h = 1.43 ± 0.12; unpaired t-test using Bonferroni's correction, $p \leq 0.016$). Meanwhile, *Jnk2* exhibited a significant decrease in mRNA synthesis levels 3 and 6 h post-tMCAO. By 24 h post-MCAO there was no significant difference in *Jnk2* mRNA synthesis levels in comparison to sham controls (RQ for sham = 1 ± 0.07; *3 h = 0.55 ± 0.02; *6 h = 0.69 ± 0.05; 24 h = 0.66 ± 0.12; unpaired t-test using Bonferroni's correction, *$p \leq 0.016$). However, levels of *Jnk3* mRNA were significantly decreased 3 h post-tMCAO but exhibited no significant difference from sham

controls at 6 or 24 h post-tMCAO (sham = 1 ± 0.05; *3 h = 0.64 ± 0.02; 6 h = 0.83 ± 0.07; 24 h = 0.71 ± 0.14; unpaired t-test using Bonferroni's correction, *p≤0.016).

In the region of the peri-infarct (Figure 4.7), levels of *Jnk1* mRNA were significantly lowered 3, 6 and 24 h post-tMCAO compared to sham controls (RQ for sham = 1 ± 0.04; *3 h = 0.15 ± 0.01; *6 h = 0.47 ± 0.05; *24 h = 0.33 ± 0.01; unpaired t-test using Bonferroni's correction, *p≤0.016). Levels of *Jnk2* mRNA were not significantly altered from sham control at any time-point post-tMCAO (RQ for sham = 1 ± 0.08; 3 h = 0.91 ± 0.07; 6 h = 1.24 ± 0.15; 24 h = 0.70 ± 0.06; unpaired t-test using Bonferroni's correction, *p≤0.016). However, levels of *Jnk3* mRNA were significantly lowered at 3 h post-tMCAO but were not altered from sham control at later time-points (sham = 1 ± 0.07; *3 h = 0.61 ± 0.08; 6 h = 0.89 ± 0.14; 24 h = 0.66 ± 0.08, unpaired t-test using Bonferroni's correction, *p≤0.016).
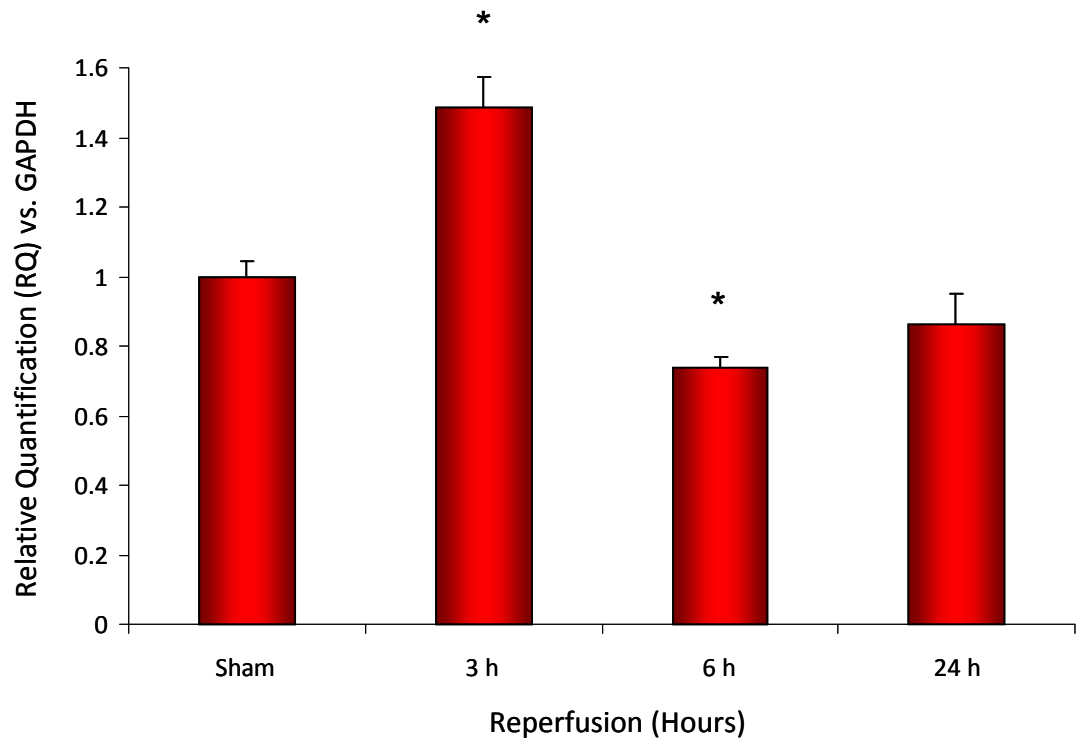
Figure 4.5: **Characterisation of Ngb synthesis post-tMCAO in infarct tissue.**

Levels of *Ngb* mRNA were quantified by TaqMan™ qRT-PCR from RNA isolated from perceived infarct tissue at increasing times from tMCAO in SHRSP and normalised to GAPDH. Conditions were run in triplicate in a duplex reaction with *a Ngb* specific probe and GADPH housekeeper. Relative quantification (RQ) was calculated from ΔΔCt (cycle threshold) and compared to sham levels. RQ ± RQmax is shown. *p<0.016, unpaired t-test compared to sham control, using Bonferroni's post-hoc correction, *n* = 4.

(A)

(B)

(C)
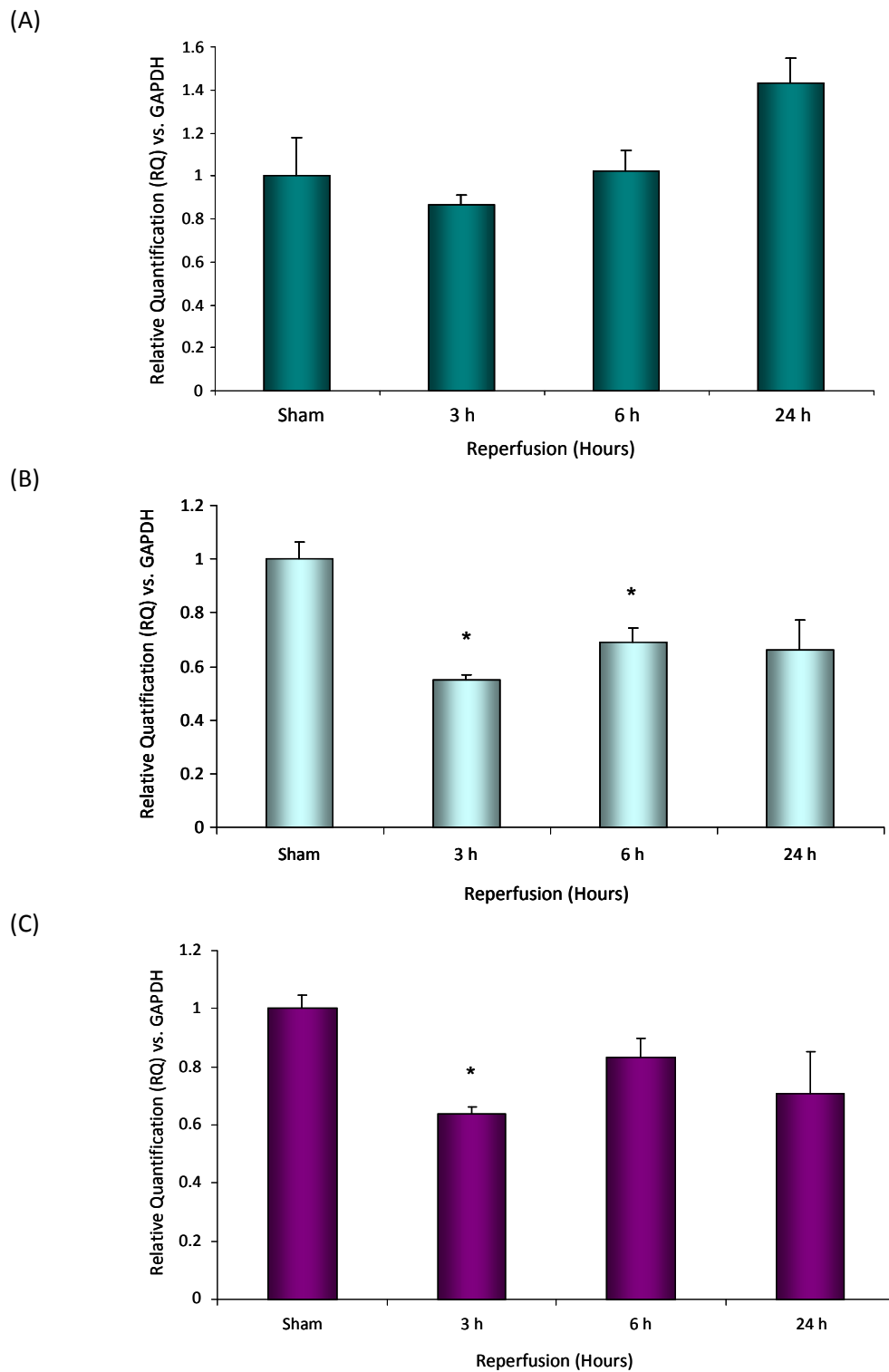
Figure 4.6:   Characterisation of *Jnk1*, *Jnk2* and *Jnk3* Synthesis post-tMCAO in Infarct tissue.

Levels of *Jnk1* (A), *Jnk2* (B) or *Jnk3* (C) mRNA were quantified by TaqMan™ qRT-PCR from RNA isolated from perceived infarct tissue at increasing times from tMCAO in SHRSP and normalised to GAPDH. Conditions were run in triplicate in a duplex reaction with *Jnk1*, *Jnk2*, and *Jnk3* specific probes and GADPH housekeeper. Relative quantification (RQ) was calculated from ΔΔCt (cycle threshold) and compared to sham levels. RQ ± RQmax is shown. *$p < 0.016$, unpaired t-test compared to sham control, using Bonferroni's post-hoc correction.

(A)

(B)

(C)

Figure 4.7:   Characterisation of *Jnk1*, *Jnk2* and *Jnk3* Synthesis post-tMCAO in Peri-Infarct Tissue.

Levels of *Jnk1* (A), *Jnk2* (B) or *Jnk3* (C) mRNA were quantified by TaqMan™ qRT-PCR from RNA isolated from perceived peri-infarct tissue at increasing times from tMCAO in SHRSP and normalised to GAPDH. Conditions were run in triplicate in a duplex reaction with *Jnk1*, *Jnk2*, and *Jnk3* specific probes and GADPH housekeeper. Relative quantification (RQ) was calculated from $\Delta\Delta$Ct (cycle threshold) and compared to sham levels. RQ ± RQmax is shown. *p<0.016, unpaired t-test compared to sham control, using Bonferroni's post-hoc correction.

145

4.2.2   Confirmation of Function and Optimisation of SP600125

4.2.2.1   *JNK inhibitor (SP600125)*

To assess the optimal SP600125 concentration for use in our *in vitro* model, cells were treated with increasing concentrations of SP600125 (1, 2, 5, 10, 20, 50 or 100 μM) in sterile DMSO for 30 min prior to 9 h hypoxia. The final concentration of DMSO did not exceed 1% (v/v) of total volume. Following 24 h reoxygenation, bright field images were taken to assess cell morphology and number before lysis in RIPA buffer to determine levels of p-JNK protein as an indicator of apoptosis with increasing [SP600125] preformed by immunoprecipitation, SDS-PAGE and subsequent western blotting.

Bright field images (Figure 4.8 A) showed high levels of cell rounding and death in untreated cells exposed to hypoxia / reoxygenation with a dose-dependent improvement in cell morphology and increase in number when pre-treated with SP600125 at concentrations of 1 - 20 μM. At 50 and 100 μM drug toxicity was observed. Time-matched control cells were treated with equal volumes of DMSO (< 1% v/v) as vehicle control and showed no difference in cell morphology or number from untreated controls. Western blot (Figure 4.8 B) shows a dose-dependent decrease in activated JNK (α-JNK).

From these studies, SP600125 was used at a concentration of 20 μM for further *in vitro* analysis.

(A)
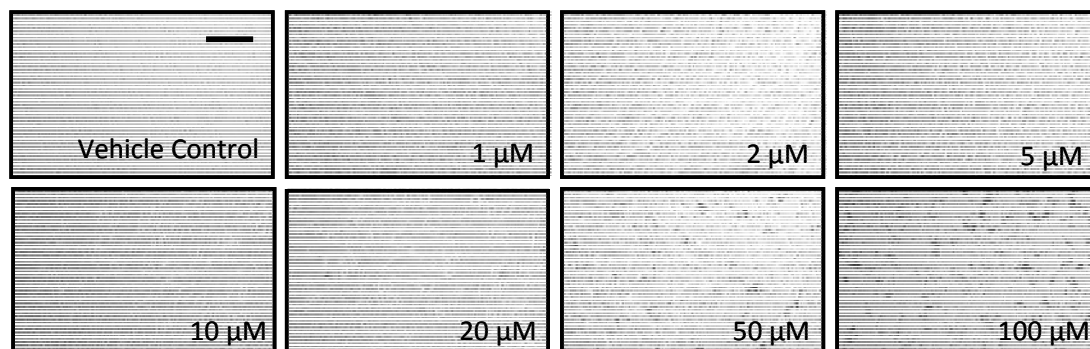
(B)
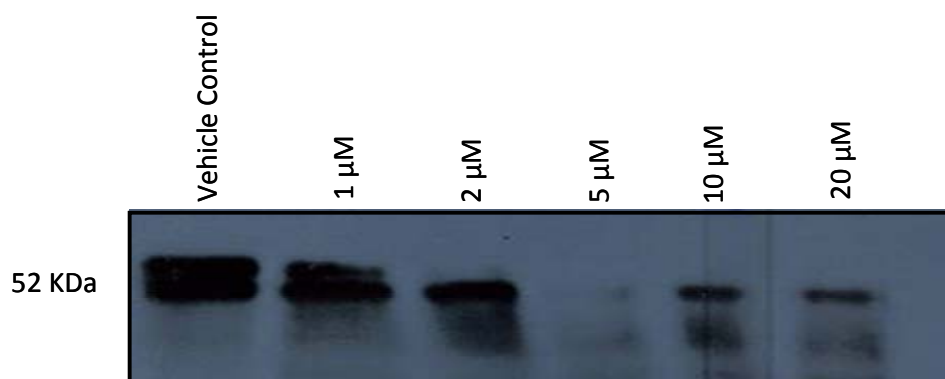
Figure 4.8:   Optimisation of SP600125.

(A) Bright field images of B50 rat neuronal cells pre-treated with increasing doses of SP600125 prior to 9 h hypoxia with 24 h reoxygenation. Scale bar = 200µm and applies to all panels. **(B)** Levels of p-JNK assessed by western blot of protein extracted from B50 rat neuronal cells pre-treated with increasing doses of SP600125 prior to 9 h hypoxia with 24 h reoxygenation.

4.2.3 Determination of combined efficacy of antioxidant and anti-apoptotic intervention in an *in vitro* model of hypoxia / reoxygenation

In assessing the efficacies of the individual therapies alone and in combination, two oxidative stress and two apoptosis assays were optimised for use. For each assay, cells were seeded and 24 h later transduced with either lenti-Ngb or control lenti-GFP (MOI 5), as previously described (section 2.4.1). 48 h post-transduction and immediately prior to hypoxia cells were incubated with 20 μM SP600125 or same volume (< 1 % v/v) DMSO (vehicle control) for 30 min. Cells were placed in the hypoxic chamber for 9 h after which time cells were returned to complete medium with SP600125 or DMSO being re-administered and left for 24 h reoxygenation in a standard incubator before experimental analysis. Each condition was duplicated in a separate plate not exposed to hypoxia to ensure no baseline toxicity of treatments and to serve as a normoxic control for each condition.

4.2.3.1 Electron Paramagnetic Resonance (EPR)

EPR and appropriate probe was used to provide a quantitative measure of superoxide (SO) released from a monolayer of cells *in situ* over a period of 60 min. Cells were incubated with 10 mM CPH spin probe in Krebs buffer for the final hour of the 24 hr reoxygenation period. After 60 min the spin probe / Krebs solution mixture was removed, and immediately read on the E-Scan Analyzer. The CPH / Krebs solution mixture was replaced with RIPA buffer and protein concentration determined by BCA assay to allow each sample to be normalised to input protein.

Hypoxic challenge in B50 rat neuronal cells resulted in a significant increase in SO levels determined by EPR (Figure 4.9). Those cells pre-treated with lenti-Ngb demonstrated significantly reduced SO levels in comparison with uninfected control and vehicle control cells. Treatment with SP600125 alone did not have a significant effect on SO levels. Importantly, the combination of SP600125 and lenti-Ngb treatment induced a further significant reduction in SO levels from lenti-Ngb or SP600125 treatment alone (Hypoxic [control = 838 ± 30; DMSO = 821 ± 19; lenti-GFP = 780 ± 54; *lenti-Ngb = 712 ± 31; *SP6001215 = 766 ± 2; *†lenti-Ngb + SP600125 = 571 ± 11; *lenti-Ngb + DMSO = 664 ± 7; *lenti-GFP + SP600125 = 744 ± 15 counts / min / *ng* protein] unpaired t-test compared to hypoxic control using Bonferroni's correction, *p<0.01 vs. unifected control and

†p<0.001 vs. lenti-Ngb alone). The combination of the two treatments reduced SO levels (571 ± 11 counts / min / *ng* protein) to that of the normoxic controls (566 ± 24 counts / min / *ng* protein), suggesting a synergistic role for the therapies in combination. All interventions showed no effect on SO levels in normoxic control cells (Normoxic [control = 551 ± 6; DMSO = 581 ± 17; lenti-GFP = 570 ± 16; lenti-Ngb = 592 ± 9; SP6001215 = 574 ± 15; lenti-Ngb + SP600125 = 566 ± 24; lenti-Ngb + DMSO = 586 ± 6; lenti-GFP + SP600125 = 553 ± 24] counts / min / *ng* protein, unpaired t-test compared to normoxic control using Bonferroni's correction).

4.2.3.2   *Malondialdehyde (MDA) Assay*

Lipid peroxidation is a well-established mechanism of cellular injury, and can be used as a marker of oxidative stress in cells and tissues. Lipid peroxides, derived from polyunsaturated fatty acids, are unstable and break down to form a number of compounds, including reactive carbonyl compounds of which the most abundant is MDA. As such, MDA can be used as a marker of lipid peroxidation. MDA reacts readily with amino groups on proteins and other biomolecules forming adducts and also reacts with DNA causing DNA-protein cross-links (reviewed in (Del Rio *et al.*, 2005)).

Hypoxic challenge in B50 rat neuronal cells resulted in a significant increase in MDA levels (Figure 4.10). Those cells pre-treated with lenti-Ngb had significantly reduced MDA levels in comparison to uninfected control and lenti-GFP control cells. Hypoxic cells pre-treated with the JNK inhibitor SP600125 (20 µM) also had significantly reduced MDA levels in comparison to uninfected control and DMSO vehicle control. Pre-treatment with lenti-Ngb and SP600125 alone resulted in a maximal reduction in MDA levels to that of the normoxic controls, and consequently no further effect of the combined therapy was observed (Hypoxic [control = 1.38 ± 0.11; DMSO = 1.33 ± 0.03; lenti-GFP = 1.32 ± 0.07; *lenti-Ngb = 0.33 ± 0.05; *SP6001215 = 0.45 ± 0.04; *lenti-Ngb + SP600125 = 0.36 ± 0.03; *lenti-Ngb+DMSO = 0.46 ± 0.08; *lenti-GFP + SP600125 = 0.41 ± 0.07] MDA µ mol / µg protein; unpaired t-test compared to hypoxic control using Bonferroni's correction, *p≤0.001). All interventions showed no effect on MDA levels in normoxic control cells (Normoxic [control = 0.37 ± 0.03; DMSO = 0.38 ± 0.07; lenti-GFP = 0.34 ± 0.09; lenti-Ngb = 0.50 ± 0.03; SP6001215 = 0.33 ± 0.1; lenti-Ngb + SP600125 = 0.46 ± 0.02; lenti-Ngb + DMSO = 0.33 ± 0.03; lenti-GFP + SP600125 = 0.52 ± 0.04] MDA µ mol / µg protein; unpaired t-test compared to hypoxic control using Bonferroni's correction).

4.2.3.3   Cell Death ELISA

A main characteristic in cells undergoing apoptosis is DNA fragmentation by endogenous endonucleases generating mono- and oligonucleosomes. The cell death ELISA (Roche, West Sussex, UK) is based on the quantitative sandwich-enzyme-immunoassay principle using antibodies directed against DNA and histones which are released into the cytoplasm of cells undergoing apoptosis.

Hypoxic challenge in B50 rat neuronal cells resulted in a significant increase in apoptosis, as assessed by a cell death ELISA (Figure 4.11).   Pre-treatment with lenti-Ngb significantly reduced levels of apoptosis from untreated hypoxic and lenti-GFP virus control cells ($p<0.01$). SP600125 also reduced apoptosis levels from untreated hypoxic and DMSO vehicle control cells ($p<0.005$). SP600125 significantly reduced levels of apoptotic cells in comparison to lenti-Ngb treatment alone ($p<0.01$ vs lenti-Ngb). Combined pre-treatment with lenti-Ngb and SP600125 lowered levels of apoptosis significantly from lenti-Ngb alone ($p<0.001$) but not SP600125 treatment alone ($p<0.03$) (Hypoxic [control = 0.30 ± 0.01; lenti-GFP = 0.27 ± 0.01; DMSO = 0.31 ± 0.01; lenti-Ngb = 0.19 ± 0.01; SP6001215 = 0.16 ± 0.01; lenti-Ngb + SP600125 = 0.11 ± 0.01; lenti-Ngb + DMSO = 0.17 ± 0.01; lenti-GFP + SP600125 = 0.16 ± 0.01] absorbance / µg protein; unpaired t-test compared to hypoxic control using Bonferroni's correction). The combined treatment is maximal, reducing levels of MDA to that seen in the normoxic controls. This quantifiable measure of apoptosis shows combination of pre-treatment with lenti-Ngb (MOI 5) and SP600125 (20 µM) resulted in a reduction in levels of apoptosis to that of normoxic control cells. No interventions showed significant effect on apoptosis levels in normoxic cells (Normoxic [control = 0.09 ± 0.01; lenti-GFP = 0.10 ± 0.02; DMSO = 0.10 ± 0.01; lenti-Ngb = 0.10 ± 0.01; SP6001215 = 0.09 ± 0.01; lenti-Ngb + SP600125 = 0.09 ± 0.02; lenti-Ngb + DMSO = 0.10 ± 0.0; lenti-GFP + SP600125 = 0.10 ± 0.01] absorbance / µg protein; unpaired t-test compared to hypoxic control using Bonferroni's correction).
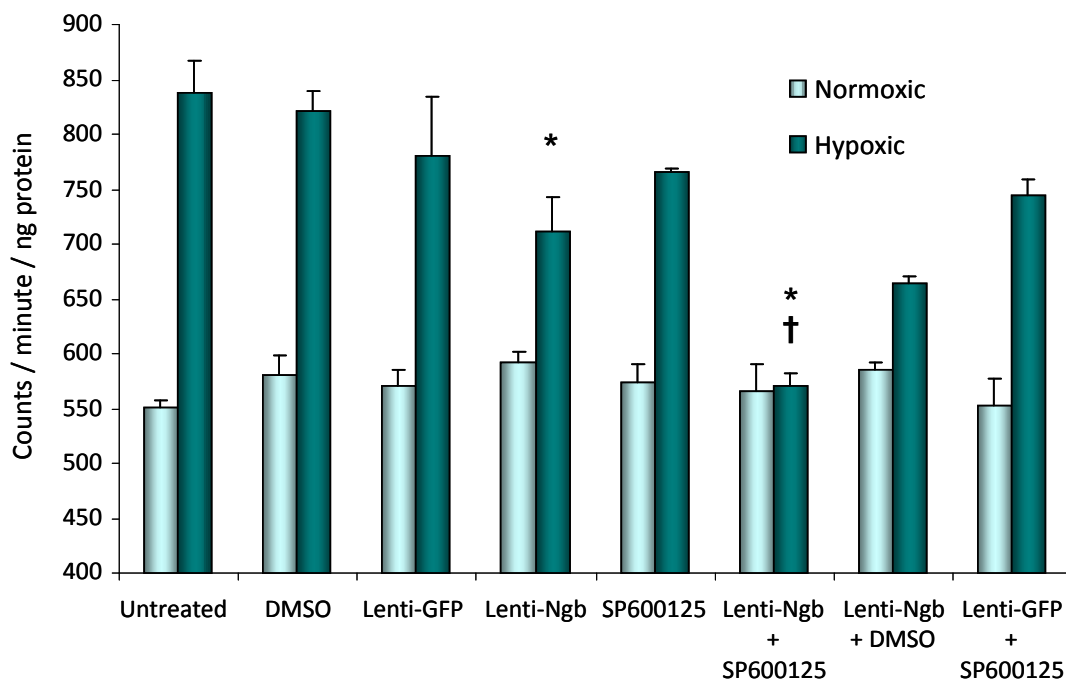
Figure 4.9:   **Quantitative determination of oxidative stress by EPR.**

Superoxide levels were determined by EPR in normoxic control B50 rat neuronal cells or cell exposed to 9 h hypoxia with 24 h reoxygenation following pre-treatment with lenti-Ngb, lenti-GFP, SP600125, or DMSO vehicle control or left as untreated controls. Data presented as mean ± SEM. Representative of n=3. *p< 0.01 and †p<0.001 using unpaired Student's t-test and Bonferroni's post-hoc correction vs. untreated hypoxic control.
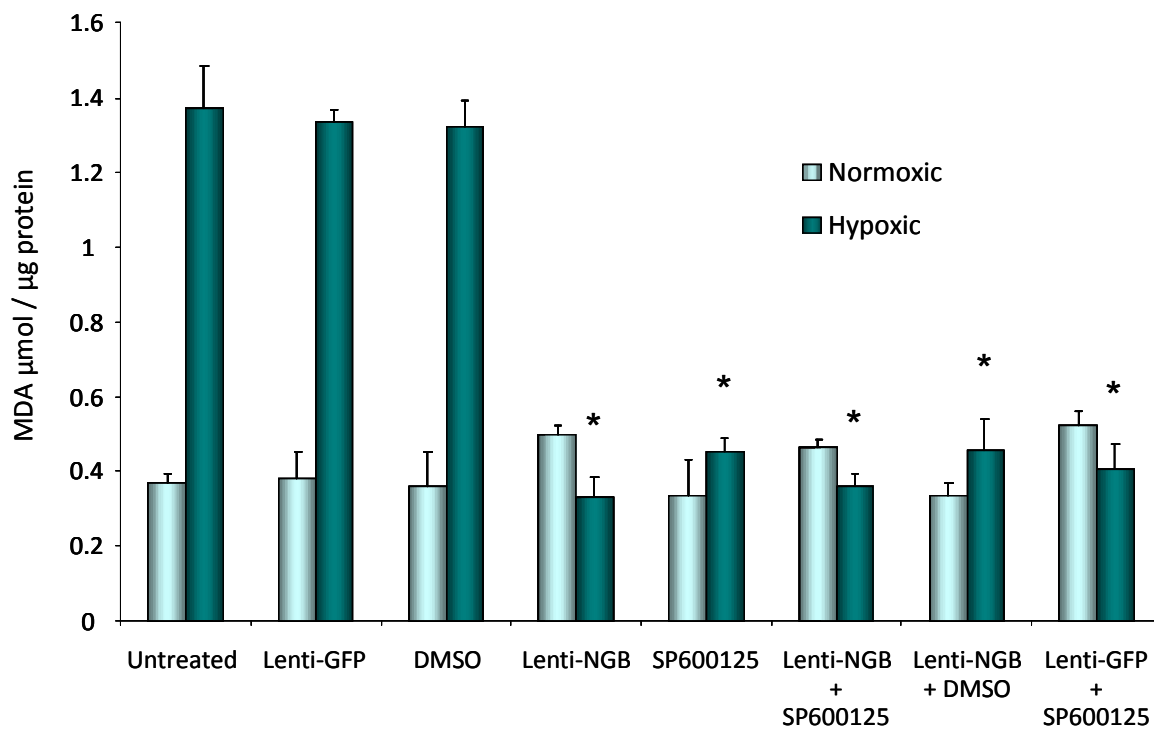
Figure 4.10:   Quantitative determination of oxidative stress by MDA assay.

Levels of MDA were determined in normoxic control B50 rat neuronal cells or cell exposed to 9 h hypoxia with 24 h reoxygenation following pre-treatment with lenti-Ngb, lenti-GFP, SP600125, or DMSO vehicle control or left as untreated controls.   Data presented as mean ± SEM. Representative of n=3.   *p< 0.01 using unpaired Student's t-test and Bonferroni's post-hoc correction vs. untreated hypoxic control.
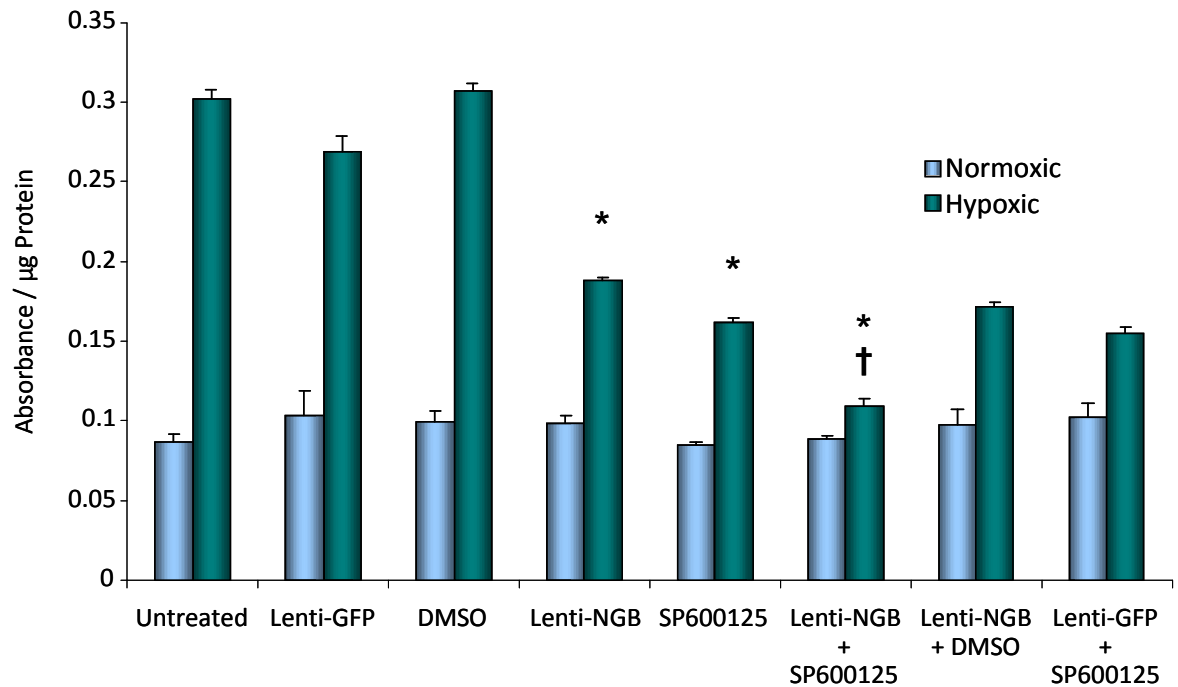
Figure 4.11:   Quantitative determination of apoptosis by cell death ELISA

Levels of DNA fragmentation were determined in normoxic control B50 rat neuronal cells or cell exposed to 9 h hypoxia with 24 h reoxygenation following pre-treatment with lenti-Ngb, lenti-GFP, SP600125, or DMSO vehicle control or left as untreated controls. Data presented as mean ± SEM. Representative of n=3. *p< 0.01 vs. untreated control and †p<0.001 vs. lenti-Ngb using unpaired Student's t-test and Bonferroni's post-hoc correction vs. untreated hypoxic control.

4.2.3.4   Caspase 3 ICC

In cells undergoing apoptosis, caspase 3 is cleaved and translocated to the nucleus. By visualising both the location and concentration of caspase-3 in cells following hypoxia, the number of cells undergoing apoptosis after 9 h of hypoxia with reoxygenation can be qualitatively assessed. ICC analysis showed a significant increase in activated caspase-3 (shown in green, FITC) localised in the nucleus (counterstained with DAPI, blue) in untreated hypoxic cells compared to normoxic controls (Figure 4.12). Pre-treatment with lenti-Ngb (MOI 5) lowered levels of nuclear-localised activated caspase-3 from untreated hypoxic cells, as did pre-treatment with SP600125 (20 µM). Combined lenti-Ngb and SP600125 pre-treatment lowered overall staining levels and reduced co-localisation with the nucleus of activated caspase-3 to that of the normoxic controls (Figure 4.12).

154
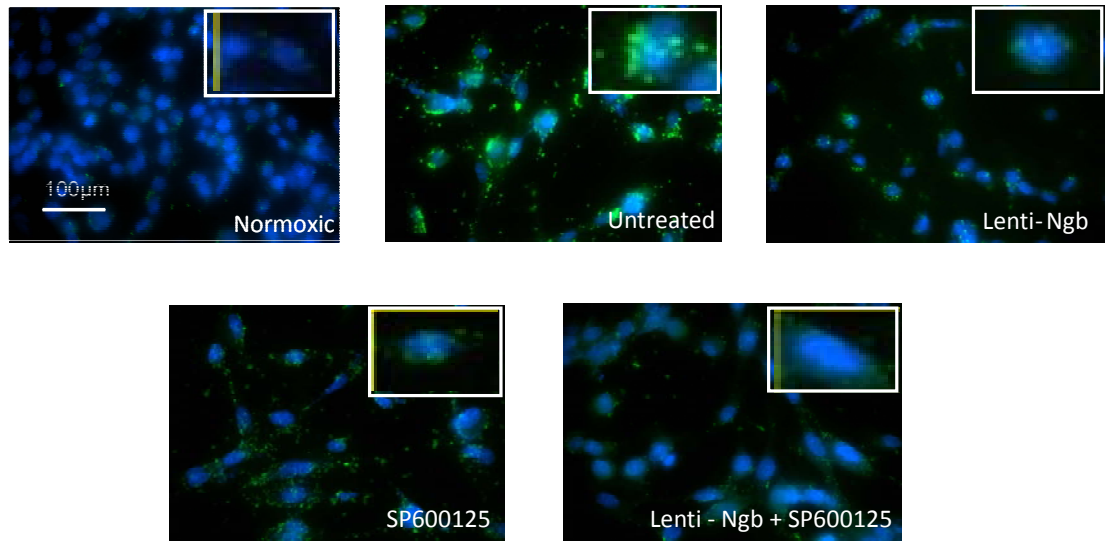
Figure 4.12:   Assessment of apoptosis from activated caspase 3 ICC.

Normoxic and hypoxic B50 rat neuronal cells either untreated, pre-treated with lenti-Ngb, or SP600125, were assayed to determine levels of apoptosis by ICC where positive caspase 3 (green) translocates to the nucleus (blue) in cells undergoing apoptosis. Representative of n=3. Scale bar = 100 μm and applicable to all panels.

4.3 DISCUSSION

Herein, the aim of the work presented in this chapter was to determine the changes in synthesis of Ngb and JNK (mRNA and protein) in B50 rat neuronal cells following hypoxia / reoxygenation *in vitro* and in *ex vivo* in the region of the infarct core and peri-infarct following tMCAO. Further, to test the hypothesis that the protective role for the combined intervention of lentivirus mediated Ngb overexpression and pharmacological JNK inhibition would have a greater effect than either treatment alone. A time-dependent endogenous increase in Ngb (mRNA and protein), *Jnk3* mRNA and p-JNK3 protein in B50 rat neuronal cells with increasing exposure to hypoxia with 24 h reoxygenation was demonstrated. *Ex vivo* analysis demonstrated varying results in *Ngb* and *Jnk1, Jnk2,* and *Jnk3* mRNA synthesis in both the region of the infarct core and peri-infarct at increasing time-points following tMCAO compared to sham control. Finally, a beneficial effect of combined intervention greater than either therapy alone in reducing oxidative stress and apoptosis was effectively shown in B50 rat neuronal cells following hypoxia and subsequent reoxygenation.

The *in vitro* model of hypoxia / reoxygenation used in the present study demonstrated that B50 rat neuronal cells respond to injury by increasing endogenous anti-oxidant capacity through Ngb upregulation. In response to injury, activation of pro-apoptotic pathways was evident with increasing JNK synthesis. These data are consistent with other *in vitro* studies (as discussed below) and the cellular injury observed in animal models of stroke.

Findings that Ngb is upregulated with increasing exposure to hypoxia is largely consistent with previous reports (Fordel *et al.*; Schwarzschild *et al.*, 1997b; Sun *et al.*, 2001), with modest variations in induction time-points and levels being explained by different technical setups and experimental designs. The cited reports vary from the present study in a number of ways, including induction of hypoxia, reoxygenation periods and controls. Sun *et al* (2001) utilised increasing lengths of exposure to an anoxic environment with respective decreasing lengths of reoxygenation in primary neuronal cells. They reported an increase in Ngb protein synthesis up to 16 h (with 8 h reoxygenation) with a reduction in protein synthesis at 24 h (with 0 h reoxygenation). The present study reported a time-dependant increase in Ngb synthesis with increasing exposure to hypoxia with 24 h reoxygenation. The differences in results in these instances are perhaps attributed to the length of reoxygenation period, and potentially suggest that endogenous upregulation of

Ngb is a mechanism, which is 'switched-on' during reoxygenation, and the subsequent increase in intracellular ROS. Sun *et al.* (2001) also failed to utilise time-matched normoxic controls, which take into account the stage of cellular respiration at the point of harvest. Although Fordel *et al* (2004) did utilise time-matched controls and a hypoxic rather than anoxic environment in assessing endogenous Ngb mRNA upregulation in HN33 neuronal cells, the study did not employ a reoxygenation period. This perhaps accounts for the relatively low levels of overexpression of Ngb they observe with up to 54 h hypoxia *in vitro*. The effect of increasing time-points of reoxygenation following 1 h anoxia was assessed in ND15 neuronal cells (Rayner *et al.*). Interestingly a time-dependent increase in Ngb mRNA synthesis with increasing lengths of reoxygenation up to 5 h, with a sharp decrease in synthesis in the following time-point of 24 h reoxygenation was reported. The decrease in synthesis between 5 and 24 h reoxygenation could be explained by an insufficient level of insult administered to the cells, as all markers of stress including HIF-1α and heme oxygenase-1 (HO-1) had decreased at this time-point, indicating a return to normal respiration (Rayner *et al.*).

Although it has been shown in the present study and elsewhere that Ngb is upregulated in response to hypoxia *in vitro*, the mechanism for the hypoxic induction of Ngb is unknown. A candidate for Ngb's activation is HIF-1α. HIF-1α is an oxygen-dependent transcriptional activator, which under normoxia is rapidly degraded *via* the von Hippel-Lindau tumour suppressor gene product (pVHL)-mediated ubiquitin-proteasome pathway (Maxwell *et al.*, 1999). Under hypoxic conditions HIF-1α becomes stable and interacts with coactivators such as p300/CBP to initiate its transcriptional activity. HIF-1α transcribes several genes which may be involved in neuroprotection in response to hypoxia, including erythropoietin (EPO) (Wang *et al.*, 1993), vascular endothelial growth factor (Forsythe *et al.*, 1996), glycolytic enzymes (Semenza *et al.*, 1994), heme oxygenase (Lee *et al.*, 1997), glucose transporters (Ebert *et al.*, 1995), and possibly Ngb (Fordel *et al.*, 2004a). In support of HIF-1α's role in Ngb synthesis, it has previously been reported that Ngb is increased in neuronal cells out with hypoxia but in the presence of iron chelators such as cobalt chloride ($CoCl_2$) and deferoxamine (Dfx) which are well established stabilisers of HIF-1α, although not entirely HIF specific (Gong *et al.*, 2001 2001). In addition to this, further evidence shows the 5'-untranslated region of Ngb contains several copies of the consensus HIF-1 binding sequence (5'-RCGTG-3') (Sun *et al.*, 2001).

Data in the present *in vitro* study demonstrating *Jnk3* but not *Jnk1* or *Jnk2* synthesis is increased in a time-dependent manner with increasing exposure to hypoxia is consistent with *in vivo* data (Kuan *et al.*, 2005) but currently there are no previous *in vitro* data showing the response of the different isoforms of JNK in neuronal cells to hypoxia. However, *ex vivo* analysis of *Jnk1*, *Jnk2*, and *Jnk3* in the present study failed to determine a change in synthesis with increasing time-points post-tMCAO for *Jnk3*. Herein, *Jnk3* displayed a significant reduction in synthesis at 3 h post-tMCAO but no significant change at longer time-points in both the infarct core and peri-infarct. Although no change in *Jnk1* in the infarct core was observed following tMCAO, *Jnk2* also displayed a significant decrease in synthesis following tMCAO at 3 and 6 h. Conversely, in the peri-infarct region, no change in *Jnk2* synthesis was observed following tMCAO but *Jnk1* synthesis levels were significantly decreased at 3, 6 and 24 h following tMCAO. Although it was not possible in our hands to detect an injury-induced increase in *Jnk3* observed *in vitro* through *ex vivo* analysis of post-ischaemic brains, previous studies have confirmed this upregulation (Irving *et al.*, 2002). The previous reports indicating *Jnk3* upregulation following cerebral ischaemia taken together with the neuroprotective effects of JNK inhibition or *Jnk3* knockout *in vivo* and the extensive *in vitro* proof-of-concept data in the present study allowed for sufficient evidence to continue with the *in vivo* intervention study.

Sun *et al.* in 2001 reported that hypoxic induction of Ngb was correlated with a decrease in DNA damage shown by staining of the Klenow fragment of DNA polymerase I in neuronal cells. They hypothesised that this suggested a role for Ngb in cells destined for survival, and as such a protective mechanism of action which they, along with the results shown presently and by other groups, went on to demonstrate *in vitro* (Sun *et al.*, 2001) and *in vivo* (Sun *et al.*, 2003). Although Sun *et al.* (2003) describe Ngb upregulation as protective and hypoxic induction of Ngb as reserved for cells destined to survive, our data assessing the synthesis of the three isoforms of *Jnk* mRNA and p-JNK3 protein, demonstrate that under hypoxic conditions neuronal cells are also expressing increasing levels of these apoptotic mediators with increasing exposure to hypoxia. As aforementioned, there is a time-dependent decrease in cell number with increasing exposure to hypoxia suggesting an inability of Ngb to endogenously protect neurons from cell death. However, limitations of this study mean that Ngb and *Jnk3* / p-JNK upregulation can only be assessed in surviving cells. Therefore, it remains to be seen whether Ngb upregulation is consistent throughout the population or if an inconsistency in upregulation accounts for the cell death observed,

confirming Ngb's endogenous protective role. Additionally, it is unknown whether *Jnk3* or p-JNK upregulation in hypoxia in surviving cells is representative of levels present in the cells destined for apoptosis, and if the levels are lower in surviving cells can this be related back to the increase in Ngb synthesis, perhaps having an attenuating effect on JNK synthesis.

Across the four *in vitro* assays, assessing oxidative stress and apoptosis, a significant improvement in both viability outcomes in cells assigned to the combined intervention compared to those administered single treatments was observed. In line with previous reports Ngb overexpression was shown to act as a powerful antioxidant (Figure 4.9 & Figure 4.10), but also acted to prevent apoptosis (Figure 4.11 & Figure 4.12), the putative mechanisms for these actions are described below. In addition to this, JNK inhibition through SP600125 effectively blocked apoptosis mediated cell death (Figure 4.11 & Figure 4.12) but also attenuated SO production when in the presence of Ngb overexpression (Figure 4.9), and interestingly, completely abolished lipid peroxidation (Figure 4.10) (discussed below).

As aforementioned, the data for Ngb overexpression and its protective action in hypoxia / reoxygenation injury broadly agrees with previous reports. EPR assessment of the reduction of SO production in neuronal cells, afforded by Ngb overexpression, has not previously been performed as an *in vitro* measure of neuroprotection, although Ngb overexpression has been shown to reduce SO in *in vitro* models of neuronal hypoxia / reoxygenation determined by alternative assays (Li *et al.*, 2011; Liu *et al.*, 2009). Liu *et al.* (2009) utilised primary cortical neurones from Ngb-transgenic mice (Ngb-Tg) or matching wild-type mice and exposed to increasing lengths of anoxia with 2 h reoxygenation. Cortical neurones from Ngb-Tg mice exhibited reduced SO production in comparison to wild-type controls following 10 h anoxia, assessed by oxidised hydroethidine production (a by-product of ROS production). EPR has provided direct evidence that Ngb overexpression lowers SO production which is consistent with its putative role as an antioxidant through ROS scavenging, which include hydroxyl radicals ($\cdot$OH) (Li *et al.*, 2011), hydrogen peroxide (H_2O_2) (Antao *et al.*, 2010; Fordel *et al.*, 2006; Li *et al.*, 2011), nitric oxide (NO$\cdot$) (Jin *et al.*, 2008b), and peroxynitrite ($ONOO^-$) (Herold *et al.*, 2004). The effective scavenging of ROS lowers oxidative stress and as such improves cell viability by inhibiting a number of ROS mediated cell stressors, such as lipid peroxidation.

Although the mechanism of Ngb's ROS scavenging ability has been widely studied, the exact mechanisms of action are still to be elucidated. Ngb exists in the ferrous (Fe(II)) and ferric (Fe(III)) oxidative forms, and in the presence of excess NO·, during hypoxia, NgbFe(III) is converted into NgbFe(II)NO by reductive nitrosylation (Herold *et al.*, 2004), similar to the reactions of NO with Fe(III)Mb and Fe(III)Hb. The Fe(II)NO form of Ngb is then oxidised back to NgbFe(III) by $ONOO^-$ and O_2^-, two reactions that also take place in Hb and Mb. In contrast to this reaction in Mb and Hb however, NgbFe(III) does not generate the cytotoxic Fe(IV) form of the protein upon addition of either $ONOO^-$ or H_2O_2 (Herold *et al.*, 2004), indicating Ngb as an highly efficient scavenger of ROS. Some putative equations for these mechanisms are shown below (Figure 4.13):

$$NgbFe(III) + NO \rightleftharpoons NgbFe(III)NO \longleftrightarrow NgbFe(II)(NO+)$$

$$\xrightarrow[\substack{OH^- \\ H_2O}]{NO^-} NgbFe(II)NO + NO_2 + (1 \text{ or } 2)\ H^+$$

$$NgbFe(II)NO \xrightarrow{ONOO^-/H_2O_2} NgbFe(III)NO \xrightarrow{-ON\bullet} NgbFe(III)$$
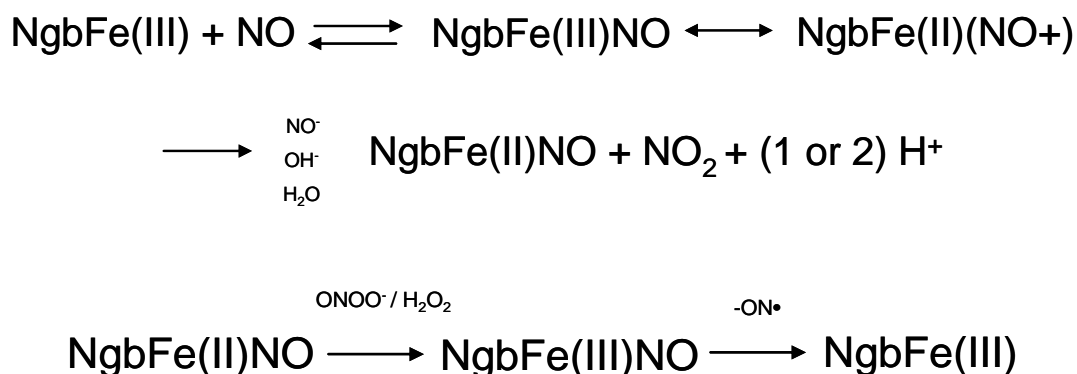
Figure 4.13:   Redox reactions of Ngb with ROS

Putative equations demonstrating possible mechanisms of Ngb's ROS scavenging.

Although Ngb's interaction with SO, as measured by EPR in the present study, is not specifically dealt with in the above equation, SO readily reacts with water or NO to form H_2O_2 or $ONOO^-$, respectively, which in turn are shown above to be readily scavenged by Ngb. Therefore, data from the present study suggest Ngb has a two-fold action on reduction of ROS following hypoxia / reoxygenation. Firstly, upregulation of Ngb has been suggested to reduce NO and SO derived ROS (H_2O_2 or $ONOO^-$) by the scavenging mechanisms shown above. In addition, Ngb upregulation has been shown in the present study to have a direct action on SO production levels, potentially through an alternative mechanism involving maintenance of the mitochondria under hypoxic stress. Antao *et al.* demonstrated an outcome of Ngb overexpression in neuronal cells exposed to hypoxia to

be maintenance of intracellular ATP concentration ($[ATP]_i$), whereas control cells exhibited the projected $[ATP]_i$ depletion under hypoxic conditions. They believed $[ATP]_i$ maintenance occurred as a result Ngb's action on the mitochondrial potassium / ATP (mito-K_{ATP}) channel through activation of phosphionositide 3-kinase (PI3K) (Antao *et al.*, 2010). PI3K acts to phosphorylate a protein within the mito-K_{ATP} channel, maintaining the mitochondrial pore (Plum *et al.*, 2006). Inhibitors of PI3K and mito-K_{ATP} channel were shown to abolish Ngb effects on $[ATP]_i$. It is important to note that maintenance of the mito-K_{ATP} channel in itself reduces ROS production by decreasing the depolarisation of the mitochondrial membrane potential ($\Delta\psi m$) and sustaining normal mitochondrial respiration (Liu *et al.*, 2009). Interestingly, the same study reported Ngb's activation of PI3K led to a subsequent phosphorylation of its downstream mediator, Akt and initation of the well-established PI3K/AKT/mTOR pathway of cell survival / inhibition of apoptosis.

Lipid peroxidation occurs as a result of an increased intracellular concentration of ROS. ROS such as $ONOO^-$ and OH^- reacting with the lipids of the cell membrane through two distinct steps, initiation and propagation, in a positive feedback chain reaction. By-products of this reaction such as malondialdehyde ($CH_2(CHO)_2$) are both mutagenic and carcinogenic, and translocate to the nucleus forming DNA adducts. The finding that lenti-virus mediated Ngb overexpression lowers lipid peroxidation in hypoxia stressed neuronal cells (Figure 4.10) in the present study, is in agreement with another report (Li *et al.*, 2008a), further supporting Ngb's role as an antioxidant. The study by Li *et al.* (2008b) utilised PC12 neuronal cells and chemical induction of hypoxic pathways through incubation with H_2O_2. Cells were transfected with an Ngb cDNA containing expression vector (pcDNA3.1; Invitrogen) with a cytomegalovirus promoter, before incubation with 0.1 mM H_2O_2 for 6 h. Consistent with the present study, Li *et al*. (2008b) reported a maximal reduction in MDA levels following pre-treatment with 1.0 µg Ngb DNA. The same study reported an anti-apoptotic capacity of Ngb, demonstrating that upregulation of Ngb caused a significant reduction in caspase 3/7 activation following incubation with 0.1 mM H_2O_2 for 6 h.

In addition to its well documented anti-oxidant effect, we have shown an anti-apoptotic effect when Ngb is overexpressed. Cells treated with lenti-Ngb exhibited a lower incidence of DNA fragmentation (Figure 4.11) and caspase-3 activation (Figure 4.12) both traditional markers of apoptosis. A number of studies have looked into potential anti-apoptotic roles for Ngb in response to stress. One potential role for Ngb in apoptosis is

inhibition of CytC, released from mitochondria into the cytosol during activation of the intrinsic pathway of apoptosis following mitochondrial outer membrane permeabilisation (MOMP). A rapid redox reaction occurs between ferrous Ngb (NgbFe(II)) and ferric CytC (CytCFe(III)). CytC is unusually basic (pI = 10.2) and Ngb is unusually acidic (pI = 4.6) and therefore under neutral conditions exhibit a highly positive and highly negative charge, respectively, allowing redox electron exchange to occur very rapidly (2000 s^{-1}) (Fago *et al.*, 2006a). Although there exists no structural determinants of an Ngb/CytC complex, computational methods determined they share a common binding site (Bonding *et al.*, 2008). Interestingly, this binding site contains the amino acids Lys25 and Lys72, which are key to the binding of CytC to apoptotic protease activating factor-1 (APAF1), to form the apoptosome which initiates caspase release and subsequent caspase-mediated cell death, in part by DNA fragmentation through caspase activation. The potential binding of Ngb at this specific region of CytC and subsequent inhibition of the formation of the apoptosome demonstrates a possible anti-apoptotic role for Ngb under hypoxic conditions. Following redox reaction with CytC, Ngb becomes oxidised to its ferric form (NgbFe(III)). Wakasugi and colleagues (Wakasugi *et al.*, 2003) showed by surface plasmon resonance that in it's ferric form Ngb binds exclusively to and inactivates the GDP-bound Gα subunit of the heterotrimeric G proteins, which are activated by GPCRs under stress conditions. Activation of the Gα subunit in hypoxia can be correlated with an increase in PKC activity and subsequent elevation of internal Ca^{2+} concentration as a result of phospholipase C-β activation (Althoefer *et al.*, 1997). This binding of Ngb to the GDP-bound Gα subunit prevents activation by GTP, even in the presence of excess GTP (Wakasugi *et al.*, 2005). This suggests another protective role for Ngb, in protection against Ca^{2+} influx and subsequent spreading depression-mediated apoptosis.

Another benefit of the previously described preservation of [ATP]$_i$ by Ngb is the maintenance of free intracellular actin. In ATP depleted cells, there is a large production of actin aggregates, decreasing the available intracellular actin and affecting cell structure. Actin has been shown to maintain intracellular homeostasis by acting on mitochondrial structure and intracellular position, and during depletion of [ATP]$_i$ free actin depletion has been shown to contribute to mitochondrial fusion (Rappaport *et al.*, 1998). In addition to its action on mitochondrial positioning, reduction of free actin can lead to reduced Δψm and sensitivity to apoptotic insult though disruption of actin's regulation of the voltage-dependent anion channel (VDAC) on the mitochondrial membrane which regulates the permeability of the Δψm. When actin is aggregated as a result of ATP depletion, the

VDAC allows release of apoptogenic proteins such as CytC which is abolished when dynamic actin is reinstated (Koya *et al.*, 2000). The maintenance of $\Delta\psi$m through $[ATP]_i$ and regulation of free intracellular actin, demonstrates an indirect mechanism through which Ngb could inhibit release of apoptotic mediators.

JNK inhibition by SP600125 showed a significant reduction in cell death as assessed by the two apoptosis assays, and as expected. JNK is a downstream mediator of apoptosis, activated by a number of apoptotic pathways and as such inhibition of JNK, reduced levels of apoptosis observed by cell death ELISA (Figure 4.11) and nuclear translocation of activated caspase-3 (Figure 4.12). Interestingly, however, incubation with SP600125 showed a complete abolishment of lipid peroxidation, a mechanism usually attributed to oxidative stress but had no significant effect on SO levels observed by EPR. This abolishment of lipid oxidation by JNK inhibition is consistent with a previous study assessing *in vitro* ischaemia / reperfusion within hepatic cells (Uehara *et al.*, 2005), however no mechanism for this result has been clarified. Although JNK inhibition by SP600125 showed no significant decrease of SO levels, SP600125 treatment potentiated the effect of Ngb overexpression on SO levels when given in combination, suggesting a synergistic role of combined treatment of Ngb and JNK through cross-talk of the pathways.

It is not possible to entirely distinguish apoptotic and oxidative stress pathways when considering the mechanisms of cell damage /death. For example, NO (Mishra *et al.*, 2004) and other ROS (Felix *et al.*, 2002) induce JNK phosphorylation, and the present study has determined JNK inhibition lowers lipid peroxidation. When considering a synergistic role for Ngb overexpression in combination with JNK inhibition in cell survival during hypoxia, it is necessary to assess Ngb's direct action on JNK (if any) and *vice versa*. Ngb's role as a ROS scavenger indicates a clear-cut mechanism by which Ngb overexpression effects JNK phosphorylation. Another protective mechanism of Ngb is its direct action on PI3K and the activation of the subsequent PI3K/AKT/mTOR pathway of cell survival. AKT is recruited to the plasma membrane after activation of PI3K and is activated through phosphorylation by phosphoinositide-dependent kinases 1 and 2. pAKT has been demonstrated to indirectly suppress JNK synthesis by disrupting several pro-apoptotic proteins which activate the JNK pathway such as MLK3 (Barthwal *et al.*, 2003), JNK-interacting protein (JIP) (Kim *et al.*, 2002), MKK4 (Park *et al.*, 2002) and in particular it has been shown to have a direct effect on ASK1 (Kim *et al.*, 2001b), the upstream mediator of JNK activation. Ngb has also been implicated in the upregulation of

14-3-3 (Ye *et al.*, 2009a), a scaffold protein that mediates apoptosis by binding essential pro-apoptotic mediators such as the members of the Bcl-2 family, Bax, Bad and Bim and ASK-1 (Porter *et al.*, 2006b). Ye and colleagues postulated that Ngb controlled 14-3-3 synthesis through G-protein-mediated signalling (Ye *et al.*, 2009a). Taken together, these data suggest Ngb has a number of possible mechanisms of action against JNK, in addition to its other actions as an anti-apoptotic agent, suggesting an explanation as to how Ngb overexpression and JNK inhibition can act synergistically.

As is observed in the data, JNK activation has a reduced ability to modulate oxidative stress pathways, than Ngb has to modulate apoptotic pathways. However, there is evidence to suggest that JNK can inhibit activation of the neuroprotective, hypoxia induced, transcription factor HIF-1α (Antoniou *et al.*, 2010). Antoniou and colleagues (2010) demonstrated that the HIF-1α exhibited a JNK binding domain (JBD) motif within the N-terminal Von Hippel-Lindau (VHL) recognition site and showed inhibition of JNK with the peptide D-JNKI-1 resulted in a marked increase in HIF-1α expression in response to hypoxia (Antoniou *et al.*, 2010). Although HIF-1α's targets are not exclusively anti-oxidants it is the prime candidate for Ngb upregulation, suggesting that JNK inhibition can potentially improve endogenous Ngb upregulation in response to hypoxia, further elucidating a synergistic role for these therapies in combination.

The findings reported herein, confirm that lentivirus mediated upregulation of Ngb (MOI 5) and pharmacological inhibition of JNK using SP600125 (20µM) can act in both an additive and sometimes synergistic manner in combination to improve cell survival beyond that seen with either therapy alone across the majority of the cell viability assays studied. In every instance, combined treatment improved cell survival to the levels of the normoxic controls. These data provide the proof-of-concept required to justify a comprehensive *in vivo* study assessing both neurological deficit and infarct size following tMCAO in spontanously hypertensive stroke-prone (SHRSP) rats.

Chapter 5

Results:

Optimisation and Refinement of the tMCAO

Experimental Stroke Model in the SHRSP

5.1   INTRODUCTION

Preclinical *in vivo* studies have generated a lot of criticism in their failure to adequately reproduce features of clinical stroke and predict therapeutic efficacy. As such, they have a very poor 'bench-to-bedside' track record. In 2009 a modified version of the S.T.A.I.R guidelines for preclinical stroke was published (Fisher *et al.*, 2009), outlining the updated requirements for a comprehensive in vivo study of stroke, one of which is the requirement and importance of a pilot study. Although there is a vast amount of information available regarding optimal surgical techniques for the MCAO procedure (such as, suture size, coating length, and insertion length) available in the literature, previously published parameters may not be entirely relevant. Therefore a pilot study can offer the opportunity to select the optimal parameters for the specific model, before initiating the comprehensive intervention study. The intraluminal filament model also demands surgical skill, and refinement of technique is required to guarantee consistent results. This period of refinement is known as the "surgeon's learning curve" (reviewed in (Renzulli *et al.*, 2005)). The "surgeon's learning curve" is of the premise that the individual surgeon is the sole factor for outcome in all surgical techniques, and experience is directly related to outcome (Renzulli *et al.*, 2005). A pilot study also allows experience can be gained on outcome assessments such as neurological scores and *ex vivo* analysis of brain tissue. Additionally, it can highlight issues with outcome assessments, and allow for alterations of the study design. Further to optimisation of techniques utilised in specific models, a pilot study addresses the 3 R's of animal research; replacement, reduction, and refinement. The 3 R's raise awareness of the ethical, scientific, legal and economic problems of animal research, and attempt to improve *in vivo* study design. In performing a pilot study, and resolving any potential problems prior to initiation of the intervention study, overall animal number is reduced and technique is refined.

The intraluminal MCAO model of experimental stroke has many benefits including the induction of stroke without having to administer a craniotomy and exposing the brain, the option of reperfusion and the reproducibility of infarct. However, more accurate modelling of human stroke can be afforded through use of aged animals and strains bred to exhibit a number of the co-morbidities of cardiovascular disease (CVD). Hypertension is by far the most significant risk factor for stroke (O'Donnell *et al.*, 2010a) is present in > 50 % of all stroke cases and increases the risk of stroke by 20 - 30 % per 10 mmHg increase from

normotension in arterial blood pressure (Alberts *et al.*).   Therefore the use of the spontaneously hypertensive stroke prone rat (SHRSP) in the present model allows closer modelling of human stroke. As a consequence of limitations within the present study aged animals could not be utilised, however at the age of use (16 wks) the SHRSP exhibits advanced hypertension, with an arterial blood pressure of ~ 185 mmHg compared to the normotensive Wistar-Kyoto (WKY) rat which exhibits an arterial blood pressure of ~ 125 mmHg at 16 wks. Unfortunately however, closer modelling of human stroke with use of animals exhibiting co-morbidities such as advanced hypertension comes with increased mortality. Interestingly the present study demonstrated a novel finding which resulted in a new methodological refinement which reduced mortality with no confounding effect on lesion size or neurological recovery observed.

In order to address the shortcomings of experimental stroke models, it was the aim of this chapter to carry out an initial pilot study of the utilised stroke model in the SHRSP to assess the value of the neurological tests, to observe the variability in lesion size, to determine if the *n* number was adequate and to allow for experience to be gained in carrying out the data analysis before initiation of the intervention study.

5.2   RESULTS

5.2.1   *In Vivo* Control Study

Early training in the tMCAO procedure utilised filaments made by forming a uniform bulb (0.28 - 0.3 mm) with a cauterising pen at the end of 3-0 nylon monofilament. However, colleagues at the Wellcome Surgical Institute began utilising a custom made silicon-coated monofilament (Doccol Corporation, USA) and reported improved survival and reduced variability in infarct volume. In an attempt to reflect these positive findings in the SHRSP, a control study to determine the reproducibility of infarct and neurological scores following 45 min tMCAO using these Doccol filaments was undertaken. 12 male SHRSP (16 – 18 weeks, 270 – 310 g) were subjected to 45 min tMCAO and neurological score assessed longitudinally at day 1, 2, 3, 7, 10, and 14 post-MCAO. Neurological score initially consisted of three tests, the 32-point neurological score, the tapered beam test and the cylinder test (Gharbawie *et al.*, 2004). However, the cylinder test was discontinued mid-study due to a lack of consistency in the response seen during both the baseline and training period and additionally post-MCAO. The animal should normally rear onto its hindlimbs and explore the cylinder with both forepaws, but this action was inconsistent pre-MCAO and the animal failed to rear at all post-MCAO.

5.2.1.1   Survival

A total of 13 rats underwent tMCAO surgery, with only one rat not completing the study, due to early sacrifice as a result of exceeding the severity limits specified for the tMCAO protocol on the project license. 4 animals were removed from the study following brain processing for histological analysis due to minimal or no infarct which likely reflected partial occlusion as a result of the filament not being advanced far enough to fully block the origin of the MCA.

5.2.1.2   Physiological Variables

Body temperature was measured during MCAO surgery and maintained at 37 °C ± 1 °C. Previous work in the group had measured blood gases with increasing time under anaesthesia and with ventilation settings (stroke rate and volume) comparable to those used currently. No significant change in pCO_2 was evident up to 180 min after artificial ventilation began (L. Work, unpublished observations). As the animals in the current study were to be recovered, arterial blood samples were not obtained to determine blood gases as

cannulation of the femoral artery can cause limb weakness or paresis which could confound behavioural testing. However, time under anaesthesia was kept to a minimum and in the main < 90 minutes.

5.2.1.3   Infarct Volume

At day 14 animals were deeply anaesthetised, perfusion fixed and the brain paraffin embedded for histological analysis. Volume of infarct was determined from haematoxylin and eosin stained sections. In the region of the infarct, neuronal cell bodies are darkly stained, shrunken and triangular in shape and the structure and organisation of the neuropil is vastly disrupted, with significant tissue loss at day 14. After 45 minutes tMCAO average infarct volume was 181.8 ± 24.7 mm3 (Figure 4.10). Infarct volume was highly variable across group (animal 1 = 246.5; animal 2 = 90.4; animal 3 = 146.9; animal 4 = 189.8; animal 5 = 191.8; animal 6 = 238.2; animal 7 = 83.3; animal 8 = 267.5).

5.2.1.4   32-Point Neurological Score

32-point neurological score for the control group is shown in (Figure 5.2 A). Although a significant drop in neurological score is observed from baseline assessment at day 1**, 2**, 3**, and 7* (**$p<0.0001$, *$p<0.01$; Student's unpaired t-test vs. baseline with Bonferroni's post-hoc correction), by day 10 and 14 animals exhibit no significant difference from baseline (baseline = 31.3 ± 0.2; day 1** = 19.0 ± 1.2; day 2** = 21.1 ± 1.4; day 3** = 21.8 ± 1.1; day 7* = 25.9 ± 1.0; day 10 = 27.0 ± 1.2; day 14 = 27.4 ± 1.1).

5.2.1.5   Tapered Beam Walk Test

Tapered beam test demonstrated a significant increase in percentage footfalls from baseline at day 1**, 2**, 3**, and 7* (**$p<0.001$, *$p<0.05$; Student's unpaired t-test vs. baseline with Bonferroni's post-hoc correction). However, by day 10 and 14 animals showed no significant difference from baseline in the percentage of footfalls observed (baseline = 0.9 % $\pm$ 0.7 %; day 1** = 36.2 % $\pm$ 2.8 %; day 2** = 23.6 % $\pm$ 2.1 %; day 3** = 21.4 % $\pm$ 2.8 %; day 7* = 14.3 % $\pm$ 3.9 %; day 10 = 12.9 % $\pm$ 3.5 %; day 14 = 11.4 % $\pm$ 3.5 %) (Figure 5.2 B).
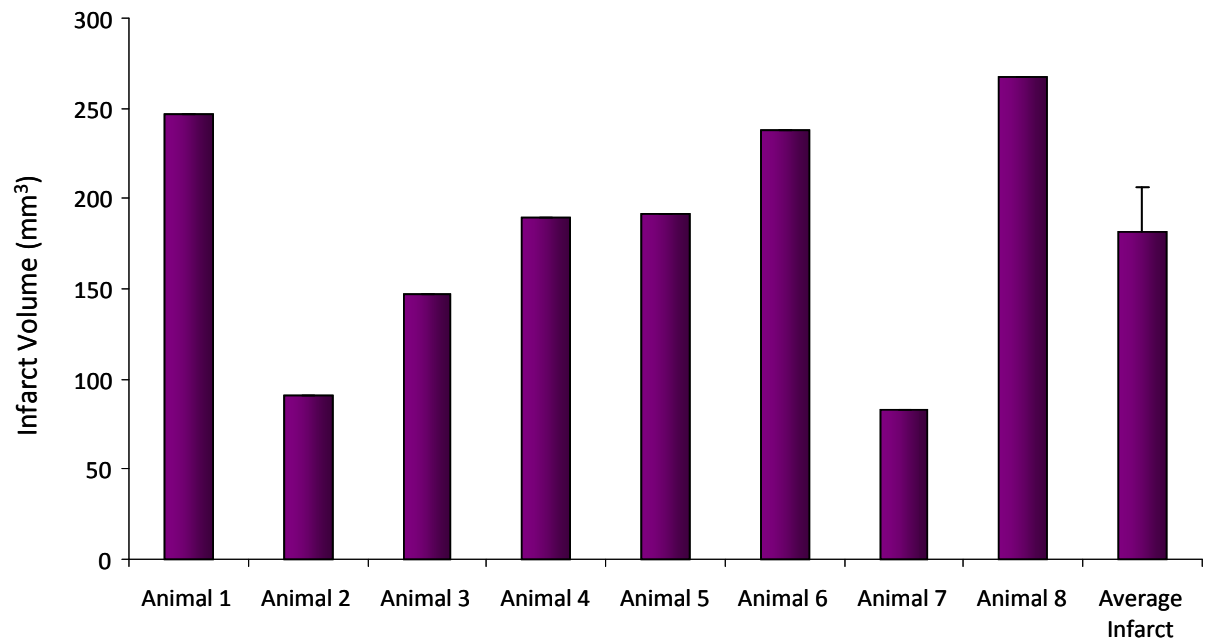
Figure 5.1:   Infarct Volume following 45 min tMCAO

Infarct volume (mm^3) measured from H&E stained sections over seven coronal levels, as previously described (section 2.7.5.1), in 8 animals that exhibited infarct out of 12 that went under procedure. Average infarct for *n* = 8 animals, expressed ± SEM.

(A)

(B)
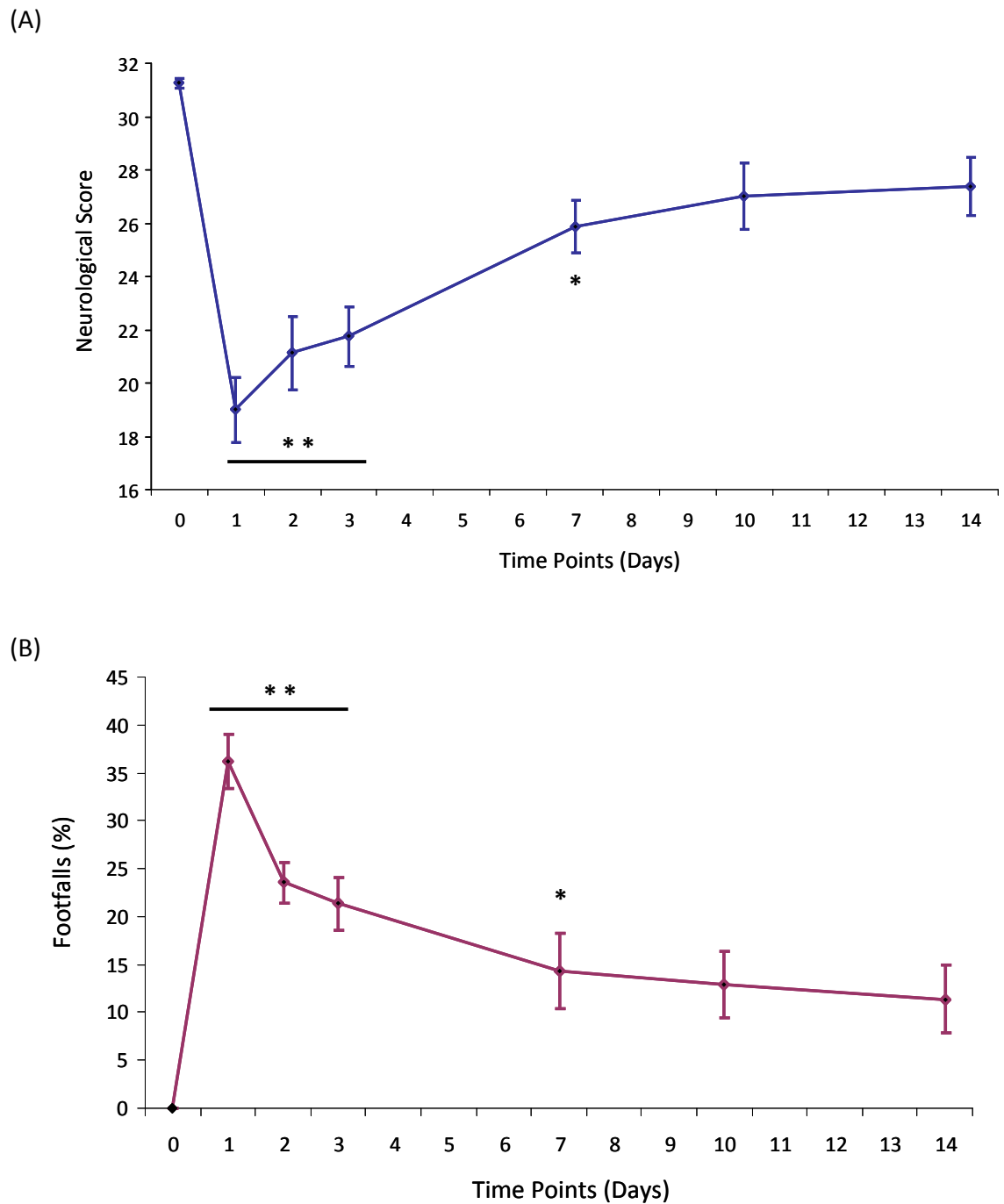
Figure 5.2:   Longitudinal Neurological Assessment following 45 min tMCAO

(A) 32-point neurological score assessed at day 1, 2, 3, 7, 10 and 14. **p<0.0001 and *p<0.001 vs. day 0, one way ANOVA using Bonferroni's post-hoc test. Data are presented as average ± SEM. (B) Tapered beam test assessed at day 1, 2, 3, 7, 10 and 14 with results expressed as % footfalls of total steps taken.   **p<0.001 and *p<0.01 vs. day 0, one way ANOVA using Bonferroni's post-hoc test. Data are presented as average ± SEM.

5.2.2   Pre-tMCAO Surgery

An early observation in the large intervention study identified that in those animals randomised to groups receiving intracranial delivery of virus there was a marked improvement in survival rates. The reduction in mortality observed lead to the hypothesis that drilling a cranial burrhole, equivalent in size to that used for stereotactic virus administration, and subsequent piercing of the dura improved survival post-MCAO. As a result, and after consultation with the named veterinary surgeon and local Home Office inspector, a change in protocol was agreed whereby all animals not randomised to virus intervention were subjected to a sham stereotactic procedure prior to tMCAO. This surgery involved a ~ 1 mm cranial burrhole being drilled into the skull at co-ordinates, AP: - 0.7 mm, ML: + 3 mm and DV: - 2 mm, relative to bregma. The Hamilton Syringe™ was subsequently lowered through the burrhole to the surface of the brain where it pierced the dura mater. Following this, the Hamilton Syringe™ was immediately raised and the burrhole filled with dental cement, as previously described (section 2.7.4). Without drilling of a cranial burrhole, the survival rate was 47 % in those animals subjected to tMCAO whose skull was intact. The survival rate was markedly improved to 93.8 % following pre-tMCAO surgery to drill a cranial burrhole (Figure 5.3). Importantly, further analysis determined infarct size was not affected by such pre-tMCAO surgery (Figure 5.4). Additionally, there was no change in the extent of neurological deficit assessed across the two neurological scores (Figure 5.5 A & B). Although there was a trend towards an improvement in percentage footfalls at day 7, 10 and 14 in the pre-tMCAO surgery group, this did not reach statistical significance. The large variation in results observed in the tapered beam test at day 7, 10 and 14 in animals without the pre-tMCAO surgery is perhaps a result of the low *n* numbers in this group, attributed to the high mortality. Additionally, of the surviving animals without the pre-tMCAO surgery a number were incapable of traversing the beam in the acute time-points following MCAO. This demonstrates a novel finding that with the pre-tMCAO drilling of a cranial burrhole survival is improved in male SHRSP rats subsequently subjected to 45 min tMCAO, with no effect on infarct size or neurological deficit to confound outcome measures.
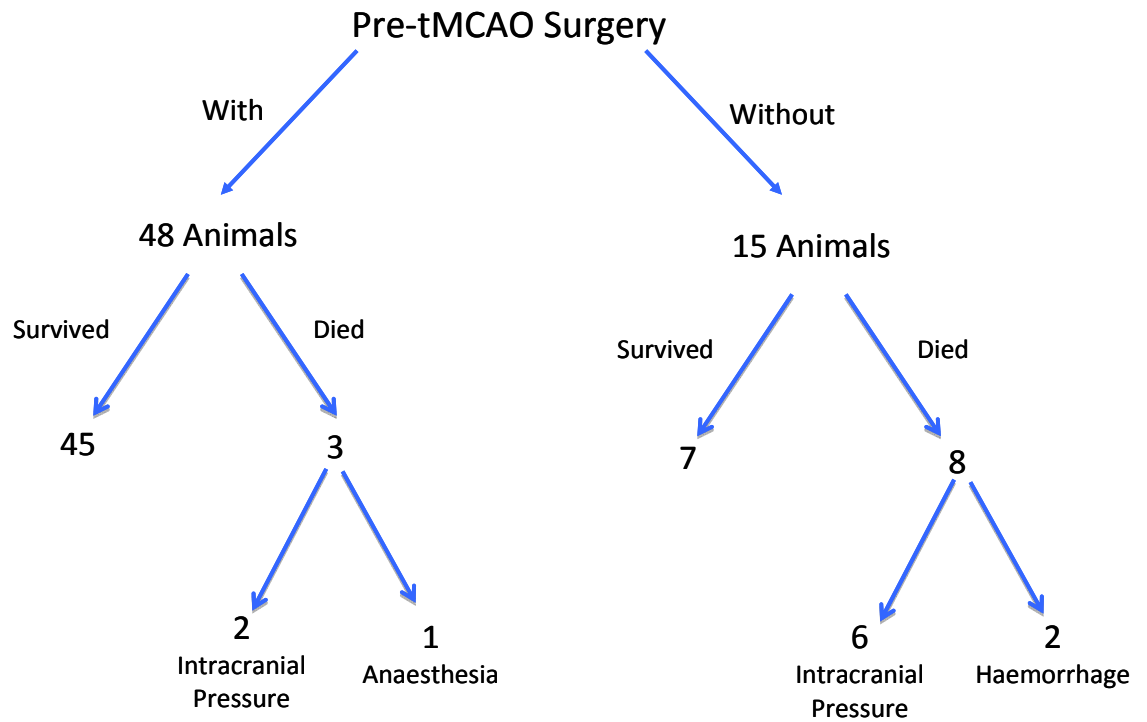
Figure 5.3: **Assessment of administration of sham stereotactic procedure on improved survival post-tMCAO**

In comparing the administration of a sham stereotactic procedure on survival, out of 15 animals that did not receive the procedure 8 died prematurely. Out of 48 animals receiving the procedure, 3 died prematurely.
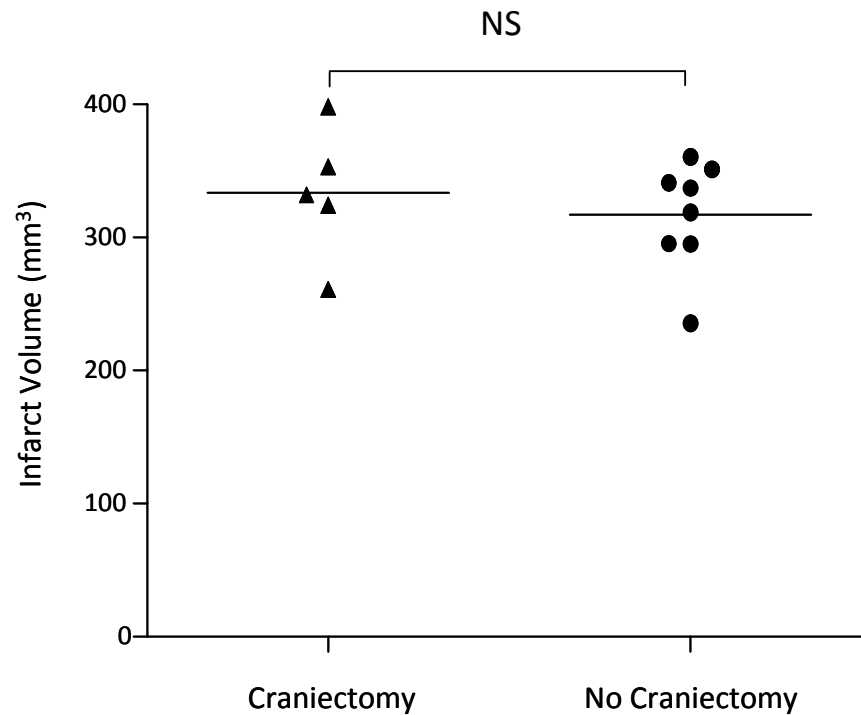
Figure 5.4:   **Assessment of administration of sham stereotactic procedure in infarct volume.**

Infarct volume (mm^3) measured from H&E stained sections over seven coronal levels, as previously described (section 2.7.5). No significant difference was observed between groups administered a craniectomy from those not administered a craniectomy, *n* = 5 and *n* = 8, respectively. Horizontal bar represents average.

(A)

(B)
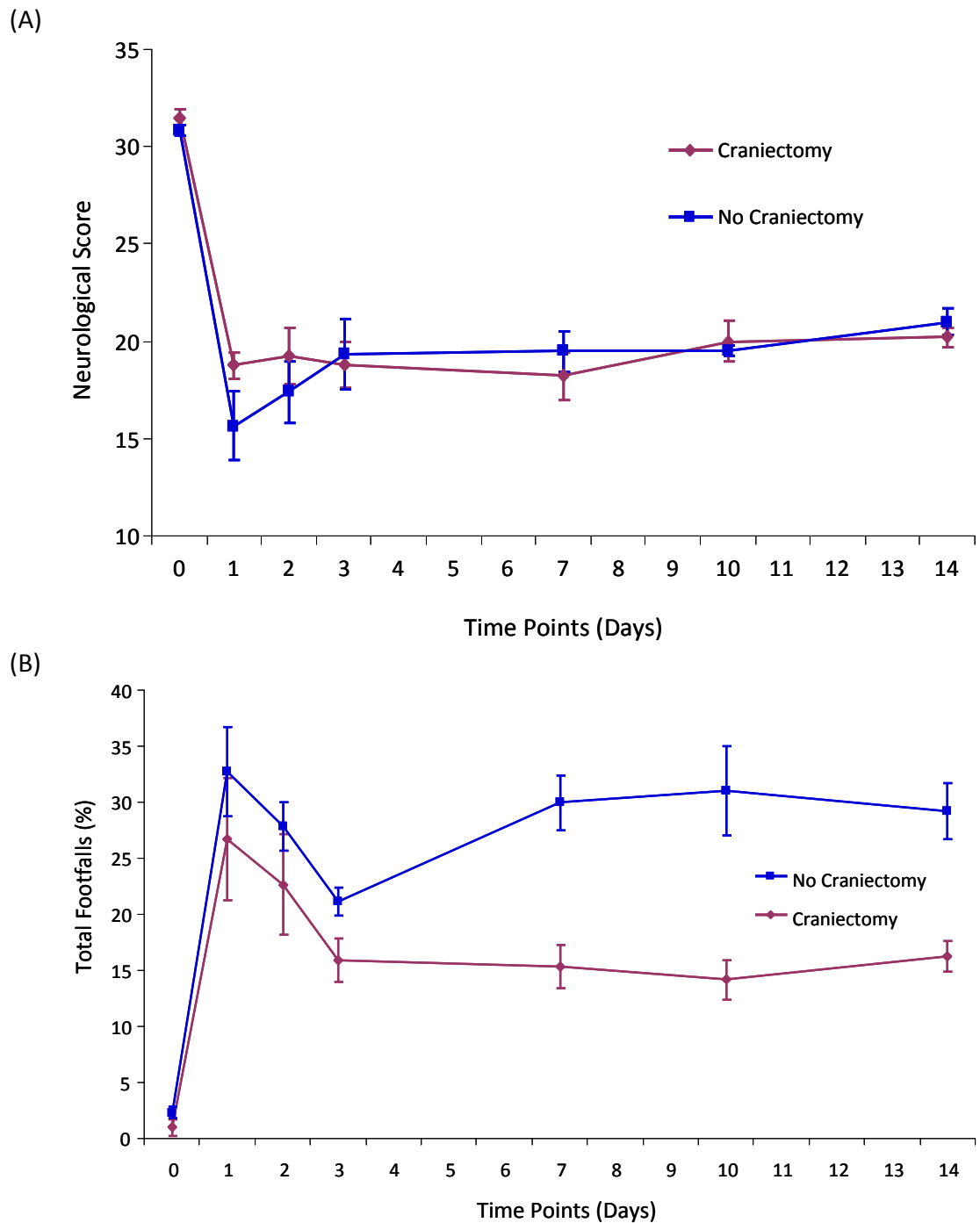
Figure 5.5: Comparative Analysis of Administration of Craniectomy on Longitudinal Neurological Assessment following 45 min tMCAO

(A) 32-point neurological score assessed at day 1, 2, 3, 7, 10 and 14. No significant difference between groups.   Craniectomy *n* = 5; no craniectomy *n* = 8. $p > 0.05$, one way ANOVA using Bonferroni's post-hoc test. Data displayed as average ± SEM. (B) Tapered beam test assessed at day 1, 2, 3, 7, 10 and 14 with results expressed as % footfalls of total steps taken. No significant difference with administration of craniectomy. Craniectomy *n*= 5; no craniectomy *n* = 8. $p > 0.05$, one way ANOVA using Bonferroni's post-hoc test. Data displayed as average ± SEM.

5.3   DISCUSSION

In accordance with the S.T.A.I.R guidelines for pre-clinical stroke studies (Fisher *et al.*, 2009), a control study was carried out in 12 animals to determine the effectiveness of the desired neurological tests and reproducibility of infarct before carrying out the comprehensive intervention study. Initial results from this study allowed exclusion of the cylinder test from the battery of neurological assessments, as no effect of MCAO was observed and baseline scores were highly variable. Analysis of the final data, indicated operational surgical issues resulting in highly variable lesion size and as such an insignificant neurological deficit at day 14 assessed by both 32-point neurological score and the tapered beam walk test. In addition, the MCA of 4 out of the 12 animals was not fully occluded during stroke surgery due to problems with fully advancing the filament. Further analysis of stroke procedure demonstrated filament was advancing into vessel wall at point of bifurcation of the ICA with the pterygopalatine, resulting in incomplete or no occlusion of the MCA. The 4 animals therefore displayed no lesion at day 14 and were removed from the study. The completion of this control study allowed for issues to be flagged and subsequent additional training to be given in surgical techniques. It also allowed for refinement in behavioural testing, operational *ex vivo* experience in assessing lesion size, and analysing neurological data before initiation of the intervention study.

The present study demonstrated that pre-tMCAO general anaesthesia and surgery to drill a cranial burrhole significantly reduced mortality following tMCAO in male SHRSP. It is well established that reduction of intracranial pressure through procedures such as decompressive craniectomy results in significantly reduced mortality following severe ischaemic strokes. In 2007, a randomised and controlled trial "Decompressive Surgery for the Treatment of Malignant Infarction of the Middle Cerebral Artery (DESTINY)" (Juttler *et al.*, 2007) published that at 30 days post stroke 88 % of patients randomised to hemicraniectomy survived, in comparison to 47 % randomised to conservative therapies. At 6 and 12 month follow up, 47 % of patients who received decompressive surgery had a modified Rankin Score (mRS) (Table 5.1) of 0-3, whilst only 27 % of patients receiving conservative treatments fell within this range.

Table 5.1:   Modified Rankin Score (mRS)

0 - No symptoms

1 - No significant disability

Able to carry out all usual activities, despite some symptoms

2 - Slight disability

Able to look after own affairs without assistance, but unable to carry out all previous

activities

3 - Moderate disability

Requires some help, but able to walk unassisted

4 - Moderately severe disability

Unable to attend to own bodily needs without assistance, and unable to walk unassisted

5 - Severe disability

Requires constant nursing care and attention, bedridden, incontinent

6 – Dead

In the clinic it may be expected that decompressive surgery in combination with rt-PA thrombolysis would improve outcome following ischaemic stroke by ameliorating the increase in pressure attributed to the oedema observed following reperfusion. However, a recent study assessing the benefit of decompressive craniectomy following intra-arterial thombosis of the MCA with or without subsequent rt-PA-mediated thrombolysis reported no significant additional benefit of outcome of decompressive surgery when in combination administration of rtPA (Fischer *et al.*, 2011). Decompressive surgery was administered in 30 ischaemic stroke patients who either received additional rt-PA thrombolysis (n = 15) or received no thrombolysis therapy (n = 15). Outcome at 3 months was reported as favourable (mRS = 0 - 3) in 47 % of thrombolysed patients and 27 % of non-thrombolysed patients (p = 0.45). In the thrombolysed group, 7 patients had a mRS of 3, 4 had a mRS of 4, and 4 patients died. In the non-thrombolysed group, 4 patients had a mRS of 2, 7 had a mRS of 4, 1 had a mRS of 5, and 3 patients died (Fischer *et al.*, 2011). Although results trended towards an improvement with combined therapy, no significant difference was observed, perhaps as a result of the relatively low *n* numbers.

In the present model, the hole created in the skull to expose the brain was subsequently sealed with dental cement in an attempt to prevent any risk of infection and also to prevent

any confounding effects of potential intracranial pressure reduction. Nevertheless, a marked improvement in survival was noted. This led to the hypothesis that piercing of the dura mater by the needle was allowing enough pressure release to reduce mortality. The dura mater (from the Latin "hard mother") is a strong and inflexible membrane surrounding the brain and spinal cord, whose primary function is to enclose the CSF. Considering the robust nature of the dura, a hole within the region of infarct could perhaps be sufficient to ameliorate pressure, reducing mortality. In addition to the potential attenuation of intracranial pressure, the hole in the dura could allow any excess CSF, as a result of brain oedema, to drain from the site of infarction, further lowering intracranial pressure. However, it is unknown whether following sham stereotactic procedure 5 days prior to MCAO, the hole remains in the dura mater up to the important acute stages following reperfusion, as it could potentially re-seal over this timecourse. Importantly for ongoing studies, there was no confounding effect of the pre-tMCAO surgery to drill a cranial burrhole on final infarct volume. Further analysis showed this reduction in mortality did not result in an improvement of neurological deficit in animals receiving the sham stereotactic procedure compared to those not receiving it. Additionally, no improvement in lesion volume was observed between groups, however it should be noted that lesion volume can only be assessed in surviving animals, and as such cannot be deemed as the primary outcome of this study. Until now it has not been reported that administration of a sham stereotactic procedure improves survival with no effect on neurological deficit or lesion size in pre-clinical models of transient ischaemic stroke using SHRSP's. Indeed, a number of other studies have assessed stereotactic administration of agents in pre-clinical models of stroke, with no improvement in mortality noted. The relatively rare of use of reperfusion models in hypertensive strains, in addition to a rare utilisation of both untreated control and stereotactically administered vehicle control groups could perhaps explain this. Unfortunately, at present there exists no mechanism to measure intracranial pressure without administration of a craniectomy to insert probe, so this hypothesis cannot currently be tested. This presents a novel finding that is of importance in the design of future studies using this model, when considering both the ethics and experimental costs involved in *in vivo* work. Specifically, this finding addresses 2 of the "3R's" of animal work; reduction, by lowering the levels of mortality observed from 53.33 % in control animals to 6.25 % in control animals; and refinement, by determining an improved method for tMCAO procedure in SHRSP.

These studies provided the substantial 'work-up' required to undertake a comprehensive in vivo intervention study. Specifically it allowed for selection of the optimal viral vector and behavioural tests for use, improvement of surgical procedure, and experience of ex vivo analysis. Additionally, following initiation of the in vivo intervention study, a novel finding allowing for refinement of the tMCAO procedure in SHRSP was identified, reducing the relatively high mortality expected with the tMCAO procedure.

Chapter 6

Results:

In Vivo Intervention Study

6.1 INTRODUCTION

Generating an effective pre-clinical animal model of stroke is challenging for a number of reasons. Human stroke generally occurs in the aged population, who often exhibit co-morbidities such as hypertension, heart disease and diabetes. Each of these factors is likely to have an effect on the efficacy of a potential therapeutic agent. Hypertension and age are the most prevalent risk factors for stroke (O'Donnell *et al.*, 2010b), but mortality following experimental stroke surgery is higher in aged and hypertensive animals. Diabetes and hyperglycemia occur in one-third of stroke patients, and are associated with poorer outcomes in large vessel stroke (Adams *et al.*, 2003). In addition, human stroke patients are often using concomitant medication which can interact with the proposed therapeutic agent; this has rarely been considered in the outcome of negative stroke trials.

In an attempt to address some of the issues highlighted in the STAIR guidelines to improve clinical translation (Fisher *et al.*, 2009), the present study was designed using male, stroke-prone spontaneously hypertensive rats (SHRSP) with experimental stroke induced at 16 weeks of age (270 – 310 g). The SHRSP is a strain of rats bred to exhibit a number of the co-morbidities of CVD. Isolated from normotensive Wistar-Kyoto (WKY) rats by Okamoto and Aoki in 1963 (Okamoto *et al.*, 1963), these animals display hypertension, nephropathy, insulin resistance, hyperinsulinemia, hypertriglyceridemia, and hypercholesterolemia (Masineni *et al.*, 2005). The SHRSP differs from the SHR in that it displays an even higher blood pressure and has a strong tendency to spontaneous stroke when aged (Nagaoka *et al.*, 1976). Use of this strain of rats therefore theoretically allows for a more robust pre-clinical model, with greater translation to human stroke.

The factor of perhaps greatest importance to pre-clinical stroke studies is outcome analysis. Outcome analysis should be assessed blinded and include factors such as infarct size, histology, mortality rate, and behavioral and motor scores. Lesion size can be measured in a number of ways including TTC staining (healthy tissue stains red, infarct does not) of coronal sections, but more accurately by haematoxylin and eosin (H&E) staining of paraffin embedded sections. However, as the infarct does not reach its maximum size until 72 h post tMCAO (Garcia *et al.*, 1997), studies should be designed with a recovery period of at least 3 days and preferably longer before infarct determination. A novel method of H&E staining of coronal sections at 8 known levels was described in 1987, where the area of lesion from each section was delineated onto scale diagrams representative of the

coronal level (Osborne *et al.*, 1987). The area (mm^2) was subsequently plotted against the anterio-ventral co-ordinates of the specific level and the area under the curve (AUC) taken to give a total volume of infarct (mm^3). Use of scale diagrams corrects for bias as a result of swelling and oedema in the region of infarct.

Neurological deficit should be assessed longitudinally throughout the recovery phase, with training or acclimatisation to the tests prior to tMCAO to generate a baseline score (reviewed in (Zarruk *et al.*, 2011)). Neurological deficit can be assessed by a number of different tests which can be largely divided into sensorimotor tests, cognitive tests and neurological scales. Sensorimotor tests include the rotarod test (Dunham *et al.*, 1957), the tapered beam walk test (Feeney *et al.*, 1982) the adhesive removal test (Schallert *et al.*, 1984), the elevated body swing test (Borlongan *et al.*, 1995), the cylinder test (Zhang *et al.*, 2002a) and the corner test (Zhang *et al.*, 2002a). Neurological scales evaluate diverse symptoms of ischaemic injury through a number of tests. A commonly used neurological scale is Bederson's neurological score (Bederson *et al.*, 1986), which consists of a 5 point scale (0 = no neurological deficit, 1 = failure to fully extent contralateral forepaw, 2 = circling, 3 = falling to the contralateral side at rest, 4 = unable to walk spontaneously and having a depressed level of consciousness, 5 = dead). A neurological score with greater sensitivity comprised of a battery of 10 tests to give a maximum score of 32 was devised by colleagues at the Wellcome Surgical Institute, University of Glasgow (McGill *et al.*, 2005).

Neuroglobin upregulation has been shown to be neuroprotective in a number of studies of *in vivo* brain ischaemia models. Stereotactic injections of 1.2×10^{11} vp of adeno-associated virus (AAV) at 2 sites in the cortex of normotensive Sprague-Dawley rats to overexpress Ngb significantly reduced infarct size and improved neurological function measured 24 h after tMCAO. The virus was administered 3 weeks prior to tMCAO (Sun *et al.*, 2003). Transgenic mice overexpressing Ngb confirmed its neuroprotective action following focal (Wang *et al.*, 2008) and global (Li *et al.*, 2010) ischaemia, respectively. A reduction in infarct size at day 1 and 14 post-tMCAO in addition to reduced MDA synthesis at 8 and 24 h post-tMCAO in Ngb transgenic animals has been reported; however no improvement in neurological function was observed (Wang *et al.*, 2008). Following global ischaemia a significant reduction in MDA, nitrotyrosine and ROS formation in comparison to controls was seen at day 3 accompanied by a reduction in neuronal death in the region of the hippocampus (Li *et al.*, 2010). Another method of upregulating Ngb from

endogenous levels is through cell-penetrating peptides (CPP). Due to its size (17 kDa), Ngb is too large to freely pass across the BBB. CPP are usually basic peptides that mediate the delivery of peptides, proteins, drugs, or even 40 nm iron beads across cellular membranes and the BBB and are regularly used in pre-clinical models of neurological disorders due to the well-established difficulties with therapeutic delivery to the tightly-controlled CNS (Dietz *et al.*, 2005). The most common CPP has been derived from the basic domain of the HIV transactivator of transcription (Tat). Delivery of 10 mg / kg Tat-Ngb *i.v.* either prior to or immediately after 24 h reperfusion following 2 h tMCAO in normotensive C57BL/6J mice resulted in significantly reduced lesion size (assessed by TTC) and improved neurological recovery (assessed by Bederson's 5 point neurological scale) when given as a pre-treatment. However, animals administered Tat-Ngb post-tMCAO at the point of reperfusion showed no improvement in infarct size or neurological score (Cai *et al.*, 2011).

In 2002, Irving and Bamford showed a specific role of JNK-mediated neuronal apoptosis in cerebral ischaemia and since then a number of groups have confirmed beneficial effects of JNK inhibition on lesion size, neurological deficit, and production of harmful stimuli following experimental stroke. A dose-dependent (0.3 mg / kg – 10 mg / kg SP600125, administered *i.v.* - 15 min and + 3 h post-MCAO) reduction in lesion size following 60 min tMCAO was demonstrated in C57/B6 mice at 48 h following the onset of stroke (Gao *et al.*, 2005). The same study also recorded a significant improvement in neurological score at day 1, 3, 5, and 7 following tMCAO assessed by 5-point numerical score and corner test (Gao *et al.*, 2005). Additionally, a reduction in neuronal cell death was observed within the hippocampal CA1 region in animals pre-treated (- 20 min) with *i.c.v.* injection of 30 µg SP600125 in a model of transient (15 min) global brain ischaemia in Sprague-Dawley rats (Guan *et al.*, 2005). Importantly, use of a peptide inhibitor of JNK, D-JNKI-1, has also showed a significant decrease in infarct volume at 48 h after *i.c.v* administration of 15.7 ng up to 6 h after the onset of stroke in a model of tMCAO (Borsello *et al.*, 2003a).

The combination of Ngb upregulation with inhibition of JNK in the treatment of stroke has not been assessed until now. Furthermore, the combination of an anti-apoptotic with an antioxidant strategy has not been assessed in a model of pre-clinical stroke. Therefore it was the aim of this study to assess the efficacy of CAV2-mediated Ngb upregulation in combination with pharmacological inhibition of JNK on survival, infarct size and neurological deficit.

6.2 RESULTS

6.2.1 Inclusion Criteria

Only animals ranging between 270 g – 310 g were included in the study and weight gain / loss was measured daily throughout the study, with monitoring of the animal occurring 3 times a day for the first 3 days post-tMCAO, and once a day thereafter. Weight at time of tMCAO had no correlation with final infarct (Figure 6.1 B). Animals having lost $\geq$20 % of body weight from time of tMCAO were euthanised as this exceeded the severity limits of the license. Animals displaying additional symptoms out with those indicated as acceptable adverse effects in the license criteria were also euthanised immediately.

6.2.2 Physiological Variables

Body temperature was maintained at 37 °C $\pm$ 1 °C and time under anaesthesia was kept to a minimum and in the main < 90 minutes at < 3 % isoflurane. To assess whether any of the intervention regimes had a confounding effect on blood pressure post-tMCAO, blood pressure was taken pre-tMCAO and at 7 and 14 days post-tMCAO (Table 6.1). No significant change in blood pressure was observed with time within any treatment group or at any point between any of the treatment groups. In addition, blood pressure at time of tMCAO was not correlated to final infarct size (Figure 6.1A).

6.2.3 Survival

A total of 63 rats underwent transient tMCAO (45 minutes) or sham procedure. A total of 13 animals did not complete the study, due to spontaneous death or early sacrifice as a result of exceeding severity limits or exhibiting adverse effects out with those included in the project license. A total of 13 animals died, as a result of increased intracranial pressure ($n = 8$); brain hemorrhage ($n = 2$) and anaesthesia ($n = 1$). 1 animal was removed from study as no infarct was observed (Figure 6.2). 4 deaths were oserved in the control MCAO group, 2 in the CAV-GFP group, 4 in the SP600125 group, and 1 in the CAV-Ngb group, with no deaths observed in the combined treatment groups. Of the surviving control animals, 3 were not administered a sham stereotactic procedure and 3 of the surviving SP600125 animals did not receive a sham stereotactic procedure. Evidence in chapter 5 demonstrated an improvement in survival with no effect on outcome measures so these animals were deemed suitable to remain in the intervention study.

Table 6.1:   Longitudinal Assessment of Blood Pressure

Conscious systolic blood pressure (mmHg) was determined in all groups by tailcuff plethysomography pre- and at 7 and 14 days post-tMCAO. Data are presented as mean ± SEM.

	Pre-tMCAO	7 d Post-tMCAO	14 d Post-tMCAO
Sham *n* = 6	177.5 ± 5.6	175.3 ± 5.1	180.7 ± 5.8
Control tMCAO *n* = 9	173.2 ± 3.8	177.8 ± 4.2	175.4 ± 4.5
CAV2-GFP *n* = 9	171.4 ± 4.3	181.3 ± 4.5	186.6 ± 3.3
SP600125 *n* = 9	179.3 ± 3.1	179.3 ± 2.8	179.3 ± 4.2
CAV2-Ngb *n* = 9	174.7 ± 4.2	182.8 ± 2.8	177.7 ± 4.1
CAV2-Ngb + SP600125 *n* = 8	173.5 ± 5.4	176.8 ± 4.3	182.6 ± 2.9

(A)
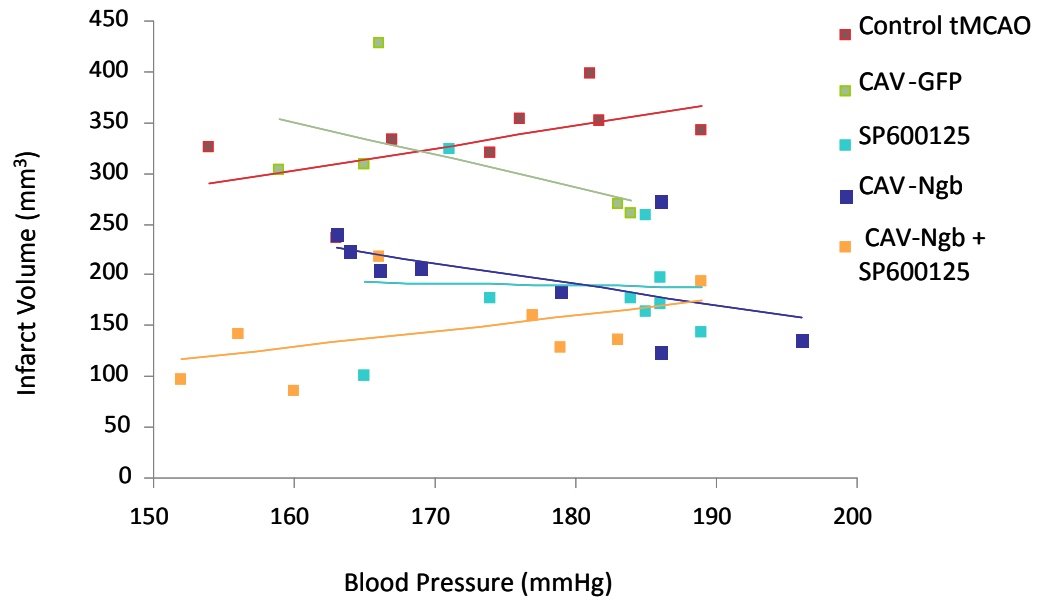
(B)
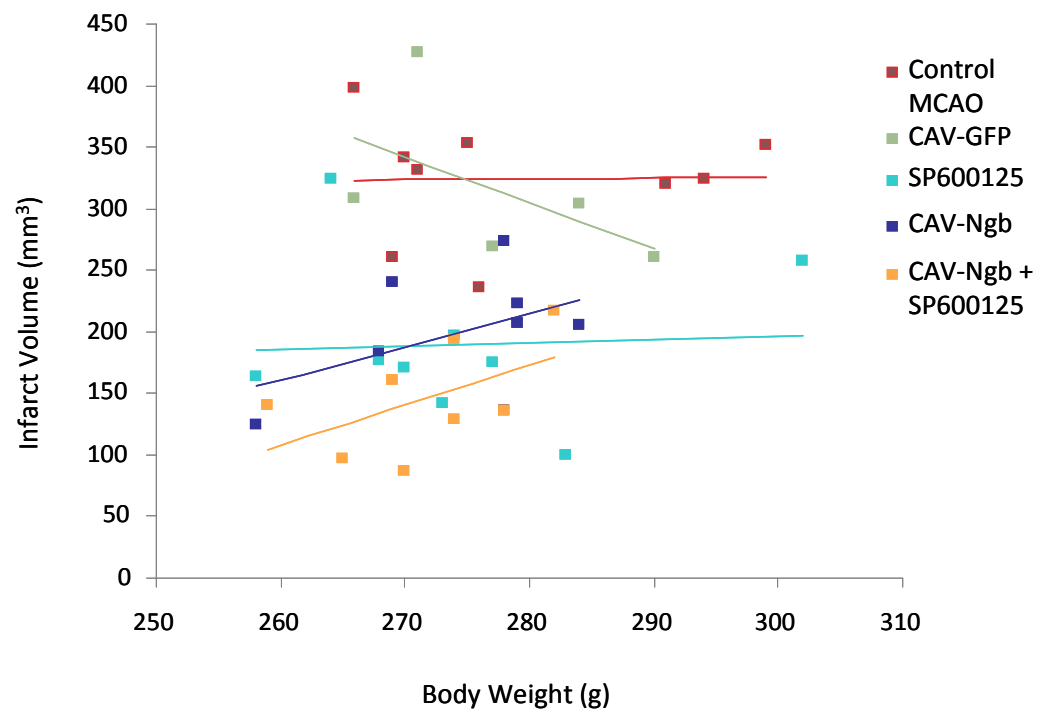
Figure 6.1: **Effect of Blood Pressure and Body Weight at Time of tMCAO on Final Lesion Size.**

Correlation between blood pressure (A) or body weight ($r^2 < 0.01$.) and (B) at time of infarct with final lesion size ($r^2 < 0.05$.).

SURVIVAL

Total = 63 Animals

Included

Excluded

50 Animals

13 Animals

6
Sham

9
Control
MCAO

9
CAV-GFP

9
SP600125

9
CAV-Ngb

8
CAV-Ngb +
SP600125

Survived

Died

1
No ischaemic
damage

11

8
Intracranial
Pressure

2
Haemorrhage

1
Anaesthesia
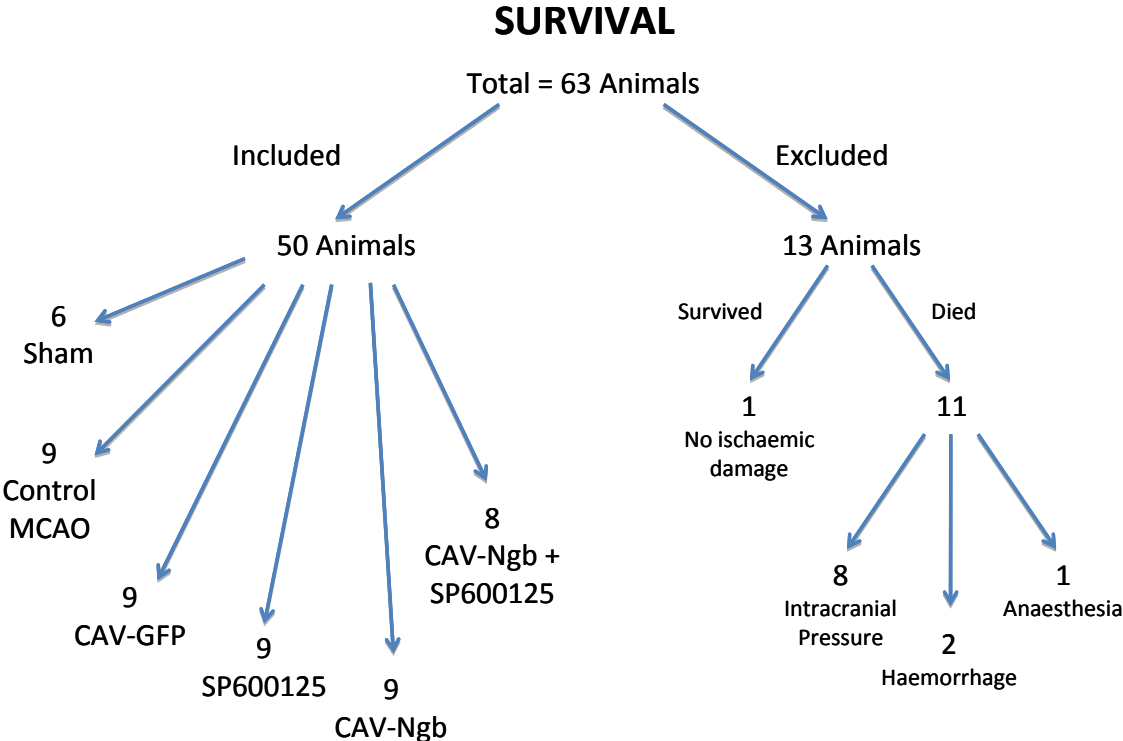
Figure 6.2:   Fate of Animals Included in the Study

Of 63 animals, 13 were excluded due to falling out with the severity limits of the project license or displaying adverse events not included in the license criteria, premature death or lack of ischaemic damage.

6.2.4 Study Design

Animals were administered virus (by single stereotactic injection into the cortex) or subjected to pre-tMCAO surgery to drill a cranial burrhole, 5 days prior to tMCAO. On the day of tMCAO surgery, animals receiving SP600125 (1 mg / kg) were administered it *i.v.* 15 minutes prior and 3 h after the onset of ischaemia. SP600125 was diluted in PPCES vehicle (30% PEG–400 / 20% polypropylene glycol / 15% cremophor EL / 5% ethanol / 30% saline). A stock solution of 200 mM SP600125 was made up in neat DMSO, and ~ 7 μl of stock was added to make a final volume of 50 μl in PPCES vehicle per injection. Neurological score and tapered beam walk test was assessed at day 1, 2, 3, 7, 10 and 14. Blood pressure was monitored with tail-cuff measurements made 3 days prior to tMCAO and day 7 and 14 post tMCAO. At the end of the study, animals were perfusion fixed under physiological pressure for histological processing of brain (Figure 6.3).

6.2.5 Infarct Analysis

6.2.5.1 Infarct Volume

At day 14 post-stroke animals were deeply anaesthetised, perfusion fixed and the brain removed for paraffin embedding for histological analysis. Volume of infarct was determined by haematoxylin and eosin staining and mapping onto seven known coronal levels (section 2.7.5). In the region of the infarct, neuronal cell bodies appeared shrunken and triangular and the structure and organisation of the brain was vastly disrupted, with significant tissue loss at day 14. After 45 minutes tMCAO infarct volume was 324.1 ± 16.4 mm^3 in control animals, and this was unaffected with pre-treatment of 3×10^9 vp control virus CAV2-GFP (313.9 ± 22.2 mm^3). Pre-treatment (-15 min) and acute post-treatment (+ 3 h) with SP600125 (1 mg / kg) *i.v* significantly reduced infarct volume (214.8 ± 34.2 mm^3, $p<0.01$ vs. control tMCAO). In addition, pre-treatment with 3×10^9 vp CAV2-Ngb (-5 days) significantly reduced infarct volume from controls (199.0 ± 14.4 mm^3, $p<0.01$ vs. control tMCAO). However, pre-treatment with the combined therapies further significantly reduced infarct volume in comparison to SP600125 alone (137.0 ± 20.7 mm^3, $p<0.01$ vs. SP600125) (Figure 6.4).
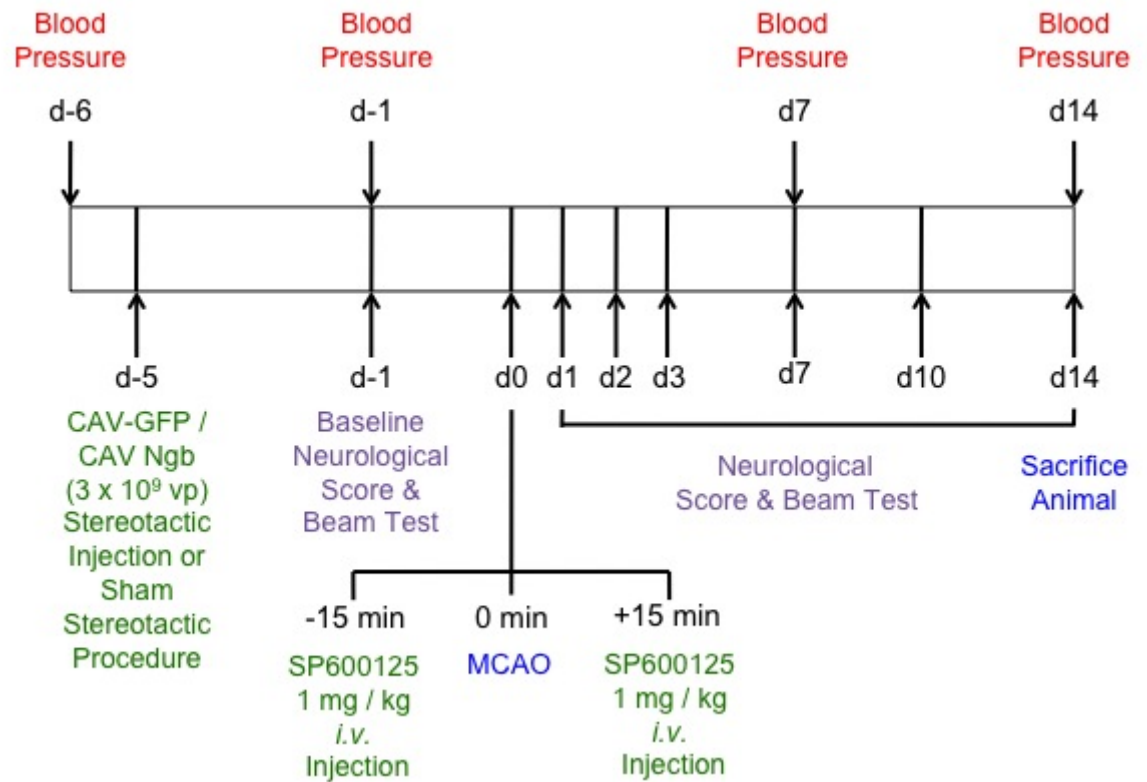
Figure 6.3:   Study Design

Animals were administered 3 x 10^9 vp virus stereotactically 5 d prior to tMCAO within the cortex (AP: - 0.7 mm, ML: + 3 mm, DV: - 2 mm), and those receiving SP600125 were administered 1 mg / kg *i.v.* via femoral infusion 15 min prior and 3 h post tMCAO onset. Baseline neurological score was assessed 1 d prior to tMCAO, with subsequent post analysis at 1 d, 2 d, 3 d, 7 d, 10 d, and 14 d. Blood pressure measured at 6 d and 1 d prior to tMCAO surgery with subsequent post analysis at 7d and 14d, before sacrifice.

6.2.6   Infarct Location

Infarct location was assessed by use of scale line diagrams of 7 known coronal levels, determined by specific anatomical markers. The mean rostra-caudal distribution of the infarct across the groups over the 7 coronal levels of the brain is shown in Figure 6.5. SP600125-treated animals showed a significant improvement from control animals at levels 4, 5, 6 and 7. CAV2-Ngb and CAV2-Ngb + SP600125 groups showed a significant reduction of infarct area at levels 3, 4, 5, 6 and 7 (Figure 6.5). There was a further significant improvement with combined treatment at level 3, and a further impovement at level 4 although this did not reach significance. Values are quantified in Table 6.2.

Representative line diagrams from median animals within each group show the rostro-caudal location of the infarct (Figure 6.6). Across all groups, the sensorimotor regions of the cortex are a highly conserved area of infarct. In contrast, the region of the striatum appears to be the most readily salvaged. Respresentative H&E images of the cortex and striatum taken from median animals at coronal level 3 (AP: - 0.12 mm, relative to bregma) are shown in Figure 6.7. Results show an reduction in lesion size within the cortex and striatum with individual treatment of CAV2-Ngb or SP600125, and a further improvement afforded by combined treatment at these distinct locations.

6.2.7   32-Point Neurological Score

Neurological scores for each treatment group at each time-point are shown in Figure 6.8. All groups, excluding sham, exhibited a significant worsening of neurological deficit score from baseline pre-tMCAO control (sham = 31.0 ± 0.4; control tMCAO = 31.6 ± 0.2; CAV2-GFP = 31.6 ± 0.3; SP600126 = 30.8 ± 0.2; CAV2-Ngb = 31.3 ± 0.3; CAV2-Ngb + SP600125 = 31.3 ± 0.2) at 24 h post-tMCAO (sham = 27.5 ± 0.6; *control tMCAO = 18.0 ± 0.2; *CAV2-GFP = 18.7 ± 0.6; *SP600126 = 19.7 ± 1.5; *CAV2-Ngb = 19.4 ± 0.1; *CAV2-Ngb + SP600125 = 20.3 ± 0.7; *$p<0.01$ vs. control tMCAO, using one way ANOVA with Bonferroni's post-hoc correction). Sham animals trended towards a drop in neurological score at day one, and never fully returned to baseline levels although no significant difference was observed.
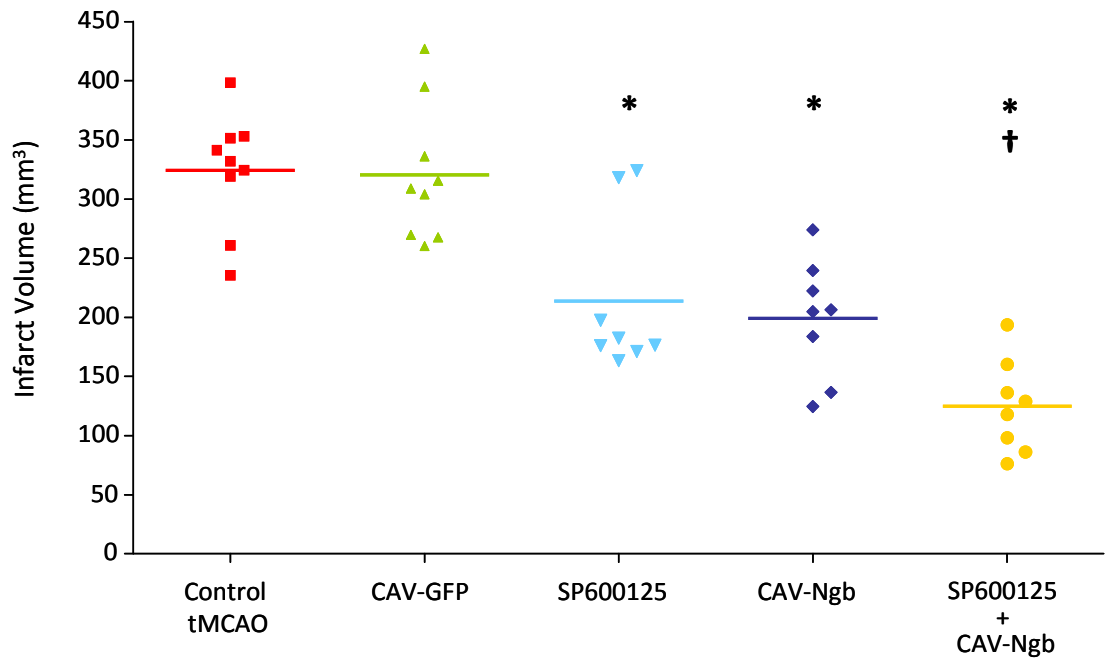
Figure 6.4:   Infarct Volume following 45 min tMCAO in SHRSP

Infarct volume in control tMCAO, CAV2-GFP, SP600125, CAV2-Ngb and CAV2-Ngb + SP600125-treated animals 14 d post-tMCAO. Data are shown from each animal in the group with the line representing the mean. *p<0.01 vs. control tMCAO and †p<0.01 vs. SP600125 by one way ANOVA with Bonferroni's post-hoc correction.
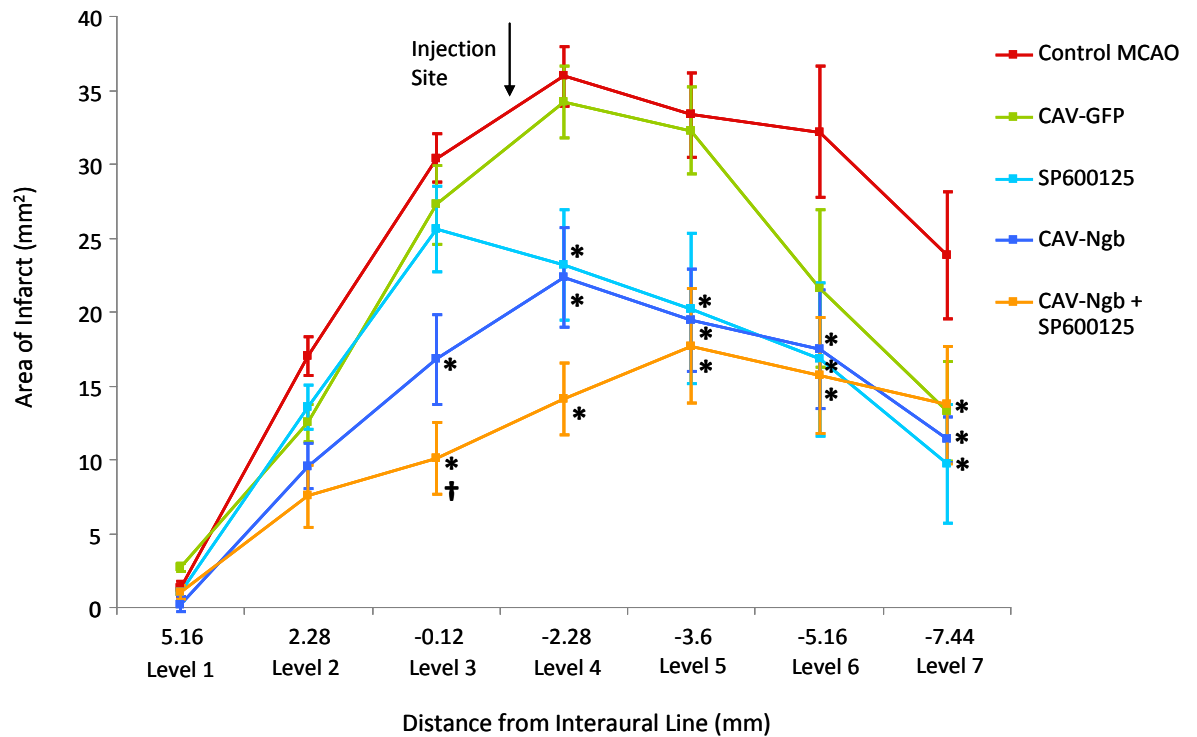
Figure 6.5:   Infarct Location following 45 min tMCAO in SHRSP

Distribution of infarct areas over 7 coronal levels in control tMCAO, CAV2-GFP, SP600125, CAV2-Ngb and CAV2-Ngb + SP600125 treated groups, 14 d post tMCAO. Area of infarct at each level (mm^2) against distance from interaural line (mm). Data point displayed as mean ± SEM. *p<0.01 vs. control tMCAO and †p<0.01 vs. SP600125 by one way ANOVA with Bonferroni's post-hoc correction.

Table 6.2: Quantified Lesion Area by Coronal Level following 45 min tMCAO in SHRSP

Average lesion area (mm^2) at each coronal level ± SEM. *p<0.01 vs. control tMCAO and †p<0.01 vs. SP600125 or CAV2-Ngb single treatment groups, by one way ANOVA with Bonferroni's post-hoc correction.

	Level 1	Level 2	Level 3	Level 4	Level 5	Level 6	Level 7
Control tMCAO	1.28 ± 0.5	17.0 ± 1.3	30.40 ± 1.6	35.97 ± 2.0	33.32 ± 2.8	32.17 ± 4.5	23.83 ± 4.3
CAV2-GFP	2.72 ± 0.3	12.51 ± 1.3	27.25 ± 2.7	34.21 ± 2.4	32.27 ± 2.9	21.55 ± 5.3	13.25 ± 3.4
SP600125	1.00 ± 0.5	13.54 ± 1.5	25.63 ± 2.9	23.18 ± 3.8*	20.23 ± 5.1*	16.78 ± 5.2*	9.71 ± 4.1*
CAV2-Ngb	0.21 ± 0.5	9.57 ± 1.5	16.7 ± 3.1*	22.36 ± 3.4*	19.40 ± 3.5*	17.46 ± 4.0*	11.38 ± 1.5*
CAV2-Ngb + SP600125	1.03 ± 0.4	7.54 ± 2.1	10.07 ± 2.4*†	14.10 ± 2.4*	17.69 ± 3.9*	15.71 ± 4.0*	13.70 ± 4.0*
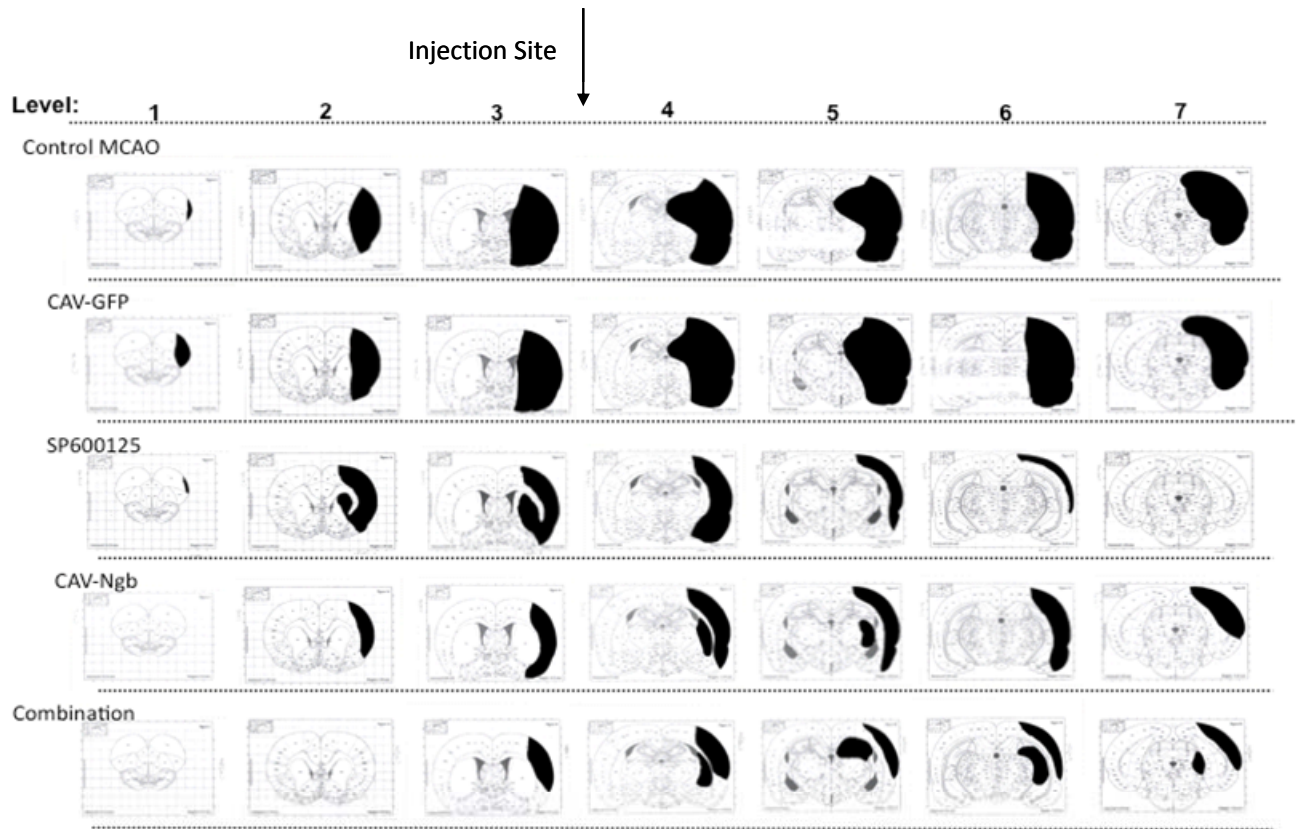
Figure 6.6:   Comparative Analysis of Infarct Location

Line diagrams of the 7 known coronal sections delineating the infarct from the median animals of each treatment group.
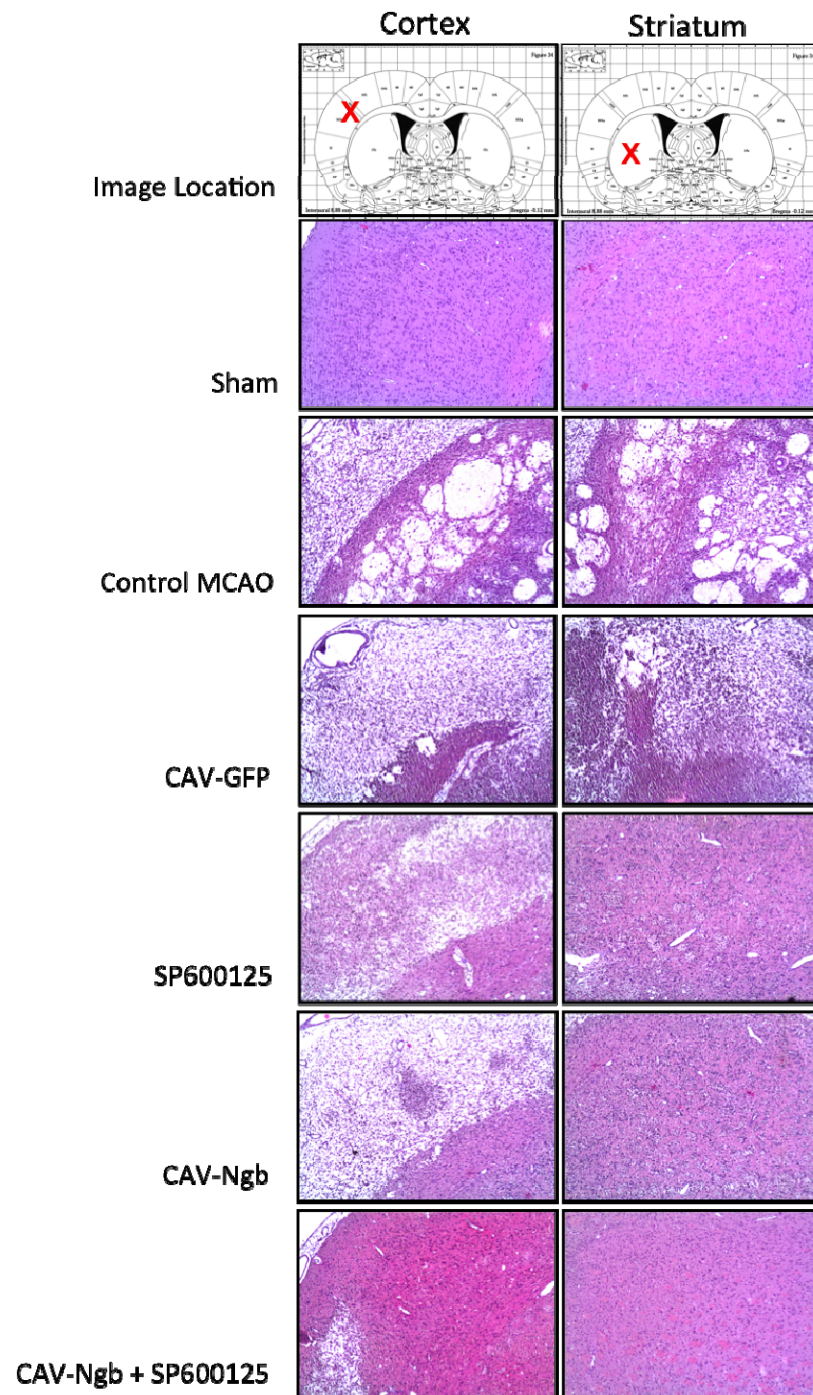
Figure 6.7:   Representative H&E Images of Infarct

Image location on coronal slice (AP: - 0.12 mm, relative to brema) is shown by red cross (top row). Normal brain tissue morphology (sham) is shown by even distribution and round nuclei of cells. Infarcted tissue (control & CAV2-GFP) is represented by neurons displaying the morphological features of ischaemic damage: pyknotic perikarya (shrunken and triangular in shape) within a highly disorganised neuropil. Images taken of median animal, x 4 magnification.

No significant difference in neurological deficit was observed at day 1, 2 or 3 between groups. At day 7 a significant improvement in neurological deficit from control was observed with combined therapy but not with either treatment alone (control tMCAO = 18.8 ± 0.8; CAV2-GFP = 20.1 ± 0.7; SP600125 = 22.7 ± 0.7; CAV2-Ngb = 22.4 ± 0.9; *CAV2-Ngb + SP600125 = 24.6 ± 0.7; *p<0.01 vs. control tMCAO, using one way ANOVA with Bonferroni's post-hoc correction). At day 10 there was a significant improvement from control tMCAO with all treatment groups, but no further improvement with combination therapy (control tMCAO = 19.8 ± 0.6; CAV2-GFP = 21.0 ± 0.3; *SP600125 = 24.0 ± 0.5; *CAV2-Ngb = 23.3 ± 0.9; *CAV2-Ngb + SP600125 = 25.8 ± 0.5, *p<0.01 vs. control tMCAO, using one way ANOVA with Bonferroni's post-hoc correction). However, at day 14 in addition to a significant improvement in neurological score from control tMCAO with all treatments groups, there was a further significant improvement with combination therapy from either treatment alone (control tMCAO = 20.6 ± 0.4; CAV2-GFP = 21.7 ± 0.3; *SP600125 = 23.1 ± 0.6; *CAV2-Ngb = 23.2 ± 0.9; *†CAV2-Ngb + SP600125 = 26.5 ± 0.5, *p<0.01 vs. control tMCAO, †p<0.01 vs. SP600125 or CAV2-Ngb, using one way ANOVA with Bonferroni's post-hoc correction).

6.2.7.1 Correlation Between 32-point Neurological Score and Infarct Volume

Figure 6.9 indicates a correlation between volume of infarct and neurological score following tMCAO. As infarct volume increases, neurological score decreases in all groups. This correlation demonstrates the outcome of the neurological score used in the present study is directly related to the extent of neurological damage.
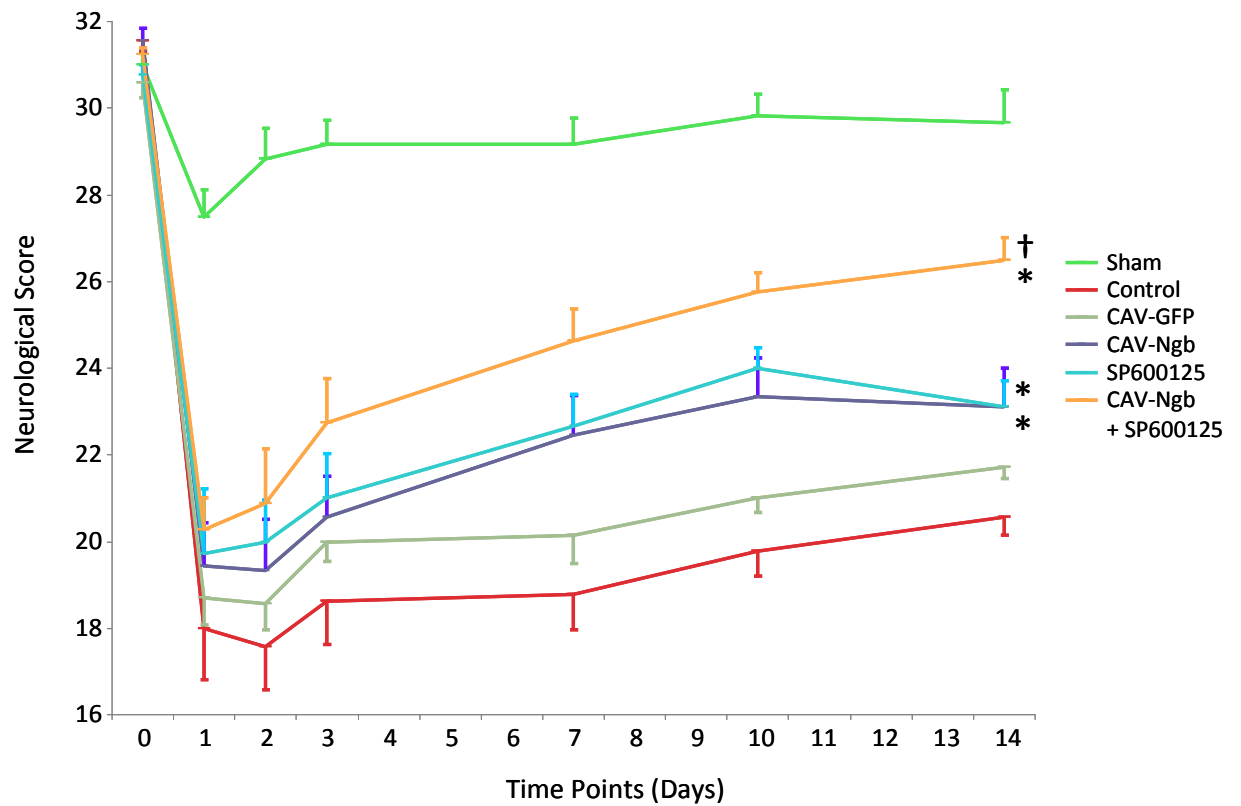
Figure 6.8: **Longitudinal Assessment of Neurological Score following 45 min tMCAO**

Neurological score measured before and after tMCAO in sham, control tMCAO, CAV2-GFP, SP600125, CAV2-Ngb and CAV2-Ngb + SP600125 treated groups up to 14 d post-tMCAO. Data points displayed as mean ± SEM, *n* = 8 - 9. *p<0.01 vs. control tMCAO and †p<0.01 vs. single treatment groups by one way ANOVA using Bonferroni's post-hoc correction.
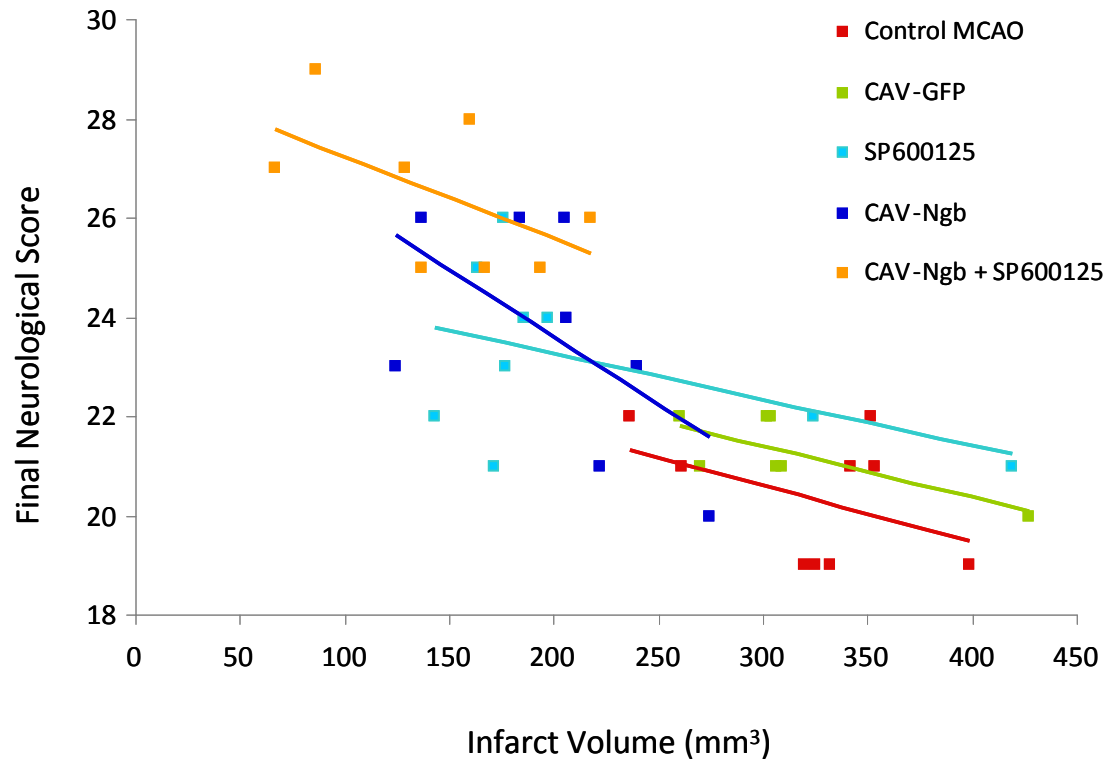
Figure 6.9:   Correlation between Final Neurological Score and Infarct Volume

Correlation between final infarct volume and final neurological score was assessed for each animal, across all groups (($r^2 > - 0.9$.).

6.2.8 Tapered Beam Walk Test

6.2.8.1 Total Footfalls

Neurological deficit assessed by the tapered beam walk test at each timepoint post-tMCAO is shown in Figure 6.10, and footfalls calculated as a percent of total number of steps taken to traverse the beam. All groups, excluding sham animals, exhibited a significant increase in percentage footfalls from baseline measure (sham = 0.6 % ± 0.1 %; control tMCAO = 1.2 % ± 0.6 %; CAV2-GFP = 3.8 % ± 0.6 %; SP600126 = 0.7 % ± 0.5 %; CAV2-Ngb = 1.8 % ± 0.8 %; CAV2-Ngb + SP600125 = 2.3 % ± 0.7 %) at 24 h post-tMCAO (sham = 1.0 % ± 0.3 %; *control tMCAO = 29.5 % ± 2.6 %; *CAV2-GFP = 31.6 % ± 3.2 %; *SP600126 = 22.6 % ± 3.1 %; *CAV2-Ngb = 20.4 % ± 0.8 %; *CAV2-Ngb + SP600125 = 20.8 % ± 2.3 %; *$p<0.01$ vs. control tMCAO using one way ANOVA using Bonferroni's post-hoc correction). Across the two-week recovery phase, percentage footfalls were consistently lower in all treatment groups but only with significance at day 3 and day 14. At day 3, a significant improvement in percentage footfalls from control animals (control tMCAO = 23.7 % ± 3.8 %) was noted with combined therapy (*CAV2-Ngb + SP600125 = 9.1 % ± 2.1 %) but no other treatment group (*$p<0.01$ vs. single treatments by one way ANOVA using Bonferroni's post-hoc correction). At day 14, a significant improvement in total footfalls was observed in all treatment groups in comparison to control animals (control tMCAO = 24.4 % ± 3.3 %; *SP600126 = 13.8 % ± 2.6 %; *CAV2-Ngb = 14.4 % ± 3.3 %; *CAV2-Ngb + SP600125 = 13.7 % ± 2.2 %; *$p<0.01$ vs. control tMCAO by one way ANOVA using Bonferroni's post-hoc correction).

6.2.8.2 Contralateral and Ipsilateral Footfalls

Total footfalls were divided into their contralateral and ipsilateral (relative to MCAO) sides (Figure 6.11). No significant difference was observed across groups for contralateral or ipsilateral sides. However, contralateral footfalls did follow a similar pattern to that seen with the total footfalls. Taken together these data suggest an important role for ipsilateral footfalls in addition to those on the contralateral side when considering neurological deficit.
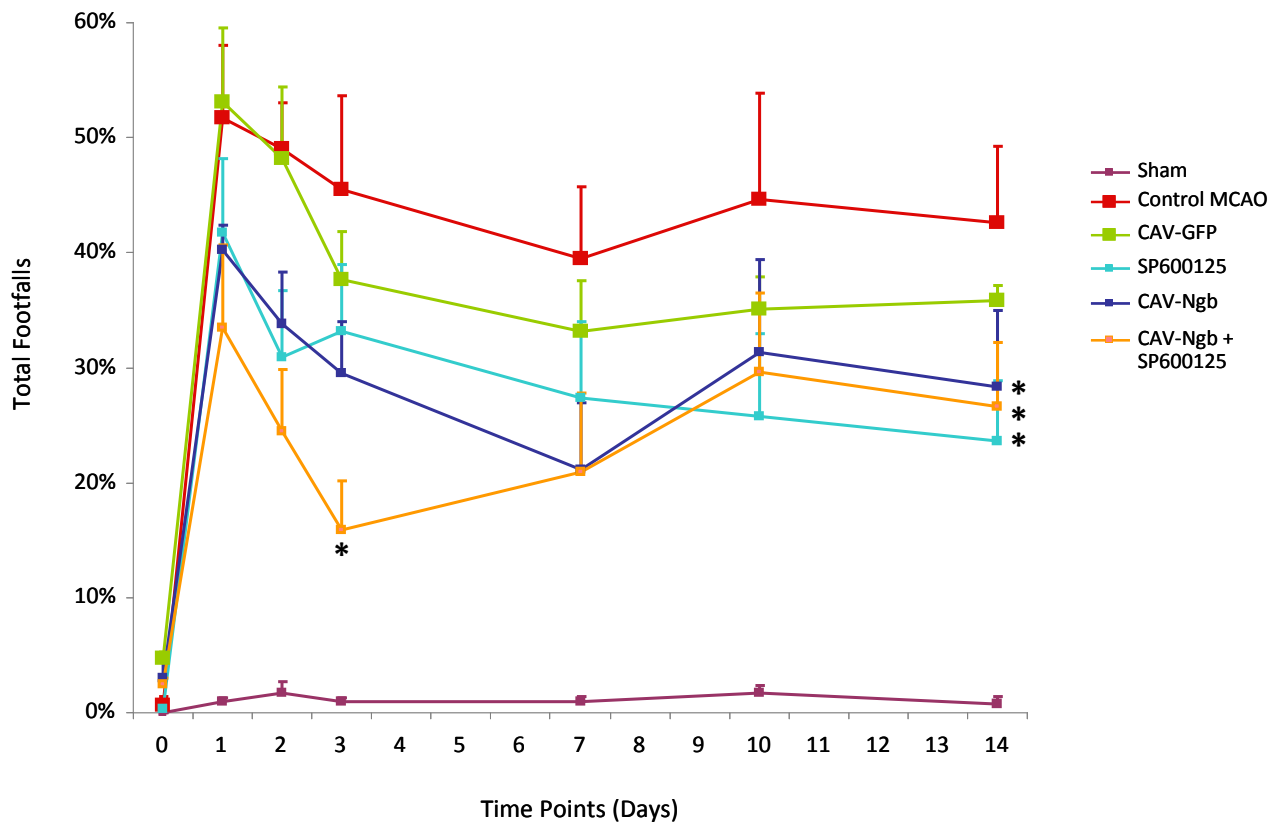
Figure 6.10:   Longitudinal Assessment of Tapered Beam Test following 45 min tMCAO

Total percentage footfalls measured before and after tMCAO in sham, control tMCAO, CAV2-GFP, SP600125, CAV2-Ngb, and CAV2-Ngb + SP600125-treated groups, up to 14 d post-tMCAO. Data points displayed as mean ± SEM, *n* = 8 - 9. *p<0.01 vs. control tMCAO by one way ANOVA with Bonferroni's post-hoc correction.

(A)

(B)
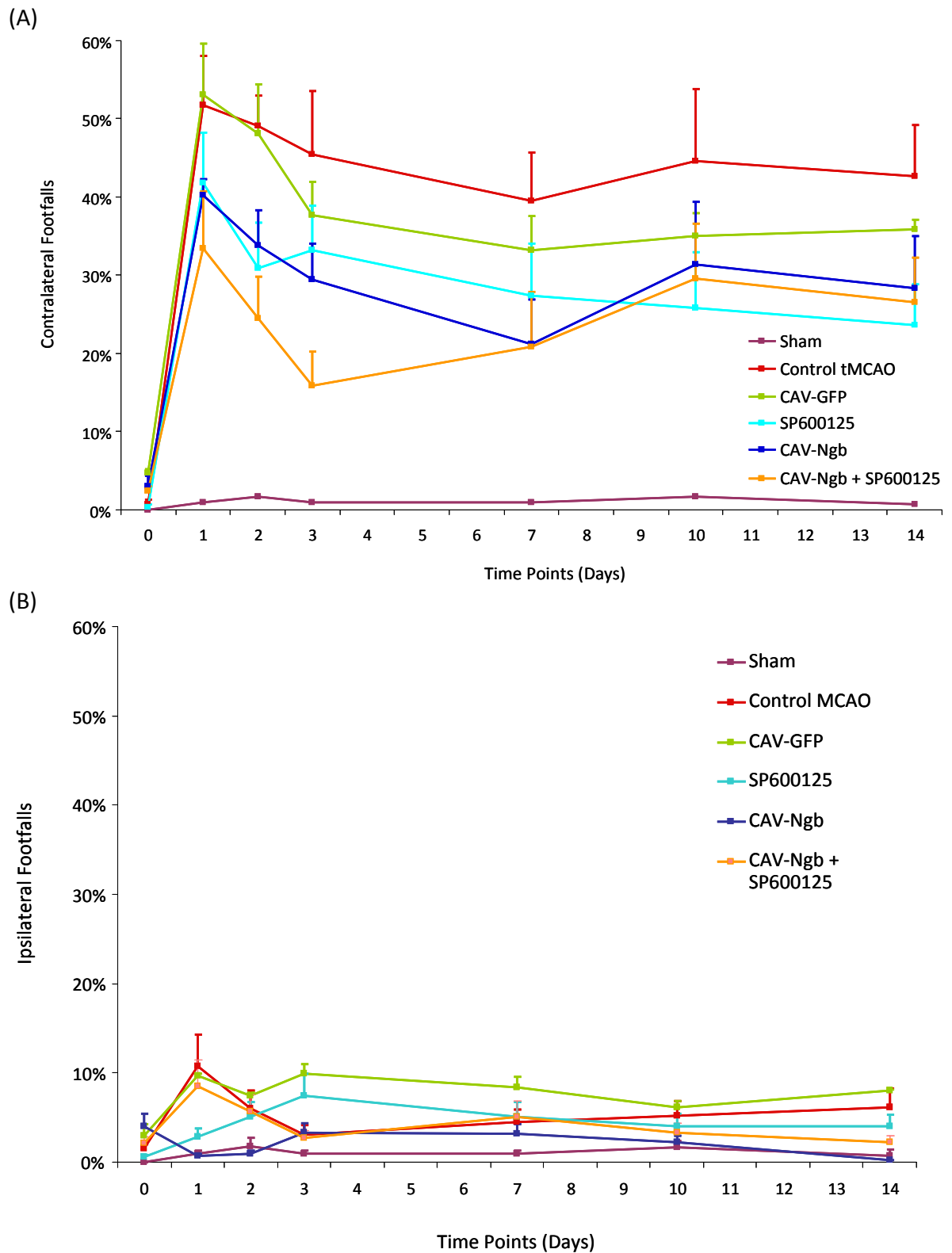
Figure 6.11: Assessment of Footfalls Contralateral or Ipsilateral to MCAO Registered During Tapered Beam Walk Test

Contralateral (A) and ipsilateral footfalls (B) measured before and after tMCAO in sham, control tMCAO, CAV2-GFP, SP600125, CAV2-Ngb and CAV2-Ngb + Sp600125 treated groups, up to 14 d post-tMCAO. Data points displayed as mean ± SEM, *n* = 8 - 9.

6.3 DISCUSSION

The hypothesis in the present study was that of gene delivery-mediated increase of Ngb in combination with pharmacological inhibition of JNK, would reduce lesion size and improve neurological recovery following 45 min tMCAO to an extent greater than either therapy alone, through anti-oxidant and anti-apoptotic capacities. Results showed that all three treatments (SP600125, CAV2-Ngb and CAV2-Ngb + SP600125) significantly reduced lesion size and reduced neurological deficit assessed by 32-point numerical score and tapered beam walk test following 45 minute tMCAO. Combined treatment further significantly reduced lesion size and improved neurological recovery, assessed by 32-point numerical score, from either treatment alone therefore showing an additive benefit. However, combined intervention showed no further improvement in neurological recovery from either treatment alone assessed by the tapered beam test.

Body temperature and level and duration of isoflurane anaesthetic were held at equivalent levels across all groups and procedures. Blood pressure assessed prior and post-tMCAO showed no confounding effect of any of the treatment regime(s) on blood pressure from the baseline measurement or longitudinally over the 2 week course of the study. Body weights at time of tMCAO did not differ between the study groups and showed no correlation with final infarct, and as such all improvements seen are accountable to treatment administered.

The ability of *in vivo* Ngb upregulation to protect the brain and thus improve lesion size and neurological recovery in the present study is in agreement with a number of pre-clinical studies of brain ischaemia. Of most relevance to the present study, Sun *et al.* in 2003 showed double injection of an AAV-1 generated to overexpress Ngb into the cortex and striatum 3 weeks prior to tMCAO significantly reduced infarct at 24 h post 90 minute tMCAO in Sprague-Dawley rats (Sun *et al.*, 2003). At present, this is the only other study evaluating the benefit of a gene delivery approach of Ngb upregulation as a therapeutic tool. They showed a reduction of 49 – 52 % of lesion size from untreated controls and control virus (AAV-GFP) groups. Neurological deficit was seen to be improved at 24 h using a numerical neurological score of 14 (where a healthy animal scores zero), from ~5 in control animals to ~3 in AAV-Ngb treated animals. Although our findings are in agreement, with CAV2-Ngb inducing a 38.5 % reduction at d 14, the study by Sun *et al.*, displays a number of common shortcomings relating to pre-clinical stroke studies. When assessing the effect of ischaemia / reperfusion models, infarct is not final until $\geq$ 72 h after

the initial onset of stroke. Therefore, by looking at an endpoint prior to this, it is unclear whether any reduction in size would still be present when the infarct had fully matured. In addition, the rat strain utilised was normotensive Sprague-Dawley rats, and as such excludes a number of the additional pathogeneses attributed to hypertension and CVD, common in stroke patients, that contribute extensively to outcome. In the present randomised and blinded study, the SHRSP was utilised as a strain which exhibits a number of the co-morbidities of CVD. Neurological recovery was assessed longitudinally over a 14 d recovery period with blinded data analysis confirmed by a second blinded observer.

Although upregulation of Ngb has been shown to be neuroprotective in the present study and elsewhere, at endogenous basal levels Ngb's role is unknown but evidence would suggest a role in maintenance of intracellular homeostasis. However, it has been demonstrated to be endogenously upregulated in response to cerebral ischaemia both in the animal brain (Fordel *et al.*, 2007b; Shang *et al.*, 2006; Sun *et al.*, 2003) in human stroke (Jin *et al.*, 2010) and repression of its synthesis has exacerbated damage following experimental stroke (Sun *et al.*, 2001; Sun *et al.*, 2003), demonstrating an endogenous role in neuroprotection. The endogenous upregulation of Ngb is perhaps critical in levels of ischaemia similar to those seen in TIA's, but it is conceivable that the system is 'overwhelmed' during longer episodes of ischaemia, such as stroke. Ngb upregulation has not only been studied within the field of cerebral ischaemia, but *in vivo* studies have also demonstrated the protection that Ngb can create in disease models of myocardial infarction (Khan *et al.*, 2006), glaucoma (Rajendram *et al.*, 2007) and traumatic brain injury (Chuang *et al.*, 2010).

The present study utilises a pre-injection (- 5 days) of CAV2-Ngb to ensure significant Ngb overexpression at the acute and critical timepoints (day 1 - 3) following tMCAO. Previous work, shown in Chapter 4, demonstrates extensive and widespread synthesis 7 days post-injection with CAV2 expressing reporter gene, GFP. Due to the 18 h delay in protein synthesis following transduction of virus, gene delivery is often dismissed as not clinically relevant in the context of stroke owing to the requirement for pre-treatment. However, pre-treatment is a currently utilised and viable option in patients who have presented with TIAs or previous strokes, as this is more often than not an indicator of a subsequent larger and more detrimental stroke (Hart *et al.*, 2001). In addition, cerebral ischaemia / reperfusion is not restricted to stroke, and is often a by-product of brain surgery, during which an artery may require clamping for relatively prolonged periods and

as such, intervention of CAV2-mediated Ngb upregulation could be administered in advance to protect from this unavoidable damage. Studies into CAV2-mediated transgene expression show overexpression could be expected for prolonged periods of up to at least 6 months (Soudais *et al.*, 2004), strengthening the potential of CAV2 as a preventative therapy.

Currently there has been no work addressing whether prolonged Ngb overexpression may have detrimental effects. However, study of the mechanism of action of Ngb suggests it is a protein which has an unknown role during normal cellular respiration but is crucial and activated in neuronal stress, indicating overexpression at baseline conditions would not have a negative effect, but further work is necessary within this area. CAV2 has been previously used therapeutically in pre-clinical models of the monogenic disorder, lysosomal storage disease (Lau *et al.*, 2010; Lau *et al.*, 2012). Lysosomal storage diseases are genetically acquired diseases where malfunctioning lysosomes result in accumulation of diverse materials normally 'recycled' by functioning lysosomes. This accumulation of material results in subsequent neurodegeneration and death within months to years of birth in the majority of cases. A form of lysosomal storage disease, mucopolysaccharidosis type IIIA (MPS IIIA) is caused by N-sulfoglucosamine sulfohydrolase (SGSH) deficiency. Therefore, a SGSH-expressing CAV2 was administered to neonatal MPS IIIA mice and transgene expression was detected up to 20 weeks (Lau *et al.*, 2010). Lysosomal storage inclusions, vacuole markers of MPS IIIA in ependymal and choroidal cells, were reduced in CAV2-SGSH-treated MPS IIIA mice treated at birth by ~ 25 % in comparison to untreated control brains (Lau *et al.*, 2010). This study was repeated the following year using a helper-dependant CAV2 (Hd-CAV2) with the premise to improve length of transgene expression following administration. However, although transgene was detected for up 8.5 months, no improvement in any of the classical markers of MPS IIIA was observed, attributed the reduced efficiency of spread within the brain parenchyma following injection with Hd-CAV2-SGSH (Lau *et al.*, 2012).

Although stereotactic administration is routinely utilised in treatment of brain cancer and Parkinson's disease, it is seen as a considerable invasive procedure and as such there is wide interest in the study of pharmacological induction of Ngb. This would potentially allow for greater options of delivery route and consequently an increase in therapeutic window. A number of short-chain fatty acids including cinnamic acid and valproic acid have been shown to induce Ngb synthesis (Jin *et al.*, 2011).

In addition to Ngb's protective effect, intravenous pre- and post-treatment with 1 mg / kg of the JNK inhibitor, SP600125, also significantly reduced lesion size and improved neurological recovery post-tMCAO. The results in the present study are in general in agreement with previously published data (Gao *et al.*, 2005; Guan *et al.*, 2005). The initial study assessing the effect of SP600125 in cerebral ischaemia, utilised a pre-clinical model of transient (15 min) global ischaemia with 30 min, 3 d or 5 d reperfusion in Sprague-Dawley rats (Gao *et al.*, 2005). Animals were administered 0.12 mg / kg SP600125, in 10 µl DMSO, by intracerebral ventricular infusion 20 min prior to onset of ischaemia. Following 5 d recovery, a significant improvement in cell survival was reported with SP600125 treatment in the CA1 neurons of the hippocampus in comparison to untreated and vehicle (DMSO)-treated control animals. With 30 min and 3 d reperfusion there was a significant upregulation in JNK1, JNK2 and JNK3 synthesis following 15 min transient global ischaemia in untreated and vehicle control animals, assessed by western blot of brain homogenates. Following 30 min and 3 d reperfusion, SP600125-treated animals exhibited a significant reduction in JNK1, JNK2 and JNK3 synthesis in comparison to untreated and vehicle control animals. Although SP600125 was also reported to reduce levels of phosphorylated c-Jun (p-c-Jun), it had no effect on the levels of c-Jun present following ischaemia. This study demonstrated a protective role for SP600125 in global cerebral ischaemia, however this pre-clinical model is not considered to be a true model of stroke, and no assessment of neurological score was determined (Gao *et al.*, 2005). In the same year, another study reported a beneficial effect of SP600125 in a model of tMCAO (60 min) in male C57/B6 mice (Guan *et al.*, 2005). It was demonstrated 4 and 8 h following tMCAO that *i.v.* administration of 1 or 3 mg / kg SP600125 15 min prior to and 3 h post onset of ischaemia significantly reduced levels of p-c-Jun, JNK1, JNK2 and JNK3 synthesis following tMCAO. Additionally, treatment with 1 , 3 and 10 mg / kg SP600125 reduced lesion size at 48 h by ~ 25 %, ~ 50 % and ~ 40 %, respectively, and administration with 3 mg / kg exhibited the same reduction in lesion size at 7 d post tMCAO. The optimal dose (3 mg / kg) was subsequently administered post-tMCAO, and a significant reduction in infarct was maintained with administration at 0 h, 0.5 h and 1 h post-tMCAO, ~ 50 %, ~ 40 % and ~ 25 % respectively, but not 2 h post-tMCAO. Behavioral outcome assessed by 5-point neurological score and corner test demonstrated a significant improvement in neurological recovery with treatment of 3 mg / kg at day 3, 5 and 7 post tMCAO (Guan *et al.*, 2005). Although JNK inhibition is beneficial in the acute stages following cerebral ischaemia, it is believed that JNK exhibits a biphasic response following cerebral ischaemia and several days following initial insult JNK may be involved in regeneration

and repair. This hypothesis has originated from *in vitro* experiments, where JNK was activated in the differentiation process of stem cells to neuronal-like cells and use of JNK inhibitors in differentiated neuronal cells significantly reduced dendritic sprouting (Waetzig *et al.*, 2006). An equivalent role might exist in the animal brain, where JNK contributes to dendritic sprouting and axonal regrowth in the late stages following neuronal injury (Waetzig *et al.*, 2006).

Until now, the combination of Ngb upregulation with JNK inhibition has not been assessed, but in the present study they have been shown to exert a beneficial effect greater than either therapy alone in reduction of lesion size and improvement in neurological deficit, assessed by 32-point neurological score but not by the tapered beam test. There are a number of postulated mechanisms by which CAV2-Ngb and SP600125 exert a synergistic role, discussed in chapter 3. Primarily, ROS activates the pathway of JNK activation by direct action on ASK1 (Pan *et al.*, 2010), and therefore Ngb's anti-oxidant role has a direct action on JNK activation. Ngb also mediates JNK indirectly through activation of the PI3K/AKT/mTOR pathway of cell survival. Following activation, pAKT disrupts JNK synthesis by inhibiting synthesis of a number of pro-apoptotic mediators of JNK including MLK3 (Barthwal *et al.*, 2003), JNK-interacting protein (JIP) (Kim *et al.*, 2002), MKK4 (Park *et al.*, 2002), and ASK1 (Kim *et al.*, 2001a). Ngb has also been implicated in the upregulation of scaffold protein 14-3-3 (Ye *et al.*, 2009b) which binds pro-apoptotic mediators including the upstream mediator of JNK activation, ASK1 (Porter *et al.*, 2006a). Although, JNK has a lesser ability to modulate Ngb, it has been demonstrated that JNK activation leads to down-regulation of HIF-1α (Antoniou *et al.*, 2010) – the leading candidate for Ngb upregulation

One explanation for the difference in the results between the 32-point neurological score and the tapered beam walk test can perhaps be explained by the location of the remaining infarct within the treatment groups, and the range of brain assessed by the two tests. The 32-point neurological score evaluates a number of diverse symptoms of ischaemic injury, which ranges from motor deficits, sensory neglect and absence of reflexes. Due to its diverse range of tests, it assesses a larger region of the brain than the tapered beam test and as such allows for a more accurate read-out of neurological recovery. The tapered beam walk test determines the number of footfalls taken by the animal when crossing the beam. As aforementioned, a specific area of the cortex (Figure 6.12 A) is a highly conserved region of infarct throughout all groups within the present model. This area of conserved

infarct is at the location of the sensorimotor regions of the cortex, in particular the forelimb and hindlimb regions (Figure 6.12 B).

(A)

(B)
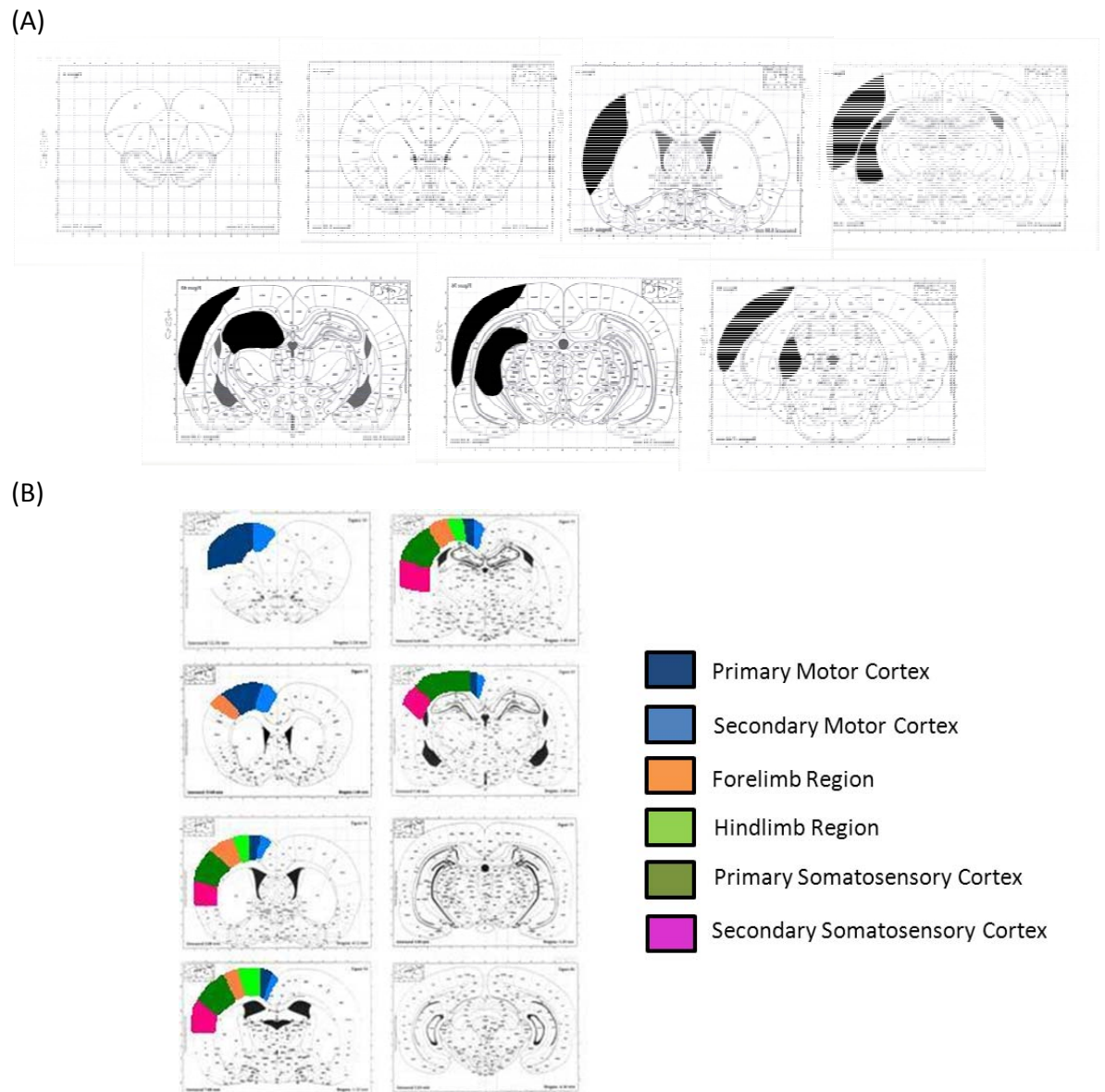
Figure 6.12:   Conserved Region of Infarct in Relation to the Motor Cortex

(A) Representative infarct location in median animal of combination treated group and (B) location of a selection of sensorimotor areas through the cortex of the rat brain.

Although one may expect the vast majority of footfalls attributed to neurological deficit to occur on the side contralateral to the lesion, when footfalls were separated into their ipsilateral and contralateral sides it was noted that no significant difference was observed between groups when assessing solely contralateral footfalls. This suggested an important role of the footfalls counted on the ipsilateral side. Following stroke, the perceived midline of the animal was observed to shift towards the ipsilateral side as a result of the significant tissue loss within this hemisphere of the brain. This caused the animal to shift its entire body weight towards the ipsilateral side, resulting in the fore and hind limb of the ipsilateral side to be more likely to fall onto the ledge below. Thus, although significant fore- and hindlimb deficit is observed within the contralateral side causing footfalls, a shift of balance towards the ipsilateral side caused footfalls to the ipsilateral side, which can be attributed to neurological deficit.

In conclusion, this study demonstrated that CAV2-mediated Ngb upregulation and pharmacological JNK inhibition led to a significant improvement in infarct size and neurological deficit in a robust pre-clinical modal of experimental stroke. Additionally, combined treatment further improved behavioural recovery and lesion size greater than either therapy alone, strengthening the argument for combination therapy in stroke.

Chapter 7:

General Discussion

7.1 GENERAL DISCUSSION

This thesis has focused on the development of a combined neuroprotective intervention strategy for stroke. The efficacy of the protection afforded by gene transfer-mediated Ngb upregulation in combination with small molecule inhibition of JNK was assessed across *in vitro* and *in vivo* models. The combined intervention was demonstrated to provide neuroprotection with either additional or synergistic benefit greater than either treatment alone across the majority of *in vitro* or *in vivo* outcome measures.

Stroke is a disease with largely unmet clinical needs, and currently the vast majority of treatment strategies are preventative. However, with the increase in prescription of preventative therapies, such as anti-coagulant and / or anti-platelet drugs, there has been a related increase in haemorrhagic stroke incidence. In addition, the only remedial therapy available is the administration of the thrombolytic rt-PA within 4.5 hours of stroke onset. However significant risk of haemorrhage exists even within this short therapeutic window in patients with advanced cardiovascular disease (CVD). Additionally, evidence has suggested rt-PA can cross the compromised BBB and cause additional neurotoxicity through mechanisms such as Ca^{2+} influx in neuronal cells and through direct action on the NMDA receptor (reviewed in (Kaur *et al.*, 2004)). Understanding of the pathophysiology of stroke has led to the development of neuroprotective stroke therapy but although pre-clinical models of neuroprotective strategies show promising results success, translation into clinical studies has been completely absent. This poor "bench-to-bedside" translation led to the generation of a list of guidelines set by a roundtable of academic and industry experts for pre-clinical models, .in an attempt to more closely mimic stroke pathology (Fisher *et al.*, 2009). The present study attempted to adhere to the majority of the guidelines, by firstly carrying out a comprehensive *in vitro* study; performing an *in vivo* control pilot study; ensuring the *in vivo* intervention study was blinded and randomised with blinded outcome analysis; using an ischaemia / reperfusion model of tMCAO in a relevant animal strain to human stroke, the SHRSP; assessing both functional and behavioural analysis with prolonged survival, 14 days post-stroke; and monitoring physiological variables to avoid interference of confounding factors, such as blood pressure effects.

Interruption of the ischaemic cascade, and saving non-dividing neurons from death, represents the goal of neuroprotection. Gene transfer-mediated neuroprotection comprises

numerous challenges including delivery, transduction efficiency, and immunogenicity, but despite these challenges pre-clinical model studies have reported successful neuroprotection. The present study initially assessed the efficiency of gene delivery with two viral vectors following stereotactic injection, and found CAV2 to exhibit significantly greater efficiency of transduction from a single injection in the cortex in comparison to a double injection of lentivirus. Extent of spread of CAV2-GFP was comparable to equivalent studies (Soudais *et al.*, 2001); however the present study demonstrates the first assessment of transduction of CAV2-GFP following cortical injection, and also the first use of CAV2 in the SHRSP. Although histological analysis of immune response was not assessed in the present study, studies performed by Dr. Eric Kremer and colleagues have shown long-term expression of transgene following injection of CAV2 with minimal immune response (especially with use of novel helper-dependent CAV2 vectors) (Soudais *et al.*, 2004), furthering the potential of CAV2-Ngb as a preventative treatment in high-risk patients. Although CAV2 has been shown to preferentially transduce neurons, further analysis would assess the transduction of CAV2 into specific cells of the neurovascular unit (neurons, cerebral endothelial cells, pericytes, astrocytes and surrounding matrix) in the present model. A number of methods have been attempted to improve the notoriously limited transduction efficiency of viral vectors following direct injection into the brain parenchyma. For example, convection-enhanced delivery (CED) is a microinfusion technique that utilises positive perfusion pressure to enhance the spread of agents being directly administered to the brain (Bobo *et al.*, 1994). However, completed clinical trials utilising CED have reported mixed results, with unpredictable spread being the major impeding factor (reviewed in (Allard *et al.*, 2009)). Although computer models / algorithms are currently in development to predict distribution, CED remains an invasive and somewhat unpredictable method to enhance spread. In addition to alternative methods to enhance intracerebral spread, pseudotyping of viral vectors has been assessed with success in *in vivo* preclinical models, although currently no clinical trials have been initiated using pseudotyped viral vectors. Use of CAV2 offers a novel viral vector which can offer predictable and efficient spread from a single injection site without the requirement of techniques such as CED or pseudotyping to enhance actions.

An *in vitro* study was performed to assess the effect of Ngb upregulation and JNK inhibition alone and in combination and to generate the proof-of-concept required for initiation of the *in vivo* study. Outcome analysis was assessed across 4 separate assays of cell viability; 2 oxidative stress assays, EPR for SO production and a MDA assay of lipid

peroxidation; and 2 measures of apoptosis, a cell death ELISA and caspase-3 ICC. All assays excluding the MDA assay of lipid peroxidation demonstrated a combined effect of Ngb upregulation and JNK inhibition greater than either therapy alone, improving cell viability to levels equivalent to the normoxic control cells. Results of the MDA assay demonstrated a maximal reduction in MDA with either treatment alone and in combination. The present *in vitro* study served as a robust indicator of the neuroprotection mediated by both strategies, allowed for dissection of the mechanisms involved and prediction of potential synergistic actions of the two therapies. The success of the present *in vitro* study could be attributed to the variety of outcome measures, spanning both oxidative stress and apoptosis and both quantitative and qualitative measures. *Ex vivo* analysis of SHRSP brains exposed to 45 min tMCAO with increasing lengths of reperfusion failed to determine an increase in *Jnk1*, *Jnk2* or *Jnk3* following ischaemia in the region of the infarct or penumbra. In the region of the infarct, *Ngb* was shown to be upregulated at 3 h post-tMCAO but not at later timepoints.

Prior to performing the full *in vivo* intervention study a small control pilot study was carried out, as is suggested by STAIR guidelines. This pilot study proved invaluable in 'flagging' issues with both the surgical technique and assessing the sensitivity of a variety of neurological scores prior to the intervention study. It allowed for additional training to be sought ensuring refinement of surgical technique, to minimise variation in insult, strengthening the significance of outcome measures in the intervention study. The pilot study also allowed for optimisation of behavioural assessment tests for use in the present model, and user experience to be gained in carrying out assessments and analysis of data, including *ex vivo* analysis of lesion size. The novel finding demonstrating improved survival with no effect on outcome measures with pre-stroke surgery to drill a cranial burrhole allowed for further refinement of the technique and reduction in overall animal numbers utilised for the *in vivo* intervention study.

The *in vivo* intervention study demonstrated an improvement in behavioural outcome and reduction in lesion size mediated by combination therapy greater than either therapy alone. The study utilised an animal strain exhibiting a number of the co-morbidities of CVD, allowing for a more clinically relevant experimental model. Additionally, a long recovery period was assessed to ensure not only that infarct was final but also behavioural recovery had plateaued prior to sacrifice. This study demonstrated the additive effect of combined gene delivery and pharmacological approach, demonstrating the importance of co-therapy

in treatment of this multifactorial disease. Furthermore, it is the first study utilising a strategy of combined anti-oxidant and anti-apoptotic neuroprotection. Further work could determine whether neuroprotection was maintained with treatment administered in the acute stages post-tMCAO. The time for translation of transgene following initial injection remains the limiting factor in gene-therapy strategies of stroke, however with the dangers directly linked to increased prescription of anti-platelet and anti-coagulant drugs, perhaps neuroprotective agents represent a promising new strategy in preventative stroke therapy. Although unlikely to reduce the incidence of stroke, pre-treatment with neuroprotective agents could reduce the severity, neurological deficit following stroke and subsequent substantial socio-economic health care costs. No clinical trials using gene delivery strategies have been commenced in stroke, however there has been a handful initiated for other neurological disorders, such as brain cancer, Parkinson's and Alzheimer's disease . Gene delivery strategies for the treatment of brain cancer have seen the furthest advancement into clinical trials, with a large multicenter double-blind phase III trial completed in Europe in 2009 reporting promising results using an adenovirus (Osborne, 2008). However, the European Medicines Agency (EMEA) recently rejected Ark Therapeutics' marketing application for this therapy after deciding that the study was statistically underpowered and failed to show sufficient efficacy in terms of postponing death, this decision is being appealed by Ark Therapeutics (Mitchell, 2010). Alzheimer's disease has seen completion of two early-phase clinical trials, using gene delivery mediated delivery of nerve growth factor, with promising results (Mandel, 2010; Tuszynski *et al.*, 2005) - phase II clinical trials have been commenced and are ongoing. There has also been success of gene delivery clinical trials for Parkinson's disease. Recently, completion of a phase II trial into AAV2-mediated glutamic acid decarboxylase (GAD) upregulation to modulate production of GABA in the subthalamic nucleus, resulted in an improvement in neurological score at 6 months with no adverse side effects compared to sham surgery procedure (LeWitt *et al.*, 2011). Although the field of gene delivery for neurological deficits is advancing, stroke still remains a challenging pathology as a result of the tight time constraints due to the rapid disease progression following onset. While gene delivery mediated neuroprotection, as a preventative measure is viable, gene delivery mediated stimulation of neurogenesis following ischaemic damage potentially represents the future of gene delivery in stroke. Importantly, the PISCES clinical trial is currently assessing the effect of administration of neuronal stem cells in disabled stroke patients up to 6 m post insult.

In summary, the present study has demonstrated successful neuroprotection mediated by combined intervention of Ngb upregulation and JNK inhibition in a robust pre-clinical model of stroke. Initial *in vitro* analysis confirmed proof-of-concept, and suggested potential mechanisms by which the combined therapies exert neuroprotection in a synergistic manner. Comparative analysis of the efficacy of available viral vectors in the present model, demonstrated highly efficient spread and neuronal specificity of CAV2 from a single injection in comparison to lentivirus. A control *in vivo* study identified the optimal neurological scoring tests and helped identify and resolve surgical inconsistencies. The statistically powered, randomised and blinded *in vivo* study illustrated a novel finding that pre-tMCAO surgery to drill a cranial burrhole improved survival following the substantial surgical tMCAO procedure without exerting a beneficial effect on lesion size or neurological deficit – an important methodological finding for reducing mortality in tMCAO studies. Finally, longitudinal analysis of neurological deficit up to 14 days and histological analysis of lesion size at 14 days post-stroke showed an improvement in neurological score and lesion size with combined therapy greater than either treatment alone. Assessment of neurological score by tapered beam test showed an overall improvement in all three treatment groups, but with no further improvement observed with combined therapy. These findings demonstrate a role for combined intervention of neuroprotection, in the complex pathogenesis of stroke, and a role for potentiation of gene-therapy strategies using complimentary pharmacological agents. Combining of different strategies could potentially hold the key to development of a successful future therapy for stroke. Further studies would seek to assess this neuroprotection with administration following cerebral ischaemia, and across a variety of different models. Also, future work would assess alternative administration routes, such as systemic and intranasal delivery. Neuroglobin upregulation through pharmacological intervention also offers an interesting and novel route of neuroprotection.

A recent review (Hossmann, 2012) has suggested better modelling of human stroke by utilisation the embolic model of MCAO with subsequent reperfusion through administration of a thrombolytic. This ischaemia / reperfusion model allows for protracted reperfusion of the previously ischaemic area, compared to the immediate reperfusion mediated by removal of a mechanical vascular occlusion device, such as an intraluminal filament. In protracted reperfusion, inhibition of expansion of the infarct core into the penumbra can only be mediated within the short time window of 3 h, as is observed in human stroke. However, prompt reperfusion initiates a 'free interval' of 6 - 12 h prior to

infarct expansion into the penumbra, which is not a naturally occurring phenomenon and is widely ignored in pre-clinical trials assessing post-ischaemic intervention timepoints. Future studies would seek to assess the benefit of post-MCAO administration of CAV2-Ngb in combination with SP600125 in the embolic model of ischaemia with protracted thrombolytic-induced reperfusion, as an improved clinical model of stroke. In addition to testing the combined therapy in a more clinically relevant model, this approach would also allow us to determine whether this combined intervention is compatible with administration of a thrombolytic.

List of References

ABORDO-ADESIDA E, FOLLENZI A, BARCIA C, SCIASCIA S, CASTRO MG, NALDINI L, *et al.* (2005). Stability of lentiviral vector-mediated transgene expression in the brain in the presence of systemic antivector immune responses. *Human gene therapy* **16**(6)**:** 741-751.

ADAMS AS, MAH C, SOUMERAI SB, ZHANG F, BARTON MB, ROSS-DEGNAN D (2003). Barriers to self-monitoring of blood glucose among adults with diabetes in an HMO: a cross sectional study. *BMC health services research* **3**(1)**:** 6.

ADAMS H, BENDIXEN B, KAPPELLE L, BILLER J, LOVE B, GORDON D, *et al.* (1993). Classification of subtype of acute ischemic stroke. Definitions for use in a multicenter clinical trial. TOAST. Trial of Org 10172 in Acute Stroke Treatment. *Stroke* **24**(1)**:** 35-41.

ADRAIN C, CREAGH EM, MARTIN SJ (2001). Apoptosis-associated release of Smac/DIABLO from mitochondria requires active caspases and is blocked by Bcl-2. *The EMBO journal* **20**(23)**:** 6627-6636.

ALBERS GW, ATKINSON RP, KELLEY RE, ROSENBAUM DM (1995). Safety, Tolerability, and Pharmacokinetics of the N-Methyl-D-Aspartate Antagonist Dextrorphan in Patients With Acute Stroke. *Stroke* **26**(2)**:** 254-258.

ALBERT MA, DANIELSON E, RIFAI N, RIDKER PM (2001). Effect of statin therapy on C-reactive protein levels: the pravastatin inflammation/CRP evaluation (PRINCE): a randomized trial and cohort study. *JAMA : the journal of the American Medical Association* **286**(1)**:** 64-70.

ALBERTS MJ, ATKINSON R (2004). Risk reduction strategies in ischaemic stroke : the role of antiplatelet therapy. *Clinical drug investigation* **24**(5)**:** 245-254.

ALBERTS MJ, BRASS LM, PERRY A, WEBB D, DAWSON DV (1993). Evaluation times for patients with in-hospital strokes. *Stroke* **24**(12)**:** 1817-1822.

ALLARD E, PASSIRANI C, BENOIT JP (2009). Convection-enhanced delivery of nanocarriers for the treatment of brain tumors. *Biomaterials* **30**(12)**:** 2302-2318.

ALTHOEFER H, EVERSOLE-CIRE P, SIMON MI (1997). Constitutively Active Gαq and Gα13 Trigger Apoptosis through Different Pathways. *Journal of Biological Chemistry* **272**(39)**:** 24380-24386.

ANSG (1992). Clinical trial of nimodipine in acute ischemic stroke. The American Nimodipine Study Group. *Stroke* **23**(1)**:** 3-8.

ANTAO ST, DUONG TT, ARAN R, WITTING PK (2010). Neuroglobin overexpression in cultured human neuronal cells protects against hydrogen peroxide insult via activating phosphoinositide-3 kinase and opening the mitochondrial K(ATP) channel. *Antioxidants & redox signaling* **13**(6)**:** 769-781.

ANTONIOU X, SCLIP A, PLOIA C, COLOMBO A, MOROY G, BORSELLO T (2010). JNK contributes to Hif-1alpha regulation in hypoxic neurons. *Molecules* **15**(1)**:** 114-127.

APOLONIA L, WADDINGTON SN, FERNANDES C, WARD NJ, BOUMA G, BLUNDELL MP*, et al.* (2007). Stable gene transfer to muscle using non-integrating lentiviral vectors. *Mol Ther* **15**(11)**:** 1947-1954.

ARUMUGAM TV, CHAN SL, JO D-G, YILMAZ G, TANG S-C, CHENG A*, et al.* (2006). Gamma secretase-mediated Notch signaling worsens brain damage and functional outcome in ischemic stroke. *Nat Med* **12**(6)**:** 621-623.

ARVIDSSON A, KIRIK D, LUNDBERG C, MANDEL RJ, ANDSBERG G, KOKAIA Z*, et al.* (2003). Elevated GDNF levels following viral vector-mediated gene transfer can increase neuronal death after stroke in rats. *Neurobiology of disease* **14**(3)**:** 542-556.

ASAHI M, ASAHI K, WANG X, LO EH (2000). Reduction of tissue plasminogen activator-induced hemorrhage and brain injury by free radical spin trapping after embolic focal cerebral ischemia in rats. *Journal of cerebral blood flow and metabolism : official journal of the International Society of Cerebral Blood Flow and Metabolism* **20**(3)**:** 452-457.

ASHKENAZI A (2002). Targeting death and decoy receptors of the tumour-necrosis factor superfamily. *Nature reviews. Cancer* **2**(6)**:** 420-430.

ASTRUP J, SIESJO BK, SYMON L (1981). Thresholds in cerebral ischemia - the ischemic penumbra. *Stroke* **12**(6)**:** 723-725.

ATKINSON C, ZHU H, QIAO F, VARELA JC, YU J, SONG H, *et al.* (2006). Complement-dependent P-selectin expression and injury following ischemic stroke. *J Immunol* **177**(10)**:** 7266-7274.

AVIVI A, GERLACH F, JOEL A, REUSS S, BURMESTER T, NEVO E, *et al.* (2010). Neuroglobin, cytoglobin, and myoglobin contribute to hypoxia adaptation of the subterranean mole rat Spalax. *Proceedings of the National Academy of Sciences of the United States of America* **107**(50)**:** 21570-21575.

AZZOUZ M, RALPH GS, STORKEBAUM E, WALMSLEY LE, MITROPHANOUS KA, KINGSMAN SM, *et al.* (2004). VEGF delivery with retrogradely transported lentivector prolongs survival in a mouse ALS model. *Nature* **429**(6990)**:** 413-417.

BADIN RA, MODO M, CHEETHAM M, THOMAS DL, GADIAN DG, LATCHMAN DS, *et al.* (2009). Protective effect of post-ischaemic viral delivery of heat shock proteins in vivo. *Journal of cerebral blood flow and metabolism : official journal of the International Society of Cerebral Blood Flow and Metabolism* **29**(2)**:** 254-263.

BAEKELANDT V, CLAEYS A, EGGERMONT K, LAUWERS E, DE STROOPER B, NUTTIN B, *et al.* (2002). Characterization of lentiviral vector-mediated gene transfer in adult mouse brain. *Human gene therapy* **13**(7)**:** 841-853.

BARCIA C, JIMENEZ-DALMARONI M, KROEGER KM, PUNTEL M, RAPAPORT AJ, LAROCQUE D, *et al.* (2007). One-year expression from high-capacity adenoviral vectors in the brains of animals with pre-existing anti-adenoviral immunity: clinical implications. *Mol Ther* **15**(12)**:** 2154-2163.

BARON JC, MARCHAL G (1999). Ischemic core and penumbra in human stroke. *Stroke* **30**(5)**:** 1150-1153.

BARR RK, BOEHM I, ATTWOOD PV, WATT PM, BOGOYEVITCH MA (2004). The critical features and the mechanism of inhibition of a kinase interaction motif-based peptide inhibitor of JNK. *The Journal of biological chemistry* **279**(35)**:** 36327-36338.

BARRETO AD, GROTTA JC (2008). The Argatroban and tPA Stroke Study. *Progress in Neurotherapeutics and Neuropsychopharmacology* **3**(01)**:** 35-47.

BARTH A, BARTH L, NEWELL DW (1996). Combination therapy with MK-801 and alpha-phenyl-tert-butyl-nitrone enhances protection against ischemic neuronal damage in organotypic hippocampal slice cultures. *Experimental neurology* **141**(2)**:** 330-336.

BARTHWAL MK, SATHYANARAYANA P, KUNDU CN, RANA B, PRADEEP A, SHARMA C, *et al.* (2003). Negative Regulation of Mixed Lineage Kinase 3 by Protein Kinase B/AKT Leads to Cell Survival. *Journal of Biological Chemistry* **278**(6)**:** 3897-3902.

BEDERSON J, PITTS L, GERMANO S, NISHIMURA M, DAVIS R, BARTKOWSKI H (1986). Evaluation of 2,3,5-triphenyltetrazolium chloride as a stain for detection and quantification of experimental cerebral infarction in rats. *Stroke* **17**(6)**:** 1304-1308.

BEDNAR MM, RAYMOND S, MCAULIFFE T, LODGE PA, GROSS CE (1991). The role of neutrophils and platelets in a rabbit model of thromboembolic stroke. *Stroke* **22**(1)**:** 44-50.

BENDINELLI P, PICCOLETTI R, MARONI P, BERNELLI-ZAZZERA A (1996). The MAP kinase cascades are activated during post-ischemic liver reperfusion. *FEBS letters* **398**(2-3)**:** 193-197.

BENNETT BL, SASAKI DT, MURRAY BW, O'LEARY EC, SAKATA ST, XU W, *et al.* (2001). SP600125, an anthrapyrazolone inhibitor of Jun N-terminal kinase. *Proceedings of the National Academy of Sciences of the United States of America* **98**(24)**:** 13681-13686.

BENVENISTE H, DREJER J, SCHOUSBOE A, DIEMER NH (1984). Elevation of the extracellular concentrations of glutamate and aspartate in rat hippocampus during transient cerebral ischemia monitored by intracerebral microdialysis. *Journal of neurochemistry* **43**(5)**:** 1369-1374.

BLITS B, DERKS S, TWISK J, EHLERT E, PRINS J, VERHAAGEN J (2010). Adeno-associated viral vector (AAV)-mediated gene transfer in the red nucleus of the adult rat brain: comparative analysis of the transduction properties of seven AAV serotypes and lentiviral vectors. *Journal of neuroscience methods* **185**(2)**:** 257-263.

BOBO RH, LASKE DW, AKBASAK A, MORRISON PF, DEDRICK RL, OLDFIELD EH (1994). Convection-enhanced delivery of macromolecules in the brain. *Proceedings of the National Academy of Sciences* **91**(6)**:** 2076-2080.

BOGOYEVITCH MA, ARTHUR PG (2008). Inhibitors of c-Jun N-terminal kinases: JuNK no more? *Biochimica et biophysica acta* **1784**(1)**:** 76-93.

BOGOYEVITCH MA, GILLESPIE-BROWN J, KETTERMAN AJ, FULLER SJ, BEN-LEVY R, ASHWORTH A, *et al.* (1996). Stimulation of the stress-activated mitogen-activated protein kinase subfamilies in perfused heart. p38/RK mitogen-activated protein kinases and c-Jun N-terminal kinases are activated by ischemia/reperfusion. *Circulation research* **79**(2)**:** 162-173.

BONDING SH, HENTY K, DINGLEY AJ, BRITTAIN T (2008). The binding of cytochrome c to neuroglobin: a docking and surface plasmon resonance study. *International journal of biological macromolecules* **43**(3)**:** 295-299.

BORDI F, PIETRA C, ZIVIANI L, REGGIANI A (1997). The glycine antagonist GV150526 protects somatosensory evoked potentials and reduces the infarct area in the MCAo model of focal ischemia in the rat. *Experimental neurology* **145**(2 Pt 1)**:** 425-433.

BORLONGAN CV, SANBERG PR (1995). Elevated body swing test: a new behavioral parameter for rats with 6-hydroxydopamine-induced hemiparkinsonism. *The Journal of neuroscience : the official journal of the Society for Neuroscience* **15**(7 Pt 2)**:** 5372-5378.

BORSELLO T, CLARKE PG, HIRT L, VERCELLI A, REPICI M, SCHORDERET DF*, et al.* (2003a). A peptide inhibitor of c-Jun N-terminal kinase protects against excitotoxicity and cerebral ischemia. *Nature medicine* **9**(9)**:** 1180-1186.

BORSELLO T, CLARKE PGH, HIRT L, VERCELLI A, REPICI M, SCHORDERET DF*, et al.* (2003b). A peptide inhibitor of c-Jun N-terminal kinase protects against excitotoxicity and cerebral ischemia. *Nat Med* **9**(9)**:** 1180-1186.

BORSELLO T, FORLONI G (2007). JNK signalling: a possible target to prevent neurodegeneration. *Curr Pharm Des* **13**(18)**:** 1875-1886.

BOURGOIN C, EMILIANI C, KREMER EJ, GELOT A, TANCINI B, GRAVEL RA*, et al.* (2003). Widespread distribution of beta-hexosaminidase activity in the brain of a Sandhoff mouse model after coinjection of adenoviral vector and mannitol. *Gene therapy* **10**(21)**:** 1841-1849.

BOWES MP, ROTHLEIN R, FAGAN SC, ZIVIN JA (1995). Monoclonal antibodies preventing leukocyte activation reduce experimental neurologic injury and enhance efficacy of thrombolytic therapy. *Neurology* **45**(4)**:** 815-819.

BRODERICK J, CONNOLLY S, FELDMANN E, HANLEY D, KASE C, KRIEGER D*, et al.* (2007). Guidelines for the management of spontaneous intracerebral hemorrhage in adults: 2007 update: a guideline from the American Heart Association/American Stroke Association Stroke Council, High Blood Pressure Research Council, and the Quality of Care and Outcomes in Research Interdisciplinary Working Group. *Circulation* **116**(16)**:** e391-413.

BROWN AT, SKINNER RD, FLORES R, HENNINGS L, BORRELLI MJ, LOWERY J, *et al.* (2010). Stroke location and brain function in an embolic rabbit stroke model. *Journal of vascular and interventional radiology : JVIR* **21**(6)**:** 903-909.

BROWN MJ, CRUICKSHANK JK, DOMINICZAK AF, MACGREGOR GA, POULTER NR, RUSSELL GI, *et al.* (2003). Better blood pressure control: how to combine drugs. *J Hum Hypertens* **17**(2)**:** 81-86.

BRUNORI M, GIUFFRÈ A, NIENHAUS K, NIENHAUS GU, SCANDURRA FM, VALLONE B (2005). Neuroglobin, nitric oxide, and oxygen: Functional pathways and conformational changes. *Proceedings of the National Academy of Sciences of the United States of America* **102**(24)**:** 8483-8488.

BUDD SL, NICHOLLS DG (1996). Mitochondria, calcium regulation, and acute glutamate excitotoxicity in cultured cerebellar granule cells. *Journal of neurochemistry* **67**(6)**:** 2282-2291.

BURMESTER T, EBNER B, WEICH B, HANKELN T (2002). Cytoglobin: a novel globin type ubiquitously expressed in vertebrate tissues. *Molecular biology and evolution* **19**(4)**:** 416-421.

BURMESTER T, GERLACH F, HANKELN T (2007). Regulation and role of neuroglobin and cytoglobin under hypoxia. *Advances in experimental medicine and biology* **618:** 169-180.

BURMESTER T, HANKELN T (2009). What is the function of neuroglobin? *The Journal of experimental biology* **212**(Pt 10)**:** 1423-1428.

BURMESTER T, WEICH B, REINHARDT S, HANKELN T (2000). A vertebrate globin expressed in the brain. *Nature* **407**(6803)**:** 520-523.

BUSTO R, DIETRICH WD, GLOBUS MY, GINSBERG MD (1989). The importance of brain temperature in cerebral ischemic injury. *Stroke* **20**(8)**:** 1113-1114.

BUTLER SL, HANSEN MS, BUSHMAN FD (2001). A quantitative assay for HIV DNA integration in vivo. *Nature medicine* **7**(5)**:** 631-634.

BYRNES AP, RUSBY JE, WOOD MJ, CHARLTON HM (1995). Adenovirus gene transfer causes inflammation in the brain. *Neuroscience* **66**(4)**:** 1015-1024.

CAI B, LIN Y, XUE XH, FANG L, WANG N, WU ZY (2011). TAT-mediated delivery of neuroglobin protects against focal cerebral ischemia in mice. *Experimental neurology* **227**(1)**:** 224-231.

CANDE C, COHEN I, DAUGAS E, RAVAGNAN L, LAROCHETTE N, ZAMZAMI N*, et al.* (2002). Apoptosis-inducing factor (AIF): a novel caspase-independent death effector released from mitochondria. *Biochimie* **84**(2-3)**:** 215-222.

CAO G, XIAO M, SUN F, XIAO X, PEI W, LI J*, et al.* (2004). Cloning of a novel Apaf-1-interacting protein: a potent suppressor of apoptosis and ischemic neuronal cell death. *The Journal of neuroscience : the official journal of the Society for Neuroscience* **24**(27)**:** 6189-6201.

CARDEN DL, GRANGER DN (2000). Pathophysiology of ischaemia-reperfusion injury. *The Journal of pathology* **190**(3)**:** 255-266.

CARLSSON Y, LEVERIN AL, HEDTJARN M, WANG X, MALLARD C, HAGBERG H (2009). Role of mixed lineage kinase inhibition in neonatal hypoxia-ischemia. *Developmental neuroscience* **31**(5)**:** 420-426.

CATHCART MK (2004). Regulation of superoxide anion production by NADPH oxidase in monocytes/macrophages: contributions to atherosclerosis. *Arteriosclerosis, thrombosis, and vascular biology* **24**(1)**:** 23-28.

CEARLEY CN, WOLFE JH (2006). Transduction characteristics of adeno-associated virus vectors expressing cap serotypes 7, 8, 9, and Rh10 in the mouse brain. *Mol Ther* **13**(3)**:** 528-537.

CECCONI F, ALVAREZ-BOLADO G, MEYER BI, ROTH KA, GRUSS P (1998). Apaf1 (CED-4 homolog) regulates programmed cell death in mammalian development. *Cell* **94**(6)**:** 727-737.

CHANG HY, NISHITOH H, YANG X, ICHIJO H, BALTIMORE D (1998). Activation of apoptosis signal-regulating kinase 1 (ASK1) by the adapter protein Daxx. *Science* **281**(5384)**:** 1860-1863.

CHEN J, JIN K, CHEN M, PEI W, KAWAGUCHI K, GREENBERG DA*, et al.* (1997). Early detection of DNA strand breaks in the brain after transient focal ischemia: implications for the role of DNA damage in apoptosis and neuronal cell death. *Journal of neurochemistry* **69**(1)**:** 232-245.

CHEN M, HE H, ZHAN S, KRAJEWSKI S, REED JC, GOTTLIEB RA (2001). Bid is cleaved by calpain to an active fragment in vitro and during myocardial ischemia/reperfusion. *The Journal of biological chemistry* **276**(33)**:** 30724-30728.

CHEN MY, HOFFER A, MORRISON PF, HAMILTON JF, HUGHES J, SCHLAGETER KS*, et al.* (2005). Surface properties, more than size, limiting convective distribution of virus-sized particles and viruses in the central nervous system. *Journal of neurosurgery* **103**(2)**:** 311-319.

CHEN T, LIU W, CHAO X, QU Y, ZHANG L, LUO P*, et al.* (2011). Neuroprotective effect of osthole against oxygen and glucose deprivation in rat cortical neurons: involvement of mitogen-activated protein kinase pathway. *Neuroscience* **183**(0)**:** 203-211.

CHENG MY, SUN G, JIN M, ZHAO H, STEINBERG GK, SAPOLSKY RM (2009). Blocking glucocorticoid and enhancing estrogenic genomic signaling protects against cerebral ischemia. *Journal of cerebral blood flow and metabolism : official journal of the International Society of Cerebral Blood Flow and Metabolism* **29**(1)**:** 130-136.

CHEUNG BM, LAUDER IJ, LAU CP, KUMANA CR (2004). Meta-analysis of large randomized controlled trials to evaluate the impact of statins on cardiovascular outcomes. *British journal of clinical pharmacology* **57**(5)**:** 640-651.

CHILLON M, KREMER EJ (2001). Trafficking and propagation of canine adenovirus vectors lacking a known integrin-interacting motif. *Human gene therapy* **12**(14)**:** 1815-1823.

CHO BB, TOLEDO-PEREYRA LH (2008). Caspase-Independent Programmed Cell Death Following Ischemic Stroke. *Journal of Investigative Surgery* **21**(3)**:** 141-147.

CHUANG PY, CONLEY YP, POLOYAC SM, OKONKWO DO, REN D, SHERWOOD PR*, et al.* (2010). Neuroglobin genetic polymorphisms and their relationship to functional outcomes after traumatic brain injury. *Journal of neurotrauma* **27**(6)**:** 999-1006.

CIPOLLA MJ, CRETE R, VITULLO L, RIX RD (2004). Transcellular transport as a mechanism of blood-brain barrier disruption during stroke. *Frontiers in bioscience : a journal and virtual library* **9:** 777-785.

CONFORTI P, RAMOS C, APOSTOL BL, SIMMONS DA, NGUYEN HP, RIESS O*, et al.* (2008). Blood level of brain-derived neurotrophic factor mRNA is progressively reduced in rodent models of Huntington's disease: restoration by the neuroprotective compound CEP-1347. *Molecular and cellular neurosciences* **39**(1)**:** 1-7.

COOK ML, STEVENS JG (1973). Pathogenesis of herpetic neuritis and ganglionitis in mice: evidence for intra-axonal transport of infection. *Infection and immunity* **7**(2)**:** 272-288.

CROALL DE, DEMARTINO GN (1991). Calcium-activated neutral protease (calpain) system: structure, function, and regulation. *Physiol Rev* **71**(3)**:** 813-847.

CULLEN DK, SIMON CM, LAPLACA MC (2007). Strain rate-dependent induction of reactive astrogliosis and cell death in three-dimensional neuronal-astrocytic co-cultures. *Brain Res* **1158:** 103-115.

DALTON TP, SHERTZER HG, PUGA A (1999). Regulation of gene expression by reactive oxygen. *Annual review of pharmacology and toxicology* **39:** 67-101.

DAVIDSON AO, SCHORK N, JAQUES BC, KELMAN AW, SUTCLIFFE RG, REID JL, *et al.* (1995). Blood Pressure in Genetically Hypertensive Rats : Influence of the Y Chromosome. *Hypertension* **26**(3)**:** 452-459.

DEL RIO D, STEWART AJ, PELLEGRINI N (2005). A review of recent studies on malondialdehyde as toxic molecule and biological marker of oxidative stress. *Nutrition, Metabolism and Cardiovascular Diseases* **15**(4)**:** 316-328.

DEL ZOPPO GJ, SHARP FR, HEISS WD, ALBERS GW (2011). Heterogeneity in the penumbra. *Journal of cerebral blood flow and metabolism : official journal of the International Society of Cerebral Blood Flow and Metabolism* **31**(9)**:** 1836-1851.

DENES A, FERENCZI S, HALASZ J, KORNYEI Z, KOVACS KJ (2008). Role of CX3CR1 (fractalkine receptor) in brain damage and inflammation induced by focal cerebral ischemia in mouse. *Journal of cerebral blood flow and metabolism : official journal of the International Society of Cerebral Blood Flow and Metabolism* **28**(10)**:** 1707-1721.

DENG X, XIAO L, LANG W, GAO F, RUVOLO P, MAY WS, JR. (2001). Novel role for JNK as a stress-activated Bcl2 kinase. *The Journal of biological chemistry* **276**(26)**:** 23681-23688.

DENG YZ, REEVES MJ, JACOBS BS, BIRBECK GL, KOTHARI RU, HICKENBOTTOM SL, *et al.* (2006). IV tissue plasminogen activator use in acute stroke: experience from a statewide registry. *Neurology* **66**(3)**:** 306-312.

DEROOSE CM, REUMERS V, GIJSBERS R, BORMANS G, DEBYSER Z, MORTELMANS L, *et al.* (2006). Noninvasive Monitoring of Long-Term Lentiviral Vector-Mediated Gene Expression in Rodent Brain with Bioluminescen ce Imaging. *Mol Ther* **14**(3)**:** 423-431.

DEVERAUX QL, TAKAHASHI R, SALVESEN GS, REED JC (1997). X-linked IAP is a direct inhibitor of cell-death proteases. *Nature* **388**(6639)**:** 300-304.

DEWILDE S, KIGER L, BURMESTER T, HANKELN T, BAUDIN-CREUZA V, AERTS T, *et al.* (2001). Biochemical characterization and ligand binding properties of neuroglobin, a novel member of the globin family. *The Journal of biological chemistry* **276**(42)**:** 38949-38955.

DIETZ GP, BAHR M (2005). Peptide-enhanced cellular internalization of proteins in neuroscience. *Brain research bulletin* **68**(1-2)**:** 103-114.

DITTMAR M, SPRUSS T, SCHUIERER G, HORN M (2003). External carotid artery territory ischemia impairs outcome in the endovascular filament model of middle cerebral artery occlusion in rats. *Stroke* **34**(9)**:** 2252-2257.

DROGE W (2002). Free radicals in the physiological control of cell function. *Physiol Rev* **82**(1)**:** 47-95.

DU C, FANG M, LI Y, LI L, WANG X (2000). Smac, a mitochondrial protein that promotes cytochrome c-dependent caspase activation by eliminating IAP inhibition. *Cell* **102**(1)**:** 33-42.

DU C, HU R, CSERNANSKY CA, LIU XZ, HSU CY, CHOI DW (1996). Additive neuroprotective effects of dextrorphan and cycloheximide in rats subjected to transient focal cerebral ischemia. *Brain research* **718**(1-2)**:** 233-236.

DUNHAM NW, MIYA TS (1957). A note on a simple apparatus for detecting neurological deficit in rats and mice. *Journal of the American Pharmaceutical Association. American Pharmaceutical Association* **46**(3)**:** 208-209.

DYKER AG, LEES KR (1999). Safety and Tolerability of GV150526 (a Glycine Site Antagonist at the N-Methyl-D-Aspartate Receptor) in Patients With Acute Stroke. *Stroke* **30**(5)**:** 986-992.

EBERT BL, FIRTH JD, RATCLIFFE PJ (1995). Hypoxia and mitochondrial inhibitors regulate expression of glucose transporter-1 via distinct Cis-acting sequences. *The Journal of biological chemistry* **270**(49)**:** 29083-29089.

EGGERT D, DASH PK, GORANTLA S, DOU H, SCHIFITTO G, MAGGIRWAR SB*, et al.* (2010). Neuroprotective Activities of CEP-1347 in Models of NeuroAIDS. *The Journal of Immunology* **184**(2)**:** 746-756.

EGLITIS MA, KANTOFF P, GILBOA E, ANDERSON WF (1985). Gene expression in mice after high efficiency retroviral-mediated gene transfer. *Science* **230**(4732)**:** 1395-1398.

ELS T, OEHM E, VOIGT S, KLISCH J, HETZEL A, KASSUBEK J (2006). Safety and therapeutical benefit of hemicraniectomy combined with mild hypothermia in comparison with hemicraniectomy alone in patients with malignant ischemic stroke. *Cerebrovasc Dis* **21**(1-2)**:** 79-85.

ELTING JW, SULTER GA, KASTE M, LEES KR, DIENER HC, HOMMEL M*, et al.* (2002). AMPA antagonist ZK200775 in patients with acute ischemic stroke: possible glial cell toxicity detected by monitoring of S-100B serum levels. *Stroke* **33**(12)**:** 2813-2818.

ENARI M, SAKAHIRA H, YOKOYAMA H, OKAWA K, IWAMATSU A, NAGATA S (1998). A caspase-activated DNase that degrades DNA during apoptosis, and its inhibitor ICAD. *Nature* **391**(6662)**:** 43-50.

FAGO A, HUNDAHL C, DEWILDE S, GILANY K, MOENS L, WEBER RE (2004). Allosteric regulation and temperature dependence of oxygen binding in human neuroglobin and cytoglobin. Molecular mechanisms and physiological significance. *The Journal of biological chemistry* **279**(43)**:** 44417-44426.

FAGO A, MATHEWS AJ, MOENS L, DEWILDE S, BRITTAIN T (2006a). The reaction of neuroglobin with potential redox protein partners cytochrome b5 and cytochrome c. *FEBS Letters* **580**(20)**:** 4884-4888.

FAGO A, MATHEWS AJ, MOENS L, DEWILDE S, BRITTAIN T (2006b). The reaction of neuroglobin with potential redox protein partners cytochrome b5 and cytochrome c. *FEBS letters* **580**(20)**:** 4884-4888.

FAN M, CHAMBERS TC (2001). Role of mitogen-activated protein kinases in the response of tumor cells to chemotherapy. *Drug resistance updates : reviews and commentaries in antimicrobial and anticancer chemotherapy* **4**(4)**:** 253-267.

FAURE S, OUDART N, JAVELLAUD J, FOURNIER A, WARNOCK DG, ACHARD JM (2006). Synergistic protective effects of erythropoietin and olmesartan on ischemic stroke survival and post-stroke memory dysfunctions in the gerbil. *Journal of hypertension* **24**(11)**:** 2255-2261.

FAWCETT JW, HOUSDEN E, SMITH-THOMAS L, MEYER RL (1989). The growth of axons in three-dimensional astrocyte cultures. *Dev Biol* **135**(2)**:** 449-458.

FEENEY D, GONZALEZ A, LAW W (1982). Amphetamine, haloperidol, and experience interact to affect rate of recovery after motor cortex injury. *Science* **217**(4562)**:** 855-857.

FELIX RA, BARRAND MA (2002). P-glycoprotein expression in rat brain endothelial cells: evidence for regulation by transient oxidative stress. *J Neurochem* **80**(1)**:** 64-72.

FISCHER U, TAUSSKY P, GRALLA J, ARNOLD M, BREKENFELD C, REINERT M*, et al.* (2011). Decompressive craniectomy after intra-arterial thrombolysis: safety and outcome. *Journal of neurology, neurosurgery, and psychiatry* **82**(8)**:** 885-887.

FISHER M, FEUERSTEIN G, HOWELLS DW, HURN PD, KENT TA, SAVITZ SI*, et al.* (2009). Update of the Stroke Therapy Academic Industry Roundtable Preclinical Recommendations. *Stroke* **40**(6)**:** 2244-2250.

FISHER M, LEES K, PAPADAKIS M, BUCHAN AM (2006). NXY-059: brain or vessel protection. *Stroke* **37**(8)**:** 2189-2190.

FLEISHAKER JC, HULST-PEARSON LK, PETERS GR (1995). Effect of Gender and Menopausal Status on the Pharmacokinetics of Tirilazad Mesylate in Healthy Subjects. *American journal of therapeutics* **2**(8)**:** 553-560.

FORDEL E, GEUENS E, DEWILDE S, DE COEN W, MOENS L (2004a). Hypoxia/ischemia and the regulation of neuroglobin and cytoglobin expression. *IUBMB life* **56**(11-12)**:** 681-687.

FORDEL E, GEUENS E, DEWILDE S, ROTTIERS P, CARMELIET P, GROOTEN J*, et al.* (2004b). Cytoglobin expression is upregulated in all tissues upon hypoxia: an in vitro and in vivo study by quantitative real-time PCR. *Biochem Biophys Res Commun* **319**(2)**:** 342-348.

FORDEL E, THIJS L, MARTINET W, LENJOU M, LAUFS T, VAN BOCKSTAELE D*, et al.* (2006). Neuroglobin and cytoglobin overexpression protects human SH-SY5Y neuroblastoma cells against oxidative stress-induced cell death. *Neuroscience Letters* **410**(2)**:** 146-151.

FORDEL E, THIJS L, MOENS L, DEWILDE S (2007a). Neuroglobin and cytoglobin expression in mice. *FEBS Journal* **274**(5)**:** 1312-1317.

FORDEL E, THIJS L, MOENS L, DEWILDE S (2007b). Neuroglobin and cytoglobin expression in mice. Evidence for a correlation with reactive oxygen species scavenging. *The FEBS journal* **274**(5)**:** 1312-1317.

FORSYTHE JA, JIANG BH, IYER NV, AGANI F, LEUNG SW, KOOS RD*, et al.* (1996). Activation of vascular endothelial growth factor gene transcription by hypoxia-inducible factor 1. *Molecular and cellular biology* **16**(9)**:** 4604-4613.

FOUST KD, NURRE E, MONTGOMERY CL, HERNANDEZ A, CHAN CM, KASPAR BK (2009). Intravascular AAV9 preferentially targets neonatal neurons and adult astrocytes. *Nat Biotech* **27**(1)**:** 59-65.

FRANTSEVA MV, CARLEN PL, PEREZ VELAZQUEZ JL (2001). Dynamics of intracellular calcium and free radical production during ischemia in pyramidal neurons. *Free radical biology & medicine* **31**(10)**:** 1216-1227.

FRIEDMANN T, ROBLIN R (1972). Gene Therapy for Human Genetic Disease? *Science* **175**(4025)**:** 949-955.

GAHN G, BARLINN K, DZIALOWSKI I, PUETZ V, KUNZ A, HENTSCHEL H*, et al.* (2010). Combined thrombolysis with abciximab and rtPA in patients with middle cerebral artery occlusion. *Acta neurologica Scandinavica* **121**(1)**:** 63-66.

GAO Y, SIGNORE AP, YIN W, CAO G, YIN XM, SUN F*, et al.* (2005). Neuroprotection against focal ischemic brain injury by inhibition of c-Jun N-terminal kinase and attenuation of the mitochondrial apoptosis-signaling pathway. *Journal of cerebral blood flow and metabolism : official journal of the International Society of Cerebral Blood Flow and Metabolism* **25**(6)**:** 694-712.

GARCIA JH, LIU KF, YE ZR, GUTIERREZ JA (1997). Incomplete infarct and delayed neuronal death after transient middle cerebral artery occlusion in rats. *Stroke* **28**(11)**:** 2303-2309; discussion 2310.

GATFIELD PD, LOWRY OH, SCHULZ DW, PASSONNEAU JV (1966). Regional energy reserves in mouse brain and changes with ischaemia and anaesthesia. *Journal of neurochemistry* **13**(3)**:** 185-195.

GEORGIADIS D, SCHWARZ S, KOLLMAR R, SCHWAB S (2001). Endovascular cooling for moderate hypothermia in patients with acute stroke: first results of a novel approach. *Stroke* **32**(11)**:** 2550-2553.

GHARBAWIE OA, WHISHAW PA, WHISHAW IQ (2004). The topography of three-dimensional exploration: a new quantification of vertical and horizontal exploration, postural support, and exploratory bouts in the cylinder test. *Behavioural brain research* **151**(1-2)**:** 125-135.

GILL R (1994). The pharmacology of alpha-amino-3-hydroxy-5-methyl-4-isoxazole propionate (AMPA)/kainate antagonists and their role in cerebral ischaemia. *Cerebrovascular and brain metabolism reviews* **6**(3)**:** 225-256.

GILLUM RF, MUSSOLINO ME, INGRAM DD (1996). Physical activity and stroke incidence in women and men. The NHANES I Epidemiologic Follow-up Study. *American journal of epidemiology* **143**(9)**:** 860-869.

GINSBERG MD (1995). REVIEW ■ : Neuroprotection in Brain Ischemia: An Update (Part I. *The Neuroscientist* **1**(2)**:** 95-103.

GOLSTEIN P, KROEMER G (2007). Cell death by necrosis: towards a molecular definition. *Trends in biochemical sciences* **32**(1)**:** 37-43.

GONG P, HU B, STEWART D, ELLERBE M, FIGUEROA YG, BLANK V*, et al.* (2001). Cobalt induces heme oxygenase-1 expression by a hypoxia-inducible factor-independent mechanism in Chinese hamster ovary cells: regulation by Nrf2 and MafG transcription factors. *J Biol Chem* **276**(29)**:** 27018-27025.

GROTTA J (2001). Combination Therapy Stroke Trial: recombinant tissue-type plasminogen activator with/without lubeluzole. *Cerebrovasc Dis* **12**(3)**:** 258-263.

GROTTA J, CLARK W, COULL B, PETTIGREW LC, MACKAY B, GOLDSTEIN LB*, et al.* (1995). Safety and Tolerability of the Glutamate Antagonist CGS 19755 (Selfotel) in Patients With Acute Ischemic Stroke : Results of a Phase IIa Randomized Trial. *Stroke* **26**(4)**:** 602-605.

GUAN QH, PEI DS, ZHANG QG, HAO ZB, XU TL, ZHANG GY (2005). The neuroprotective action of SP600125, a new inhibitor of JNK, on transient brain ischemia/reperfusion-induced neuronal death in rat hippocampal CA1 via nuclear and non-nuclear pathways. *Brain research* **1035**(1)**:** 51-59.

HACEIN-BEY-ABINA S, VON KALLE C, SCHMIDT M, MCCORMACK MP, WULFFRAAT N, LEBOULCH P, *et al.* (2003). LMO2-associated clonal T cell proliferation in two patients after gene therapy for SCID-X1. *Science* **302**(5644)**:** 415-419.

HACKE W, DONNAN GA, FIESCHI C (2004). Association of outcome with early stroke treatment: pooled analysis of ATLANTIS, ECASS, and NINDS rt-PA stroke trials. *The Lancet* **363**(9411)**:** 768-774.

HACKE W, KASTE M, BLUHMKI E, BROZMAN M, DAVALOS A, GUIDETTI D, *et al.* (2008). Thrombolysis with alteplase 3 to 4.5 hours after acute ischemic stroke. *The New England journal of medicine* **359**(13)**:** 1317-1329.

HADACZEK P, EBERLING JL, PIVIROTTO P, BRINGAS J, FORSAYETH J, BANKIEWICZ KS (2010). Eight Years of Clinical Improvement in MPTP-Lesioned Primates After Gene Therapy With AAV2-hAADC. *Mol. Ther.* **18**(8)**:** 1458-1461.

HANUS J, KALINOWSKA-HEROK M, WIDLAK P (2008). The major apoptotic endonuclease DFF40/CAD is a deoxyribose-specific and double-strand-specific enzyme. *Apoptosis : an international journal on programmed cell death* **13**(3)**:** 377-382.

HARDING TC, DICKINSON PJ, ROBERTS BN, YENDLURI S, GONZALEZ-EDICK M, LECOUTEUR RA, *et al.* (2006). Enhanced gene transfer efficiency in the murine striatum and an orthotopic glioblastoma tumor model, using AAV-7- and AAV-8-pseudotyped vectors. *Human gene therapy* **17**(8)**:** 807-820.

HART CL, HOLE DJ, SMITH GD (2001). The relation between questions indicating transient ischaemic attack and stroke in 20 years of follow up in men and women in the Renfrew/Paisley Study. *Journal of Epidemiology and Community Health* **55**(9)**:** 653-656.

HARVEY BK, AIRAVAARA M, HINZMAN J, WIRES EM, CHIOCCO MJ, HOWARD DB, *et al.* (2011). Targeted over-expression of glutamate transporter 1 (GLT-1) reduces ischemic brain injury in a rat model of stroke. *PloS one* **6**(8)**:** e22135.

HARVEY BK, CHANG CF, CHIANG YH, BOWERS WJ, MORALES M, HOFFER BJ, *et al.* (2003). HSV amplicon delivery of glial cell line-derived neurotrophic factor is neuroprotective against ischemic injury. *Experimental neurology* **183**(1)**:** 47-55.

HEGDE R, SRINIVASULA SM, ZHANG Z, WASSELL R, MUKATTASH R, CILENTI L, *et al.* (2002). Identification of Omi/HtrA2 as a Mitochondrial Apoptotic Serine Protease That Disrupts Inhibitor of Apoptosis Protein-Caspase Interaction. *Journal of Biological Chemistry* **277**(1)**:** 432-438.

HEISS WD, GRAF R, LOTTGEN J, OHTA K, FUJITA T, WAGNER R, *et al.* (1997). Repeat positron emission tomographic studies in transient middle cerebral artery occlusion in cats: residual perfusion and efficacy of postischemic reperfusion. *Journal of cerebral blood flow and metabolism : official journal of the International Society of Cerebral Blood Flow and Metabolism* **17**(4)**:** 388-400.

HERCULANO-HOUZEL S (2011). Scaling of brain metabolism with a fixed energy budget per neuron: implications for neuronal activity, plasticity and evolution. *PloS one* **6**(3)**:** e17514.

HERDEGEN T, CLARET FX, KALLUNKI T, MARTIN-VILLALBA A, WINTER C, HUNTER T, *et al.* (1998). Lasting N-terminal phosphorylation of c-Jun and activation of c-Jun N-terminal kinases after neuronal injury. *The Journal of neuroscience : the official journal of the Society for Neuroscience* **18**(14)**:** 5124-5135.

HEROLD S, FAGO A, WEBER RE, DEWILDE S, MOENS L (2004). Reactivity Studies of the Fe(III) and Fe(II)NO Forms of Human Neuroglobin Reveal a Potential Role against Oxidative Stress. *Journal of Biological Chemistry* **279**(22)**:** 22841-22847.

HIRT L, BADAUT J, THEVENET J, GRANZIERA C, REGLI L, MAURER F, *et al.* (2004). D-JNKI1, a cell-penetrating c-Jun-N-terminal kinase inhibitor, protects against cell death in severe cerebral ischemia. *Stroke* **35**(7)**:** 1738-1743.

HOLZBERG D, KNIGHT CG, DITTRICH-BREIHOLZ O, SCHNEIDER H, DORRIE A, HOFFMANN E, *et al.* (2003). Disruption of the c-JUN-JNK complex by a cell-permeable peptide containing the c-JUN delta domain induces apoptosis and affects a distinct set of

interleukin-1-induced inflammatory genes. *The Journal of biological chemistry* **278**(41)**:** 40213-40223.

HORN J, LIMBURG M (2000). Calcium antagonists for acute ischemic stroke. *Cochrane Database Syst Rev*(2)**:** CD001928.

HOSSMANN KA (2012). The two pathophysiologies of focal brain ischemia: implications for translational stroke research. *Journal of cerebral blood flow and metabolism : official journal of the International Society of Cerebral Blood Flow and Metabolism*.

HPSCG (2002). MRC/BHF Heart Protection Study of cholesterol lowering with simvastatin in 20,536 high-risk individuals: a randomised placebo-controlled trial. *Lancet* **360**(9326)**:** 7-22.

HU FB, STAMPFER MJ, COLDITZ GA, ASCHERIO A, REXRODE KM, WILLETT WC*, et al.* (2000). Physical activity and risk of stroke in women. *JAMA : the journal of the American Medical Association* **283**(22)**:** 2961-2967.

HU Q, CHEN C, KHATIBI NH, LI L, YANG L, WANG K*, et al.* (2011). Lentivirus-mediated transfer of MMP-9 shRNA provides neuroprotection following focal ischemic brain injury in rats. *Brain research* **1367:** 347-359.

HU Q, CHEN C, YAN J, YANG X, SHI X, ZHAO J*, et al.* (2009). Therapeutic application of gene silencing MMP-9 in a middle cerebral artery occlusion-induced focal ischemia rat model. *Experimental neurology* **216**(1)**:** 35-46.

HUANG J, CHOUDHRI TF, WINFREE CJ, MCTAGGART RA, KISS S, MOCCO J*, et al.* (2000). Postischemic cerebrovascular E-selectin expression mediates tissue injury in murine stroke. *Stroke* **31**(12)**:** 3047-3053.

HUDGINS WR, GARCIA JH (1970). The effect of electrocautery, atmospheric exposure, and surgical retraction on the permeability of the blood-brain-barrier. *Stroke* **1**(5)**:** 375-380.

HUNDAHL C, KELSEN J, KJAER K, RONN LC, WEBER RE, GEUENS E, *et al.* (2006a). Does neuroglobin protect neurons from ischemic insult? A quantitative investigation of neuroglobin expression following transient MCAo in spontaneously hypertensive rats. *Brain research* **1085**(1)**:** 19-27.

HUNDAHL C, KELSEN J, KJÆR K, RØNN LCB, WEBER RE, GEUENS E, *et al.* (2006b). Does neuroglobin protect neurons from ischemic insult? A quantitative investigation of neuroglobin expression following transient MCAo in spontaneously hypertensive rats. *Brain Research* **1085**(1)**:** 19-27.

HUNDAHL C, STOLTENBERG M, FAGO A, WEBER RE, DEWILDE S, FORDEL E, *et al.* (2005). Effects of short-term hypoxia on neuroglobin levels and localization in mouse brain tissues. *Neuropathology and applied neurobiology* **31**(6)**:** 610-617.

HUNDAHL CA, ALLEN GC, HANNIBAL J, KJAER K, REHFELD JF, DEWILDE S, *et al.* (2010). Anatomical characterization of cytoglobin and neuroglobin mRNA and protein expression in the mouse brain. *Brain research* **1331:** 58-73.

HUNTER AJ, HATCHER J, VIRLEY D, NELSON P, IRVING E, HADINGHAM SJ, *et al.* (2000). Functional assessments in mice and rats after focal stroke. *Neuropharmacology* **39**(5)**:** 806-816.

IADECOLA C, ANRATHER J (2011). The immunology of stroke: from mechanisms to translation. *Nature medicine* **17**(7)**:** 796-808.

IADECOLA C, ZHANG F, XU X (1995). Inhibition of inducible nitric oxide synthase ameliorates cerebral ischemic damage. *The American journal of physiology* **268**(1 Pt 2)**:** R286-292.

IM JY, LEE KW, KIM MH, LEE SH, HA HY, CHO IH, *et al.* (2003). Repression of phospho-JNK and infarct volume in ischemic brain of JIP1-deficient mice. *Journal of neuroscience research* **74**(2)**:** 326-332.

IMAI H, MASAYASU H, DEWAR D, GRAHAM DI, MACRAE IM (2001). Ebselen protects both gray and white matter in a rodent model of focal cerebral ischemia. *Stroke* **32**(9)**:** 2149-2154.

INVESTIGATORS TPSGP (2007). Mixed lineage kinase inhibitor CEP-1347 fails to delay disability in early Parkinson disease. *Neurology* **69**(15)**:** 1480-1490.

IRVING EA, BAMFORD M (2002). Role of mitogen- and stress-activated kinases in ischemic injury. *Journal of cerebral blood flow and metabolism : official journal of the International Society of Cerebral Blood Flow and Metabolism* **22**(6)**:** 631-647.

ISHIKAWA E, OOBOSHI H, KUMAI Y, TAKADA J, NAKAMURA K, AGO T*, et al.* (2009). Midkine gene transfer protects against focal brain ischemia and augments neurogenesis. *Journal of the neurological sciences* **285**(1-2)**:** 78-84.

ISO H, REXRODE KM, STAMPFER MJ, MANSON JE, COLDITZ GA, SPEIZER FE*, et al.* (2001). Intake of fish and omega-3 fatty acids and risk of stroke in women. *JAMA : the journal of the American Medical Association* **285**(3)**:** 304-312.

ITRAT A, AHMED B, KHAN M, MUHAMMAD M, THAVER D, KHOWAJA Z*, et al.* (2011). Risk factor profiles of South Asians with cerebrovascular disease. *International journal of stroke : official journal of the International Stroke Society* **6**(4)**:** 346-348.

IZUMI Y, ROUSSEL S, PINARD E, SEYLAZ J (1991). Reduction of infarct volume by magnesium after middle cerebral artery occlusion in rats. *Journal of cerebral blood flow and metabolism : official journal of the International Society of Cerebral Blood Flow and Metabolism* **11**(6)**:** 1025-1030.

JÄNICKE RU, SPRENGART ML, WATI MR, PORTER AG (1998). Caspase-3 Is Required for DNA Fragmentation and Morphological Changes Associated with Apoptosis. *Journal of Biological Chemistry* **273**(16)**:** 9357-9360.

JIN K, MAO XO, XIE L, JOHN V, GREENBERG DA (2011). Pharmacological induction of neuroglobin expression. *Pharmacology* **87**(1-2)**:** 81-84.

JIN K, MAO XO, XIE L, KHAN AA, GREENBERG DA (2008a). Neuroglobin protects against nitric oxide toxicity. *Neurosci Lett* **430**(2)**:** 135-137.

JIN K, MAO XO, XIE L, KHAN AA, GREENBERG DA (2008b). Neuroglobin protects against nitric oxide toxicity. *Neuroscience Letters* **430**(2)**:** 135-137.

JIN K, MAO Y, MAO X, XIE L, GREENBERG DA (2010). Neuroglobin Expression in Ischemic Stroke. *Stroke* **41**(3)**:** 557-559.

JOHNSON GL, NAKAMURA K (2007). The c-jun kinase/stress-activated pathway: regulation, function and role in human disease. *Biochimica et biophysica acta* **1773**(8)**:** 1341-1348.

JOSHIPURA KJ, ASCHERIO A, MANSON JE, STAMPFER MJ, RIMM EB, SPEIZER FE*, et al.* (1999). Fruit and vegetable intake in relation to risk of ischemic stroke. *JAMA : the journal of the American Medical Association* **282**(13)**:** 1233-1239.

JUTTLER E, SCHWAB S, SCHMIEDEK P, UNTERBERG A, HENNERICI M, WOITZIK J*, et al.* (2007). Decompressive Surgery for the Treatment of Malignant Infarction of the Middle Cerebral Artery (DESTINY): a randomized, controlled trial. *Stroke* **38**(9)**:** 2518-2525.

KAGI D, VIGNAUX F, LEDERMANN B, BURKI K, DEPRAETERE V, NAGATA S*, et al.* (1994). Fas and perforin pathways as major mechanisms of T cell-mediated cytotoxicity. *Science* **265**(5171)**:** 528-530.

KAMMERSGAARD LP, RASMUSSEN BH, JORGENSEN HS, REITH J, WEBER U, OLSEN TS (2000). Feasibility and safety of inducing modest hypothermia in awake patients with acute stroke through surface cooling: A case-control study: the Copenhagen Stroke Study. *Stroke* **31**(9)**:** 2251-2256.

KAUR J, ZHAO Z, KLEIN GM, LO EH, BUCHAN AM (2004). The neurotoxicity of tissue plasminogen activator? *Journal of cerebral blood flow and metabolism : official journal of the International Society of Cerebral Blood Flow and Metabolism* **24**(9)**:** 945-963.

KAWASAKI H, MOROOKA T, SHIMOHAMA S, KIMURA J, HIRANO T, GOTOH Y*, et al.* (1997a). Activation and involvement of p38 mitogen-activated protein kinase in glutamate-induced apoptosis in rat cerebellar granule cells. *J Biol Chem* **272**(30)**:** 18518-18521.

KAWASAKI H, MOROOKA T, SHIMOHAMA S, KIMURA J, HIRANO T, GOTOH Y*, et al.* (1997b). Activation and Involvement of p38 Mitogen-activated Protein Kinase in Glutamate-induced Apoptosis in Rat Cerebellar Granule Cells. *Journal of Biological Chemistry* **272**(30)**:** 18518-18521.

KAWASE M, FUJIMURA M, MORITA-FUJIMURA Y, CHAN PH (1999). Reduction of apurinic/apyrimidinic endonuclease expression after transient global cerebral ischemia in rats: implication of the failure of DNA repair in neuronal apoptosis. *Stroke* **30**(2)**:** 441-448; discussion 449.

KERIEL A, RENE C, GALER C, ZABNER J, KREMER EJ (2006). Canine adenovirus vectors for lung-directed gene transfer: efficacy, immune response, and duration of transgene expression using helper-dependent vectors. *Journal of virology* **80**(3)**:** 1487-1496.

KHAN AA, MAO XO, BANWAIT S, DERMARDIROSSIAN CM, BOKOCH GM, JIN K*, et al.* (2008). Regulation of hypoxic neuronal death signaling by neuroglobin. *The FASEB journal : official publication of the Federation of American Societies for Experimental Biology* **22**(6)**:** 1737-1747.

KHAN AA, WANG Y, SUN Y, MAO XO, XIE L, MILES E*, et al.* (2006). Neuroglobin-overexpressing transgenic mice are resistant to cerebral and myocardial ischemia. *Proceedings of the National Academy of Sciences of the United States of America* **103**(47)**:** 17944-17948.

KIM AH, KHURSIGARA G, SUN X, FRANKE TF, CHAO MV (2001a). Akt Phosphorylates and Negatively Regulates Apoptosis Signal-Regulating Kinase 1. *Molecular and cellular biology* **21**(3)**:** 893-901.

KIM AH, KHURSIGARA G, SUN X, FRANKE TF, CHAO MV (2001b). Akt Phosphorylates and Negatively Regulates Apoptosis Signal-Regulating Kinase 1. *Mol. Cell. Biol.* **21**(3)**:** 893-901.

KIM AH, YANO H, CHO H, MEYER D, MONKS B, MARGOLIS B, *et al.* (2002). Akt1 Regulates a JNK Scaffold during Excitotoxic Apoptosis. *Neuron* **35**(4)**:** 697-709.

KIM HW, CHO KJ, PARK SC, KIM HJ, KIM GW (2009). The adenoviral vector-mediated increase in apurinic/apyrimidinic endonuclease inhibits the induction of neuronal cell death after transient ischemic stroke in mice. *Brain research* **1274:** 1-10.

KIRKLAND RA, WINDELBORN JA, KASPRZAK JM, FRANKLIN JL (2002). A Bax-induced pro-oxidant state is critical for cytochrome c release during programmed neuronal death. *The Journal of neuroscience : the official journal of the Society for Neuroscience* **22**(15)**:** 6480-6490.

KOIZUMI J, YOSHIDA Y, NAKAZAWA T (1986). Experimental studies of ischemic brain edema: a new experimental model in which recirculation can be reintroduced. *Jpn J Stroke* **8:** 1-8.

KOLLMAR R, HENNINGER N, BARDUTZKY J, SCHELLINGER PD, SCHABITZ WR, SCHWAB S (2004). Combination therapy of moderate hypothermia and thrombolysis in experimental thromboembolic stroke--an MRI study. *Experimental neurology* **190**(1)**:** 204-212.

KONSMAN JP, DRUKARCH B, VAN DAM AM (2007). (Peri)vascular production and action of pro-inflammatory cytokines in brain pathology. *Clin Sci (Lond)* **112**(1)**:** 1-25.

KORCOK J, RAIMUNDO LN, KE HZ, SIMS SM, DIXON SJ (2004). Extracellular nucleotides act through P2X7 receptors to activate NF-kappaB in osteoclasts. *Journal of bone and mineral research : the official journal of the American Society for Bone and Mineral Research* **19**(4)**:** 642-651.

KOYA RC, FUJITA H, SHIMIZU S, OHTSU M, TAKIMOTO M, TSUJIMOTO Y, *et al.* (2000). Gelsolin Inhibits Apoptosis by Blocking Mitochondrial Membrane Potential Loss and Cytochrome c Release. *Journal of Biological Chemistry* **275**(20)**:** 15343-15349.

KOZIOL JA, FENG AC (2006). On the analysis and interpretation of outcome measures in stroke clinical trials: lessons from the SAINT I study of NXY-059 for acute ischemic stroke. *Stroke* **37**(10)**:** 2644-2647.

KUAN CY, BURKE RE (2005). Targeting the JNK signaling pathway for stroke and Parkinson's diseases therapy. *Current drug targets. CNS and neurological disorders* **4**(1)**:** 63-67.

KUAN CY, WHITMARSH AJ, YANG DD, LIAO G, SCHLOEMER AJ, DONG C, *et al.* (2003). A critical role of neural-specific JNK3 for ischemic apoptosis. *Proceedings of the National Academy of Sciences of the United States of America* **100**(25)**:** 15184-15189.

KURODA S, TSUCHIDATE R, SMITH ML, MAPLES KR, SIESJO BK (1999). Neuroprotective effects of a novel nitrone, NXY-059, after transient focal cerebral ischemia in the rat. *Journal of cerebral blood flow and metabolism : official journal of the International Society of Cerebral Blood Flow and Metabolism* **19**(7)**:** 778-787.

LAU AA, HOPWOOD JJ, KREMER EJ, HEMSLEY KM (2010). SGSH gene transfer in mucopolysaccharidosis type IIIA mice using canine adenovirus vectors. *Molecular genetics and metabolism* **100**(2)**:** 168-175.

LAU AA, ROZAKLIS T, IBANES S, LUCK AJ, BEARD H, HASSIOTIS S, *et al.* (2012). Helper-dependent canine adenovirus vector-mediated transgene expression in a neurodegenerative lysosomal storage disorder. *Gene* **491**(1)**:** 53-57.

LEAVITT AD, ROBLES G, ALESANDRO N, VARMUS HE (1996). Human immunodeficiency virus type 1 integrase mutants retain in vitro integrase activity yet fail to integrate viral DNA efficiently during infection. *Journal of virology* **70**(2)**:** 721-728.

LEE BI, LEE DJ, CHO KJ, KIM GW (2005). Early nuclear translocation of endonuclease G and subsequent DNA fragmentation after transient focal cerebral ischemia in mice. *Neuroscience letters* **386**(1)**:** 23-27.

LEE EM, HONG SH, LEE YJ, KANG YH, CHOI KC, CHOI SH, *et al.* (2004). Liposome-complexed adenoviral gene transfer in cancer cells expressing various levels of coxsackievirus and adenovirus receptor. *Journal of Cancer Research and Clinical Oncology* **130**(3)**:** 169-177.

LEE PJ, JIANG BH, CHIN BY, IYER NV, ALAM J, SEMENZA GL*, et al.* (1997). Hypoxia-inducible factor-1 mediates transcriptional activation of the heme oxygenase-1 gene in response to hypoxia. *The Journal of biological chemistry* **272**(9)**:** 5375-5381.

LEES KR, ASPLUND K, CAROLEI A, DAVIS SM, DIENER HC, KASTE M*, et al.* (2000). Glycine antagonist (gavestinel) in neuroprotection (GAIN International) in patients with acute stroke: a randomised controlled trial. GAIN International Investigators. *Lancet* **355**(9219)**:** 1949-1954.

LEES KR, DAVALOS A, DAVIS SM, DIENER HC, GROTTA J, LYDEN P, *et al.* (2006). Additional outcomes and subgroup analyses of NXY-059 for acute ischemic stroke in the SAINT I trial. *Stroke* **37**(12)**:** 2970-2978.

LEWITT PA, REZAI AR, LEEHEY MA, OJEMANN SG, FLAHERTY AW, ESKANDAR EN*, et al.* (2011). AAV2-GAD gene therapy for advanced Parkinson's disease: a double-blind, sham-surgery controlled, randomised trial. *Lancet neurology* **10**(4)**:** 309-319.

LI H, BUCHAN AM (1993). Treatment with an AMPA antagonist 12 hours following severe normothermic forebrain ischemia prevents CA1 neuronal injury. *Journal of cerebral blood flow and metabolism : official journal of the International Society of Cerebral Blood Flow and Metabolism* **13**(6)**:** 933-939.

LI RC, GUO SZ, LEE SK, GOZAL D (2010). Neuroglobin protects neurons against oxidative stress in global ischemia. *Journal of cerebral blood flow and metabolism : official journal of the International Society of Cerebral Blood Flow and Metabolism* **30**(11)**:** 1874-1882.

LI RC, MORRIS MW, LEE SK, POURANFAR F, WANG Y, GOZAL D (2008a). Neuroglobin protects PC12 cells against oxidative stress. *Brain Research* **1190**(0)**:** 159-166.

LI RC, MORRIS MW, LEE SK, POURANFAR F, WANG Y, GOZAL D (2008b). Neuroglobin protects PC12 cells against oxidative stress. *Brain Res* **1190:** 159-166.

LI T, YU HM, SUN YF, SONG YJ, ZHANG GY, PEI DS (2009). Inhibition of cerebral ischemia/reperfusion-induced injury by adenovirus expressed C-terminal amino acids of GluR6. *Brain research* **1300:** 169-176.

LI W, WU Y, REN C, LU Y, GAO Y, ZHENG X, *et al.* (2011). The activity of recombinant human neuroglobin as an antioxidant and free radical scavenger. *Proteins: Structure, Function, and Bioinformatics* **79**(1)**:** 115-125.

LILLEY CE, GROUTSI F, HAN Z, PALMER JA, ANDERSON PN, LATCHMAN DS, *et al.* (2001). Multiple immediate-early gene-deficient herpes simplex virus vectors allowing efficient gene delivery to neurons in culture and widespread gene delivery to the central nervous system in vivo. *Journal of virology* **75**(9)**:** 4343-4356.

LIN TN, CHEUNG WM, WU JS, CHEN JJ, LIN H, CHEN JJ, *et al.* (2006). 15d-prostaglandin J2 protects brain from ischemia-reperfusion injury. *Arteriosclerosis, thrombosis, and vascular biology* **26**(3)**:** 481-487.

LIN YC, HUANG ZH, JAN IS, YEH CC, WU HJ, CHOU YC, *et al.* (2002). Development of excitatory synapses in cultured neurons dissociated from the cortices of rat embryos and rat pups at birth. *J Neurosci Res* **67**(4)**:** 484-493.

LIU J, YU Z, GUO S, LEE S-R, XING C, ZHANG C, *et al.* (2009). Effects of neuroglobin overexpression on mitochondrial function and oxidative stress following hypoxia/reoxygenation in cultured neurons. *Journal of Neuroscience Research* **87**(1)**:** 164-170.

LIU PK, HSU CY, DIZDAROGLU M, FLOYD RA, KOW YW, KARAKAYA A, *et al.* (1996a). Damage, repair, and mutagenesis in nuclear genes after mouse forebrain ischemia-reperfusion. *The Journal of neuroscience : the official journal of the Society for Neuroscience* **16**(21)**:** 6795-6806.

LIU S, MANSON JE, STAMPFER MJ, REXRODE KM, HU FB, RIMM EB, *et al.* (2000). Whole grain consumption and risk of ischemic stroke in women: A prospective study. *JAMA : the journal of the American Medical Association* **284**(12)**:** 1534-1540.

LIU X, KIM CN, YANG J, JEMMERSON R, WANG X (1996b). Induction of apoptotic program in cell-free extracts: requirement for dATP and cytochrome c. *Cell* **86**(1)**:** 147-157.

LO EH, DALKARA T, MOSKOWITZ MA (2003). Mechanisms, challenges and opportunities in stroke. *Nat Rev Neurosci* **4**(5)**:** 399-415.

LONGA E, WEINSTEIN P, CARLSON S, CUMMINS R (1989). Reversible middle cerebral artery occlusion without craniectomy in rats. *Stroke* **20**(1)**:** 84-91.

LU H, WANG Y, HE X, YUAN F, LIN X, XIE B, *et al.* (2012). Netrin-1 Hyperexpression in Mouse Brain Promotes Angiogenesis and Long-Term Neurological Recovery After Transient Focal Ischemia. *Stroke*.

LUNDBERG C, BJORKLUND T, CARLSSON T, JAKOBSSON J, HANTRAYE P, DEGLON N, *et al.* (2008). Applications of lentiviral vectors for biology and gene therapy of neurological disorders. *Current gene therapy* **8**(6)**:** 461-473.

LYDEN PD, JACKSON-FRIEDMAN C, SHIN C, HASSID S (2000). Synergistic combinatorial stroke therapy: A quantal bioassay of a GABA agonist and a glutamate antagonist. *Experimental neurology* **163**(2)**:** 477-489.

LYONS A, DOWNER EJ, CROTTY S, NOLAN YM, MILLS KH, LYNCH MA (2007). CD200 ligand receptor interaction modulates microglial activation in vivo and in vitro: a role for IL-4. *The Journal of neuroscience : the official journal of the Society for Neuroscience* **27**(31)**:** 8309-8313.

MA J, ENDRES M, MOSKOWITZ MA (1998). Synergistic effects of caspase inhibitors and MK-801 in brain injury after transient focal cerebral ischaemia in mice. *British journal of pharmacology* **124**(4)**:** 756-762.

MACRAE IM (2011). Preclinical stroke research--advantages and disadvantages of the most common rodent models of focal ischaemia. *British journal of pharmacology* **164**(4)**:** 1062-1078.

MACRAE IM, ROBINSON MJ, GRAHAM DI, REID JL, MCCULLOCH J (1993). Endothelin-1-induced reductions in cerebral blood flow: dose dependency, time course, and neuropathological consequences. *Journal of cerebral blood flow and metabolism : official journal of the International Society of Cerebral Blood Flow and Metabolism* **13**(2)**:** 276-284.

MAGNONI S, BAKER A, THOMSON S, JORDAN G, GEORGE SJ, MCCOLL BW, *et al.* (2007). Neuroprotective effect of adenoviral-mediated gene transfer of TIMP-1 and -2 in ischemic brain injury. *Gene therapy* **14**(7)**:** 621-625.

MANDEL RJ (2010). CERE-110, an adeno-associated virus-based gene delivery vector expressing human nerve growth factor for the treatment of Alzheimer's disease. *Current opinion in molecular therapeutics* **12**(2)**:** 240-247.

MANDIC A, VIKTORSSON K, STRANDBERG L, HEIDEN T, HANSSON J, LINDER S, *et al.* (2002). Calpain-mediated Bid cleavage and calpain-independent Bak modulation: two separate pathways in cisplatin-induced apoptosis. *Molecular and cellular biology* **22**(9)**:** 3003-3013.

MARCHAL G, FURLAN M, BEAUDOUIN V, RIOUX P, HAUTTEMENT JL, SERRATI C*, et al.* (1996). Early spontaneous hyperperfusion after stroke. A marker of favourable tissue outcome? *Brain : a journal of neurology* **119 (Pt 2):** 409-419.

MARINOV MB, HARBAUGH KS, HOOPES PJ, PIKUS HJ, HARBAUGH RE (1996). Neuroprotective effects of preischemia intraarterial magnesium sulfate in reversible focal cerebral ischemia. *Journal of neurosurgery* **85**(1)**:** 117-124.

MARONEY AC, GLICKSMAN MA, BASMA AN, WALTON KM, KNIGHT E, JR., MURPHY CA*, et al.* (1998). Motoneuron apoptosis is blocked by CEP-1347 (KT 7515), a novel inhibitor of the JNK signaling pathway. *The Journal of neuroscience : the official journal of the Society for Neuroscience* **18**(1)**:** 104-111.

MARSHALL JW, CUMMINGS RM, BOWES LJ, RIDLEY RM, GREEN AR (2003). Functional and histological evidence for the protective effect of NXY-059 in a primate model of stroke when given 4 hours after occlusion. *Stroke* **34**(9)**:** 2228-2233.

MARSHALL JW, DUFFIN KJ, GREEN AR, RIDLEY RM (2001). NXY-059, a free radical--trapping agent, substantially lessens the functional disability resulting from cerebral ischemia in a primate species. *Stroke* **32**(1)**:** 190-198.

MARTIN-VILLALBA A, HERR I, JEREMIAS I, HAHNE M, BRANDT R, VOGEL J*, et al.* (1999). CD95 ligand (Fas-L/APO-1L) and tumor necrosis factor-related apoptosis-inducing ligand mediate ischemia-induced apoptosis in neurons. *The Journal of neuroscience : the official journal of the Society for Neuroscience* **19**(10)**:** 3809-3817.

MASINENI SN, CHANDER PN, SINGH GD, POWERS CA, STIER CT, JR. (2005). Male gender and not the severity of hypertension is associated with end-organ damage in aged stroke-prone spontaneously hypertensive rats. *American journal of hypertension* **18**(6)**:** 878-884.

MASTAKOV MY, BAER K, KOTIN RM, DURING MJ (2002). Recombinant adeno-associated virus serotypes 2- and 5-mediated gene transfer in the mammalian brain: quantitative analysis of heparin co-infusion. *Mol Ther* **5**(4)**:** 371-380.

MASTAKOV MY, BAER K, XU R, FITZSIMONS H, DURING MJ (2001). Combined Injection of rAAV with Mannitol Enhances Gene Expression in the Rat Brain. *Mol Ther* **3**(2)**:** 225-232.

MATSUDA S, UMEDA M, UCHIDA H, KATO H, ARAKI T (2009). Alterations of oxidative stress markers and apoptosis markers in the striatum after transient focal cerebral ischemia in rats. *J Neural Transm* **116**(4)**:** 395-404.

MAXWELL PH, WIESENER MS, CHANG GW, CLIFFORD SC, VAUX EC, COCKMAN ME*, et al.* (1999). The tumour suppressor protein VHL targets hypoxia-inducible factors for oxygen-dependent proteolysis. *Nature* **399**(6733)**:** 271-275.

MAZARAKIS ND, AZZOUZ M, ROHLL JB, ELLARD FM, WILKES FJ, OLSEN AL*, et al.* (2001). Rabies virus glycoprotein pseudotyping of lentiviral vectors enables retrograde axonal transport and access to the nervous system after peripheral delivery. *Human molecular genetics* **10**(19)**:** 2109-2121.

MCCABE C, WHITE F, BROWN SM, MACRAE IM (2008). GADD34 gene restores virulence in viral vector used in experimental stroke study. *Journal of cerebral blood flow and metabolism : official journal of the International Society of Cerebral Blood Flow and Metabolism* **28**(4)**:** 747-751.

MCCRACKEN E, VALERIANI V, SIMPSON C, JOVER T, MCCULLOCH J, DEWAR D (2000). The Lipid Peroxidation By-product 4-Hydroxynonenal Is Toxic to Axons and Oligodendrocytes. *Journal of cerebral blood flow and metabolism : official journal of the International Society of Cerebral Blood Flow and Metabolism* **20**(11)**:** 1529-1536.

MCGEEHAN M, BUSH RK (2002). The mechanisms of aspirin-intolerant asthma and its management. *Current allergy and asthma reports* **2**(2)**:** 117-125.

MCGILL JK, GALLAGHER L, CARSWELL HV, IRVING EA, DOMINICZAK AF, MACRAE IM (2005). Impaired functional recovery after stroke in the stroke-prone spontaneously hypertensive rat. *Stroke* **36**(1)**:** 135-141.

MCMENAMIN MM, BYRNES AP, CHARLTON HM, COFFIN RS, LATCHMAN DS, WOOD MJ (1998). A gamma34.5 mutant of herpes simplex 1 causes severe inflammation in the brain. *Neuroscience* **83**(4)**:** 1225-1237.

MEDEN P, OVERGAARD K, SEREGHY T, BOYSEN G (1993). Enhancing the efficacy of thrombolysis by AMPA receptor blockade with NBQX in a rat embolic stroke model. *Journal of the neurological sciences* **119**(2)**:** 209-216.

MELANI A, TURCHI D, VANNUCCHI MG, CIPRIANI S, GIANFRIDDO M, PEDATA F (2005). ATP extracellular concentrations are increased in the rat striatum during in vivo ischemia. *Neurochemistry international* **47**(6)**:** 442-448.

MELONI BP, ZHU H, KNUCKEY NW (2006). Is magnesium neuroprotective following global and focal cerebral ischaemia? A review of published studies. *Magnesium research : official organ of the International Society for the Development of Research on Magnesium* **19**(2)**:** 123-137.

MILTON SL, NAYAK G, LUTZ PL, PRENTICE HM (2006). Gene transcription of neuroglobin is upregulated by hypoxia and anoxia in the brain of the anoxia-tolerant turtle Trachemys scripta. *Journal of biomedical science* **13**(4)**:** 509-514.

MINNERUP J, HEIDRICH J, ROGALEWSKI A, SCHABITZ WR, WELLMANN J (2009). The efficacy of erythropoietin and its analogues in animal stroke models: a meta-analysis. *Stroke* **40**(9)**:** 3113-3120.

MISHRA OP, ZUBROW AB, ASHRAF QM (2004). Nitric oxide-mediated activation of extracellular signal-regulated kinase (erk) and c-jun n-terminal kinase (jnk) during hypoxia in cerebral cortical nuclei of newborn piglets. *Neuroscience* **123**(1)**:** 179-186.

MITCHELL P (2010). Ark's gene therapy stumbles at the finish line. *Nature biotechnology* **28**(3)**:** 183-184.

MIYAKE N, MIYAKE K, YAMAMOTO M, HIRAI Y, SHIMADA T (2011). Global gene transfer into the CNS across the BBB after neonatal systemic delivery of single-stranded AAV vectors. *Brain research* **1389:** 19-26.

MOHR J, GAUTIER JC, HIER DB, STEIN RW (1986). *Stroke: Pathophysiology, Diagnosis and Management*. edn, vol. 1. Churchill Livingston: New York.

MONAHAN PE, SAMULSKI RJ (2000). AAV vectors: is clinical success on the horizon? *Gene therapy* **7**(1)**:** 24-30.

MORI S, TAKEUCHI T, ENOMOTO Y, KONDO K, SATO K, ONO F*, et al.* (2006). Biodistribution of a low dose of intravenously administered AAV-2, 10, and 11 vectors to cynomolgus monkeys. *Japanese journal of infectious diseases* **59**(5)**:** 285-293.

MUHAMMAD AK, PUNTEL M, CANDOLFI M, SALEM A, YAGIZ K, FARROKHI C*, et al.* (2010). Study of the efficacy, biodistribution, and safety profile of therapeutic gutless adenovirus vectors as a prelude to a phase I clinical trial for glioblastoma. *Clinical pharmacology and therapeutics* **88**(2)**:** 204-213.

MUIR KW (2001). Magnesium for neuroprotection in ischaemic stroke: rationale for use and evidence of effectiveness. *CNS drugs* **15**(12)**:** 921-930.

MULLER TB, HARALDSETH O, UNSGARD G (1994). Characterization of the microcirculation during ischemia and reperfusion in the penumbra of a rat model of temporary middle cerebral artery occlusion: a laser Doppler flowmetry study. *International journal of microcirculation, clinical and experimental / sponsored by the European Society for Microcirculation* **14**(5)**:** 289-295.

MUUL LM, TUSCHONG LM, SOENEN SL, JAGADEESH GJ, RAMSEY WJ, LONG Z*, et al.* (2003). Persistence and expression of the adenosine deaminase gene for 12 years and immune reaction to gene transfer components: long-term results of the first clinical gene therapy trial. *Blood* **101**(7)**:** 2563-2569.

NAGAOKA A, IWATSUKA H, SUZUOKI Z, OKAMOTO K (1976). Genetic predisposition to stroke in spontaneously hypertensive rats. *The American journal of physiology* **230**(5)**:** 1354-1359.

NAGAYAMA T, SIMON RP, CHEN D, HENSHALL DC, PEI W, STETLER RA*, et al.* (2000). Activation of poly(ADP-ribose) polymerase in the rat hippocampus may contribute to cellular recovery following sublethal transient global ischemia. *Journal of neurochemistry* **74**(4)**:** 1636-1645.

NALDINI L, BLÖMER U, GAGE FH, TRONO D, VERMA IM (1996a). Efficient transfer, integration, and sustained long-term expression of the transgene in adult rat brains injected with a lentiviral vector. *Proceedings of the National Academy of Sciences* **93**(21)**:** 11382-11388.

NALDINI L, BLOMER U, GALLAY P, ORY D, MULLIGAN R, GAGE FH*, et al.* (1996b). In vivo gene delivery and stable transduction of nondividing cells by a lentiviral vector. *Science* **272**(5259)**:** 263-267.

NAMURA S, NAGATA I, TAKAMI S, MASAYASU H, KIKUCHI H (2001). Ebselen reduces cytochrome c release from mitochondria and subsequent DNA fragmentation after transient focal cerebral ischemia in mice. *Stroke* **32**(8)**:** 1906-1911.

NISHITOH H, SAITOH M, MOCHIDA Y, TAKEDA K, NAKANO H, ROTHE M*, et al.* (1998). ASK1 is essential for JNK/SAPK activation by TRAF2. *Molecular cell* **2**(3)**:** 389-395.

NOMOTO T, OKADA T, SHIMAZAKI K, YOSHIOKA T, NONAKA-SARUKAWA M, ITO T*, et al.* (2009). Systemic delivery of IL-10 by an AAV vector prevents vascular remodeling and end-organ damage in stroke-prone spontaneously hypertensive rat. *Gene therapy* **16**(3)**:** 383-391.

O'COLLINS VE, MACLEOD MR, DONNAN GA, HORKY LL, VAN DER WORP BH, HOWELLS DW (2006). 1,026 experimental treatments in acute stroke. *Annals of neurology* **59**(3)**:** 467-477.

O'DONNELL M, XAVIER D, DIENER C, SACCO R, LISHENG L, ZHANG H, *et al.* (2010a). Rationale and design of INTERSTROKE: a global case-control study of risk factors for stroke. *Neuroepidemiology* **35**(1)**:** 36-44.

O'DONNELL MJ, XAVIER D, LIU L, ZHANG H, CHIN SL, RAO-MELACINI P, *et al.* (2010b). Risk factors for ischaemic and intracerebral haemorrhagic stroke in 22 countries (the INTERSTROKE study): a case-control study. *Lancet* **376**(9735)**:** 112-123.

OKAMOTO K, AOKI K (1963). Development of a strain of spontaneously hypertensive rats. *Japanese circulation journal* **27:** 282-293.

ONAL MZ, LI F, TATLISUMAK T, LOCKE KW, SANDAGE BW, JR., FISHER M (1997). Synergistic effects of citicoline and MK-801 in temporary experimental focal ischemia in rats. *Stroke* **28**(5)**:** 1060-1065.

ORRENIUS S, ZHIVOTOVSKY B, NICOTERA P (2003). Regulation of cell death: the calcium-apoptosis link. *Nature reviews. Molecular cell biology* **4**(7)**:** 552-565.

ORSET C, MACREZ R, YOUNG AR, PANTHOU D, ANGLES-CANO E, MAUBERT E, *et al.* (2007). Mouse model of in situ thromboembolic stroke and reperfusion. *Stroke* **38**(10)**:** 2771-2778.

OSBORNE KA, SHIGENO T, BALARSKY AM, FORD I, MCCULLOCH J, TEASDALE GM, *et al.* (1987). Quantitative assessment of early brain damage in a rat model of focal cerebral ischaemia. *Journal of Neurology, Neurosurgery & Psychiatry* **50**(4)**:** 402-410.

OSBORNE R (2008). Ark floats gene therapy's boat, for now. *Nature biotechnology* **26**(10)**:** 1057-1059.

OSE L, DAVIDSON MH, STEIN EA, KASTELEIN JJ, SCOTT RS, HUNNINGHAKE DB, *et al.* (2000). Lipid-altering efficacy and safety of simvastatin 80 mg/day: long-term

experience in a large group of patients with hypercholesterolemia. World Wide Expanded Dose Simvastatin Study Group. *Clinical cardiology* **23**(1)**:** 39-46.

PAN J, CHANG Q, WANG X, SON Y, ZHANG Z, CHEN G, *et al.* (2010). Reactive oxygen species-activated Akt/ASK1/p38 signaling pathway in nickel compound-induced apoptosis in BEAS 2B cells. *Chemical research in toxicology* **23**(3)**:** 568-577.

PANCIOLI AM, BRODERICK J, BROTT T, TOMSICK T, KHOURY J, BEAN J, *et al.* (2008). The combined approach to lysis utilizing eptifibatide and rt-PA in acute ischemic stroke: the CLEAR stroke trial. *Stroke* **39**(12)**:** 3268-3276.

PARK CK, HALL ED (1994). Dose-response analysis of the effect of 21-aminosteroid tirilazad mesylate (U-74006F) upon neurological outcome and ischemic brain damage in permanent focal cerebral ischemia. *Brain research* **645**(1-2)**:** 157-163.

PARK H-S, KIM M-S, HUH S-H, PARK J, CHUNG J, KANG SS, *et al.* (2002). Akt (Protein Kinase B) Negatively Regulates SEK1 by Means of Protein Phosphorylation. *Journal of Biological Chemistry* **277**(4)**:** 2573-2578.

PASSINI MA, WOLFE JH (2001). Widespread gene delivery and structure-specific patterns of expression in the brain after intraventricular injections of neonatal mice with an adeno-associated virus vector. *Journal of virology* **75**(24)**:** 12382-12392.

PAUWELS PJ, OPPERDOES FR, TROUET A (1985). Effects of antimycin, glucose deprivation, and serum on cultures of neurons, astrocytes, and neuroblastoma cells. *Journal of neurochemistry* **44**(1)**:** 143-148.

PELTEKIAN E, GARCIA L, DANOS O (2002). Neurotropism and retrograde axonal transport of a canine adenoviral vector: a tool for targeting key structures undergoing neurodegenerative processes. *Mol Ther* **5**(1)**:** 25-32.

PERONI D, NEGRO A, BAHR M, DIETZ GP (2007). Intracellular delivery of Neuroglobin using HIV-1 TAT protein transduction domain fails to protect against oxygen and glucose deprivation. *Neuroscience letters* **421**(2)**:** 110-114.

PIRIANOV G, BRYWE KG, MALLARD C, EDWARDS AD, FLAVELL RA, HAGBERG H*, et al.* (2007). Deletion of the c-Jun N-terminal kinase 3 gene protects neonatal mice against cerebral hypoxic-ischaemic injury. *Journal of cerebral blood flow and metabolism : official journal of the International Society of Cerebral Blood Flow and Metabolism* **27**(5)**:** 1022-1032.

PLUM L, MA X, HAMPEL B, BALTHASAR N, COPPARI R, MUNZBERG H*, et al.* (2006). Enhanced PIP3 signaling in POMC neurons causes KATP channel activation and leads to diet-sensitive obesity. *J Clin Invest* **116**(7)**:** 1886-1901.

PORTER GW, KHURI FR, FU H (2006a). Dynamic 14-3-3/client protein interactions integrate survival and apoptotic pathways. *Seminars in cancer biology* **16**(3)**:** 193-202.

PORTER GW, KHURI FR, FU H (2006b). Dynamic 14-3-3/client protein interactions integrate survival and apoptotic pathways. *Seminars in Cancer Biology* **16**(3)**:** 193-202.

RAHIM AA, WONG AM, HOWE SJ, BUCKLEY SM, ACOSTA-SALTOS AD, ELSTON KE*, et al.* (2009). Efficient gene delivery to the adult and fetal CNS using pseudotyped non-integrating lentiviral vectors. *Gene therapy* **16**(4)**:** 509-520.

RAHIM AA, WONG AMS, HOEFER K, BUCKLEY SMK, MATTAR CN, CHENG SH*, et al.* (2011). Intravenous administration of AAV2/9 to the fetal and neonatal mouse leads to differential targeting of CNS cell types and extensive transduction of the nervous system. *The FASEB Journal*.

RAJENDRAM R, RAO NA (2007). Neuroglobin in normal retina and retina from eyes with advanced glaucoma. *The British journal of ophthalmology* **91**(5)**:** 663-666.

RAMPLING R, CRUICKSHANK G, PAPANASTASSIOU V, NICOLL J, HADLEY D, BRENNAN D, *et al.* (2000). Toxicity evaluation of replication-competent herpes simplex virus (ICP 34.5 null mutant 1716) in patients with recurrent malignant glioma. *Gene therapy* **7**(10)**:** 859-866.

RANTTAS (1996). A randomized trial of tirilazad mesylate in patients with acute stroke (RANTTAS). The RANTTAS Investigators. *Stroke* **27**(9)**:** 1453-1458.

RAPPAPORT L, OLIVIERO P, SAMUEL JL (1998). Cytoskeleton and mitochondrial morphology and function. *Mol Cell Biochem* **184**(1-2)**:** 101-105.

RAYNER BS, DUONG TTH, MYERS SJ, WITTING PK (2006). Protective effect of a synthetic anti-oxidant on neuronal cell apoptosis resulting from experimental hypoxia re-oxygenation injury. *Journal of Neurochemistry* **97**(1)**:** 211-221.

REEDER BJ (2010). The redox activity of hemoglobins: from physiologic functions to pathologic mechanisms. *Antioxidants & redox signaling* **13**(7)**:** 1087-1123.

RENZULLI P, LAFFER UT (2005). Learning curve: the surgeon as a prognostic factor in colorectal cancer surgery. *Recent results in cancer research. Fortschritte der Krebsforschung. Progres dans les recherches sur le cancer* **165:** 86-104.

RINCON F, MAYER SA (2006). Therapeutic hypothermia for brain injury after cardiac arrest. *Seminars in neurology* **26**(4)**:** 387-395.

ROESNER A, HANKELN T, BURMESTER T (2006). Hypoxia induces a complex response of globin expression in zebrafish (Danio rerio). *The Journal of experimental biology* **209**(Pt 11)**:** 2129-2137.

ROSENBAUM DM, GUPTA G, D'AMORE J, SINGH M, WEIDENHEIM K, ZHANG H, *et al.* (2000). Fas (CD95/APO-1) plays a role in the pathophysiology of focal cerebral ischemia. *Journal of neuroscience research* **61**(6)**:** 686-692.

ROSSI DJ, OSHIMA T, ATTWELL D (2000). Glutamate release in severe brain ischaemia is mainly by reversed uptake. *Nature* **403**(6767)**:** 316-321.

SACCO RL (2001). Newer risk factors for stroke. *Neurology* **57**(5 Suppl 2)**:** S31-34.

SACCO RL, DEROSA JT, HALEY EC, JR., LEVIN B, ORDRONNEAU P, PHILLIPS SJ*, et al.* (2001). Glycine antagonist in neuroprotection for patients with acute stroke: GAIN Americas: a randomized controlled trial. *JAMA : the journal of the American Medical Association* **285**(13)**:** 1719-1728.

SALINAS S, BILSLAND LG, HENAFF D, WESTON AE, KERIEL A, SCHIAVO G*, et al.* (2009). CAR-associated vesicular transport of an adenovirus in motor neuron axons. *PLoS pathogens* **5**(5)**:** e1000442.

SAMULSKI RJ, BERNS KI, TAN M, MUZYCZKA N (1982). Cloning of adeno-associated virus into pBR322: rescue of intact virus from the recombinant plasmid in human cells. *Proceedings of the National Academy of Sciences of the United States of America* **79**(6)**:** 2077-2081.

SAVER JL (2007). Clinical impact of NXY-059 demonstrated in the SAINT I trial: derivation of number needed to treat for benefit over entire range of functional disability. *Stroke* **38**(5)**:** 1515-1518.

SCAPIN G, PATEL SB, LISNOCK J, BECKER JW, LOGRASSO PV (2003). The structure of JNK3 in complex with small molecule inhibitors: structural basis for potency and selectivity. *Chemistry & biology* **10**(8)**:** 705-712.

SCARBOROUGH P, PETO V, BHATNAGAR P, KAUR A, LEAL J, LUENGO-FERNANDEZ R*, et al.* (2009). *Stroke Statistics 2009*
edn. British Heart Foundation & Stroke Association: Oxford, England.

SCHALLERT T, FLEMING SM, LEASURE JL, TILLERSON JL, BLAND ST (2000). CNS plasticity and assessment of forelimb sensorimotor outcome in unilateral rat models

of stroke, cortical ablation, parkinsonism and spinal cord injury. *Neuropharmacology* **39**(5)**:** 777-787.

SCHALLERT T, WHISHAW IQ (1984). Bilateral cutaneous stimulation of the somatosensory system in hemidecorticate rats. *Behavioral neuroscience* **98**(3)**:** 518-540.

SCHMID-ELSAESSER R, HUNGERHUBER E, ZAUSINGER S, BAETHMANN A, REULEN HJ (1999). Neuroprotective efficacy of combination therapy with two different antioxidants in rats subjected to transient focal ischemia. *Brain research* **816**(2)**:** 471-479.

SCHMID-ELSAESSER R, ZAUSINGER S, HUNGERHUBER E, BAETHMANN A, REULEN HJ (1998). A critical reevaluation of the intraluminal thread model of focal cerebral ischemia: evidence of inadvertent premature reperfusion and subarachnoid hemorrhage in rats by laser-Doppler flowmetry. *Stroke* **29**(10)**:** 2162-2170.

SCHMIDT-KASTNER R, HABERKAMP M, SCHMITZ C, HANKELN T, BURMESTER T (2006). Neuroglobin mRNA expression after transient global brain ischemia and prolonged hypoxia in cell culture. *Brain Research* **1103**(1)**:** 173-180.

SCHMIDT M, GERLACH F, AVIVI A, LAUFS T, WYSTUB S, SIMPSON JC, *et al.* (2004). Cytoglobin is a respiratory protein in connective tissue and neurons, which is up-regulated by hypoxia. *The Journal of biological chemistry* **279**(9)**:** 8063-8069.

SCHMIDT M, GIESSL A, LAUFS T, HANKELN T, WOLFRUM U, BURMESTER T (2003). How Does the Eye Breathe? *Journal of Biological Chemistry* **278**(3)**:** 1932-1935.

SCHWAB S, SCHWARZ S, SPRANGER M, KELLER E, BERTRAM M, HACKE W (1998). Moderate hypothermia in the treatment of patients with severe middle cerebral artery infarction. *Stroke* **29**(12)**:** 2461-2466.

SCHWARZSCHILD MA, COLE RL, HYMAN SE (1997a). Glutamate, But Not Dopamine, Stimulates Stress-Activated Protein Kinase and AP-1-Mediated Transcription in Striatal Neurons. *The Journal of Neuroscience* **17**(10)**:** 3455-3466.

SCHWARZSCHILD MA, COLE RL, HYMAN SE (1997b). Glutamate, but not dopamine, stimulates stress-activated protein kinase and AP-1-mediated transcription in striatal neurons. *J Neurosci* **17**(10)**:** 3455-3466.

SCORRANO L, PENZO D, PETRONILLI V, PAGANO F, BERNARDI P (2001). Arachidonic acid causes cell death through the mitochondrial permeability transition. Implications for tumor necrosis factor-alpha aopototic signaling. *The Journal of biological chemistry* **276**(15)**:** 12035-12040.

SEGAL JB, MCNAMARA RL, MILLER MR, KIM N, GOODMAN SN, POWE NR*, et al.* (2000). Prevention of thromboembolism in atrial fibrillation. A meta-analysis of trials of anticoagulants and antiplatelet drugs. *Journal of general internal medicine* **15**(1)**:** 56-67.

SEGGEWISS R, PITTALUGA S, ADLER RL, GUENAGA FJ, FERGUSON C, PILZ IH*, et al.* (2006). Acute myeloid leukemia is associated with retroviral gene transfer to hematopoietic progenitor cells in a rhesus macaque. *Blood* **107**(10)**:** 3865-3867.

SEHBA FA, SCHWARTZ AY, CHERESHNEV I, BEDERSON JB (2000). Acute decrease in cerebral nitric oxide levels after subarachnoid hemorrhage. *Journal of cerebral blood flow and metabolism : official journal of the International Society of Cerebral Blood Flow and Metabolism* **20**(3)**:** 604-611.

SEITZ RJ, MEISEL S, MOLL M, WITTSACK HJ, JUNGHANS U, SIEBLER M (2004). The effect of combined thrombolysis with rtPA and tirofiban on ischemic brain lesions. *Neurology* **62**(11)**:** 2110-2112.

SEMENZA GL, ROTH PH, FANG HM, WANG GL (1994). Transcriptional regulation of genes encoding glycolytic enzymes by hypoxia-inducible factor 1. *The Journal of biological chemistry* **269**(38)**:** 23757-23763.

SENA E, WHEBLE P, SANDERCOCK P, MACLEOD M (2007). Systematic review and meta-analysis of the efficacy of tirilazad in experimental stroke. *Stroke* **38**(2)**:** 388-394.

SEVER PS, DAHLOF B, POULTER NR, WEDEL H, BEEVERS G, CAULFIELD M, *et al.* (2003). Prevention of coronary and stroke events with atorvastatin in hypertensive patients who have average or lower-than-average cholesterol concentrations, in the Anglo-Scandinavian Cardiac Outcomes Trial--Lipid Lowering Arm (ASCOT-LLA): a multicentre randomised controlled trial. *Lancet* **361**(9364)**:** 1149-1158.

SHANG A, ZHOU D, WANG L, GAO Y, FAN M, WANG X, *et al.* (2006). Increased neuroglobin levels in the cerebral cortex and serum after ischemia-reperfusion insults. *Brain research* **1078**(1)**:** 219-226.

SHARKEY J, RITCHIE IM, KELLY PA (1993). Perivascular microapplication of endothelin-1: a new model of focal cerebral ischaemia in the rat. *Journal of cerebral blood flow and metabolism : official journal of the International Society of Cerebral Blood Flow and Metabolism* **13**(5)**:** 865-871.

SHEN F, FAN Y, SU H, ZHU Y, CHEN Y, LIU W, *et al.* (2008). Adeno-associated viral vector-mediated hypoxia-regulated VEGF gene transfer promotes angiogenesis following focal cerebral ischemia in mice. *Gene therapy* **15**(1)**:** 30-39.

SHEN F, SU H, FAN Y, CHEN Y, ZHU Y, LIU W, *et al.* (2006). Adeno-associated viral-vector-mediated hypoxia-inducible vascular endothelial growth factor gene expression attenuates ischemic brain injury after focal cerebral ischemia in mice. *Stroke* **37**(10)**:** 2601-2606.

SHERMAN D, BES A, EASTON JD (2001). Use of anti-ICAM-1 therapy in ischemic stroke: results of the Enlimomab Acute Stroke Trial. *Neurology* **57**(8)**:** 1428-1434.

SHI N, PARDRIDGE WM (2000). Noninvasive gene targeting to the brain. *Proceedings of the National Academy of Sciences of the United States of America* **97**(13)**:** 7567-7572.

SHI Q, ZHANG P, ZHANG J, CHEN X, LU H, TIAN Y, *et al.* (2009). Adenovirus-mediated brain-derived neurotrophic factor expression regulated by hypoxia response element protects brain from injury of transient middle cerebral artery occlusion in mice. *Neuroscience letters* **465**(3)**:** 220-225.

SHIBER JR, FONTANE E, ADEWALE A (2010). Stroke registry: hemorrhagic vs ischemic strokes. *The American journal of emergency medicine* **28**(3)**:** 331-333.

SHUAIB A, LEES KR, LYDEN P, GROTTA J, DAVALOS A, DAVIS SM*, et al.* (2007). NXY-059 for the treatment of acute ischemic stroke. *The New England journal of medicine* **357**(6)**:** 562-571.

SIMON R, SHIRAISHI K (1990). N-methyl-D-aspartate antagonist reduces stroke size and regional glucose metabolism. *Annals of neurology* **27**(6)**:** 606-611.

SIMS NR, MUYDERMAN H (2010). Mitochondria, oxidative metabolism and cell death in stroke. *Biochimica et biophysica acta* **1802**(1)**:** 80-91.

SOBERANES S, URICH D, BAKER CM, BURGESS Z, CHIARELLA SE, BELL EL*, et al.* (2009). Mitochondrial complex III-generated oxidants activate ASK1 and JNK to induce alveolar epithelial cell death following exposure to particulate matter air pollution. *The Journal of biological chemistry* **284**(4)**:** 2176-2186.

SOUDAIS C, LAPLACE-BUILHE C, KISSA K, KREMER EJ (2001). Preferential transduction of neurons by canine adenovirus vectors and their efficient retrograde transport in vivo. *The FASEB journal : official publication of the Federation of American Societies for Experimental Biology* **15**(12)**:** 2283-2285.

SOUDAIS C, SKANDER N, KREMER EJ (2004). Long-term in vivo transduction of neurons throughout the rat CNS using novel helper-dependent CAV-2 vectors. *The FASEB journal : official publication of the Federation of American Societies for Experimental Biology* **18**(2)**:** 391-393.

STEELE EC, JR., GUO Q, NAMURA S (2008). Filamentous middle cerebral artery occlusion causes ischemic damage to the retina in mice. *Stroke* **39**(7)**:** 2099-2104.

STITELMAN DH, ENDO M, BORA A, MUVARAK N, ZOLTICK PW, FLAKE AW, *et al.* (2010). Robust in vivo transduction of nervous system and neural stem cells by early gestational intra amniotic gene transfer using lentiviral vector. *Mol Ther* **18**(9)**:** 1615-1623.

SUGAWARA T, LEWEN A, GASCHE Y, YU F, CHAN PH (2002). Overexpression of SOD1 protects vulnerable motor neurons after spinal cord injury by attenuating mitochondrial cytochrome c release. *The FASEB journal : official publication of the Federation of American Societies for Experimental Biology* **16**(14)**:** 1997-1999.

SUGIURA S, KITAGAWA K, TANAKA S, TODO K, OMURA-MATSUOKA E, SASAKI T, *et al.* (2005). Adenovirus-mediated gene transfer of heparin-binding epidermal growth factor-like growth factor enhances neurogenesis and angiogenesis after focal cerebral ischemia in rats. *Stroke* **36**(4)**:** 859-864.

SUN H, LE T, CHANG TT, HABIB A, WU S, SHEN F, *et al.* (2011). AAV-mediated netrin-1 overexpression increases peri-infarct blood vessel density and improves motor function recovery after experimental stroke. *Neurobiology of disease* **44**(1)**:** 73-83.

SUN Y, JIN K, MAO XO, ZHU Y, GREENBERG DA (2001). Neuroglobin is up-regulated by and protects neurons from hypoxic-ischemic injury. *Proceedings of the National Academy of Sciences of the United States of America* **98**(26)**:** 15306-15311.

SUN Y, JIN K, PEEL A, MAO XO, XIE L, GREENBERG DA (2003). Neuroglobin protects the brain from experimental stroke in vivo. *Proceedings of the National Academy of Sciences of the United States of America* **100**(6)**:** 3497-3500.

SUTC'S (2002). Organised inpatient (stroke unit) care for stroke. *Cochrane Database Syst Rev*(4)**:** CD000197.

SUZUKI Y, IMAI Y, NAKAYAMA H, TAKAHASHI K, TAKIO K, TAKAHASHI R (2001). A serine protease, HtrA2, is released from the mitochondria and interacts with XIAP, inducing cell death. *Molecular cell* **8**(3)**:** 613-621.

SYDSERFF SG, BORELLI AR, GREEN AR, CROSS AJ (2002). Effect of NXY-059 on infarct volume after transient or permanent middle cerebral artery occlusion in the rat; studies on dose, plasma concentration and therapeutic time window. *British journal of pharmacology* **135**(1)**:** 103-112.

TABAKMAN R, JIANG HAO, SHAHAR I, ARIEN-ZAKAY H, LEVINE RA, LAZAROVICI P (2005). Neuroprotection by NGF in the PC12 In Vitro OGD Model. *Annals of the New York Academy of Sciences* **1053**(1)**:** 84-96.

TAKANO K, LATOUR LL, FORMATO JE, CARANO RA, HELMER KG, HASEGAWA Y, *et al.* (1996). The role of spreading depression in focal ischemia evaluated by diffusion mapping. *Annals of neurology* **39**(3)**:** 308-318.

TAKASAGO T, PETERS EE, GRAHAM DI, MASAYASU H, MACRAE IM (1997). Neuroprotective efficacy of ebselen, an anti-oxidant with anti-inflammatory actions, in a rodent model of permanent middle cerebral artery occlusion. *British journal of pharmacology* **122**(6)**:** 1251-1256.

TAMURA A, GRAHAM DI, MCCULLOCH J, TEASDALE GM (1981). Focal cerebral ischaemia in the rat: 1. Description of technique and early neuropathological consequences following middle cerebral artery occlusion. *Journal of cerebral blood flow and metabolism : official journal of the International Society of Cerebral Blood Flow and Metabolism* **1**(1)**:** 53-60.

TAYMANS JM, VANDENBERGHE LH, HAUTE CV, THIRY I, DEROOSE CM, MORTELMANS L, *et al.* (2007). Comparative analysis of adeno-associated viral vector serotypes 1, 2, 5, 7, and 8 in mouse brain. *Human gene therapy* **18**(3)**:** 195-206.

TOBIUME K, SAITOH M, ICHIJO H (2002). Activation of apoptosis signal-regulating kinase 1 by the stress-induced activating phosphorylation of pre-formed oligomer. *Journal of Cellular Physiology* **191**(1)**:** 95-104.

TOMASSONI D, LANARI A, SILVESTRELLI G, TRAINI E, AMENTA F (2008). Nimodipine and its use in cerebrovascular disease: evidence from recent preclinical and controlled clinical studies. *Clin Exp Hypertens* **30**(8)**:** 744-766.

TOURNIER C, DONG C, TURNER TK, JONES SN, FLAVELL RA, DAVIS RJ (2001). MKK7 is an essential component of the JNK signal transduction pathway activated by proinflammatory cytokines. *Genes & development* **15**(11)**:** 1419-1426.

TRENT JT, 3RD, HARGROVE MS (2002). A ubiquitously expressed human hexacoordinate hemoglobin. *The Journal of biological chemistry* **277**(22)**:** 19538-19545.

TRENT JT, WATTS RA, HARGROVE MS (2001). Human Neuroglobin, a Hexacoordinate Hemoglobin That Reversibly Binds Oxygen. *Journal of Biological Chemistry* **276**(32)**:** 30106-30110.

TRIALISTS'COLLABORATION A (2002). Collaborative meta-analysis of randomised trials of antiplatelet therapy for prevention of death, myocardial infarction, and stroke in high risk patients. *BMJ* **324**(7329)**:** 71-86.

TRUST (1990). Randomised, double-blind, placebo-controlled trial of nimodipine in acute stroke. Trust Study Group. *Lancet* **336**(8725)**:** 1205-1209.

TUSZYNSKI MH, THAL L, PAY M, SALMON DP, U HS, BAKAY R, *et al.* (2005). A phase 1 clinical trial of nerve growth factor gene therapy for Alzheimer disease. *Nature medicine* **11**(5)**:** 551-555.

UEHARA T, BENNETT B, SAKATA ST, SATOH Y, BILTER GK, WESTWICK JK, *et al.* (2005). JNK mediates hepatic ischemia reperfusion injury. *Journal of Hepatology* **42**(6)**:** 850-859.

UTTARA B, SINGH AV, ZAMBONI P, MAHAJAN RT (2009). Oxidative stress and neurodegenerative diseases: a review of upstream and downstream antioxidant therapeutic options. *Current neuropharmacology* **7**(1)**:** 65-74.

VAN DER WORP HB, SENA ES, DONNAN GA, HOWELLS DW, MACLEOD MR (2007). Hypothermia in animal models of acute ischaemic stroke: a systematic review and meta-analysis. *Brain : a journal of neurology* **130**(Pt 12)**:** 3063-3074.

VAN LOO G, SCHOTTE P, VAN GURP M, DEMOL H, HOORELBEKE B, GEVAERT K*, et al.* (2001). Endonuclease G: a mitochondrial protein released in apoptosis and involved in caspase-independent DNA degradation. *Cell death and differentiation* **8**(12)**:** 1136-1142.

VEMUGANTI R, DEMPSEY RJ, BOWEN KK (2004). Inhibition of intercellular adhesion molecule-1 protein expression by antisense oligonucleotides is neuroprotective after transient middle cerebral artery occlusion in rat. *Stroke* **35**(1)**:** 179-184.

VERHAGEN AM, SILKE J, EKERT PG, PAKUSCH M, KAUFMANN H, CONNOLLY LM*, et al.* (2002). HtrA2 Promotes Cell Death through Its Serine Protease Activity and Its Ability to Antagonize Inhibitor of Apoptosis Proteins. *Journal of Biological Chemistry* **277**(1)**:** 445-454.

WAETZIG V, ZHAO Y, HERDEGEN T (2006). The bright side of JNKs-Multitalented mediators in neuronal sprouting, brain development and nerve fiber regeneration. *Progress in neurobiology* **80**(2)**:** 84-97.

WAHLGREN NG, MACMAHON DG, DE KEYSER J, INDREDAVIK B, RYMAN T (1994). Intravenous Nimodipine West European Stroke Trial (INWEST) of Nimodipine in the Treatment of Acute Ischaemic Stroke. *Cerebrovascular Diseases* **4**(3)**:** 204-210.

WAKASUGI K, KITATSUJI C, MORISHIMA I (2005). Possible Neuroprotective Mechanism of Human Neuroglobin. *Annals of the New York Academy of Sciences* **1053**(1)**:** 220-230.

WAKASUGI K, NAKANO T, MORISHIMA I (2003). Oxidized Human Neuroglobin Acts as a Heterotrimeric Gα Protein Guanine Nucleotide Dissociation Inhibitor. *Journal of Biological Chemistry* **278**(38)**:** 36505-36512.

WANG CY, MAYO MW, KORNELUK RG, GOEDDEL DV, BALDWIN AS, JR. (1998). NF-kappaB antiapoptosis: induction of TRAF1 and TRAF2 and c-IAP1 and c-IAP2 to suppress caspase-8 activation. *Science* **281**(5383)**:** 1680-1683.

WANG GL, SEMENZA GL (1993). Desferrioxamine induces erythropoietin gene expression and hypoxia-inducible factor 1 DNA-binding activity: implications for models of hypoxia signal transduction. *Blood* **82**(12)**:** 3610-3615.

WANG P, XU TY, GUAN YF, TIAN WW, VIOLLET B, RUI YC*, et al.* (2011). Nicotinamide phosphoribosyltransferase protects against ischemic stroke through SIRT1-dependent adenosine monophosphate-activated kinase pathway. *Annals of neurology* **69**(2)**:** 360-374.

WANG X, LIU J, ZHU H, TEJIMA E, TSUJI K, MURATA Y*, et al.* (2008). Effects of neuroglobin overexpression on acute brain injury and long-term outcomes after focal cerebral ischemia. *Stroke* **39**(6)**:** 1869-1874.

WANG X, TSUJI K, LEE SR, NING M, FURIE KL, BUCHAN AM*, et al.* (2004). Mechanisms of hemorrhagic transformation after tissue plasminogen activator reperfusion therapy for ischemic stroke. *Stroke* **35**(11 Suppl 1)**:** 2726-2730.

WARNER DS (1995). Meta-analysis of oral nimodipine trials in acute ischemic stroke. *Journal of Neurosurgical Anesthesiology* **7**(1)**:** 69.

WELSH FA, SIMS RE, HARRIS VA (1990). Mild hypothermia prevents ischemic injury in gerbil hippocampus. *Journal of cerebral blood flow and metabolism : official journal of the International Society of Cerebral Blood Flow and Metabolism* **10**(4)**:** 557-563.

WESTERMAIER T, ZAUSINGER S, BAETHMANN A, SCHMID-ELSAESSER R (2005). Dose finding study of intravenous magnesium sulphate in transient focal cerebral ischemia in rats. *Acta neurochirurgica* **147**(5)**:** 525-532; discussion 532.

WHITMARSH AJ, KUAN CY, KENNEDY NJ, KELKAR N, HAYDAR TF, MORDES JP*, et al.* (2001). Requirement of the JIP1 scaffold protein for stress-induced JNK activation. *Genes & development* **15**(18)**:** 2421-2432.

WIDLAK P, LI P, WANG X, GARRARD WT (2000). Cleavage preferences of the apoptotic endonuclease DFF40 (caspase-activated DNase or nuclease) on naked DNA and chromatin substrates. *The Journal of biological chemistry* **275**(11)**:** 8226-8232.

WIGLER M, SILVERSTEIN S, LEE LS, PELLICER A, CHENG Y, AXEL R (1977). Transfer of purified herpes virus thymidine kinase gene to cultured mouse cells. *Cell* **11**(1)**:** 223-232.

WILLIAMS B (2003). Treatment of hypertension in the UK: simple as ABCD? *JRSM* **96**(11)**:** 521-522.

WITLIN AG, SIBAI BM (1998). Magnesium sulfate therapy in preeclampsia and eclampsia. *Obstetrics and gynecology* **92**(5)**:** 883-889.

WOLF PA, D'AGOSTINO RB, KANNEL WB, BONITA R, BELANGER AJ (1988). Cigarette smoking as a risk factor for stroke. The Framingham Study. *JAMA : the journal of the American Medical Association* **259**(7)**:** 1025-1029.

WU Z, ASOKAN A, SAMULSKI RJ (2006). Adeno-associated Virus Serotypes: Vector Toolkit for Human Gene Therapy. *Mol Ther* **14**(3)**:** 316-327.

XU H, DAWSON R, CRANE IJ, LIVERSIDGE J (2005). Leukocyte diapedesis in vivo induces transient loss of tight junction protein at the blood-retina barrier. *Investigative ophthalmology & visual science* **46**(7)**:** 2487-2494.

XUE D, HUANG ZG, BARNES K, LESIUK HJ, SMITH KE, BUCHAN AM (1994). Delayed treatment with AMPA, but not NMDA, antagonists reduces neocortical infarction. *Journal of cerebral blood flow and metabolism : official journal of the International Society of Cerebral Blood Flow and Metabolism* **14**(2)**:** 251-261.

XUE D, SLIVKA A, BUCHAN AM (1992). Tirilazad reduces cortical infarction after transient but not permanent focal cerebral ischemia in rats. *Stroke* **23**(6)**:** 894-899.

XUE YQ, MA BF, ZHAO LR, TATOM JB, LI B, JIANG LX, *et al.* (2009). AAV9-mediated erythropoietin gene delivery into the brain protects nigral dopaminergic neurons in a rat model of Parkinson's disease. *Gene therapy* **17**(1)**:** 83-94.

YAMAGUCHI T, SANO K, TAKAKURA K, SAITO I, SHINOHARA Y, ASANO T, *et al.* (1998). Ebselen in acute ischemic stroke: a placebo-controlled, double-blind clinical trial. Ebselen Study Group. *Stroke* **29**(1)**:** 12-17.

YAMASHIMA T, TONCHEV AB, TSUKADA T, SAIDO TC, IMAJOH-OHMI S, MOMOI T, *et al.* (2003). Sustained calpain activation associated with lysosomal rupture executes necrosis of the postischemic CA1 neurons in primates. *Hippocampus* **13**(7)**:** 791-800.

YANEZ-MUNOZ RJ, BALAGGAN KS, MACNEIL A, HOWE SJ, SCHMIDT M, SMITH AJ, *et al.* (2006). Effective gene therapy with nonintegrating lentiviral vectors. *Nature medicine* **12**(3)**:** 348-353.

YANG DD, KUAN C-Y, WHITMARSH AJ, RINOCN M, ZHENG TS, DAVIS RJ, *et al.* (1997a). Absence of excitotoxicity-induced apoptosis in the hippocampus of mice lacking the Jnk3 gene. *Nature* **389**(6653)**:** 865-870.

YANG J, LIU X, BHALLA K, KIM CN, IBRADO AM, CAI J, *et al.* (1997b). Prevention of Apoptosis by Bcl-2: Release of Cytochrome c from Mitochondria Blocked. *Science* **275**(5303)**:** 1129-1132.

YANG X, KHOSRAVI-FAR R, CHANG HY, BALTIMORE D (1997c). Daxx, a novel Fas-binding protein that activates JNK and apoptosis. *Cell* **89**(7)**:** 1067-1076.

YANG Y, LI Q, AHMAD F, SHUAIB A (2000). Survival and histological evaluation of therapeutic window of post-ischemia treatment with magnesium sulfate in embolic stroke model of rat. *Neuroscience letters* **285**(2)**:** 119-122.

YE S-Q, ZHOU X-Y, LAI X-J, ZHENG L, CHEN X-Q (2009a). Silencing neuroglobin enhances neuronal vulnerability to oxidative injury by down-regulating 14-3-3[gamma]. *Acta Pharmacol Sin* **30**(7)**:** 913-918.

YE SQ, ZHOU XY, LAI XJ, ZHENG L, CHEN XQ (2009b). Silencing neuroglobin enhances neuronal vulnerability to oxidative injury by down-regulating 14-3-3gamma. *Acta pharmacologica Sinica* **30**(7)**:** 913-918.

YIN T, SANDHU G, WOLFGANG CD, BURRIER A, WEBB RL, RIGEL DF*, et al.* (1997). Tissue-specific pattern of stress kinase activation in ischemic/reperfused heart and kidney. *The Journal of biological chemistry* **272**(32)**:** 19943-19950.

YU C, MINEMOTO Y, ZHANG J, LIU J, TANG F, BUI TN*, et al.* (2004). JNK suppresses apoptosis via phosphorylation of the proapoptotic Bcl-2 family protein BAD. *Molecular cell* **13**(3)**:** 329-340.

YU S-W, WANG H, POITRAS MF, COOMBS C, BOWERS WJ, FEDEROFF HJ*, et al.* (2002). Mediation of Poly(ADP-Ribose) Polymerase-1-Dependent Cell Death by Apoptosis-Inducing Factor. *Science* **297**(5579)**:** 259-263.

ZARRUK JG, GARCIA-YEBENES I, ROMERA VG, BALLESTEROS I, MORAGA A, CUARTERO MI*, et al.* (2011). Neurological tests for functional outcome assessment in rodent models of ischaemic stroke. *Revista de neurologia* **53**(10)**:** 607-618.

ZAUSINGER S, BAETHMANN A, SCHMID-ELSAESSER R (2002). Anesthetic methods in rats determine outcome after experimental focal cerebral ischemia: mechanical ventilation is required to obtain controlled experimental conditions. *Brain research. Brain research protocols* **9**(2)**:** 112-121.

ZHANG L, SCHALLERT T, ZHANG ZG, JIANG Q, ARNIEGO P, LI Q*, et al.* (2002a). A test for detecting long-term sensorimotor dysfunction in the mouse after focal cerebral ischemia. *Journal of neuroscience methods* **117**(2)**:** 207-214.

ZHANG RL, CHOPP M, CHEN H, GARCIA JH (1994). Temporal profile of ischemic tissue damage, neutrophil response, and vascular plugging following permanent and transient (2H) middle cerebral artery occlusion in the rat. *Journal of the neurological sciences* **125**(1)**:** 3-10.

ZHANG XY, LA RUSSA VF, BAO L, KOLLS J, SCHWARZENBERGER P, REISER J (2002b). Lentiviral vectors for sustained transgene expression in human bone marrow-derived stromal cells. *Mol Ther* **5**(5 Pt 1)**:** 555-565.

ZHANG Y, ZHU C, PARDRIDGE WM (2002c). Antisense gene therapy of brain cancer with an artificial virus gene delivery system. *Mol Ther* **6**(1)**:** 67-72.

ZHANG Z, YANG X, ZHANG S, MA X, KONG J (2007). BNIP3 upregulation and EndoG translocation in delayed neuronal death in stroke and in hypoxia. *Stroke* **38**(5)**:** 1606-1613.

ZHAO Z, CHENG M, MAPLES KR, MA JY, BUCHAN AM (2001). NXY-059, a novel free radical trapping compound, reduces cortical infarction after permanent focal cerebral ischemia in the rat. *Brain research* **909**(1-2)**:** 46-50.

ZHENG XR, ZHANG SS, YANG YJ, YIN F, WANG X, ZHONG L*, et al.* (2010). Adenoviral vector-mediated transduction of VEGF improves neural functional recovery after hypoxia-ischemic brain damage in neonatal rats. *Brain research bulletin* **81**(4-5)**:** 372-377.

ZHOU GY, ZHOU SN, LOU ZY, ZHU CS, ZHENG XP, HU XQ (2008). Translocation and neuroprotective properties of transactivator-of-transcription protein-transduction domain-neuroglobin fusion protein in primary cultured cortical neurons. *Biotechnol Appl Biochem* **49**(Pt 1)**:** 25-33.

ZHOU L, LI F, XU HB, LUO CX, WU HY, ZHU MM*, et al.* (2010). Treatment of cerebral ischemia by disrupting ischemia-induced interaction of nNOS with PSD-95. *Nature medicine* **16**(12)**:** 1439-1443.

ZHU W, FAN Y, FRENZEL T, GASMI M, BARTUS RT, YOUNG WL, *et al.* (2008). Insulin growth factor-1 gene transfer enhances neurovascular remodeling and improves long-term stroke outcome in mice. *Stroke* **39**(4)**:** 1254-1261.

ZHU W, FAN Y, HAO Q, SHEN F, HASHIMOTO T, YANG GY, *et al.* (2009). Postischemic IGF-1 gene transfer promotes neurovascular regeneration after experimental stroke. *Journal of cerebral blood flow and metabolism : official journal of the International Society of Cerebral Blood Flow and Metabolism* **29**(9)**:** 1528-1537.

ZIPOREN L, DONIN N, SHMUSHKOVICH T, GROSS A, FISHELSON Z (2009). Programmed necrotic cell death induced by complement involves a Bid-dependent pathway. *J Immunol* **182**(1)**:** 515-521.

ZIVIN JA, MAZZARELLA V (1991). Tissue plasminogen activator plus glutamate antagonist improves outcome after embolic stroke. *Archives of neurology* **48**(12)**:** 1235-1238.

ZOU H, HENZEL WJ, LIU X, LUTSCHG A, WANG X (1997). Apaf-1, a human protein homologous to C. elegans CED-4, participates in cytochrome c-dependent activation of caspase-3. *Cell* **90**(3)**:** 405-413.